THE BASIS OF THERMOFORMING POLY(ETHYLENE-TEREPHTHALATE) CONTAINERS

by

A O Ola, B.Sc Chem, M.Sc

- Doctoral Thesis -

Submitted in partial fulfillment of the
requirements for the award of the degree of
Doctor of Philosophy of the
Loughborough University of Technology

September 1987

Supervisors :
Professor A W Birley, M.A., D. Phil., F.P.R.I.
Institute of Polymer Technology
Mr B Haworth, B.Sc., M.Sc., M.P.R.I.
Institute of Polymer Technology

CERTIFICATE OF ORIGINALITY

This is to certify that I am responsible for the work submitted in this thesis, that the original work is my own except as specified in acknowledgements and that neither the thesis nor the original work contained herein has been submitted to this or any other institution for a degree.

A O Ola

LIST OF CONTENTS

LIST OF FIGURES

LIST OF TABLES

ACKNOWLEDGEMENTS

I am very grateful for the invaluable advice and suggestions given by Professor A W Birley and Mr B Haworth, my supervisors, throughout the period of this project.

I would also like to thank my colleagues, staff and technical staff of IPT for their cooperation during my stay in the department.

Special thanks to my friends especially Messers O Odusote and P Olomolaiye for their support during difficult times.

Finally, I wish to express my deepest gratitude to God, my family especially my father for his financial support, love and encouragement which made this work possible.

SYNOPSIS

Thermoforming characteristics of amorphous Poly (ethylene-terephthalate) (PETP) were investigated. Tensile drawing behavior were used to predict thermoformability within 80 - 110°C temperature range. From the analysis of non-linear visco-elastic behavior of PETP a strain hardening equation :

$$\sigma_t = K\varepsilon_t^n$$

defined the strain hardening regime of the stress-strain curve. The strain hardening index 'n' was related to formability. A high strain hardening index ensures thickness uniformity in formed parts. In addition, for uniform thickness to achieved, the draw ratio must be in excess of the uniform deformation regime (Engineering strain > 2) especially for high rigidity and creep resistance which is required for packaging carbonated beverages.

The processing characteristics of PETP sheet during thermoforming were determined in terms of stretch and cooling factors. The influence of each processing conditions on forming characteristics was investigated. For both vacuum and Plug-assist formed containers, a low stretch factor and a low cooling factor promote eveness in thickness distribution. In thermoforming PETP, it is essential to maintain processing conditions that ensure isothermal deformation of the polymer especially in deep draw containers.

Factorial experimental design was used to optimize processing conditions for both vacuum and plug-assist formings. From the analysis of the contour plots, the best thickness distribution was obtained when the sheet temperature range was 80 - 90 °C and the mould temperature range , 70 - 85 °C for vacuum drawn containers. In the plug-assist mode, 80 - 90 °C sheet temperature, 70 - 85 °C mould temperature and plug temperature of 100 °C - 112 °C promoted evenness in thickness distribution. In shallow drawn containers similar conditions prevailed except that much lower mould temperature 50 - 70 °C was required to promote thickness uniformity.

Chapter 1

1. POLY(ETHYLENE -TEREPHTHALATE) (PETP)

1.1 Introduction

Commercially important thermoplastic polyesters are based on such polymers, of which Poly(ethylene-terephthalate) (PETP) is the major product. These polymers are commonly used both for films and fibres.

Fibre-forming polyesters based on aliphatic polyesters were first reported in 1932 by Carothers and Hill [1]. These polymers were found to have low melting point and poor hydrolytic stability. These characteristics excluded aliphatic polyesters as textile fibres. Therefore research was concentrated in the late 1930s on hydrolytically stable polyamides. However, by 1941 Whinfield and Dickson [2] working at the Calico Printers Association in England discovered poly(ethylene-terephthalate). Further research was conducted around the world for the exploitation of the material. PETP fibre was marketed as Terylene and Dacron in the U.K. and U.S.A. respectively after the war.

PETP fibres have the following properties [3].

1) high strength and modulus
2) good recovery properties
3) resistance to heat, light and chemical attack

and 4) capable of being heat crystallized (i.e. heat setting of orientation in the fibre)

In addition to PETP's role as a fibre in the textile industry, it found use as biaxially drawn films. In addition to the properties associated with the fibres, the films are noted for[4]:

1) high tear strength
2) low water absorption
3) low gas permeability
4) high transparency
5) good dimensional stability
6) good electrical properties

and 7) high-temperature performance

Thus its application in photography, bases for magnetic recording tapes, type writer ribbons etc. More recently, combination of PETP's properties with safe toxicology has made it acceptable for food packaging (e.g. boil in bag applications).

Despite PETP's widespread use for fibres and films, it was considered unsuitable as a thermoplastic moulding resin because of relative brittleness of thick sections when crystallized from the melt [5,6,7]. Also because of the melt shear

sensitivity and the sensitivity of melt to traces of moisture. If PETP is processed with a significant moisture content (>.005 %), the resin will undergo a molecular weight (and viscosity) loss, which will result in deterioration of physical properties [8]. However, developments with nucleating agents in the early 1960's led to the production in 1966 of semi-finished products such as rod and pipe by a continuous casting process developed by Glanzstoff AG of Obernbung/Main. These materials had a :

1) high degree of surface hardness and abrasion resistance
2) low surface friction
3) high rigidity
4) high yield strength and modulus

and 5) good creep resistance

This led to the use of PETP as an engineering resin. In the 1970s it became recognised that reinforcement of the polymer with glass fibre had an even greater influence on modulus and rigidity than with other engineering plastics. For example, at 23 °C and 5O% R.H the flexural modulus of unfilled crystalline PETP is slightly less than that of a polyacetal.

On the other hand, at a glass fibre loading of 30% the modulus of polyester was found to be 10% higher (11 GPa c.f 10 GPa) than that of equivalent loading of polyacetal. At 50% fibre loading the modulus was as high as 15GPa [5].

In addition, further development of PETP resins improved its processability and broadened its scope of applications. For instance, the incorporation of Diethylene glycol (DEG), which is one of the by-products of PETP Synthesis, into the polyester chain reduces the melting point and therefore permits lower extruder temperature during moulding operations. The DEG interrupts the regularity of the PETP morphology and reduces the crystallization tendency of the resin. Other modifications include incorporation of isophthalic acid or Cyclohexanedimethanol Comonomers [8]. These give reduction in melting point and crystallization tendency and also widen the processing window. These developments led to the introduction of biaxially oriented bottles into the market. In fact, PETP bottles are the polymer success story of the 1980s[9]. Since the introduction of 1 litre and 2 litres PETP bottles in 1977 by Goodyear Tyre and Rubber Company the growth has been phenomenal. It now constitutes the highest volume usage of PETP. This application takes advantage of PETP being strain crystallizable. Crystallinity and orientation increases the mechanical strength and improves the barrier properties to gas and water vapour, and improves the heat-resistance. From the original market of carbonated drinks, PETP bottles are now used in new applications for packaging spirits, beer, wine, perfume, cooking oil etc.

The introduction of a nucleating agent which makes PETP crystallize at a much faster rate has opened up new packaging market [10,11]. This is thermoformed

crystallized PETP trays, with much improved high service temperature (150 - 220°C). This makes crystallized PETP trays suitable for dual oven capability. A dual ovenable tray is one that can be used in either a conventional oven or a microwave oven to constitute or reheat food. Crystallizable PETP trays are now displacing traditional materials for prepared food packaging like aluminium foil and compression moulded thermoset. It has been shown that PETP trays cost two to four times less than thermoset polyester. Apart from economy, it is lighter, tougher and has longer reuse life. These advantages have convinced Airlines in U.S.A. to adopt crystallizable PETP trays for hot-food service trays for in flight feeding [12]. Further applications include food trays for frozen prepared meals in the supermarkets in the U.K.

Another application of thermoformed PETP which is of primary interest to the present programme is PETP Cans of 200-500 cm^3 capacity. The production of biaxially oriented bottles blown from an amorphous injection moulded preform was limited to 1 and 2 litres capacities because it was not economically efficient in the production of smaller capacities especially in the early 1980s [14]. .Plastona Ltd - Waddington group in England was the first to introduce 300 cm^3 PETP Cans to compete with aluminium and tin-plate containers which had dominated the market. However, they used nucleated PETP to make their containers. Unfortunately, the crystallized PETP 'Cans' suffered from splitting during service. This is because crystallized PETP is brittle. This problem kindled the interest in thermoforming amorphous PETP 'Cans' below 1 litre capacity. Although there was little information available on thermoforming of amorphous homopolymer PETP, the need to open-up a new market for containers below 1 litre capacity forms the basis for this study. The general objectives are discussed later.

1.2 POLY(ETHYLENE-TEREPHTHALATE):Chemistry and Manufacture

After discussing the reasons for the success of PETP in a wide number of applications, it is necessary to understand the chemistry and manufacturing process involved. There are two main routes to produce PETP commercially [5-8].

First is the direct esterification of ethylene glycol with terephthalic acid and the second is the ester-interchange reaction between ethylene glycol and dimethyl ester of terephthalic acid.

The reactions proceed via a two stage process [7]:

1) the ester-exchange reaction resulting in bis (ß -hydroxethyl) terephthalate (bis HET)

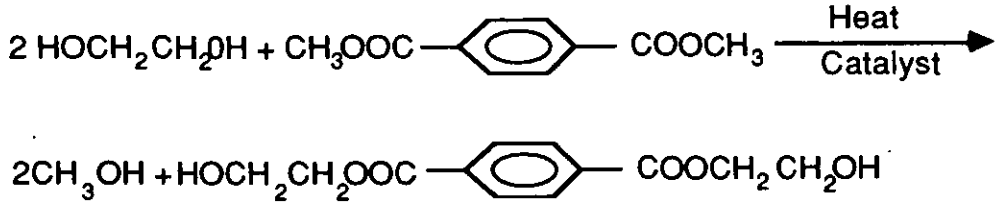

(Reaction 1.1)

2) poly condensation under vacuum to higher molecular weight polyester

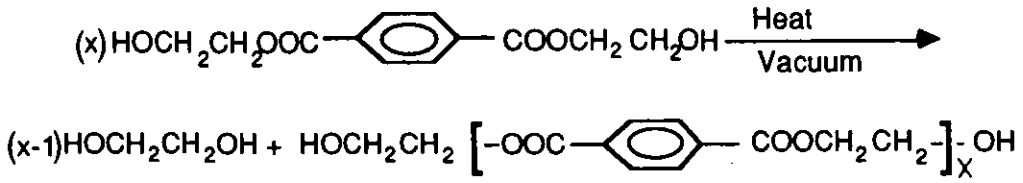

(Reaction 1.2)

In recent years, the direct esterification of ethylene glycol with terephthalic acid has replaced the ester-exchange process. This is because apart from not requiring a first stage catalyst, the initial esterification product is a low molecular weight mixture of PETP oligomers.

The molten mass of PETP produced is then extruded from the reactor, quenched rapidly with water cooling and pelletized to small chips. These pellets are further poly condensed in a solid state polymerization reactor operating at a safe temperature below the melting point of PETP [8]. During this process, the initially amorphous transparent pellets are thermally crystallized and turn opaque.

Kinetics of PETP polymerization have been studied by various workers but findings are not sufficiently consistent for easy summary [7,10,15-18]. However, it has been shown that the reaction is reversible necessitating removal of methanol, water and ethylene glycol to increase the molecular weight to the desired level [8].

Poly(ethylene- terephthalate) is a colourless material (opaque if crystalline) which melts when crystalline at about 260 - 265 °C with a glass transition temperature

of around 70 - 80 °C. The structural features of PETP which influence the high melting point are, the regularity in structure and chain stiffness. Other factors include interaction between the polarizable benzene ring and the polyester groups. All these factors contribute to the ability to develop crystallinity which also contributes to the physical properties.

1.3 Evaluation of Plastic sheet for Thermoforming

There are several concise laboratory procedures for predicting performance of various plastics in most types of thermoplastic processing, but simulation of thermoforming has received only minor attention.

Over the years research has been concentrated on flow behaviour of bulk polymers almost exclusively on flows which are viscometric, and especially on those which involve steady shears [19,20,21]. This is not surprising, since this is related to melt processing of polymers in extrusion, calendering, injection and blow moulding and related melt processing techniques.

For instance, the flow properties of polymer melts in extrusion dies of different geometries have been used in solving complex flow problems such as radial flow in injection moulding and two dimensional annular convergence in blow moulding dies [21]. In addition, recent studies have focused attention on the extensional viscosity component of polymer melts during fabrication operations [22,23,24,25]. These analyses enabled proper evaluation of new polymer materials in the various polymer melt fabrication processes, since they are not governed by shear viscosity only.

Until recently, there has been little attempt at relating common laboratory procedures to performance of thermoplastics in fabrication processes below their melting temperatures (i.e. thermoforming). The various procedures put forward by a number of workers are described briefly, one of which will be adopted later to determine formability of Poly(ethylene-terephthalate) (PETP) sheet.

It is essential at this point to state the main requirements of thermoplastics for thermoforming operations. Thermoforming implies stretching and deforming sheet above its softening point. Therefore, in order to form articles of useable draw ratios, the sheet must have capacity to thin appreciably. This means the plastic sheet must have significant elongation to break and relatively low elongation at yield and low elongation modulus in the forming conditions. For the sheet to retain the mould shape, it must have relatively little elasticity or memory when cold. These requirements are adequately met by most amorphous plastics (e.g. PS, ABS, PMMA) because they have wide softening ranges. Thus their domination of thermoforming market. Also they do not suffer excessive sagging and localised melting problems associated with some semi-crystalline materials like PP, HDPE and polyamide [26]. However, developments in polymer materials have broadened the range of plastics thermoformable for various applications. This makes it essential to have concise laboratory procedure to evaluate and predict behaviour of thermoplastic during forming operations.

1.3.1 Uniaxial Tensile Testing

Malpass and White [28] employed a number of procedures to determine thermoforming properties of ABS one of which was the Isothermal Uniaxial tensile test. They were able to determine the following parameters: tensile strength, yield elongation, maximum forming elongation, break elongation and elongation recovery. They concluded that the tensile data gave a good definition of the material property within the forming temperature because it provides the window to determine forming conditions for the material - like the optimum draw conditions (i.e. the temperature draw ratio and stress required). Thus, it can be used to screen thermoplastics for thermoformability. Fig. 1.1 shows the thermoforming region from a typical stress-strain curve.

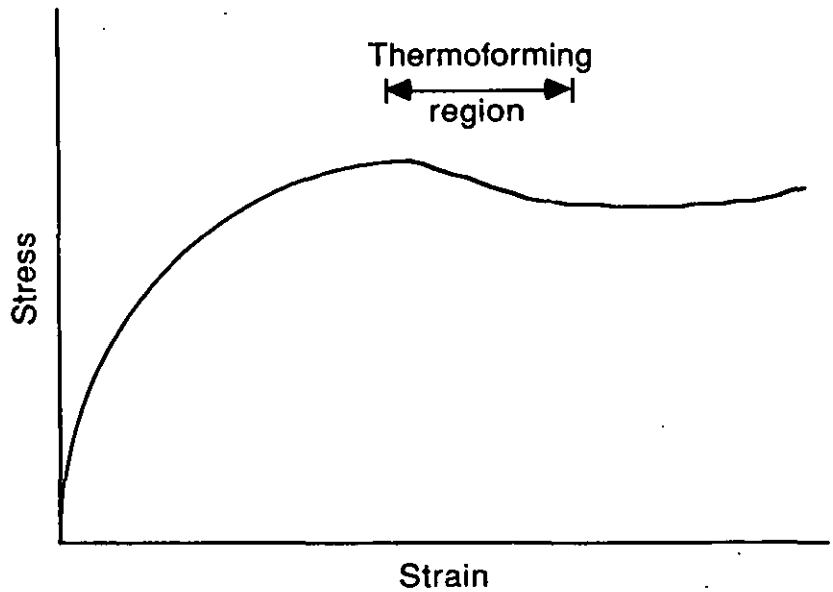

Figure 1.1 Shematic diagram strain of thermoforming region of a typical ductile material.

The Uniaxial tensile test was used by Lai and Holt [29] to analyse thermoforming behaviour of HIPS and PMMA. They proposed a relationship between the stress-strain curve and formability as follows: $\sigma = K\, t^m . \varepsilon^n$ where K is a temperature dependent constant, m is stress relaxation constant and n is strain hardening index. They established that high strain hardening index promotes thickness uniformity in formed parts. It is apparent that a strain crystallizing material such as PETP may require further development of this type of model.

1.3.2 Biaxial Deformation Testing

This is perhaps the closest procedure to simulate forming operations. Biaxial stretching of polymers had been undertaken by Rivlin and Saunders [30] in the early

1950s in order to gain insight into the large deformation behaviour of rubbers (visco-elastic properties), at room temperature. Recently, biaxial deformation of plastics at elevated temperatures was carried out by other workers [25,27,31,32] to study thermoforming behaviour of some thermoplastics Schmidt et al [31] worked on HIPS and Cellulose acetate butyrate while deVeries et al [32] worked on PVC. They were able to relate the stress-strain data to formability.

Problems with this technique are that data collection is prone to error as shown by Denson and Gallo [27], it is laborious and it requires special purpose built equipment.

1.3.3 Uniaxial Creep Testing

Viscoelastic creep is the time dependent deformation of a plastic specimen subjected to a constant load. Harris and Bruins [33] have been able to draw an analogy between creep phenomena and thermoforming of thermoplastics. Their comparison of both processes is given in table 1.1 [33].

	Thermoforming	Creep
Time scale	< 1sec	up to 3 years
Temperature	Forming temperature	Variable
Direction of applied stress	Biaxial	Uniaxial
Nature of load	Constant	Constant
Nature of strain	Time - dependent	Time - dependent

Table 1.1 Comparison of Thermoforming and Creep

They could not find a simple relationship between temperature and draw ratio. Also, the creep test did not give a good definition of material behaviour as shown by Malpass and White [28]. However, it can be used qualitatively to compare formability of various thermoplastic materials.

1.3.4 Melt flow

Malpass and White [28] attempted to use melt flow properties of ABS sheet to determine forming behaviour. The rheology of the resin was extrapolated into the low-shear condition of a stretched sheet at temperatures considered to be below those required for normal viscous flow. They assumed that amorphous polymers are essentially "fluids" above their softening temperature and that it is in this temperature regime that they are thermoformable. The evaluation of the 'extensibility' of the sheet was determined by measuring the melt viscosity. The melt viscosity was related to hot tensile strength of the sheet. Also, the swell ratio, a measure of degree of molecular

entanglement and elastic recovery, was determined. This was related to the tensile elastic recovery. However, they could not determine the thermoforming processing conditions for the materials from the melt flow properties, probably because of the dominating role which elasticity plays, for most thermoplastics in the thermoforming region.

1.4 General Objectives of this Research

With the brief Review of Properties of Poly(ethylene-terephthalate) PETP the following are the basic aims:

1) To characterise the PETP sheet and determine the processing window for PETP.
2) Simulate the thermoforming behaviour of the sheet by one of the laboratory procedures outlined in 1.3
3) Assess formability of amorphous PETP sheet at the processing window established.
4) Optimise the thermoforming processing conditions for amorphous PETP sheet.

Further objectives are outlined in the subsequent sections of this study. The work is effectively divided into two sections. First, the characterisation and simulation work is covered whilst the second part is the processing (which encompasses the assessment of formability and optimization of PETP thermoforming processing conditions).

The relevant review of literature for each part of the work is discussed separately. Chapter 2 deals with the characterization procedures used to analyse the PETP sheet supplied. Chapter 3 simulates the thermoforming behaviour of PETP sheet. Chapter 4 gives an overview of the thermoforming process and terminology. In Chapter 5, the formability of amorphous PETP sheet is assessed. Chapter 6 deals with analysis of PETP containers formed and optimization of the process respectively. Finally, in Chapter 7, the general conclusions of the research are presented

Chapter 2

2.0 Characterization of Poly(ethylene-terephthalate)PETP Sheet

2.1 Introduction

Polymer characterization involves the use of different analytical methods to identify, analyse and determine the molecular size and arrangement of polymers.

The identification tests include simple direct observation,physical tests for density ,refractive index, melting or softening temperature and solubility, and various spectroscopic techniques. These, are Infra-red (IR), Ultra Violet (UV) spectroscopy and Nuclear Magnetic Resonance (NMR) can be used to identify monomers, polymers, additives and impurities [34]. They are useful for detecting and determining crystallinity, end groups, chain microstructure, chain branching and investigation of various decomposition processes.

Other analytical techniques include chromatography, thermal analysis, microscopy and X-ray diffraction. Chromatography is particularly useful for analysis of blends and copolymers. Thermal analysis is used to determine energy changes and transition temperatures in polymers. Microscopy and X-ray diffraction methods are useful for morphology, crystallinity and the process of crystallization of polymers. Microscopy is also used to determine particle size distribution,general microstructure and features such as fracture surface,cracks and voids.

For the purpose of this work, there are three main analyses to be considered: the first is the determination of the chemical composition of the PETP sheet. It is essential to determine if the sheet is a homopolymer or a copolymer of PETP. Comonomers are sometimes added to enhance a desired aspect of processability and/or product properties(eg. supression of parison sag in blow moulding). Thus IR spectroscopy has been used because of its relative ease of operation and interpretation.

The determination of molecular weight is desirable because it influences physical properties such as crystallization rate (and thus crystallinity) and viscosity. The rate of crystallisation decreases with increasing molecular weight [35]. Therefore, the determination of the molecular weight of the sheet gives an idea of the physical properties. The intrinsic viscosity (IV) is determined as PETP is usually categorised on this basis for different applications. Dilute solution viscosity technique is employed because it has the advantage of being related to idealized state - the separation of molecules appropriate to a reliable molecular weight measurement for a given polymer system. In addition, the viscosity of dilute solutions depends on the molecular weight in a less sensitive fashion than does a molten polymer or concentrated solution since these are influenced to greater extent by molecular weight distribution.

The third analysis is thermal transition determination. This is very important in order to determine a thermoforming window of operation. Since PETP is crystallizable the processing region is limited to the rubbery region (at $T>T_g$,which may vary according the grade of PETP). Thus the glass transition T_g, crystallisation temperature (T_c), and crystalline melting temperature (T_m) must be determined. The processing region is between the T_g and T_c - the thermo-elastic region.

The material studied was PETP sheet extruded from 'Melinar' B90 (bottle grade) supplied by I.C.I. Fibres Ltd., Wilton, U.K. The sheet was optically clear and no crystallinity could be detected by density ($1.335 g/cm^3$) and wide angle X-ray diffraction measurements.

A brief exposition of each technique used for characterizing the PETP sheet is given in sub-sections of this chapter.

2.2 Infra-red Spectroscopy

Coblentz[34] discovered in the early 1900s that the infrared spectrum of a material is a highly sensitive characteristic of that substance; this led to the development of infrared absorption spectroscopy as a powerful analytical tool.

Absorption bands in the IR spectrum result from energy changes arising as a consequence of change in molecular vibrations accompanied by change in molecular dipole moments. The intensity of the absorption bands depends upon the magnitude of the change in dipole moment of the bands during the transition.

There are two main types of molecular vibrations: stretching and bending. A stretching vibration is along the bond axis while bending vibration (deformation) involves a change in bond angles. With poly-atomic molecules many more fundamental vibrational modes are possible. These include symmetrical and assymmetrical stretching modes, bending vibrations of various forms: scissoring and rocking (which are in-plane deformations) twisting and wagging (which are out-of-plane deformation) [36]. Frequencies of the stretching and bending vibrations depend largely on the vibrating atomic masses and the orders of the chemical bonds joining them. The lighter the atoms and/or the higher the bond order, the higher the frequency of vibration.

However, not all absorption bands can be accounted for from the basis of infrared-active fundamental vibrations. This is because of the presence of combination bands, overtone bands,and difference bands. These bands are frequently of lower intensity than the fundamental absorption bands but their presence,particularly the overtone bands, can be of diagnostic value for confirming the presence of a particular bonding system.

The infra-red is the portion in the electromagnetic spectrum between the visible and the microwave but for practical purposes the wavelength range of analysis is normally taken between 2.5-15μm (or 4000-600cm^{-1} wave numbers) [36]. The IR spectrum can be divided into two: the first between 4000-1600cm^{-1} and the second from 1600-660cm^{-1}. In the former, there are relatively few absorptions but in the latter a greater number of absorptions is usually observed. The second region is commonly called the 'finger print region' since complete imposability of two spectra in this region provides confirmation of identity. The former region is termed the "functional group region" since the fundamental vibrational modes of most of the principal functional groups absorb radiation in this part of the spectrum.

The most remarkable property of IR spectra interpretation is the fact that many stretching and bending modes in a molecule are virtually independent of changes of structure at more remote sites. Structural modifications closer to the absorbing center do, of course, affect the energy associated with absorption, and lead to a shift of the absorption band to higher or lower frequencies. These frequency shifts however, lie

within defined limits. For instance, the absorption maximum for C-H stretching frequency lies in the region around 3000cm^{-1}.

Infra-red spectroscopy has emerged as an important tool for studying the chemistry and physics of polymers. The analysis of functional group and finger print regions of the spectra enables qualitative and quantitative estimates of type, chemical composition in polymers and copolymers. Structural factors such as branching,cross-linking,steric hindrance,crystallinity,orientation in polymers and copolymer sequence distribution are some of the characteristics that can be studied using IR technique[37].

The infra-red absorption spectra of polymers are surprisingly simple,considering the large number of atoms involved. This simplicity results from the fact that many normal vibrations have almost the same frequency and therefore appear in the spectrum as one absorption band; and the second from the strict selection rules that prevent many vibrations from causing absorption[39].

Among the infra-red absorption of interest in polymers are C-H stretching (~3000cm^{-1}), C-H bending of CH_2 groups (1450cm^{-1}). Other absorption bands are those due to C=C at 1680-1620cm^{-1} (depending upon the substituents), carboxyl groups around 1700cm^{-1}, aromatic structures at 2000cm^{-1}, 1600cm^{-1}, 850cm^{-1} and 800cm^{-1} [39].

The infra-red absorption spectrum of PETP has been studied by a number of workers[40-43]. The most exhaustive is by Miller and Willis[44]. There is a general agreement among other workers with most of their assignments.

2.2.1 Experimental

A comprehensive list of sample preparation methods for IR spectroscopy applicable to polymers is given in the literature[36,37]. The two techniques used are solution film cast and direct transmission of this sheet.

(i) Film Cast Technique:

A 1% solution of PETP was made in 60/40 phenol/tetrachloroethane solvent at room temperature. A thin film was cast on an infra-red transparent plate from a few drops of the solution; the solvent was removed by exposing the film to a radiant heater. Care was taken to avoid crystallization or thermal degradation.

(ii) Direct Film Transmission

A biaxially drawn film of about 0.01mm thickness was cut from a vacuum formed container. The PETP sheet (as supplied) was too thick (1mm) for direct exposure to IR radiation. It was expected that the influence of biaxial orientation of the spectrum would be small. The main purpose of this procedure was to check for influence of solvent residue in the former technique.

2.2.2 Result and Discussion

The IR spectra from the two techniques are shown in figs.2.1 and 2..2. The interpretation of an infra-red spectrum of an unknown polymer can be very difficult. So a direct method is to compare the unknown with a standard spectrum, usually in the 'finger print' region (1600-650cm^{-1} If the two spectra correlate, it can be assumed that the two compounds are identical[37].

The two spectra in figs. 2.1 and 2.2 match very closely at all the major absorption bands. The band assignments are given in table 2.1.

The absorption band assignment at 2600cm^{-1} (-C=O stretching) and 1100cm^{-1} (-C=O stretching) confirms the presence of an ester group. The absorption bands at 1500cm^{-1} (Aromatic conjugated) and 870cm^{-1} (Aromatic C-H bending) and the absence of characteristic absorption bands for other carbonyl containing groups (acids and aldehydes) suggests an Aromatic polyester since Ketonic Polyesters are rarely encountered.

Comparison with a standard PETP homopolyester spectrum[43,49] shows a very close correlation. In addition, there is very close agreement with bands assignment of Miller and Willis [44]. The small difference in intensity of the absorption bands around 1100cm^{-1} in figs. 2.1 and 2.2 is influenced by orientation and crystallinity in the stretched sample[37,43,44].

From the results discussed, it is concluded that the sheet is homopolymer PETP.

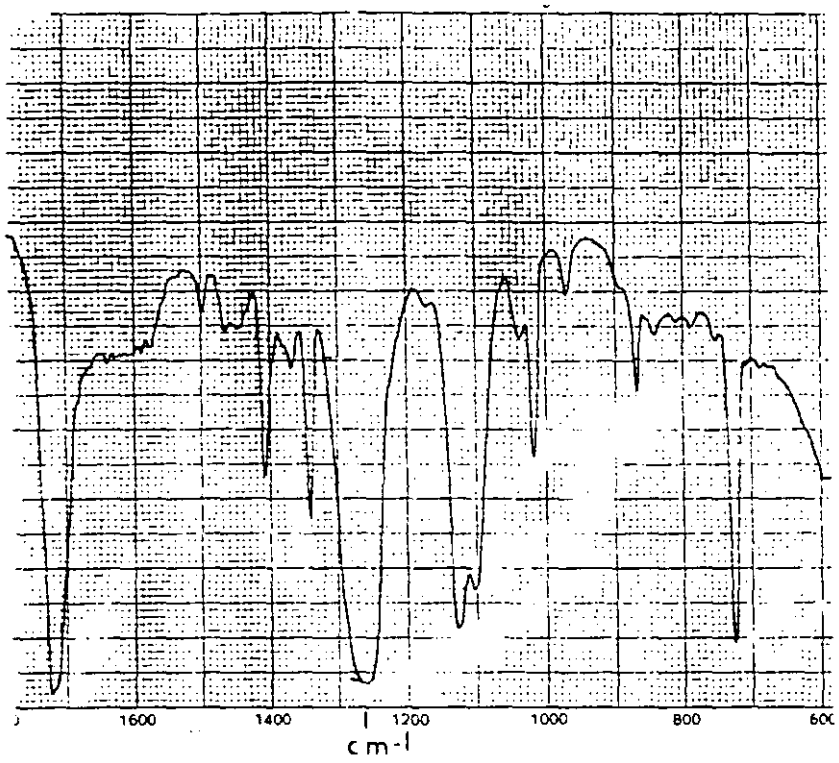

Figure 2.1 Infra-red spectrum of cast PETP film

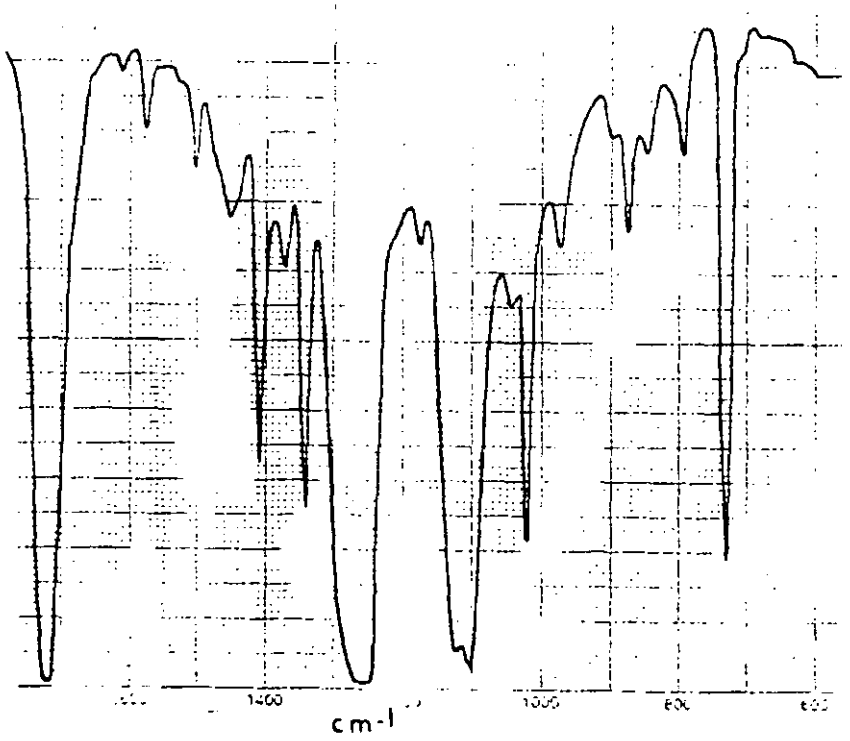

Figure 2.2 Infra-red spectrum of PETP film (direct transmission)

Sample IR Spectrum Analysis

Frequency(cm-1)	Relative intensity	Assignment
730	strong	C-O-C deformation in-plane of C-atoms.
870	medium	Aromatic C-H deformation out-of-plane of benzene ring
1100	strong	-C=O stretching Aryl conjugated.
1260	v.strong	-C-=O stretching Aryl conjugated.
1340	medium	CH_2 deformation out-of-plane of H atoms.
1410	medium	CH_2 deformation in-plane of H atoms.
1500	weak	Aromatic in-plane deformation.
1580	weak	Aromatic in-plane stretching.
1720	v.strong	O=C stretching.

Table 2.1 Band Assignments for PETP

2.3 Molecular Weight Determination

The molecular chain length of polymers is usually expressed in terms of an 'average' molecular weight. The kind of average obtained from measurement of the molecular weight is generally characteristic of the method used[45,46]. The most commonly used terms describing the experimental data are number average molecular weight ,M_n; viscosity average molecular weight,M_v; weight average molecular weight, M_w; the "Z-average" M_z and "z+1 average",M_{z+1}.[46,47] Each of these will be briefly considered for their meaning and interelationships.

(i) Number Average Molecular Weight.

The number average molecular weight is defined as

$$M_n = \frac{\text{weight of molecules}}{\text{number of molecules}} = \frac{W}{\sum N_i} = \frac{\sum N_i M_i}{\sum N_i} \qquad \text{----------2.1(a)}$$

where $W = \sum N_i M_i$

N_i = is the number of molecules of molecular weight M_i for every species i

or $M_n = \sum n_i M_i$ ----------2.1(b)

(where n_i is the number of fraction of molecules of molecular weight M_i)

Since determination of the number average molecular weight M_n involves counting the total number of molecules, regardless of their shape or size, present in a unit mass of a polymer, it is readily measured by measurement of colligative properties. A colligative property is defined as one which is a function only of the number, and not of the nature, of the solute molecules contained in a unit volume of solution [48]. Therefore, colligative properties such as osmotic pressure, elevation of boiling point, depression of freezing point, and lowering of vapour pressure provide a convenient means of determining M_n. End-group analysis also provides a direct measurement of M_n. However, the sensitivity of the method decreases rapidly as the chain length increases and the number of end group drops. Osmometry is inherently more sensitive than the other methods and is used to obtain M_n in the range of 100,000 or higher. The method suffers from the disadvantage that it is slow and consequently diffusion of low molecular weight material could introduce serious error in the measurement. These

draw backs have been rectified with the introduction of high-speed automatic membrane-osmometers.

(ii) Weight Average Molecular Weight

The weight average molecular weight is defined as

$$M_w = \frac{\sum M_i W_i}{\sum W_i} \qquad \text{---------- 2.2 (a)}$$

Where $W_i = N_i M_i$

$$\therefore M_w = \frac{\sum N_i M_i^2}{\sum N_i M_i} \qquad \text{---------- 2.2 (b)}$$

(where W_i - weight fraction of each species of molecular weight M_i.)

The weight average molecular weight measures the contribution from each molecular weight species proportional to the 'weight' of the molecules in that species. Light scattering is one of the most popular methods for determining the weight average molecular weight M_w. It has the virtue of being an absolute method, independent of other measurements [49]. Other methods include ultracentrifugation and for certain systems, from viscosity measurements.

(iii) Viscosity Average Molecular Weight

The viscosity average molecular weight M_v has been derived from the Mark-Houwink relationship of viscosity to molecular weight which is defined as [46]:

$$[\eta] = K(M)^a \qquad \text{.....2.3}$$

where $[\eta]$ = intrinsic viscosity

M = molecular weight

K and a = constants which depend on polymer-solvent system in use.

M_v is defined as

$$M_v = \left[\frac{\sum N_i M_i^{a+1}}{\sum N_i M_i} \right]^{\frac{1}{a}} \qquad \text{----------2.4}$$

It should be stated that M_v is not a true average number but a range dependent on the value of 'a', which changes with polymer-solvent interaction parameters. M_v is commonly used to characterize PVC resins. Solution viscosity measurement is the most common method for determining M_v..

(iv) Z and Z + 1 average molecular weights

The z and z+1 average molecular weights are not commonly used. They are higher than M_w and are obtained from sedimentation experiments. They are defined as follows:

$$M_z = \frac{\sum N_i M_i^3}{\sum N_i M_i^2} \qquad \text{---------- 2.5 (a)}$$

and

$$M_{z+1} = \frac{\sum N_i M_i^4}{\sum N_i M_i^3} \qquad \text{---------- 2.5 (b)}$$

2.3.1 Molecular Weight Distribution

The relationship that exists between the molecular weight 'averages' gives a measure of molecular weight distribution in a polymer since polymers are usually heterogenous in terms of weight distribution. From the relationships (2.1 - 2.5) it is obvious that

$$M_n < M_v < M_w < M_z < M_{z+1}$$

Fig (2.3) gives a typical differential weight-distribution curve. It shows that M_n is largely affected by the low-molecular weight components of a polymer sample, because they are represented most frequently in the sample and because in this average, each molecule contributes identically, regardless of its size. The higher averages are determined to an increasing extent by the high-molecular-weight 'tail' of the distribution. For this reason, the ratio M_w/M_n is often used as a measure of the width of a distribution [50].

Knowledge of the breadth of weight distribution in any polymer serves two purposes:

(a) It gives an understanding of the mechanism of polymer-forming reactions and

(b) the processability, mechanical properties, and use performance characteristics can be inferred from the shape of the distribution curve.

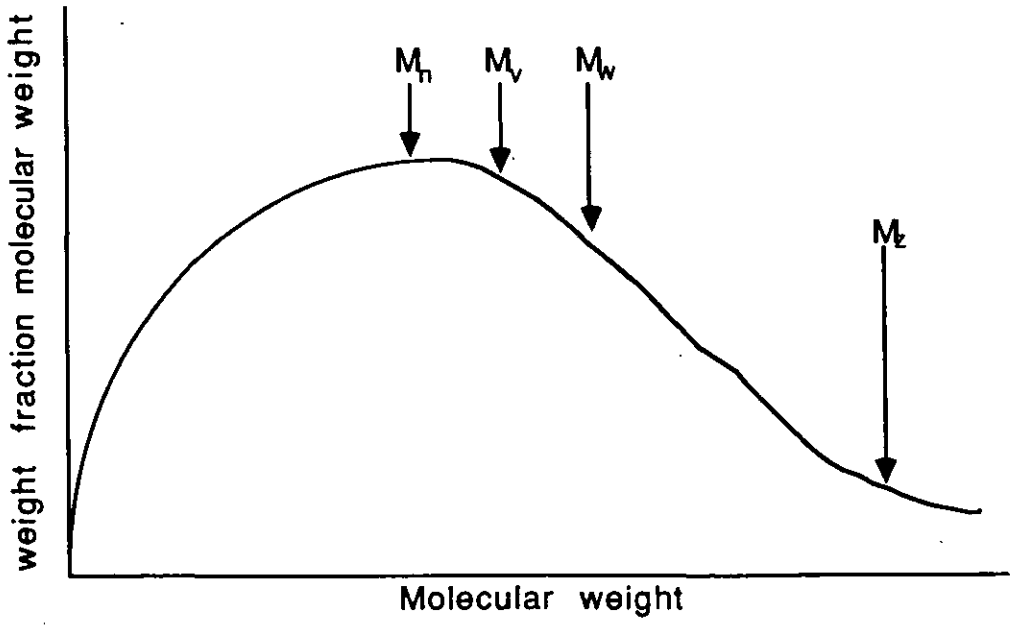

Figure 2.3 *Differential weight distribution curve with various averages indicated*

The determination of the molecular weight distribution by conventional fractionation techniques is time consuming, and a rapid, efficient, and reliable method has been developed. This is gel-permeation chromatography (GPC) which separates polymer samples into fractions according to their molecular size, by means of a reverse sieve action [51].

In section 1.1 it was stated that solution viscosity was used in this work for the reasons attributed. In addition, it is by far the quickest and simplest diagnostic tool for molecular weight although it is not an absolute method.

In practice, poly(ethylene-terephthalate) is usually characterised in terms of an intrinsic viscosity (I.V) to designate different grades for different applications. The I.V grades for PETP range from 0.7 for blow moulding to 1.0 for injection moulding. Since the IV is readily obtained from dilute solution viscosity, it was adopted in this work.

2.3.2 Solution Viscosity Measurements

Solution viscosity is a measure of the size or extension in space of polymer molecules. Measurement is made by comparing the efflux time (t) required for a specific volume of a polymer solution to flow through a capillary tube with corresponding efflux time (t_o), for the solvent. From the value of 't' and the solution concentration are derived several qualities with the following defining equations [47,52].

Relative viscosity	η_r	=	t/to
Specific viscosity	η_{sp}	=	t-to/to or η_r -1
Reduced Viscosity	η_{red}	=	η_{sp}/c
Inherent viscosity	η_{inh}	=	$(\eta_{sp}/c)/c$
Intrinsic viscosity	$[\eta]$	=	(η_{sp}/c) c=o or $(\ln \eta_r/c)$ c=o

c = concentration of polymer solution (g/dl)

The intrinsic viscosity [η]is independent of concentration by virtue of extrapolation of concentration to zero (c = o), but it is a function of the solvent used.

Typical measurements are made in a suspended level viscometer (Ubbelohde viscometer) fig (2.4) [48]. A solution of known concentration and volume is pipetted into a tube A, and with tube C closed, solution from bulb D is forced up into bulb E. Opening tube C and releasing pressure on tube A results in formation of a 'suspended level' at the lower end of the capillary. This suspended level is the feature which allows dilution to be carried out in D without affecting the efflux time t. The efflux time t is the time taken for the solution meniscus to pass from x to y in bulb F.

In the calculations of molecular weight of PETP grades, there is a relationship between intrinsic viscosity (I.V) and weight average molecular weight (M_w) which is given as [53].

$$I.V = 4.68 \times 10^{-4} (M_w)^{0.68}$$

This relationship will be used to calculate the molecular weight of PETP sheet.

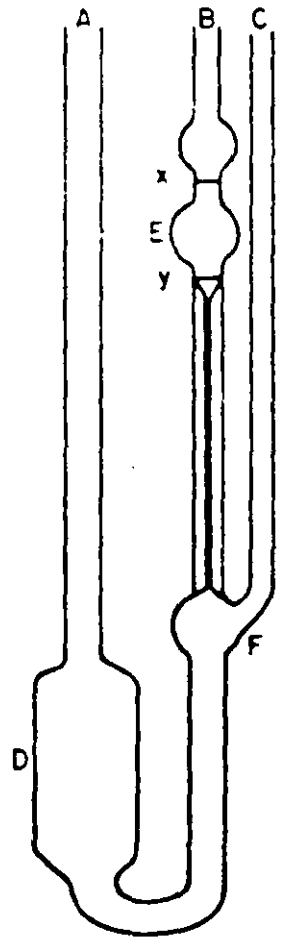

Figure 2.4 Suspended level dilution viscometer

2.3.3 Experimental

63.46 g of phenol crystals were dissolved in 40 ml of Tetracholorethane (TCE) to form a 60/40 mixture by volume. Phenol crystals were used because liquid phenol is highly hygroscopic and susceptible to oxidation.

0.5 g of PETP cut from the roll of sheet was dissolved in 50 ml of 60/40 Phenol/TCE mixture to make a 1% solution; a nitrogen atmosphere was used to eliminate any possibility of oxidation.

The flow times for successive dilutions (from 1 - 0.2 % concentrations) were determined in a suspended level viscometer maintained at 25°C in a constant temperature water bath. An equilibration time of 10 minutes was allowed for each run. Efflux time for three readings were taken, assuming agreement within 0.1 s of their mean values.

2.3.4 Results and Discussion

The results of the solution viscosity measurements are shown in table 2.2.

Solution Conc. g/dl	Efflux time (sec)			Rel. Visc η_r	Spec. Visc η_{sp}	Red.Visc η_{sp}/c	Inh. Visc $[\ln\eta_r]/c$
0	82.0	81.9	82.0	-	-	-	-
0.2	94.2	94.4	94.2	1.149	.149	.745	.694
0.4	107.4	107.4	107.4	1.310	.310	.775	.675
0.6	122.2	122.2	122.2	1.490	.490	.817	.666
0.8	138.0	137.9	138.0	1.682	.682	.852	.650
1.0	155.0	155.1	155.0	1.890	.890	.890	.637

Table 2.2 Dilute Solution Viscosity of PETP in 60/40 phenol/TCE mixture

Also, Fig 2.5 shows the plot of reduced viscosity and inherent viscosity versus concentration. The double extrapolation to zero concentration gives intrinsic viscosity $[\eta]$ value of 0.71 dl/g from the relationship[53].

$$[\eta] = 4.68 \times 10^{-4} (M_w)^{.68}$$

$$M_w = 4.73 \times 10^4 \text{ g/mol}$$

The I.V of 0.7 dl/g is fairly on the low side for bottle grade PETP. Commonly quoted I.V value for bottle grade PETP are 0.73-0.80 dl/g.

There are two possible reasons for the low value obtained; the first could be attributed to degradation during extrusion of the sheet; the other could be due to

absorption of water by phenol and oxidation during the equilibration time for each reading. This could introduce error into the calculation.

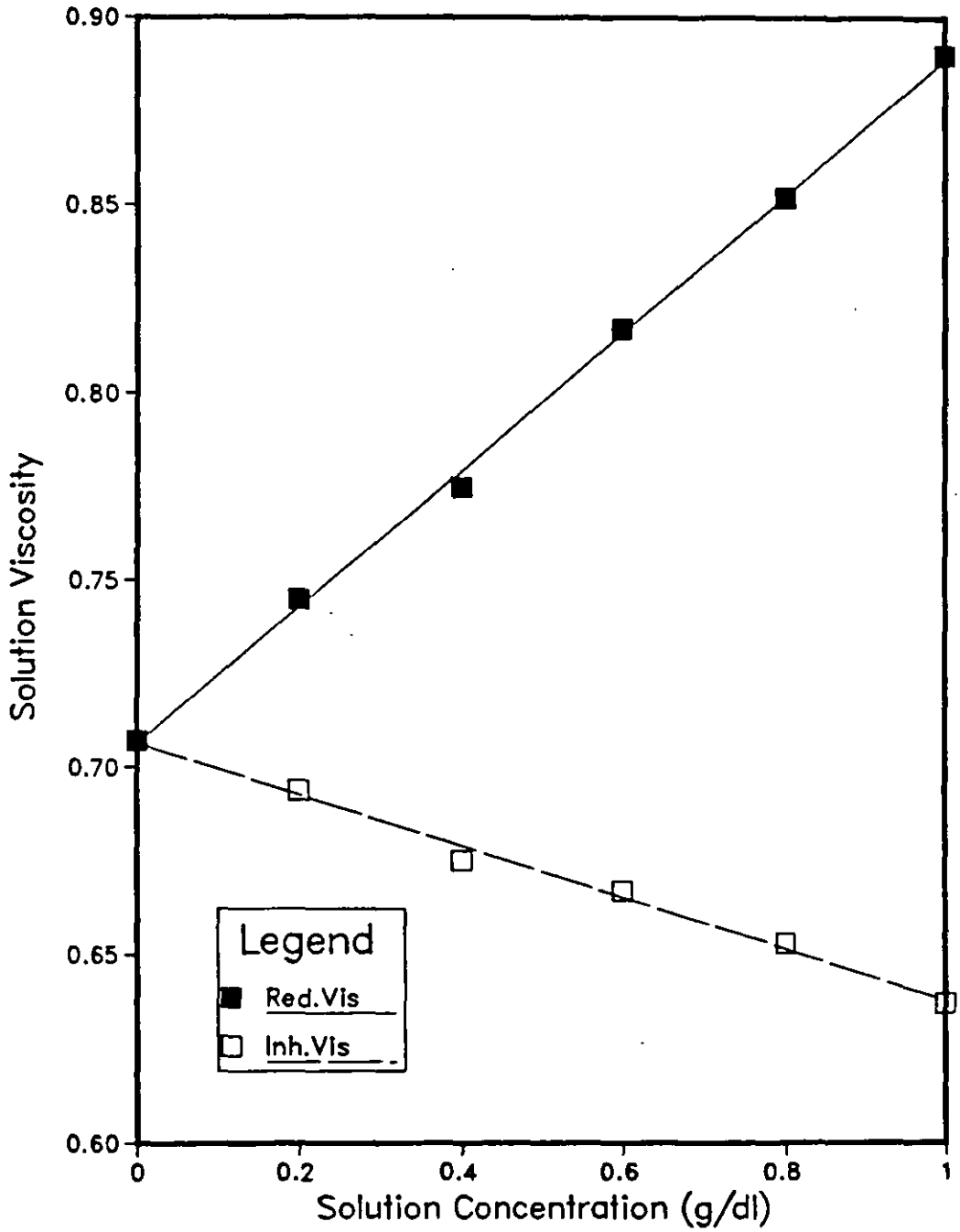

Figure 2.5 Solution viscosity as a function of concentration

2.4 Thermal Analysis

The physical or chemical change in a substance, accompanied by corresponding change in enthalpy forms the basis of Differential Thermal Analysis (DTA). DTA has its beginning in Le Chatelier's work in the fields of metallurgy and ceramics for identification and analytical purposes. [54]

Early applications in polymeric materials were in proteins, cellulose nitrate and polyethylene. Compared with other methods of analysis DTA provides a valuable and powerful tool for the study of polymer formation, stability, decompositions and transition temperatures [51] among many others.

The sample and a reference material which should undergo no phase changes (over the relevant temperature span) are placed in two cells in a heating block . The sample and the reference material are heated at a constant rate. The sample temperature T_s is then monitored by means of a thermocouple and compared with temperature of the reference material T_r. The plot of the temperature difference ΔT versus the block temperature results in a "thermogram" with a maximum or minimum as the change is exothermic or endothermic [51]. The thermogram gives the transformation temperatures such as melting or crystallization onset. A third type of change can be detected, the glass transition temperature. This is associated with a change in heat capacity of the sample and reference material. The change in heat capacity causes a shift in the base line. Because the heat of fusion represents the enthalpy difference between crystalline and amorphous phases in a material, the degree of crystallinity of the polymer can be calculated [48]. A typical DTA curve for a crystallizing polymer is shown in figure (2.6).

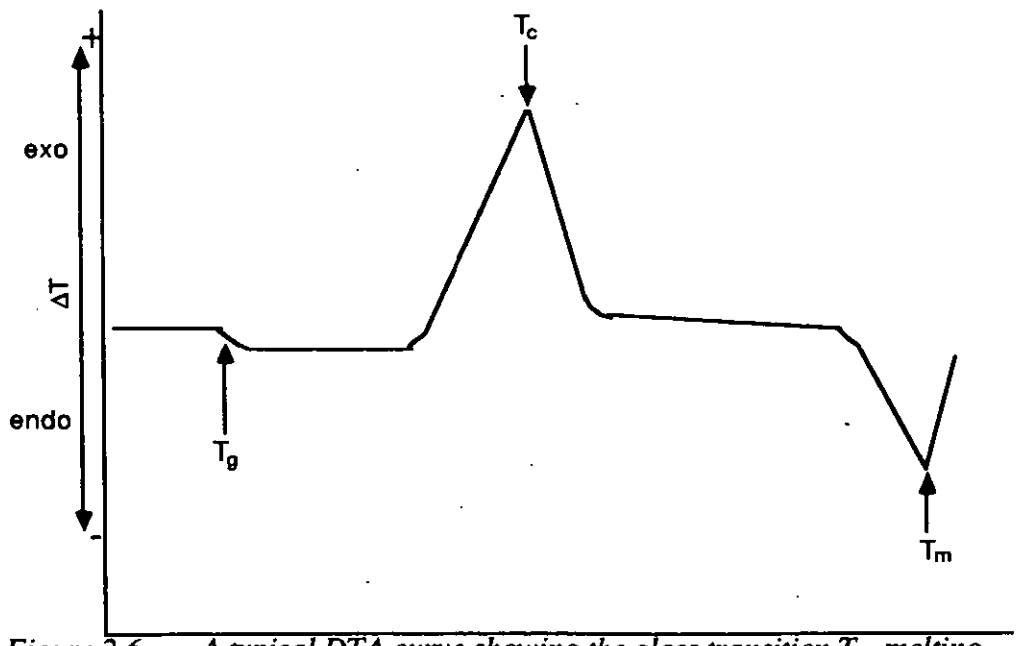

Figure 2.6 A typical DTA curve showing the glass transition T_g, melting endotherm Tm, and a crystallization exotherm T_c

Apart from the detection of transformation temperatures, DTA has been used to determine composition of blended polymers. The blends of polyethylene have been observed to show the respective melting points of the components. In addition, ethylene-propylene copolymers show the characteristic endothermic peaks for each of the moieties present. [55].

It has been reported that chemical composition of a polymer affects the transition temperatures from DTA trace [56]. A classical example of this is the replacement of one monomer partially or completely in saturated polyesters which resulted in changes in thermograms. The compositional changes alters the spatial relationship or the intermolecular forces in the polymer. Also, the effect of thermal and/or mechanical history of a polymer can be detected by DTA, since crystallinity of a polymer can be largely controlled by these treatments.

The main interest in the thermal analysis of the PETP as stated in section 2.1 is to identify the transition temperatures (eg T_g, T_c, and T_m) in order to determine the thermoforming processing window. The DSC technique was used.

In the thermoforming of crystallizable polymers, like PETP, it is essential to avoid over heating, to prevent excessive sagging, yet avoid also the induction of crystallinity which will inhibit the deformation of the polymer. In addition, the temperature of the sheet must be above the T_g to enhance chain mobility during deformation. In other words, the operating window should be within the rubbery region of the material. This is determined from the thermal analysis.

2.4.1 Experimental

A Du Pont 990 Thermal Analyser with DSC cell was used. The test conditions were as follows:

Sample weight	12 mg
Sample atmosphere	N_2
Gas flow rate (N_2)	60 ml/min
Temperature range of test	20 - 280 °C
Temperature scanning rate	20°C/min
Sensitivity (Highest)	2 mV/cm

An empty aluminium pan was used as reference sample.

2.4.2 Result and Discussion

The transitions temperatures determined from the thermogram fig 2.7 are shown in table 2.2.

PETP Sheet Transitions	Temperature
Glass Transition Temperature (T_g)	70 °C
Crystallization Temperature range	130 - 180 °C
Max. Crystallization Temperature T_c	160 °C
Melting Temperature T_m	250 °C

Table 2.3 Transition temperature of PETP sheet

There is a difference in the thermogram obtained in this work and that obtained by Ke [55]. He worked on 'Mylar' PETP which is crystallized (by strain and probably also 'heat-set'). Whereas, the sheet used in this work was amorphous and unoriented. Ke (55) obtained four transitions; the glass transition, 'cold' crystallization, pre-melt crystallization and melting temperature. In this work, three transitions were observed as shown in Fig 2.6. The difference in structure of two PETP samples is responsible for the difference in thermogram. However, similar T_g values were observed - 70 °C but a higher melting temperature 262 °C was reported by Ke [55].

From the transition temperatures of the PETP sheet, the thermoforming region can be determined. In order to enhance chain mobility and reduce the possibility of inducing crystallinity, the thermoforming range must be between the glass transition temperature T_g and the lower point of the crystallization temperature range. Therefore, the thermoforming window for amorphous PETP sheet supplied is between 70-130 °C.

However, it should be realised that the result were obtained at one heating rate. Variation of the heating rate may increase or decrease the value of the transitions.The transition values determined were used only as a guide to determine forming temperature range of PETP.

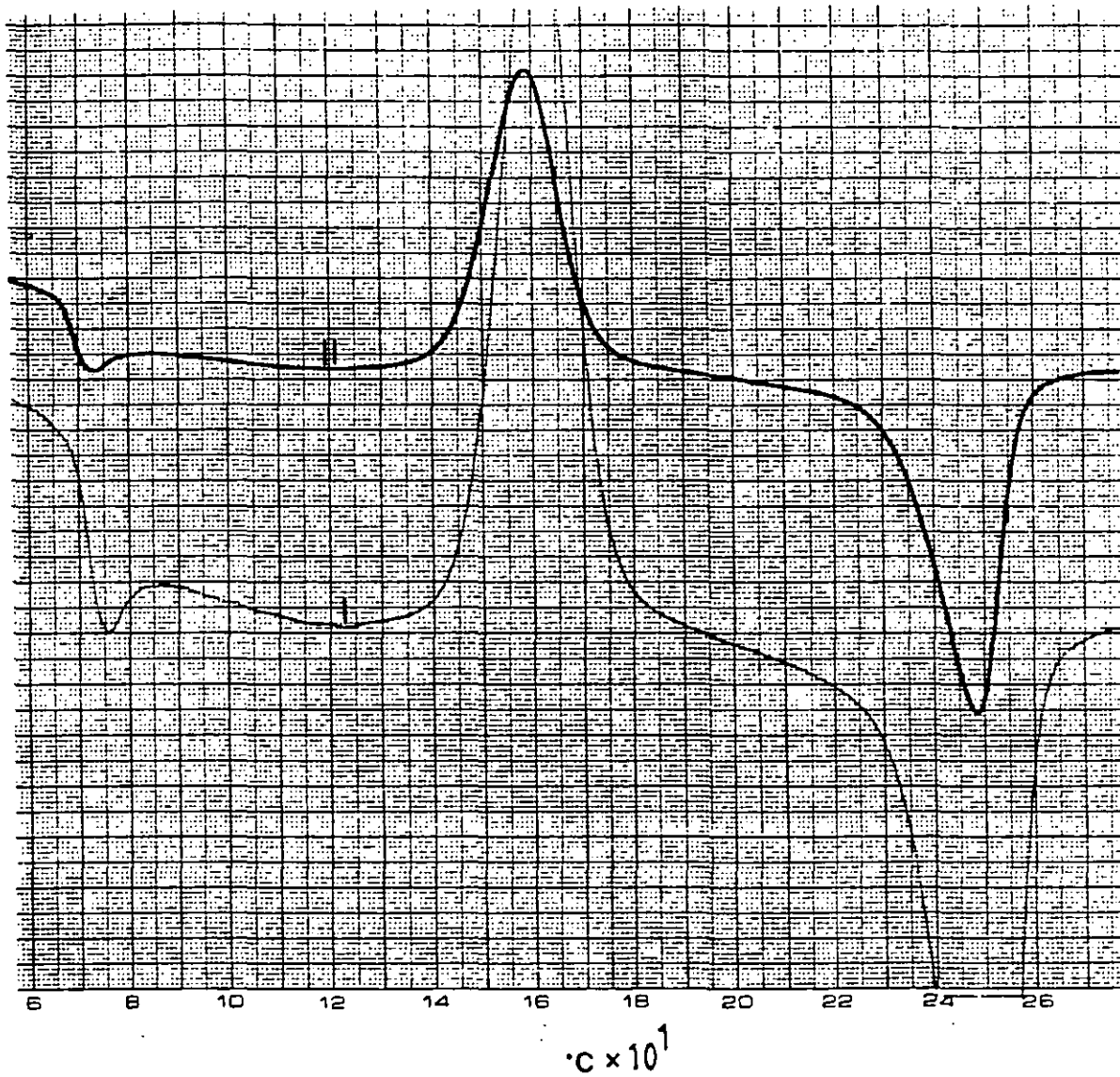

Figure 2.7 *Thermogram of Amorphous PETP*
Curve I sensitivity = 2mV/cm
Curve II sensitivity = 5mV/cm

2.5 Conclusions - characterization

The characterization techniques chosen gave the chemical composition, molecular weight and thermal transitions of the PETP sheet used in this work.

Infra-red spectroscopy analysis confirmed that the sheet supplied by I.C.I Ltd is homopolymer PETP.

Intrinsic viscosity value of the PETP sheet is 0.71 dl/g which corresponds to 4.73 x 10^4g/mol weight average molecular weight (M_w). The low I.V suggests a fast crystallizing PETP.

The processing window of operation determined by the DTA technique is between 70 - 130 °C (ie T_g to onset of crystallization). In order to enhance chain mobility during deformation and at the same time avoid inducing crystallinity, the thermoforming temperature is between 80 - 120 °C. The simulation test to predict performance of the PETP sheet and thermoforming operations were performed within the range specified.

Chapter 3

3 Physical Properties of Poly(ethylene-terephthalate)

3.1 Introduction

Various procedures for characterising the plastic sheet behaviour for thermoforming were discussed in Chapter 1, one of which is now adopted.

The use of melt flow properties is inappropriate for PETP, since it involves extrapolation to thermoforming temperatures where PETP will crystallize. Although it has been shown that uniaxial creep is analogous to the thermoforming process, the results do not define the material behaviour. The closest procedure to the thermoforming operation is biaxial deformation. However, this requires purpose-built equipment to carry out meaningful experiments. deVries et al [32] working with PVC have shown that biaxial and uniaxial deformation studies in terms of stress-stain relations give the same information about material behaviour and properties with respect to thermoforming. Malpass et al [28] have also shown that a uniaxial tensile test gives a good definition of material's behaviour. In addition to its simplicity, subsequent analysis is relatively easy. The uniaxial tensile procedure was therefore adopted in this programme to simulate thermoforming behaviour of PETP.

Apart from predicting thermoformability, the structural changes due to tensile drawing as a function of temperature strain rate and engineering strain were investigated using density, x-ray diffraction and birefringence measurements.

Before the drawing tests were made the effect of moisture absorption by amorphous PETP from its surrounding environment was investigated. This became necessary because in the preliminary tensile tests; it was realised that the tensile properties varied according to the prevailing humidity conditions. The investigation had implications for storing PETP sheet before processing.

3.2 Measurement of Moisture uptake by Amorphous PETP sheet

3.2.1 Introduction

The effect of humidity on polymer deterioration is well recognised. Also, the propensity of polymers containing ester groups to undergo chain scission during processing by hydrolysis resulting in deterioration of polymer properties is well documented. However, it was somewhat surprising that the tensile properties of PETP are influenced by the prevailing laboratory relative humidity. This made it necessary to study the influence of relative humidity on the tensile properties because of the implications on the deformation behaviour during fabrication processes.

Extensive investigation of PETP degradation at the melting temperatures has been reported. Goodings [59] monitored thermal degradation in terms of acetaldehyde generation, changes in carboxyl end-group concentration, and inherent viscosity. Marshall and Todd [60] studied thermal and hydrolytic degradation of PETP on the melt : moisture was found to cause rapid hydrolytic degradation. Melt flow rate changes was used to determine hydrolytic degradation by PETP by Kelleher et al [61].

Zimmerman [62] studied hydrolytic degradation at lower temperatures (100°C) in relation to carboxyl end-group concentration. He found the reaction to be autocatalytic. The kinetics of degradation process of PETP melt have been reported [63 - 65]. Jabarin et al [63] found that thermooxidative degradation of PETP is an exothermic reaction. The rate of hydrolysis was studied by Mc Mahon [64] as a function of temperature, relative humidity, and film thickness. He determined the effects of hydrolysis at temperatures from 50 - 99°C and relative humidity conditions from 20 to 95% upon the electrical properties of PETP. Ito and Kobayashi [65] studied hydrolytic degradation in terms of changing dielectric constant. They found that water absorption causes increments in dielectric constant. They also found water to be absorbed physically, not chemically, in terms of activation energy calculations.

Surprisingly, there has been little research on the effect of moisture on the mechanical properties of amorphous PETP. The change in tensile strength with ageing time in PETP has been reported by Gardner et al [66]. They presented an empirical equation to predict the half-life in days as a function of humidity and temperature. Jabarin [67] very recently found that absorbed moisture leads to significant deterioration in physical properties of PETP (ie large decreases in T_g, T_C and birefringence).

The present investigation was undertaken in order to establish, for amorphous PETP sheet, the relationships among : exposure time, relative humidity and mechanical properties. Also, to determine exposure time, and storage condition for PETP sheet before thermoforming.

3.2.2 Experimental

Humidity conditioning was achieved by ageing samples in controlled temperature chambers (Desiccator), with relative humidities ranging from 20 to 76%. The humidity conditions were obtained from saturated solutions of sodium acetate, sodium chromate and potassium chromate at 20°C to maintain 76, 52, and 20% relative humidities respectively.

The thin sheet samples were vacuum dried at 60°C for five hours and the weight of each sample was measured before exposure to the various relative humidity storage conditions.

Percent moisture content (% weight gain) of PETP as a fraction of time (t) was determined as :

$$\% \text{ Weight gain } W_t = \frac{\text{Weight of moist sample - Weight of dry sample}}{\text{Weight of dry sample}} * 100 \quad \text{---------- 3.1}$$

The equilibrium moisture absorbed was determined at the times the weight gain is within ±0.001 of the mean values.

The diffusivity of the material in the direction normal to the surface is described by the Fickian equation [69] as :

$$D = \frac{\pi}{t}\left[\frac{h W_t}{4 W_m}\right]^2 = \pi\left[\frac{h \phi}{4 W_m}\right]^2 \quad \text{---------- 3.2}$$

where
- h = thickness of the material
- W_t = % weight gained at time (t)
- W_m = equilibrium weight gained
- ϕ = slope of the linear position of plot of W_t vs $t^{1/2}$
- D = Diffusion Coefficient

Mechanical properties in tension were determined with J.J Extensometer at 80°C with a cross head speed of 300 mm/min on equilibrated samples at each relative humidity condition. The tensile samples were stamped from the roll of 1mm thickness PETP sheet according to B.S.2782.Part 3 method 302A (gauge length = 20mm). At least three samples were tested at each condition.

3.2.3 Results and Discussion

The moisture absorption of amorphous PETP sheet stored/aged at various relative humidity conditions is presented as a function of square root of time (min) in Fig 3.1. The results show that moisture diffusion through amorphous PETP is Fickian at least at the initial stages. The diffusion coefficient determined from equation 3.2 is $6.31 \times 10^{-5} \pm 0.25$ (mm^2/min) which shows that diffusion coefficient is independent of relative humidity (moisture concentration) as predicted by Fick's and Henry's law [68].

Also, the rate of diffusion increases with increasing relative humidity determined from the slope of the linear portion of the plot table (3.1). In diffusion through polymers, it is generally assumed that free volume is the controlling factor.

Relative Humidity (%)	76	52	20
Rate of Diffusion (Ø) x 10^{-3}(g/min $^{1/2}$)	10.70	8.9	3.91
Diffusion Coefficient (mm^2/min) x 10^{-5}	5.97	6.58	6.39

Table 3.1 Rate of Moisture Diffusion in PETP

The free volume (or holes) is not fixed in space because of thermal fluctuations; but on the average, with time and constant temperature the 'holes' are of definite size distribution [69]. Thus, the rate of diffusion depends on the concentration of the holes that are of sufficient size to receive the diffusing molecules. In PETP, the presence of carboxyl centres seems as point of attachment for the water molecules by Van der Waal forces. This increases the size of the 'holes' in the molecular structure. Therefore, the higher the moisture concentration, the greater the rate of absorption. This is analogous to ascribing the driving force to the ratio of the vapours pressure of the internal solution to that of the external pressure (ie osmotic pressure of the internal solution).

The equilibrium moisture uptake increases with increasing relative humidity as shown in Fig 3.2. This is in agreement with Henry's Law - below relative humidity of 75%, the ultimate amount of water uptake at the saturation point is roughly proportional to the relative humidity.[68]

In figs 3.3 and 3.4 are presented the effect of moisture uptake on yield stress and ultimate tensile strength of the PETP sheet. Both decrease with increasing relative humidity. Also, the elongation to break decreases with increasing relative humidity in Fig 3.5. The reduction in tensile properties with increasing relative humidity shows plasticisation by water.

There is a sharp drop in yield stress, ultimate strength, and elongation to break between 20 and 52 % R.H. The drop eases off towards 76 % R.H. This is because once the moisture absorbed is up to 60% of the uptimum uptake at equilibrium, the

tendency for increasing absorption decreases, with a similar effect on deterioration in mechanical properties.

The plasticization of the molecular chains suggests a physical phenomenon. A similar view has been reported by Ito and Koboyashi [65] in their tests on various polyesters. This leads to the determination of relative humidity storage condition for the PETP sheet. Since the prevailing relative humidity in the laboratory, monitored by a hygrometer varies about 50% R.H, the 52% relative humidity storage condition was chosen for the tensile test pieces. The equilibration time was 5 days. The conditions ensured consistent tensile response of the amorphous PETP sheet because the tendency to absorb moisture from the atmosphere is highly reduced. The sheets for thermoforming were kept in a constant relative humidity room (50% R.H) maintained at 20°C.

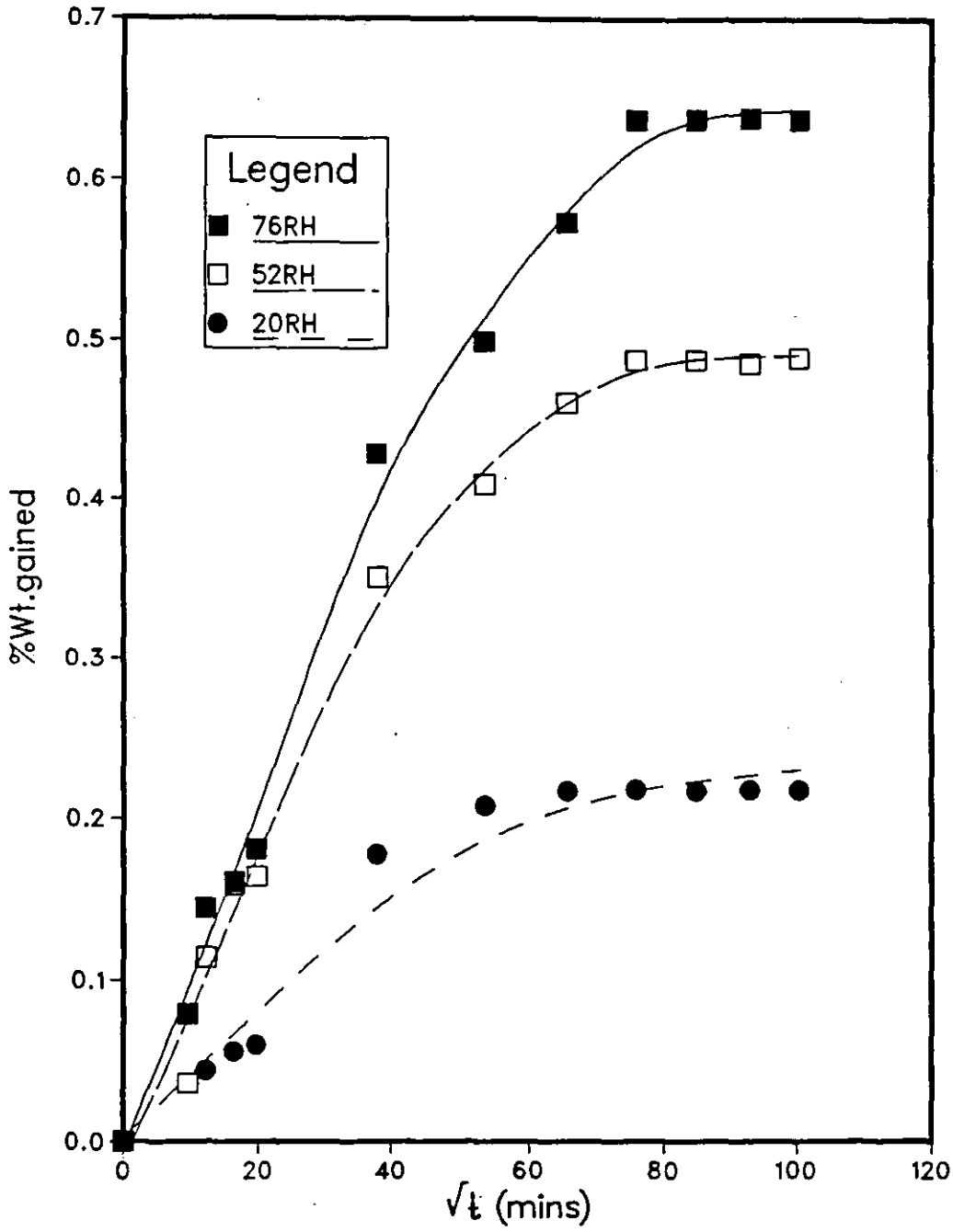

Figure 3.1 *Amount of water absorbed as a function of square root of time by PETP at different relative humidities. Initial straight lines indicate Fickian diffusion.*

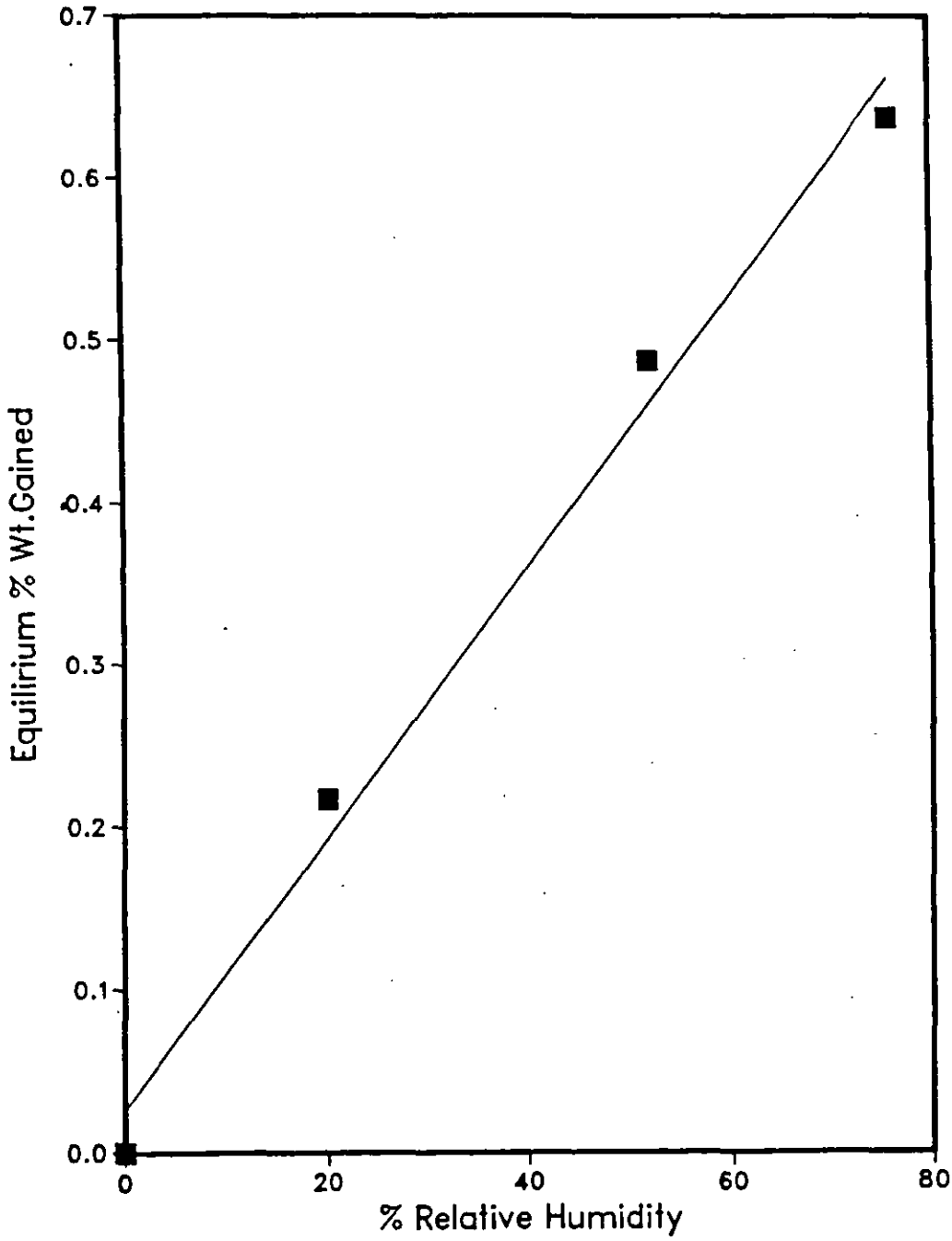

Figure 3.2 *Equilibrium moisture absorbed by PETP sheet at varying relative humidities.*

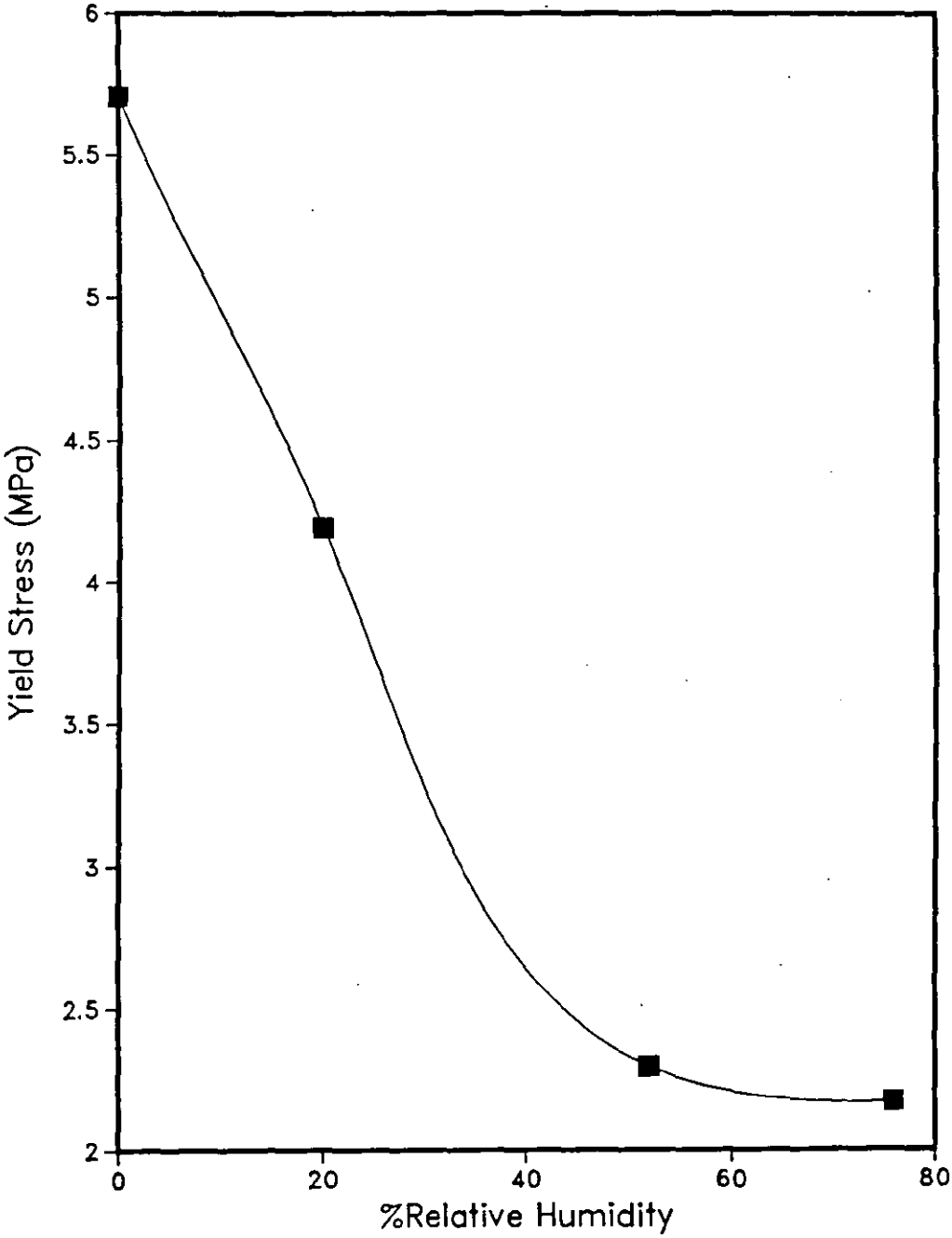

Figure 3.3 *Effect of amount of moisture absorbed on yield stress of PETP sheet*

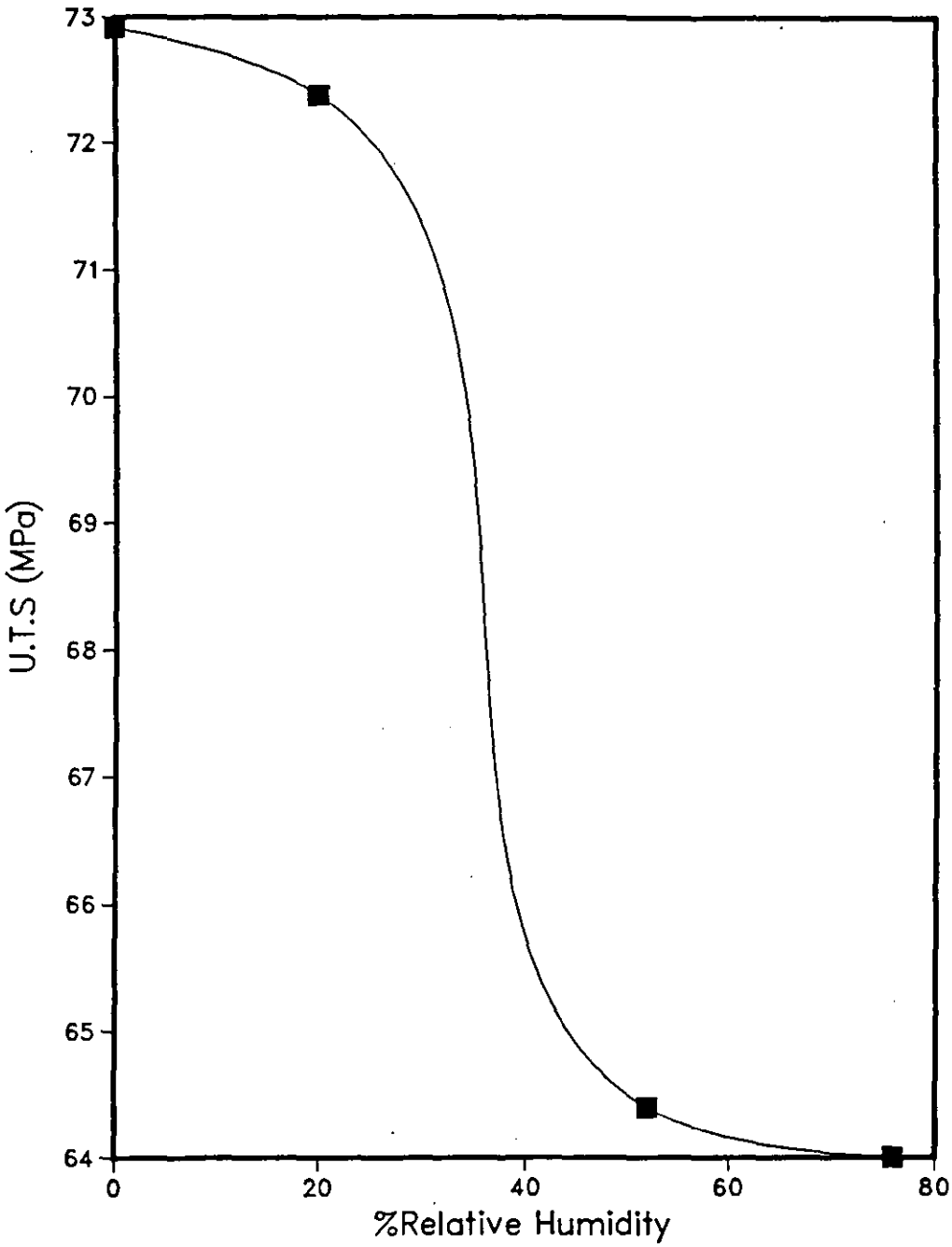

Figure 3.4 *Effect of amount of moisture absorbed on the ultimate tensile strength of PETP sheet*

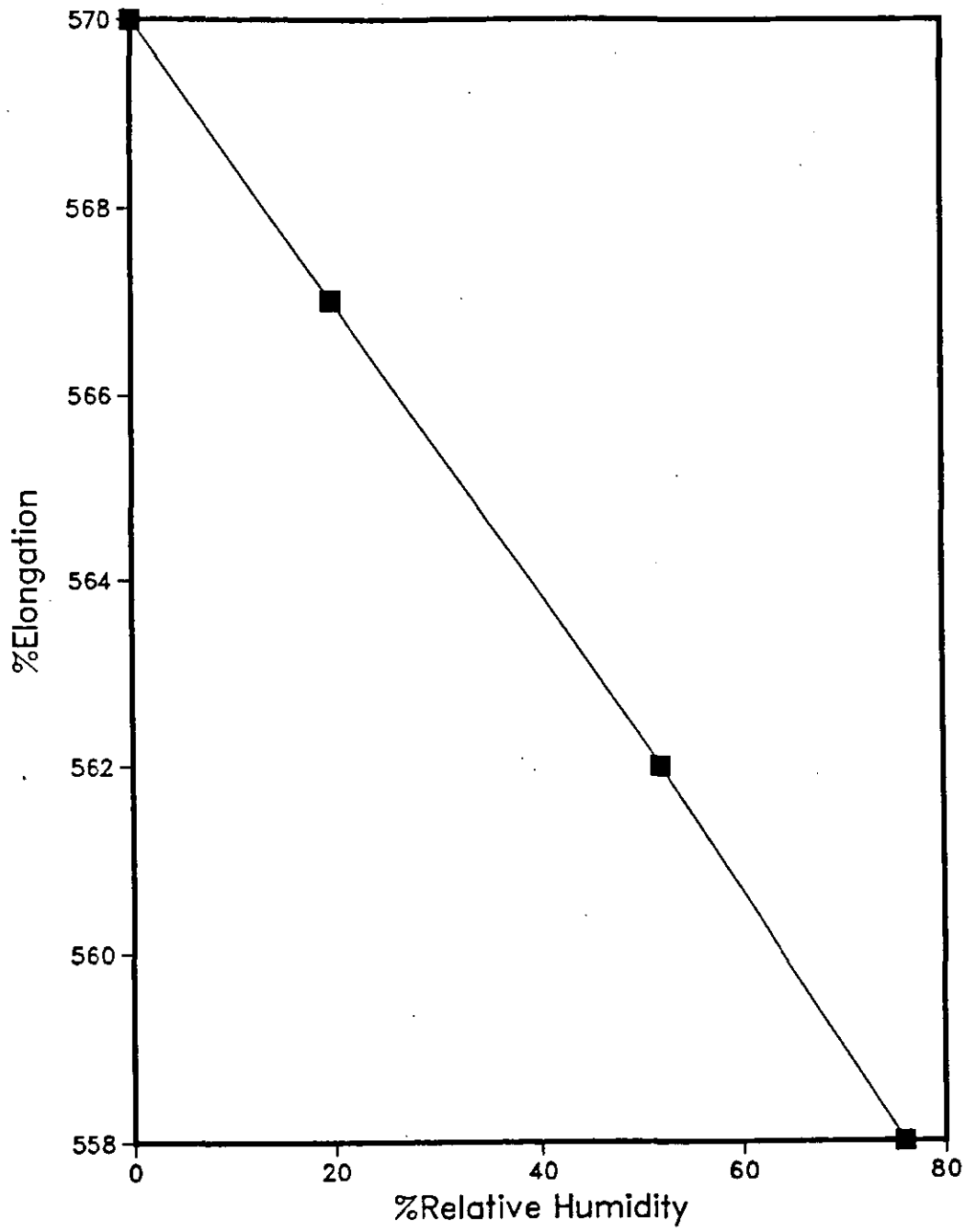

Figure 3.5 *Effect of amount of moisture absorbed on elongation to failure of PETP sheet*

3.2.4 Conclusions - Moisture uptake

Predried (amorphous) PETP sheet absorbs water from the surrounding atmosphere as a function of relative humidity and square root of time (Fickian).

The diffusion coefficient is independent of relative humidity.

Equilibrium moisture absorbed increases with increasing relative humidity (20 - 76 % R.H).

Absorbed moisture in PETP has a pronounced effect on mechanical properties. Consistent mechanical properties were obtained at 52% R.H storage condition.

3.3 Isothermal Uniaxial Tensile Testing

3.3.1 Introduction

Poly (ethylene-terephthalate) (PETP) is one of the most successful polymers commercially, particularly, in the forms of fibres and films. It has been studied extensively in connection with these applications. It has also attracted considerable attention from a more fundamental point of view because of its ability to exist in a variety of physical states.

In addition to the numerous investigations of the structure of unoriented PETP and of the tensile drawing behaviour, the structure of drawn PETP fibres and films below and above Tg have been studied using x-ray techniques [74-78], birefringence, [79, 80] infra-red absorption [81, 82] and microscopical techniques [81-83]

Marshall and Thompson [84] were early investigators of the tensile drawing behaviour of PETP. They analysed the continuous drawing process of filaments in terms of basic load/extension/temperature properties of the polymer. Their results showed that the filaments exhibit uniform deformation above T_g and necking below T_g. Similar results were obtained by Rietzh, Duckett and Ward [85]. Engelaere et al [86] studied the tensile drawing behaviour of PETP above T_g as a function of molecular weight and pre-orientation. They found that the formation of permanent physical network is very sensitive to molecular weight.

Oriented semi-crystalline polymers, such as poly (ethylene-terephthalate) consists of crystalline and amorphous regions distributed in various ways depending on the extent of strain and type of processing techniques used. This has been demonstrated by Heffelfinger and Schmidt [76] in their study of the contribution of amorphous regions to structural changes and how they influence the mechanical and thermal properties of oriented crystalline films. X-ray diffraction, infra-red, density and stress-strain measurements were used to obtain information on the amount and direction of orientation of both crystalline and amorphous regions of the films. A comprehensive study of characterization methods that distinguish between orientation distributions in both crystalline and amorphous regions in a polymer is given in ref 87.

Padibjo and Ward [88] also studied the structural changes in two stage drawing of PETP films, using similar techniques as above. The molecular orientation during drawing was discussed in terms of the deformation of a molecular network. Pinnock and Ward [89] showed that at temperatures above T_g, amorphous PETP fibres possess optical and mechanical properties similar to those of a rubber. X-ray studies have shown that amorphous PETP becomes crystalline when drawn, even at temperature below its nominal T_g [91 - 98]. The effects of draw ratio, temperature and strain rate on the orientation and crystallinity produced have been reported [92]. This is also the

subject of the investigation on PETP sheet in this report. Misra and Stein [93] established from light micrographs and x-ray diffraction patterns that at low elongations a rodlike superstructure exists that does not contribute to crystallinity and is oriented in the direction normal to stretching. At higher elongations the rods changed into spherulites which are elongated normal to stretching (Figs 3.6, 3.7). Similar studies were reported by Dulmage and Geddes [76] using birefringence, infra-red dichroism and x-ray diffraction. They found that at higher elongations, stretching induces linear orientation of chain molecules parallel to the direction of stretch. The orientation was enhanced by crystallization, owing to directional crystal growth on oriented crystal nuclei which develop during the stretching operation. Jabarin [95] reported recently that the degree of molecular orientation and the physical properties are strongly dependent on strain rate, extension ratio, molecular weight and stretch temperature.

However, most of the tensile drawing of amorphous PETP was carried out at low strain rates compared to the strain rates encountered in industrial processes. The primary interest in this work is the determination of the thermoforming region of amorphous PETP sheet from isothermal uniaxial tensile tests. These tests were conducted at strain rates which covered the range encountered in thermoforming operations (.08 - .42 s^{-1}). Also, the tensile draw behaviour was studied over a wider range of temperatures (80 - 110°C) relevant to thermoforming PETP. Most of the reports in the literature are limited to drawing at 80°C. In addition, the tensile drawing behaviour reported is not directed to any industrial process except recent reports; relation of uniaxial and biaxial drawing of PETP to bottle manufacture [96,97]. The relationship between preform temperature, stretching rate and physical properties was studied.

It is known that tensile behaviour of uniaxially orientated amorphous PETP becomes highly non-linear for relatively small strains. Linear visco-elastic theory is applicable for representing mechanical properties of polymers only within the range of small strains; thus it is of limited value in predicting behaviour of polymers under practical applications, like thermoforming.

The non-linear relationship between stress and strain occurs for two main reasons :

(i) Under most test conditions, relaxation of stress takes place continuously during the test ie short relaxation times.

(ii) Even in the absence of stress relaxation, the stress-strain curve at $T > T_g$ is non-linear, as is well known and can be predicted by the statistical theory of rubber-like elasticity.

This has been shown by T L Smith [100] working on polyisobutylene and SBR Vulcanisates (which can be considered "cross-linked molten plastics" at room

temperature) ie the true flow stress determined for tensile tests at constant strain rates is separable into a time and a strain effect. His theory was based on a generalized Maxwell model which is characterized by a stress relaxation spectrum and equilibrium modulus. He used a semi-empirical extension of linear visco-elastic theory to explain the large strain behaviour of elastomers as follows :

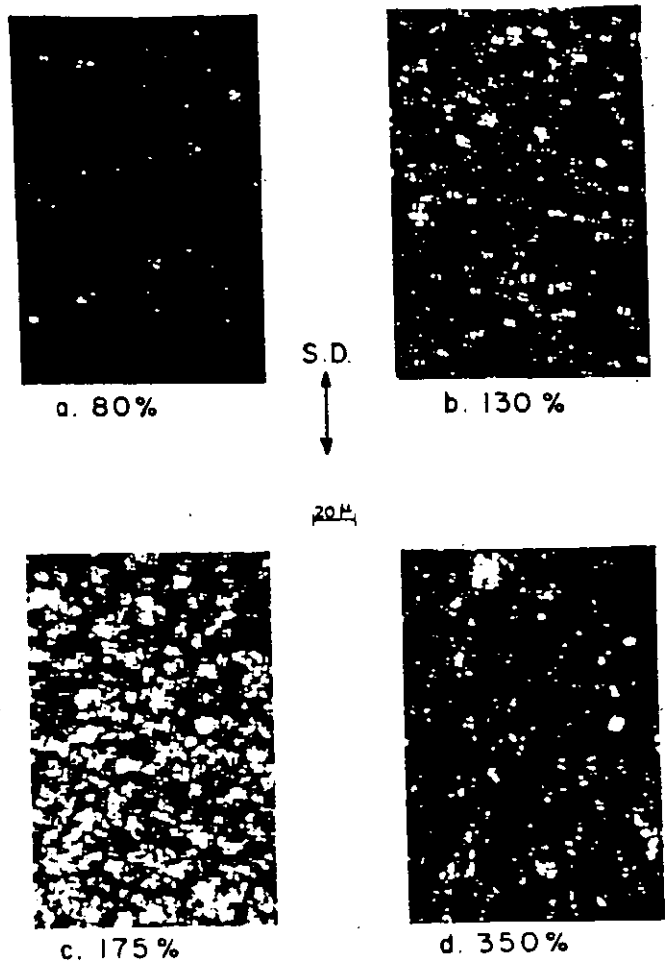

Figure 3.6 *Photomicrographs of PETP stretched at 80 oC between crossed polars.(a) 80 %; (b) 130 %; (c) 175 %; (d) 350 %.*

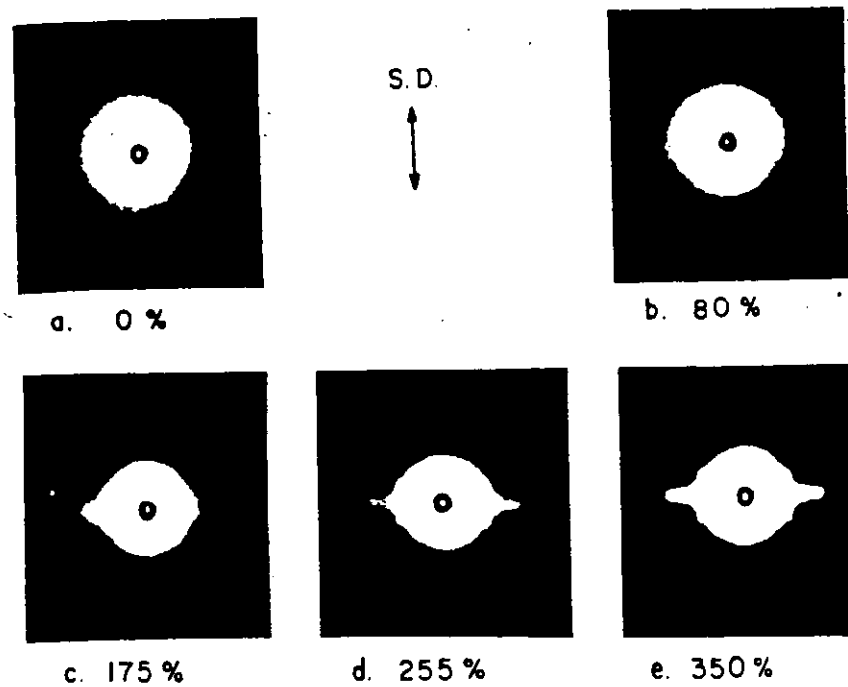

Figure 3.7 *Wide-angle diffraction patterns for PETP stretched at 80 °C (a) Amorphous PETP, 0 % (b) 80 %; (c) 175 %; (d) 255 %; (e) 250 %*

For continuous distribution of relaxation times

$$\sigma = R \int_{-\infty}^{\infty} \tau H(\tau) (1 - \exp -t/\tau) \, d \ln \tau \qquad \text{----------3.1}$$

For constant strain rate R, $R = \varepsilon/t$

$$\sigma / \varepsilon = 1/t \int_{-\infty}^{\infty} \tau H(\tau) (1 - \exp -t/\tau) \, d\ln \tau + E \qquad \text{----------3.2}$$

Where ε = strain

t = time

$H(\tau)$ = relaxation time distribution

E = equilibrium modulus.

The quantity

$$\sigma/\varepsilon = \sigma(\varepsilon,t)/\varepsilon \qquad \text{---------- (3.3)}$$

which is a function of time only termed "constant strain-rate modulus F (t)[69]. Smith [98] assumes that for large strains F(t) can be written as

$$F(t) = g(\varepsilon) \, \sigma(\varepsilon,t) / \varepsilon \qquad \text{----------3.4(a)}$$

$$\log F(t) = \log[g(\varepsilon) / \varepsilon] + \log \sigma(\varepsilon,t) \qquad \text{----------3.4(b)}$$

where g (ε) is a function of strain which approaches unity as strain approaches zero.

Also Meissner [101] working with a molten semi-crystalline branched polymer (LDPE at 150°C) found that the stress at different strain rates superpose at small times but separate at larger times with the separation increasing with strain rate Fig 3.8 [101]. The separation represents a non-linear effect (ie one which cannot be described by linear visco-elastic theory).

Lai and Holt [29,103] working along the lines developed by Smith [100] were able to show the stress-strain-time relationship at forming temperatures for some thermoformable plastics (ie PMMA and HIPS at 165 °C and 122 °C respectively). The relationship was correlated with sheet formability at these temperatures. It was found that the true-flow stress (σ) was related to true-strain (ε) and elapsed time (t) by a relation:

$$\sigma = K t^m \varepsilon^n \qquad \text{----------3.5}$$

where m = stress relaxation index

n = strain hardening index

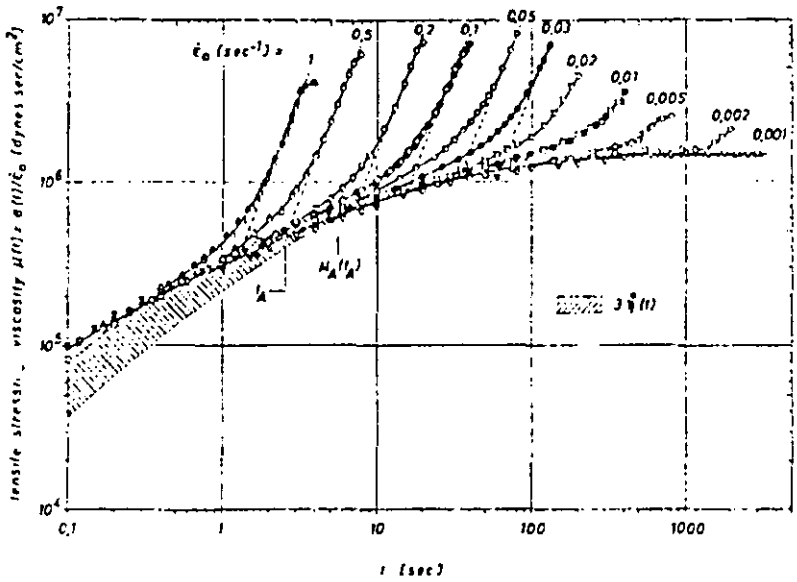

Figure 3.8 *Extensional stress viscosity and comparison with the (linear-viscoelasticity) shear stressing viscosity. Melt I, T =150°C, $\dot{\varepsilon}_o$ = constant*

They concluded that a large negative value of 'stress relaxation index' in a material reduces the degree of uniformity of sheet thickness in a formed part and a large value of 'strain hardening index' increases the degree of uniformity of sheet thickness in a formed part. This approach is of significant interest to the present work, and will be referred to in a subsequent section, when the effect of strain induced crystallization of PETP on the indices m and n will be discussed.

3.3.2 Experimental

3.3.2.1 Isothermal Uniaxial Tensile Test

The PETP sheet studied is as described in section 2.1. In addition, there is no preferred orientation in any direction in the sheet. Total extinction was observed when the sheet was placed between crossed polars at all angles between 0° and 90 °. This shows that any orientation in PETP induced during extrusion through a sheet die is quickly relaxed, before chill roll cooling (quenching) occurs.

Dumb-bell shaped samples were cut from the roll of PETP sheet according to B.S.2782 part 3 method 302A of gauge length 20 mm and 1 mm thickness.

The samples were vacuum dried at 60 °C for 5 hours before exposure to 52 % relative humidity storage condition for 5 days as explained earlier (Sec 3.2.2)

The test was carried out on a J.J Lloyd, tensile tester with extensometer and a thermostatically controlled conditioning chamber. Each sample was conditioned in the chamber for 10 minutes at the chosen temperature. The extensometer was fitted with two infra-red sensor follower heads. Strips of infra-red reflective tapes were used to mark the gauge points on each sample. In the 'follow' mode the infra-red follower heads lock on to the strips (ie gauge marks) and follow the gauge marks as the sample extends during deformation as shown in Fig 3.9 [104]. The crosshead movement and the load was registered on a conventional x - y recorder. The tests were conducted at strain rates ranging from $0.08s^{-1}$ to $0.42s^{-1}$ over a temperature range of 80 - 110 °C.

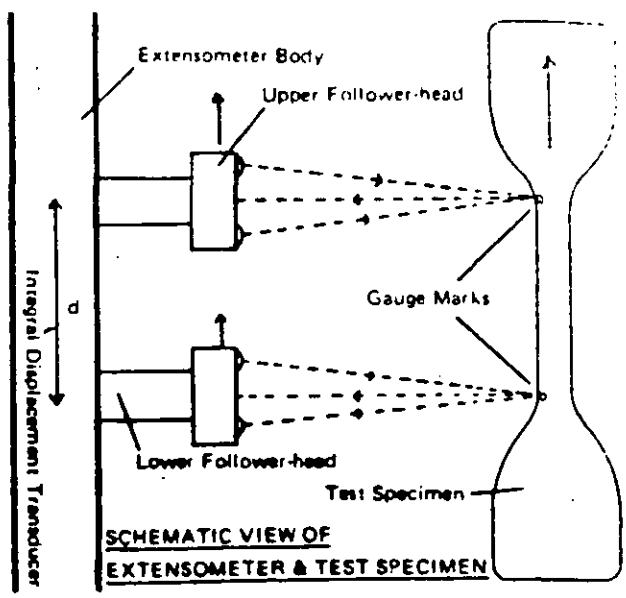

Figure 3.9 Schematic view of Extensometer and test specimen

The non-linear viscoelastic properties of PETP sheet at selected strain levels were determined. The nominal stress (σ) and strain (ε) are defined by:

$$\sigma = \frac{F}{A_o} \qquad \text{——————————} \quad 3.6$$

$$\varepsilon = (l - l_o)/l_o \qquad \text{----------} \quad 3.7$$

where A_o and l_o are the cross-sectional area and the gauge length of the undeformed sample; F and l are the force and length (respectively) of the same sample during deformation.

The true stress and true strain are estimated from the nominal stress (σ) and strain (ε) values

$$\sigma_t = F/A = [F/A_o]\,[l/l_o] = \sigma\,(1 + \varepsilon) \qquad \text{----------} \quad 3.8$$

$$\varepsilon_t = \int dl / l = \ln [l / l_o] = \ln (1 + \varepsilon) \qquad \text{----------} \quad 3.9$$

Where σ_t= true stress

ε_t = true strain

These relations are based on the assumptions of uniform deformation and constancy of volume of deformed samples. Also the time elapsed at each chosen strain for all strain rates was estimated from

$$t = \varepsilon / \dot{\varepsilon} \qquad \text{----------} \quad 3.10$$

Where ε is the selected strain

$\dot{\varepsilon}$ strain rate.

The large deformation behaviour of PETP sheet was related to thermoformability as a function of stretch temperature with the selected range relevant to PETP (80 - 110 °C).

3.3.2.2 Uniaxial Stress Relaxation test

Isothermal stress relaxation test in tension was performed. The tensile samples were prepared as described for uniaxial tensile test 3.2.2.1. Samples were deformed at 300 mm/min cross head speed ($0.25 s^{-1}$) to predetermined strain levels at temperatures 80 - 110 °C. On attaining the desired strain level, the deformation was stopped and the stress decay with time was monitored for only one hour because of influence of thermal induced crystallinity in PETP. The tests covered engineering strain 1 - 4 at each temperature chosen.

The stress decay was determined from Maxwell model:

At constant strain, the stress decay

$$\sigma_t / \sigma_o = \exp(-t/\tau) \qquad \text{----------3.11}$$

Where $\tau = \eta/E$ - the relaxation time

η = viscous constant

E = equilibrium modulus

t = time

σ_t = stress at time (t)

σ_o = initial stress at a predetermined strain

3.3.2.3 Density Measurement

The density of the samples at selected strain levels was measured at 23 °C in a gradient column from a mixture of carbon-tetrachloride and n-heptane calibrated by inserting glass beads of known densities. The samples chosen were those deformed at cross head speed of 500 mnm/min ($0.42 s^{-1}$) in the temperature range 80 - 110 °C.

The Density of unoriented samples exposed to the deformation temperatures for 10 minutes soaking time was also determined for reference purposes.

3.3.2.4 X-Ray Diffraction

Wide-angle x-ray diffraction patterns of drawn samples were taken, on Jeol x-ray Diffractometer, using CuKα radiation at 40 kV and 20 mA. The sample plate distance was 5 cm. All exposures were made with x-ray beam normal to the plane of the sample. The samples exposed were previously deformed at 80 °C to strain levels 1 - 5 at cross head speed of 500 mm/min or $0.42 s^{-1}$ (strain rate).

3.3.2.5 Birefringence Measurements

The usual method of measuring birefringence on a polarizing microscope with a compensator could not be used because of high dispersion effects (splitting of white light into the spectrum colours) which make it difficult to determine the extinction position. Instead, a spectrophotometric method proposed by Yang et al [106] was used; this technique has been shown to be efficient in determining high birefringence levels in polyester, and in aramid fibres. Also, it overcomes the problem of dispersion associated with the compensator method in highly oriented polymers.

The basic principle of the method is to measure the distribution of intensity versus wave length with a spectrophotometer and compute the optical retardation of the drawn sample. In this work, a U.V spectrophotometer was used.

A drawn sample was placed in a polarized light field in the sample chamber of the U.V spectrophotometer. The monochromatic light transmitted from the analyser is measured by a detector and compared with a reference beam, and the difference is recorded.

The phase difference is characterized by the optical path difference (OPD) in the equation

$$OPD = (n_{//} - n_{\perp})\, t = t\, \Delta n \qquad \text{----------3.12}$$

where t = thickness of sample

Δn = Birefringence

The phase difference $\Delta \varnothing$ for wavelength λ is

$$\Delta\varnothing = \frac{2\pi\, t\, \Delta n}{\lambda} \qquad \text{——————— 3.13}$$

$$\text{where } \frac{\Delta\varnothing}{2\pi} = m \qquad \text{---------- 3.14}$$

$$\text{and } m\lambda = t\Delta n \qquad \text{---------- 3.15}$$

The condition for constructive interference is met when m is an integer (ie m = 1, 2, 3 -). The value of m is chosen arbitrarily for successive light intensity peaks. The optical path difference was determined from a plot of m Vs $1/\lambda$. The thickness (t) was measured with a micrometer. The slope of the curve gives the optical path difference. At low wavelengths, dispersion distorts the location of the peaks and makes the curve non-linear. A typical calculation is shown in Figs 3.10 and 3.11.

Sample Preparation: The same sample preparation for tensile testing (section 3.2.2.1) was adopted, except that samples were deformed to pre-selected strain

levels. On attaining the desired strain level, the sample was quickly removed and quenched in cold water to prevent orientation and elastic recovery.

The degree of orientation was determined as a function of stretch temperature, strain, strain rate and deformation stress.

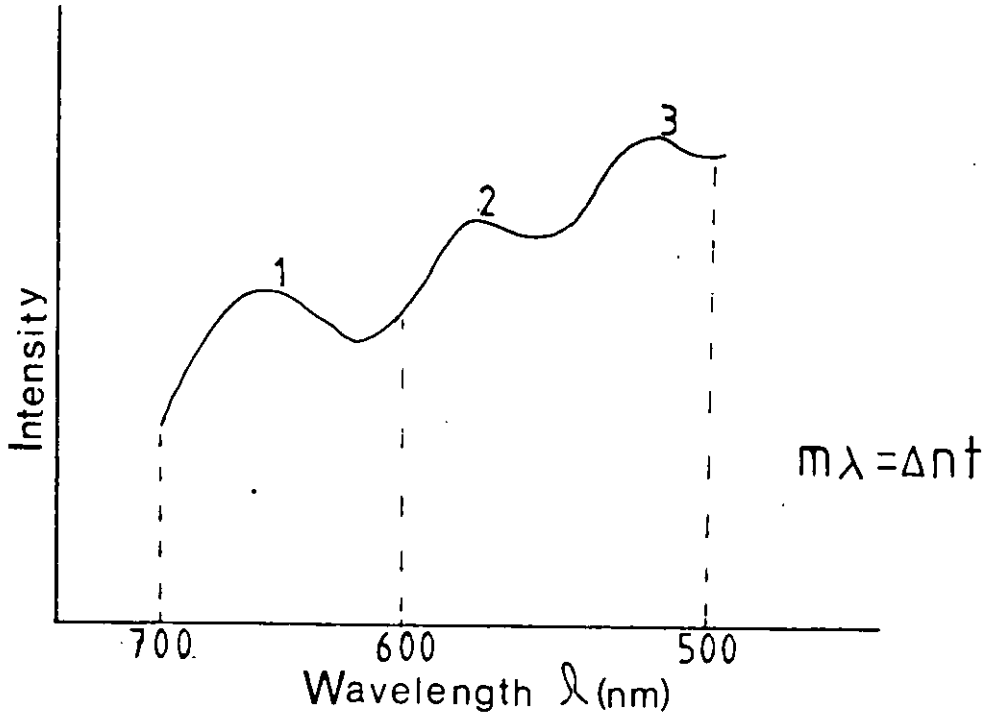

Figure 3.10 Intensity vs wavelength of light

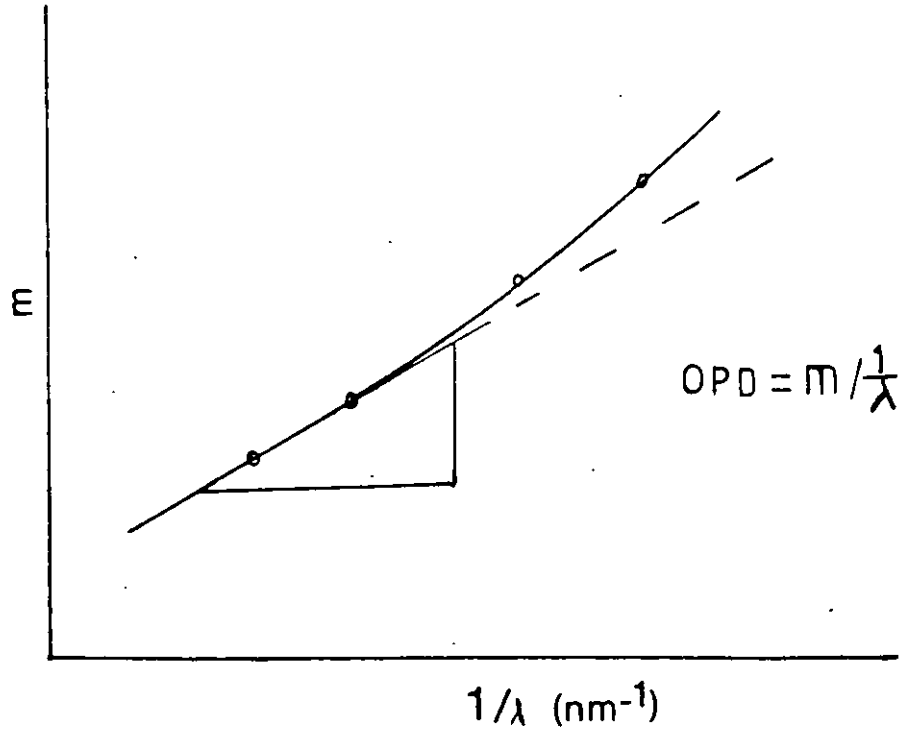

Figure 3.11 Number of each waveform (m) vs reciprocal of wavelength

3.3.3 Results and Discussion

3.3.3.1 Isothermal Uniaxial Tensile

Typical (nominal) stress-strain curves for temperatures between 80 - 110 °C are shown in Fig 3.12. The deformation is characterized by three regimes:

(i) yield (maximum load before drawing)

(ii) deformation at uniform stress (similar to natural draw) ε^N and

(iii) strain hardening

The sigmoidal shape of the stress-strain curve has been reported by others [84-88]. It is normally associated with rubber-like materials, and the reasons for the shape are well understood. [107].

Homogeneous deformation was observed throughout the tests. This has been reported and found to be consistent with the deformation of a molecular network in the rubbery state [85] at moderate strains ($< \varepsilon = 2$).

The 'natural draw' ε^N regime is characterized by a low stress which remains practically constant up to a critical strain whose value increases with increasing temperature. Similar observations have been noted by deVries [97]. This could be explained in terms of breakdown of a limited number of entanglement points beyond the yield. Increasing temperature enhances chain mobility and thus the 'extensibility' of molecular network.

The strain hardening regime is attributable to strain-induced crystallization in PETP. Although, crystallisation of isotropic PETP is negligible at temperatures the tests were conducted (< 120 °C) over short time scales, it has been established that limited crystallization does occur at lower temperatures in oriented polymers [108]. This can be explained in terms of finite extensibility of the molecular network which creates a condition in which the configurational entropy of the material is decreased by formation of extended-chain crystallites [85,92].

The rate dependence of the tensile properties is shown in Figs 3.13 - 3.15. Fig3.13 illustrates the dependence of yield stress on strain rate. The yield stress shows a small increase with increasing strain rate but decreases with temperature. Figs 3.14 and 3.15 show the rate dependence of ultimate properties. The tensile strength increases with increasing strain rate and decreasing temperature (Fig 3.14). However the elongation to failure unexpectedly increases with increasing strain rate and decreasing temperature (Fig 3.15). The rate dependence of ultimate properties has been reported in rubbery materials by others [109 - 111]. The ultimate properties vary with temperature because the internal viscosity varies with temperature.

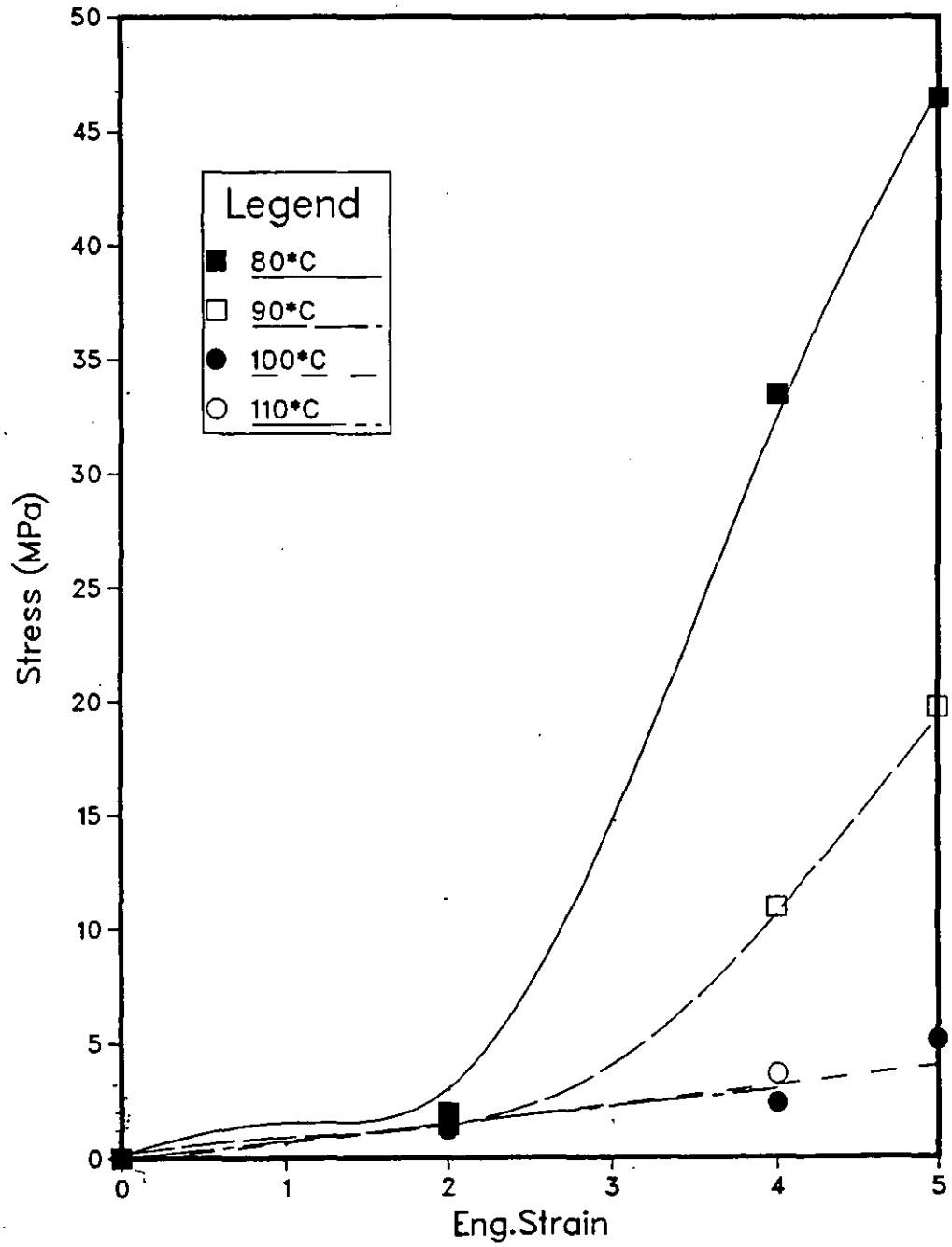

Figure 3.12 *Nominal stress-strain curve of PETP sheet at the thermoforming temperatures*

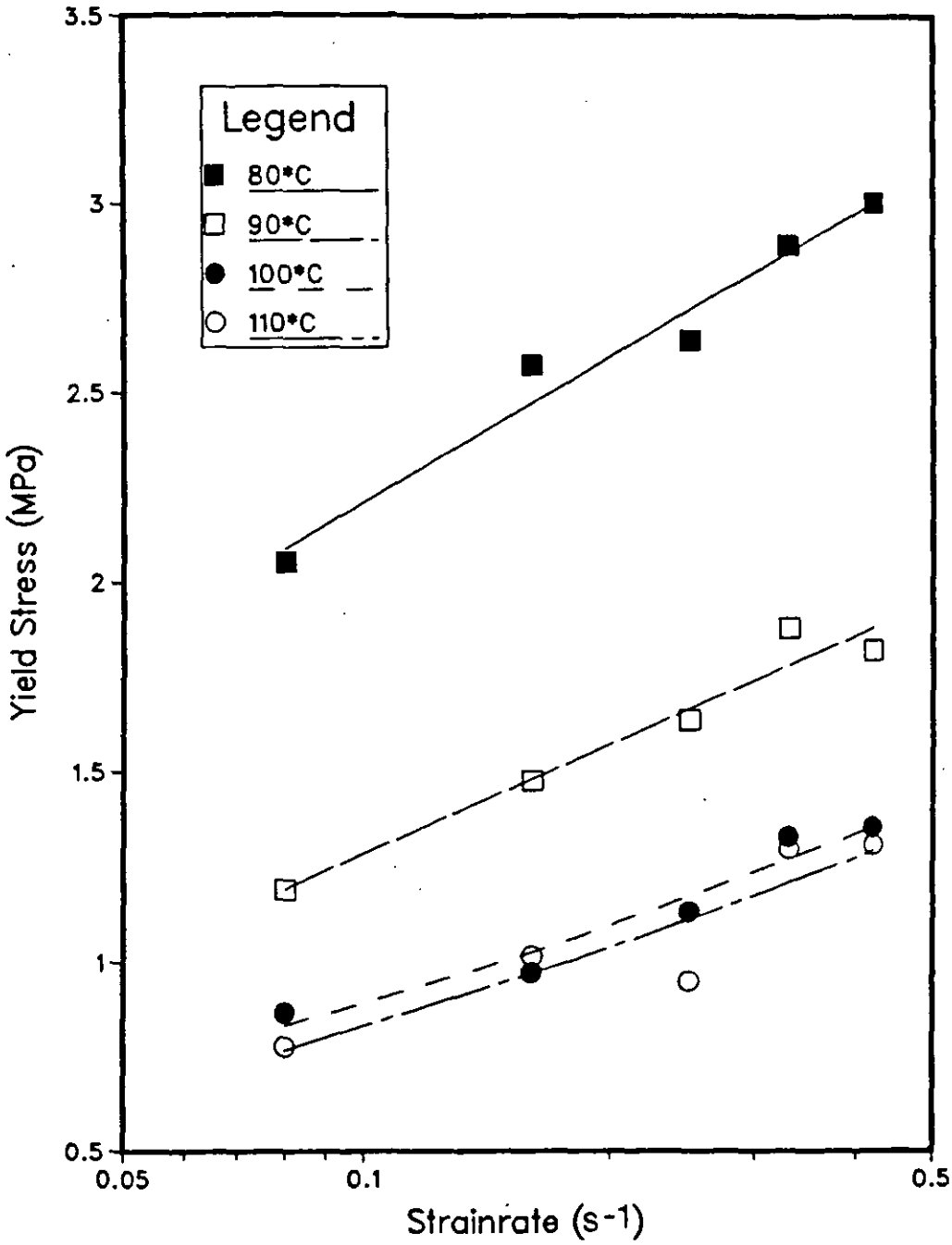

Figure 3.13 *Yield stress as a function of strainrate at the thermoforming temperatures*

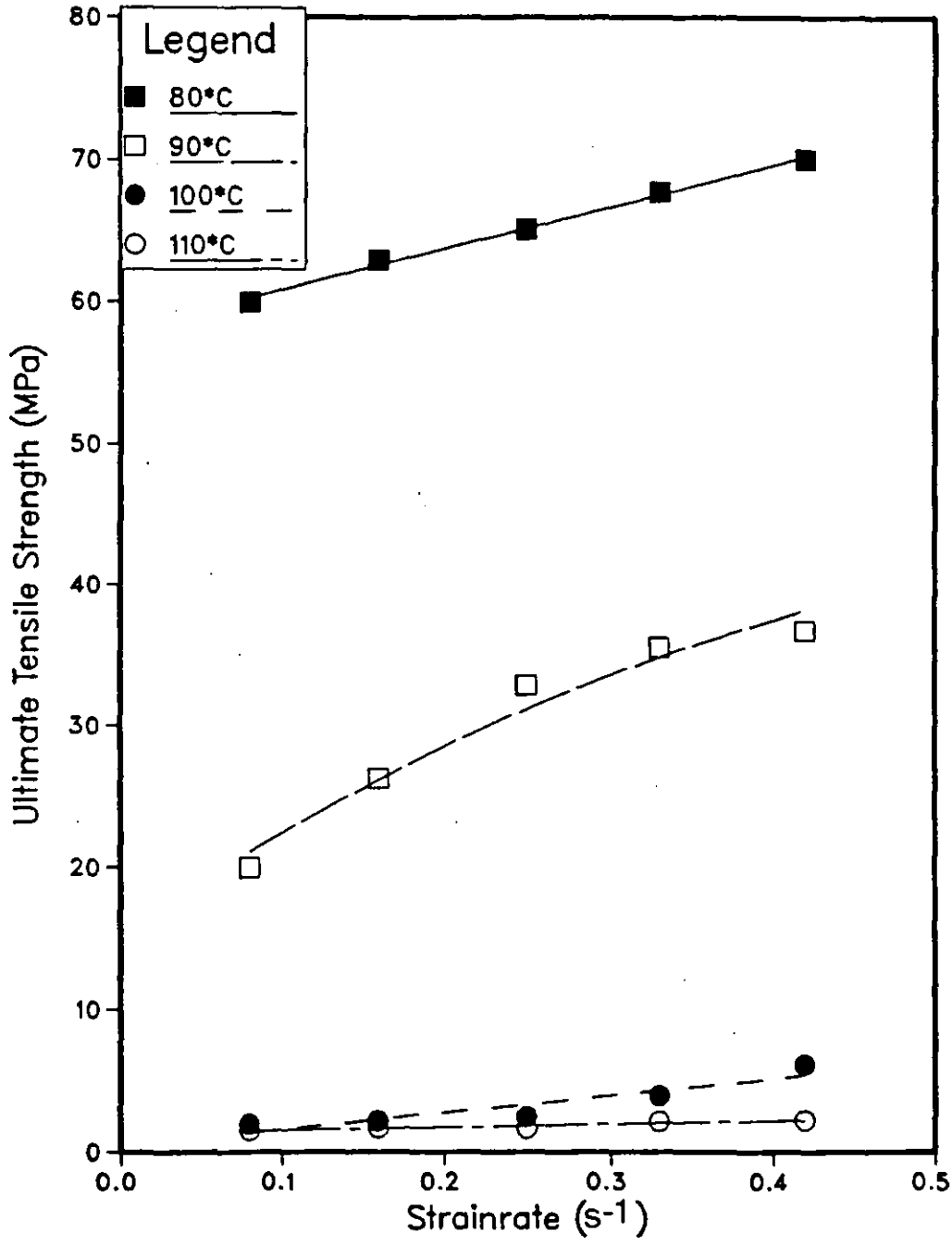

Figure 3.14 Ultimate Tensile strength as a function of strainrate at the thermoforming temperatures

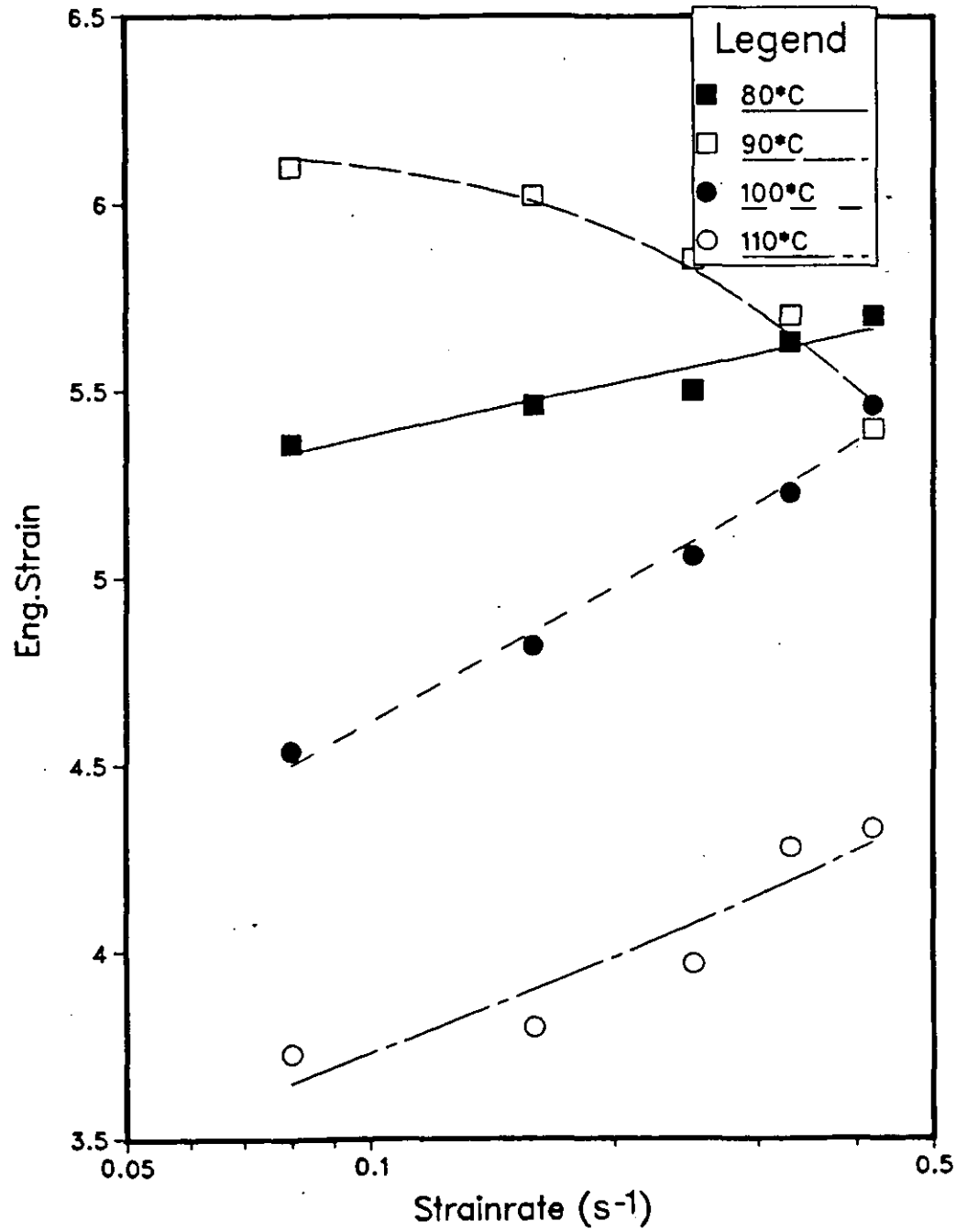

Figure 3.15 *Elongation to break as a function of strainrate at the thermoforming temperatures*

Increasing temperature enhances chain mobility and reduces chain relaxation time. This explains the decrease in ultimate strength with increasing temperature and also the lesser rate dependence of ultimate strength with increasing temperature.

For completely amorphous polymers above T_g, the rate dependence of ultimate strength could be explained in terms of increase in viscous resistance to network deformation with strain rate. In PETP, the increase in tensile strength with increasing strain rate is due to a combination of viscous resistance and strain induced crystallization. The crystallization process during deformation of PETP is enhanced by molecular alignment. The influence of heat build up at the high deformation rates employed has not been investigated. However, there is evidence in the literature [94, 111] of heat build up in PETP during deformation. The heat build up at the lower temperatures due to frictional effects promotes crystallite formation. The proportion of heat build up from mechanical slip decreases with increasing temperature.

Fig 3.15 illustrates the influence of strain rate on elongation to failure. At 80, 100 and 110 °C, the elongation to failure increases with strain rate unexpectedly. However at 90°C, the elongation to failure decreases with increasing strain rate. In addition, the greatest elongation to failure was recorded for each strain rate at 90 °C. The unexpected behaviour can be explained as follows: The elongation to failure increases with strain rate because the break down of network junctions is compensated with formation of crystallites which reinforces the chain segments. The deformation behaviour of PETP is influenced by two competing mechanisms; strain and thermally induced crystallisation. Thus at the lower temperatures, the strain effect dominates while as temperature increases the thermal effect gradually assumes greater importance. However, at 90 °C, the behaviour is that of typical rubbery plastics (ie the strain effect is reduced and the temperature is low for thermal effect to prevail). This could be explained in terms of relaxation processes taking place. The higher, the strain rate, the faster the chain relaxation process is overcome, thus the lower the elongation to failure.

In most typical amorphous plastics like ABS and PVC used in thermoforming, the forming region could be determined from stress-strain curves [26, 28]. This is usually in the uniform deformation region beyond yield in order to reduce the effect of stress and elastic recovery. Prior to yield, the deformation is purely elastic, beyond yield, it is visco-elastic where most forming takes place. While yield elongation in amorphous plastics could be in excess of engineering strain of 2, in PETP, it is less than 0.1; and the 'natural draw' ε^N is within engineering strain of 2. The bulk of PETP deformation is in the strain hardening regime. Therefore the criteria that hold for determining the forming region in amorphous plastics may not hold for a crystallizable polymer like PETP. The strain hardening exhibited makes prediction of formability from the stress-strain curve difficult. Strain hardening has been shown to enhance

formability in HIPS and PMMA [29, 103]. The limitation of nominal stress-strain behaviour in predicting large deformation behaviours has been shown (see 3.1). Therefore it is more appropriate to use the true stress - true strain relationship for interpreting the deformation mechanisms.

The true stress - true strain plots are shown in Fig 3.16 (a - d). The true stress and true strain were calculated according to equations 3.8 - 3.9. The curves are shifted for clarity by indicated value of A, because the deformation was strain-rate insensitive (ie the curves overlap). Over the strain range studied, (ε_t - 0.7 - 1.8) the extent of convex upward position of the curves decreases with increasing temperature.

The same data are replotted on logarithmic coordinates in Fig 3.17 (a - d). The curves are shifted by indicated values of A. The plots show a flat region in the ε^N regime and a linear relationship in the strain hardening regime. The linear portion (ie strain hardening regime) is replotted in Fig 3.18 (a - d). The true stress-time data are plotted on logarithmic coordinates in Fig 3.19 (a - d). The elapsed time was determined according to equation 3.10. The degree of scatter of points increases with increasing temperature.

From Fig 3.16 it seems that the strain hardening effect starts from true strain (ε_t) of 1.2 (or engineering strain of 2). This means sufficient molecular alignment has been generated at this strain level for crystallite formation which reinforces the system, thus the marked rise in stress with strain especially at the lower temperatures. It has been shown by Smith and Steward [108] that molecular alignment speeds up the rate of crystallization in oriented PETP. Therefore attainment of critical engineering strain level of 2 is needed to generate the strain hardening effect in PETP at the thermoforming temperatures.

From the true stress-strain curve Fig 3.18 an empirical model of the form

$$\sigma_t = K (\varepsilon_t)^n \qquad \text{3.15 (a)}$$

or

$$\log \sigma_t = \log K + n \log \varepsilon_t \qquad \text{3.15 (b)}$$

where σ_t = true stress

ε_t = true strain

K = constant

n = strain hardening index

describes the strain hardening behaviour of PETP. The strain hardening index 'n' and the K values are given in table 3.2. The K value is related to the yield stress/stiffness, since it is the deformation stress at the 'natural' draw' regime. The strain hardening indices are strain rate independent but temperature dependent. Also the

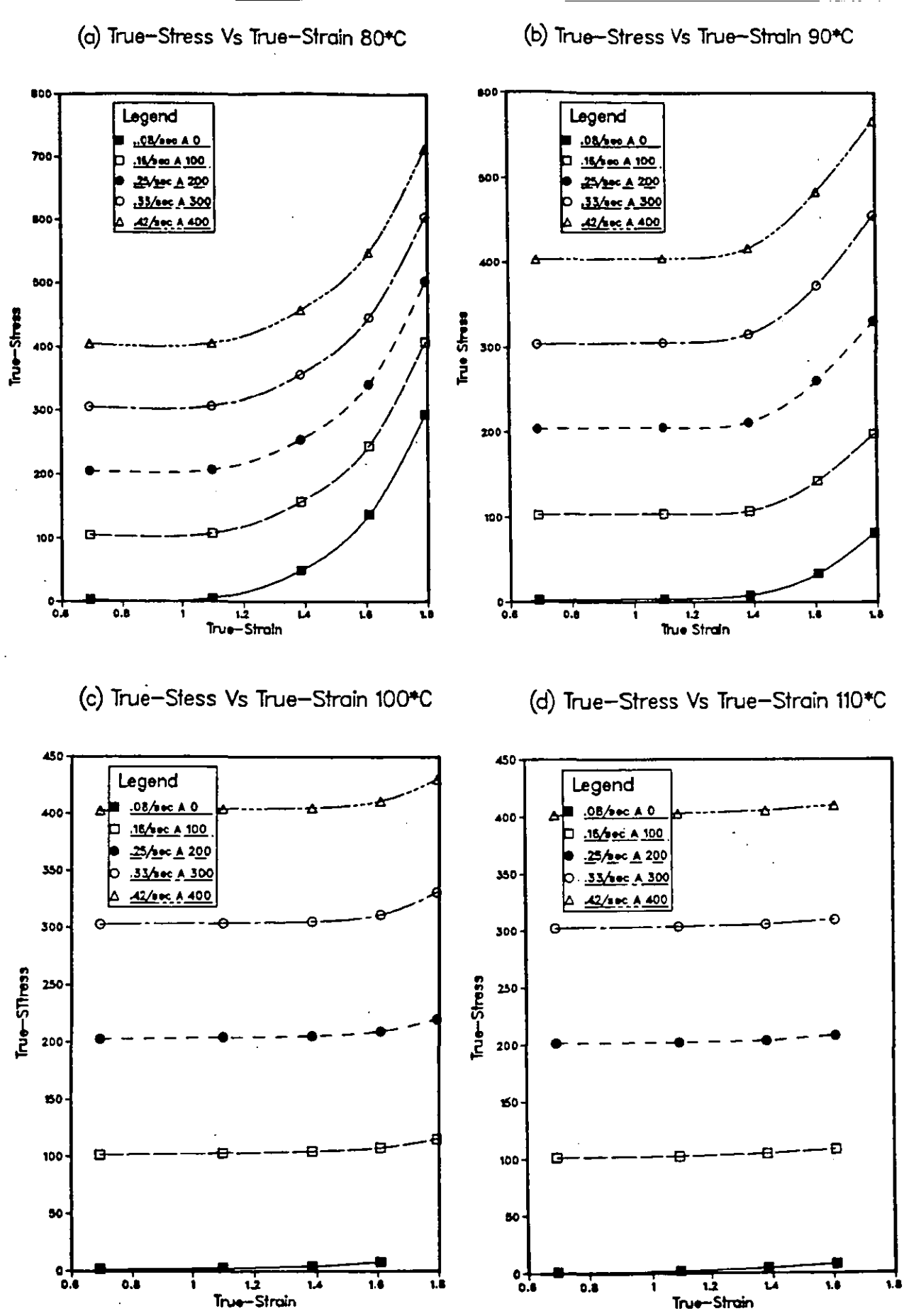

Figure 3.16 True stress-strain relationship of PETP at strainrates between 0.08 and 0.42 s^{-1}

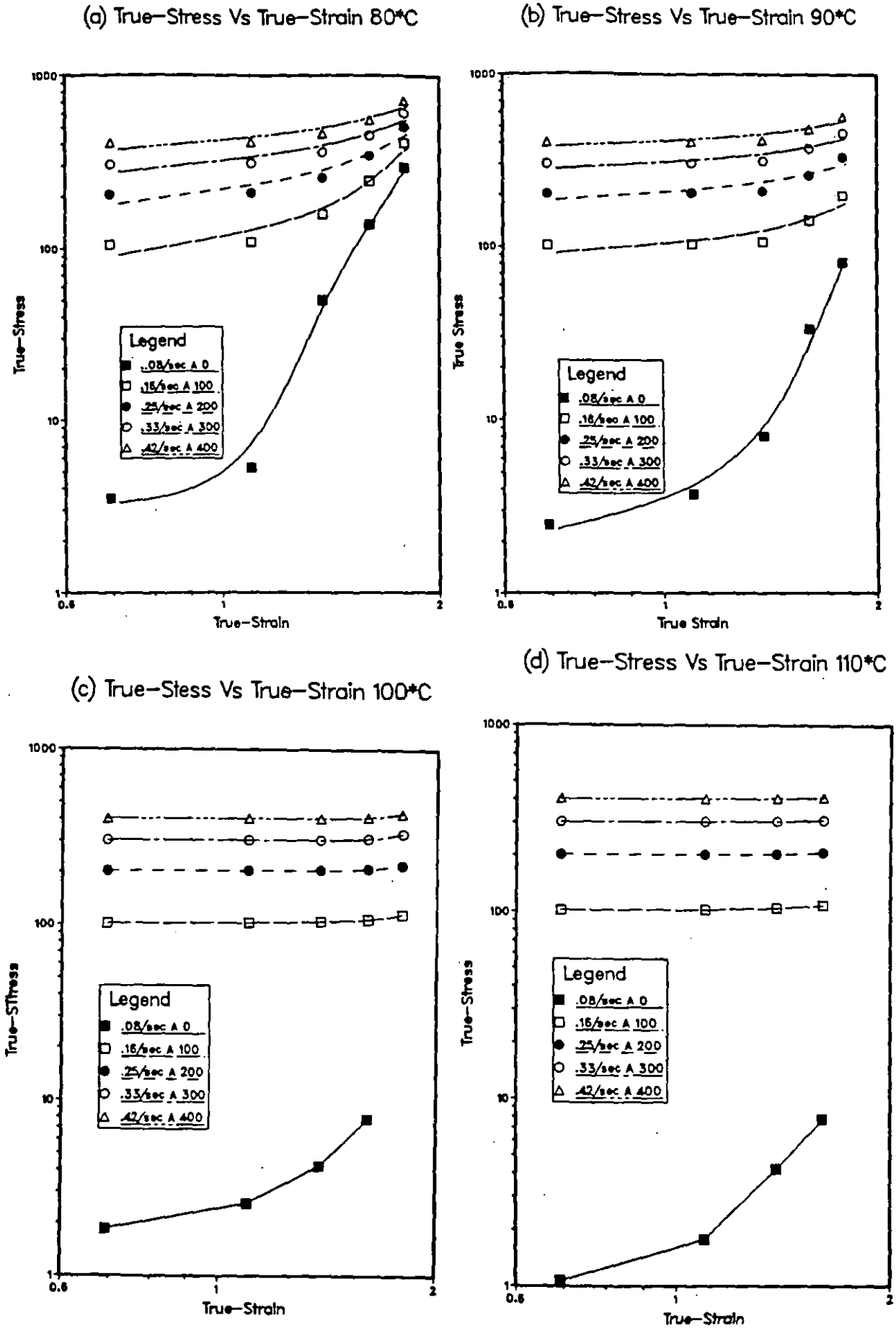

Figure 3.17 *Logarithmic True stress-strain relationship of PETP at strainrates between 0.08 and 0.42 s^{-1}*

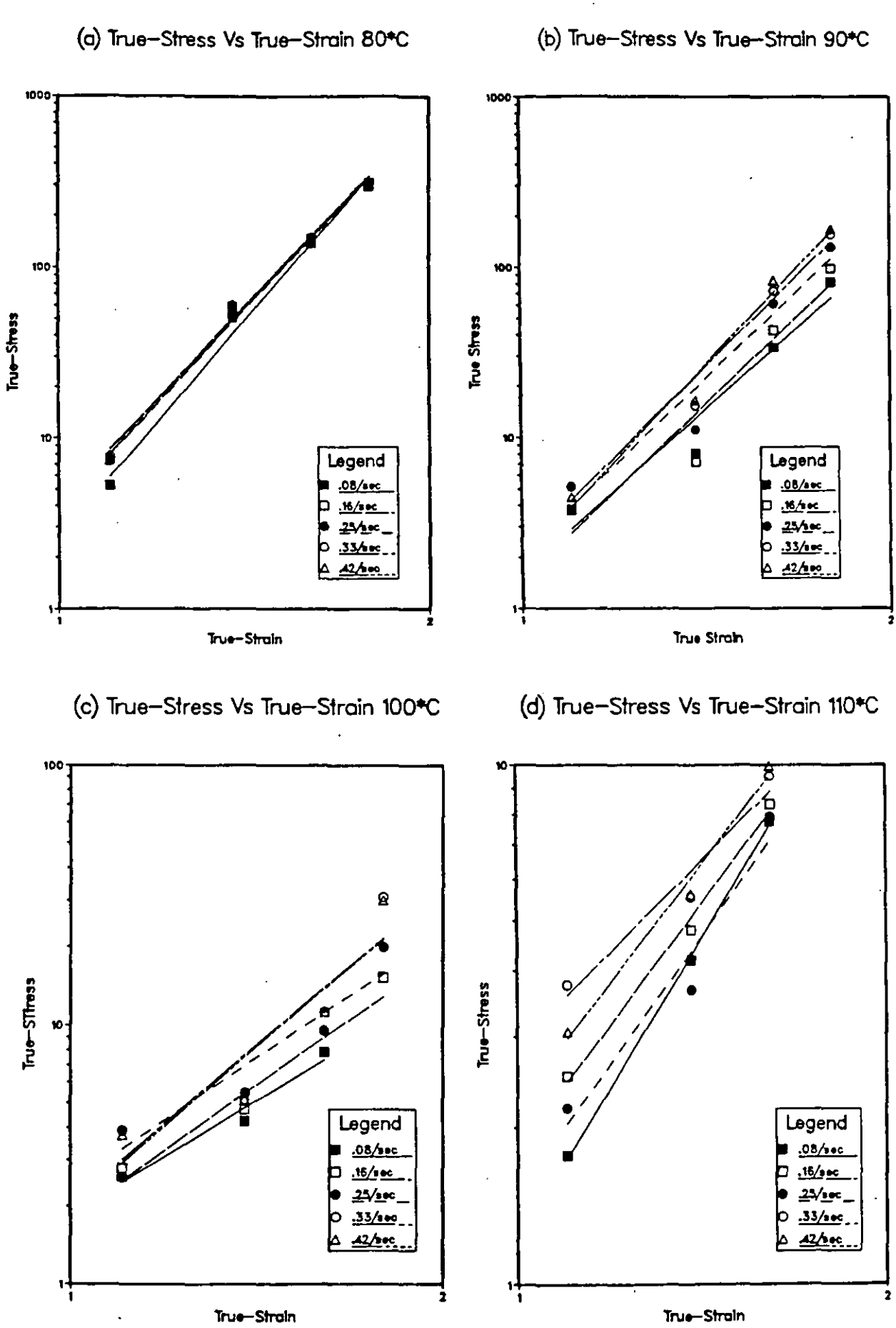

Figure 3.18 Logarithmic True stress-strain relationship in the strain hardening regime

K values are strain rate and temperature independent except at 80 °C where the sheet exhibits high stiffness. The insensitivity to strain rate, of K is similar to the yield stress behaviour shown in Fig 3.13. A similar strain-hardening equation [112] $\sigma = \sigma_o \varepsilon^m$ (where σ and ε are the true stress and the true strain respectively, and σ_o and m are constants) has been used to express plastic deformation behaviour of ductile metals. Budiansky and Wang [114] assumed the same relationship to hold for polymers. Warshavsky and Tokita [115] later pointed out that the equation is not valid for polymeric materials. This was supported by Bahadhar [116] who proposed that strainhardening equation of the form $\sigma = \sigma_o \exp m\varepsilon$ (where σ_o and m are constants) describe the large deformation behaviour of polymers.

Temperature °C	K	n
80	0.57	7.69
90	0.26	6.95
100	0.32	3.32
110	0.26	3.14

Table 3.2 *Strain hardening indices 'n' and Kvalues for PETP at the thermoforming temperatures*

All the above reports were on plastics at room temperature.Takayanagi et al [117]working at elevated temperatures on crystalline polymers found that,

$$\log(\sigma/\sigma^*) \log(\varepsilon/\varepsilon^*) = -C$$

(where σ^* and ε^* are shift parameters and C is a constant) describes the large deformation of crystalline polymers. C is a measure of deviation of deformation of polymers from the idealized system. The model was not related to any fabrication process. Also, they reported uniform deformation in nylon 6.

The main interest in this work is to relate the model to formability of PETP sheet. The strain hardening equation is only valid for the strain hardening regime of the stress-strain curve. It does not cover the entire deformation process:The strain hardening index (Table 3.2) increases with decrease in sheet temperature. The strain hardening indices varied from 7.7 at 80 °C to 3.1 at 110 °C compared to 1 and 1.1 obtained for PMMA and HIPS [103] respectively. The higher strain hardening indices recorded for PETP are due to influence of strain induced crystallinity. Whereas, in amorphous polymers, strain hardening effect is mainly due to attainment of a highly ordered state as opposed to crystalline texture in strain crystallizable polymers. Since strain hardening has been shown to promote thickness uniformity in formed parts [103],

it is proposed that a high strain hardening index 'n' ensures thickness uniformity in parts. This implies that formings at 100 and 110 °C with 3.3 and 3.1 'n' values respectively are less desirable than formings at 80 and 90 °C, with 7.7 and 7.0 'n' values (respectively) which will produce formings of even thickness. Further more, at each temperature, for even thickness in formings the draw ratio should exceed the 'natural draw' ε^N values. This has been shown to be true in stretch blown PETP bottles [96]. Between 90-110 °C where the chain mobility is enhanced, the K values are the same within experimental error. This shows that the stiffness within the rubbery region can be regarded as uniform (ie temperature insensitive below crystallization temperature but above T_g) for PETP. The higher K value recorded at 80 °C shows that the chain mobility is not fully enhanced at this temperature. Thus, it is suspected that vacuum forming at this temperature may result in formings of uniform thickness but the mould may be incompletely filled because of higher stress required.

The logarithmic plot of true stress and time (fig 3.19) is intended to show the influence of continuous stress relaxation during deformation. An empirical relation of the form

$$\sigma_t = b\, t^{m} \qquad \text{---------- 3.16}$$

where m = stress relaxation index
b = constant

fits the plot. The values of stress relaxation index 'm' and b (constant) are presented in table 3.3. 'm' and b vary with strain and temperature. b is related to the stress at each strain level. It decreases with increasing temperature at equivalent strain level as expected. However, the stress relaxation indices 'm' at strain 1 and 2 are virtually the same within experimental error at all the temperatures except at 110 °C. This is the regime within the 'natural draw' ε^N. This is not surprising, since, the deformation in this region is rubber-elastic. The slight deviation at 110 °C could be attributed to thermal induced crystallization which inhibits chain relaxation. However, at the strain hardening regime (ie ε 3 – 5) there is a marked change in stress relaxation indices. At 80 °C, where there is considerable influence of strain hardening, there is drastic reduction in chain relaxation, thus the low 'm' values. The highest stress relaxation indices 'm' are recorded at 90 °C. This shows that greater relaxation process takes place at this temperature. This supports the contention that PETP behaviour at 90 °C is similar to that of typical rubbery plastics. This fact is further investigated in the stress relaxation test at constant deformation (next section). In PETP, the stress relaxation indices cannot alone be used to determine thickness variation in formings because of complications introduced by strain hardening mechanism.

(a) True–Stress Vs Elapsed Time 80 C

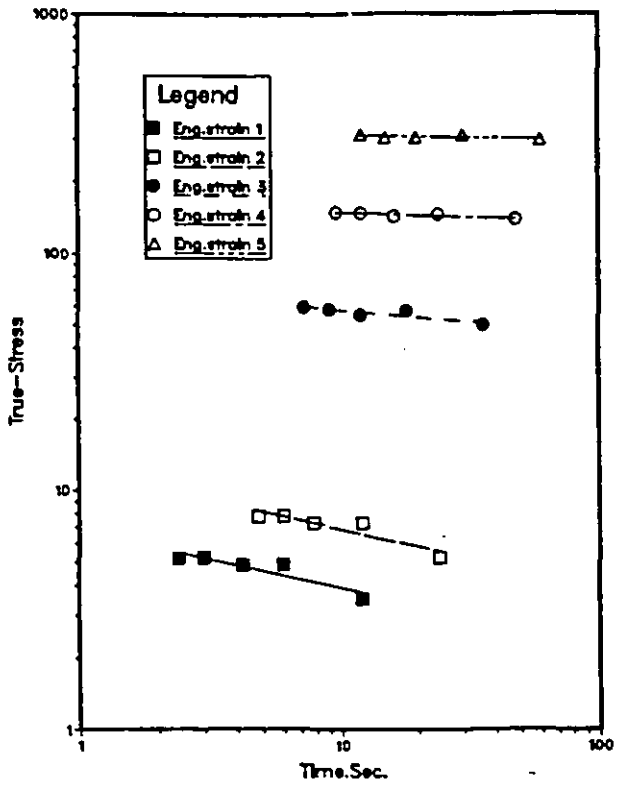

(b) True–Stress Vs Elapsed Time 90 C

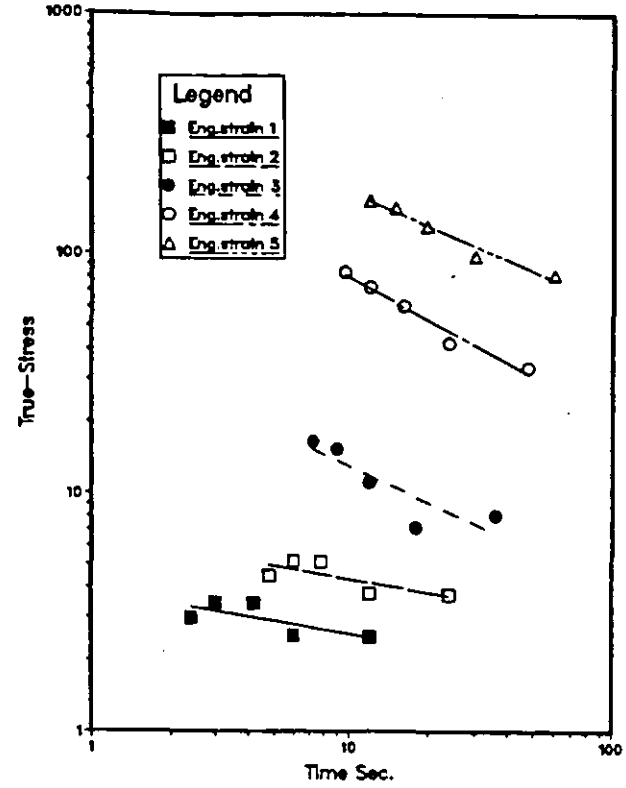

(c) True–Stress Vs Elapsed Time 100 C

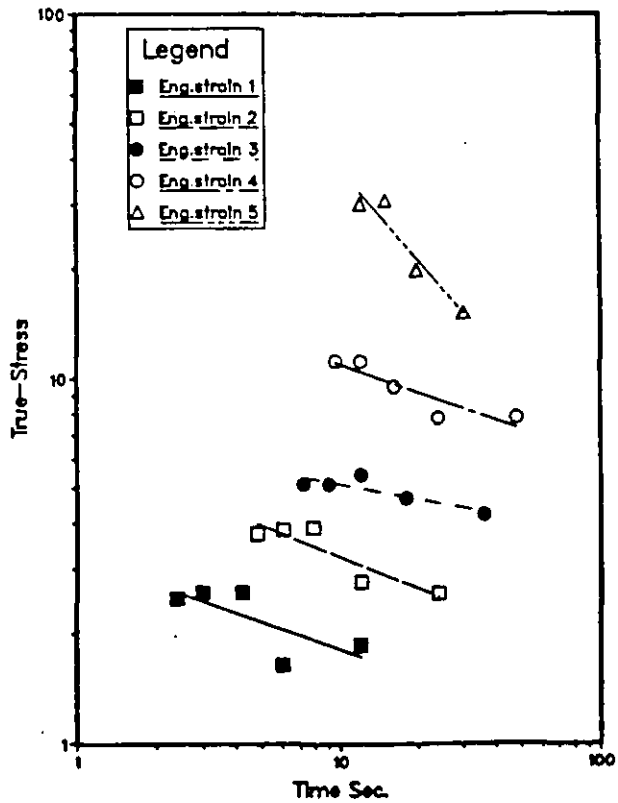

(d) True–Stress Vs Elapsed Time 110 C

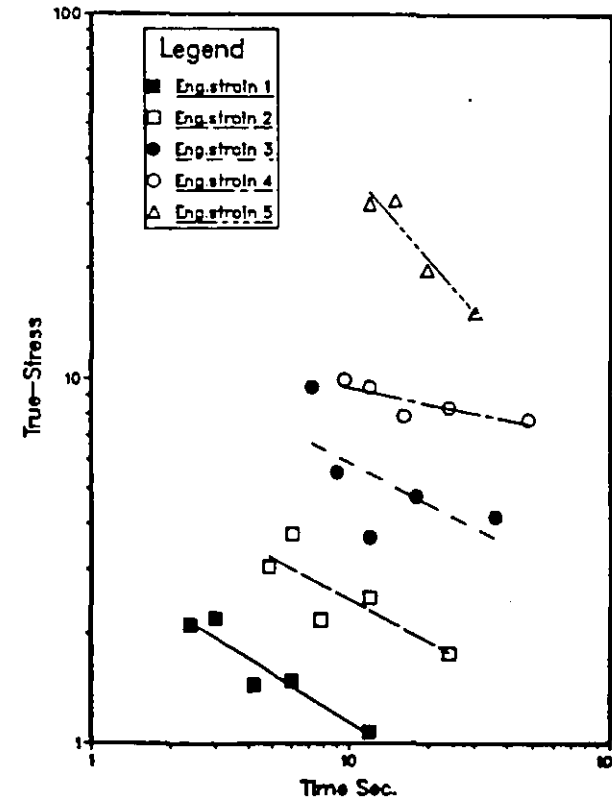

Figure 3.19 Variation of Log stress with Log time at different strain values for PETP

To determine if equation 3.4 (in section 3.3.1) represents stress-strain curve for PETP, the logarithmic plot of true stress - time must yield parallel curves (ie stress relaxation should be independent of strain) at each temperature. This is not the case as shown in fig3.19 (a - d) and this shows that the equation is not valid for PETP at the temperatures tested. Contrary to behaviour of vulcanized rubbers [108] the stress relaxation behaviour of PETP is temperature and strain dependent.

In addition, the temperature dependence of the strain hardening index show that equation 3.4 does not describe the non-linear stress-strain behaviour of PETP above T_g. HIPS and PMMA conform to equation 3.4 as shown by Lai and Holt [103] because they are not strain crystallizable, whereas PETP does strain crystallize. Since there is no correlation between the two empirical equations given (ie $\sigma = K \varepsilon^n$ and $\sigma = bt^m$) and equation 3.4, the constant velocity stress-strain-time relationship of the form $\sigma = Kt^m\varepsilon^n$ [29] does not hold for PETP. Therefore, the strain hardening equation ($\sigma = K \varepsilon^n$) similar to that of ductile metals is related to PETP formability at the strain hardening regime.

Temperature °C	Eng. strain	b	m
80	1	0.83	- 0.23
	2	1.07	- 0.23
	3	1.86	- 0.10
	4	2.22	- 0.05
	5	2.53	- 0.03
90	1	0.59	- 0.18
	2	0.82	- 0.18
	3	1.62	- 0.50
	4	2.89	- 0.86
	5	2.73	- 0.47
100	1	0.51	- 0.26
	2	0.79	- 0.28
	3	0.88	- 0.17
	4	1.23	- 0.21
110	1	0.49	- 0.43
	2	0.76	- 0.37
	3	0.94	- 0.22
	4	1.12	- 0.15

Table 3.3 *Stress relaxation index 'm' and b values for PETP at the thermoforming temperatures*

3.3.3.2 Uniaxial Stress Relaxation Tensile Test

Figure 3.20 (a - d) show the influence of temperature on stress decay of PETP with log time. The data are replotted as strain dependence of stress relaxation at each temperature (80, 90, 100, 110 °C) in fig 3.2.1 (a - d). The results show discontinuity in the slopes; from 80 to 100 °C, the relaxation slopes exhibit a discontinuity while at 110 °C, there are two discontinuities, In order to explain the relaxation behaviour observed in this experiment, the plot was divided into two parts at the lower temperatures (80 - 100 °C) and into three parts at 110 °C as shown in fig 3.22. Part 'a' is assumed to be due to normal chain relaxation at constant strain as predicted by Maxwell model; part 'b' is due to change in molecular motions as a result of strain hardening effect while part 'c' is due to combination of strain and thermally induced crystallization.

The reciprocal of relaxation times (τ) [ie relaxation rates ($1/\tau$) for part 'a' of the curves are presented in table 3.4 Relaxation time was determined according to equation 3.11

$$\sigma_t / \sigma_o = \exp(-t/\tau)$$

At 80 and 110 °C the relaxation rate decreases with increasing strain, while at 90 and 100 °C the relaxation rate increases with increasing strain. These observations could be explained as follows: At 80 °C, the decrease in relaxation rate with increasing strain is due to increasing influence of strain hardening (strain induced crystallization). Strain induced crystallization inhibit chain movements, thus the low rate of relaxation. At 110 °C, increasing influence of strain and thermally induced crystallinity (due to increasing soaking time) is responsible for the decrease in relaxation rate with increasing strain. The stress relaxation rate at 90 and 100 °C increase unexpectedly with increasing strain. This is because we expect strain hardening with increasing strain to decrease relaxation rate in PETP. The behaviour at these temperatures is typical of rubbery plastics, due to enhancement of chain mobility which over-rides strain hardening effect. However, at sufficiently long times, the strain induced crystallization changes the relaxation process which is responsible for the part 'b' of the relaxation curves.

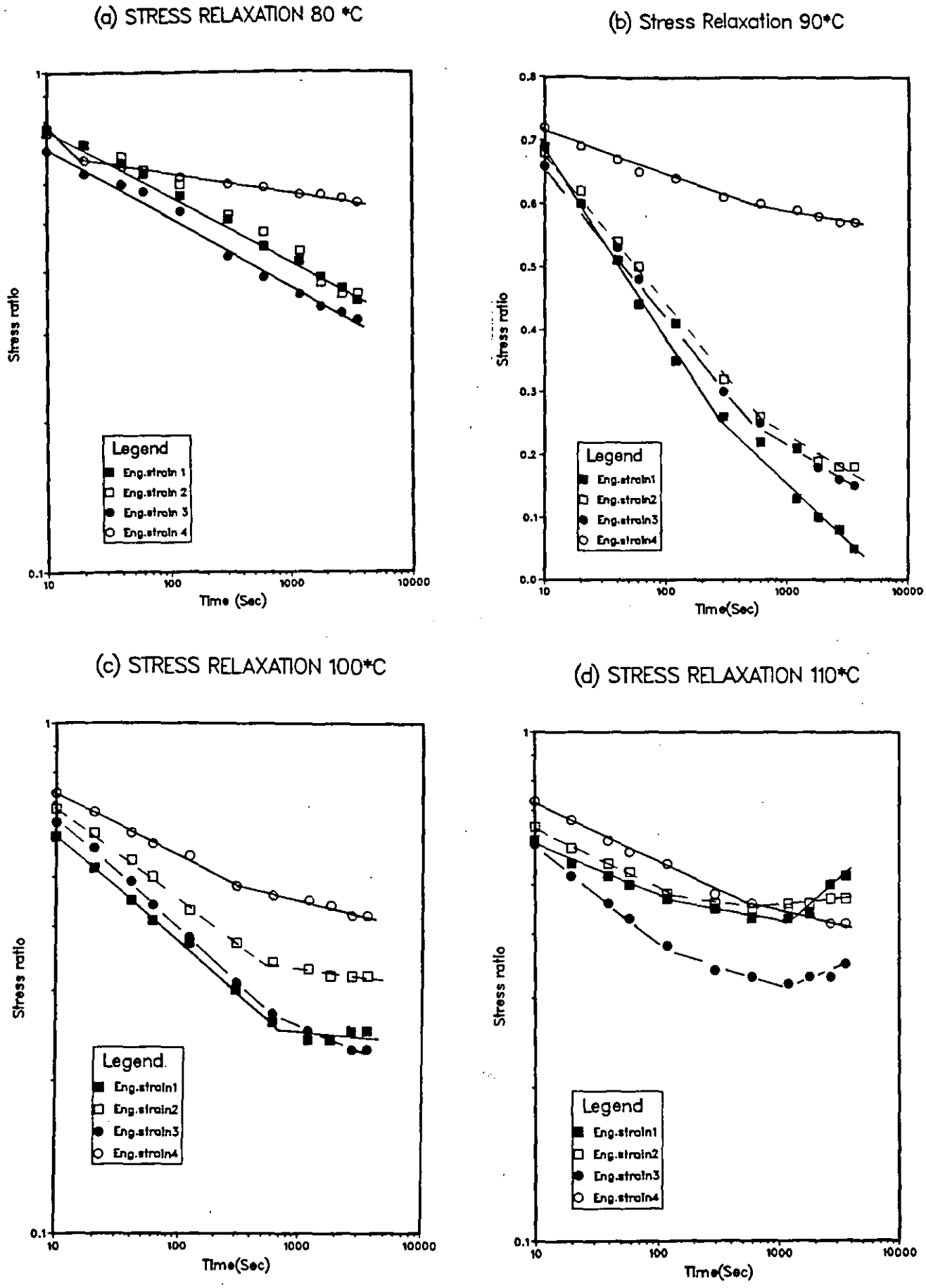

Figure 3.20 Stress relaxation of PETP at different temperatures

(a) STRESS RELAXATION.Eng.strain 1

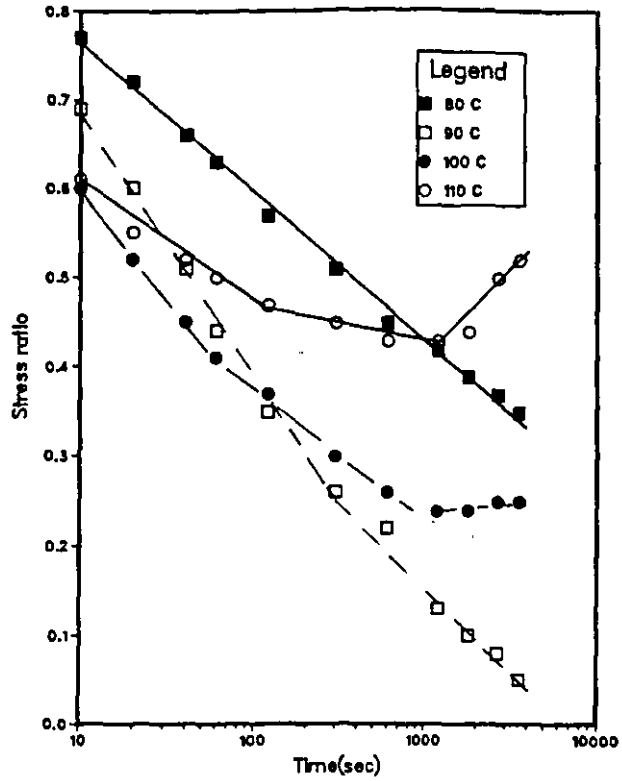

(b) STRESS RELAXATION.Eng.strain 2

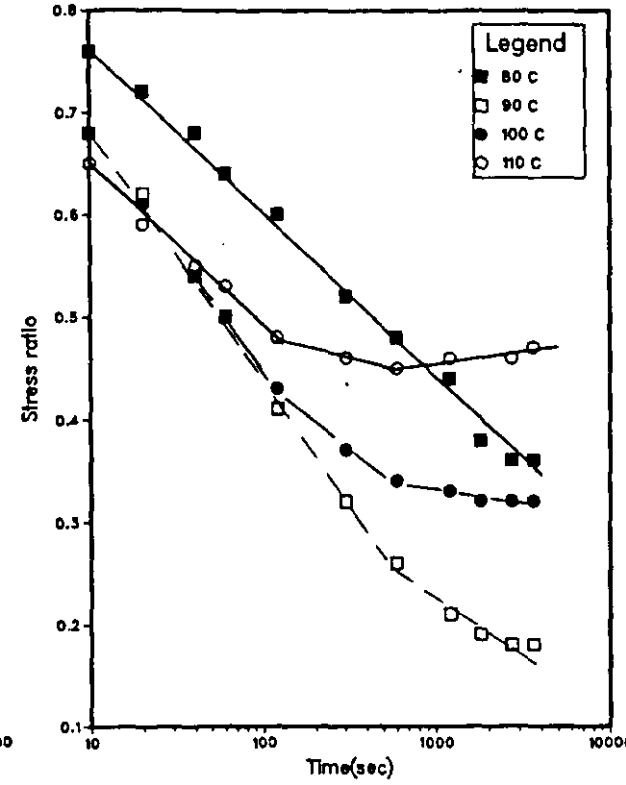

(c) STRESS RELAXATION.Eng.strain 3

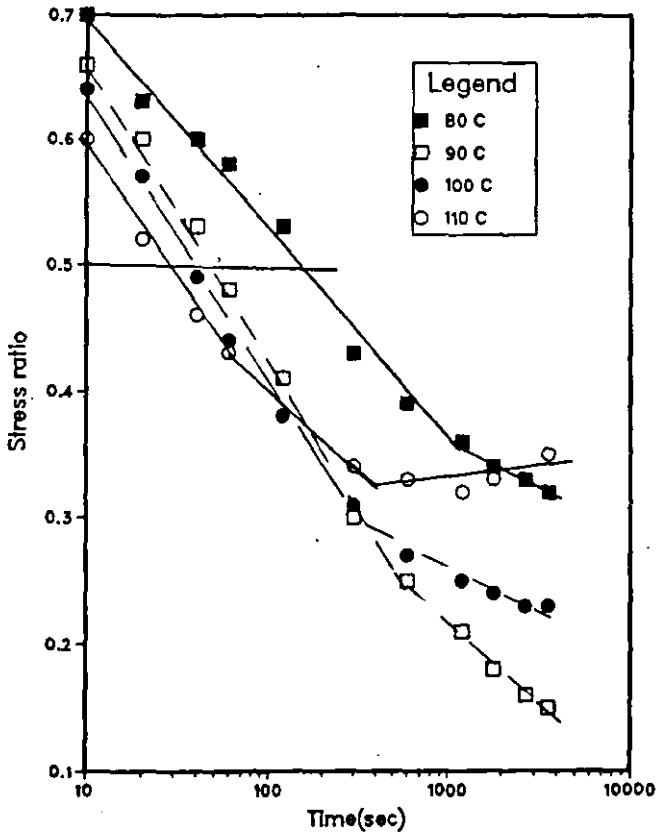

(d) STRESS RELAXATION.Eng.strain 4

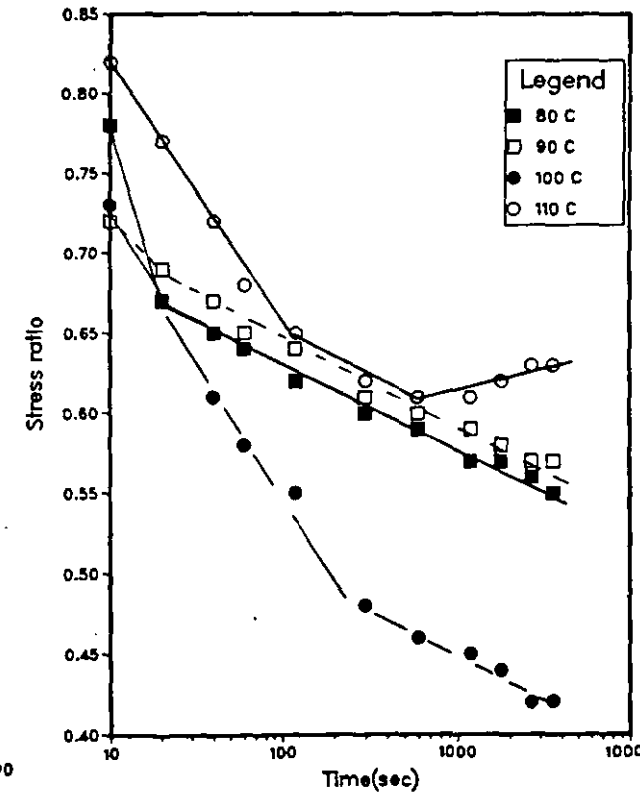

Figure 3.21 Strain dependence of stress relaxation of PETP

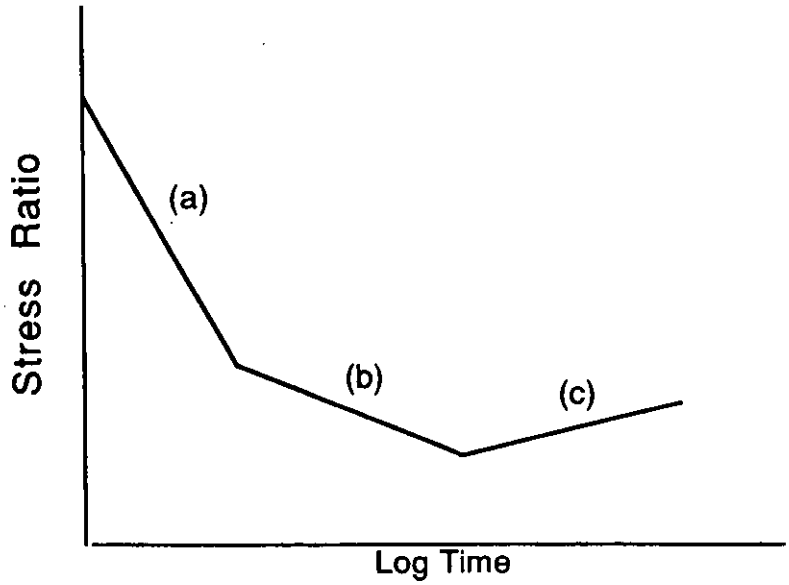

Figure 3.22 Stress relaxation model for PETP.

	Strain			
Temperature °C	1	2	3	4
80	6.10	6.06	5.75	2.74
90	3.44	4.24	4.33	13.51
100	4.10	4.31	4.67	5.92
110	7.69	6.33	4.90	6.37

Table 3.4 Relaxation rate ($1/\tau$) s^{-1} of PETP (part 'a')

	Strain			
Temperature °C	1	2	3	4
80	-	-	11.11	18.87
90	12.20	8.13	7.81	27.03
100	11.90	7.75	12.92	17.86
110	25.00	23.26	50.00	17.54

Table 3.5 Relaxation rate ($1/\tau$) s^{-1} of PETP (part 'b')

Fig 3.23, confirms the deduction from the tensile test that behaviour of PETP at 90 °C is typical of rubbery plastics. The stress ratio goes through a minimum at 90 °C at selected times in the natural draw (strain = 1) and strain hardening (strain = 3) regimes of the stress-strain curve of PETP. This is similar to elongation to failure going through a maximum at 90 °C reported in the tensile test results.

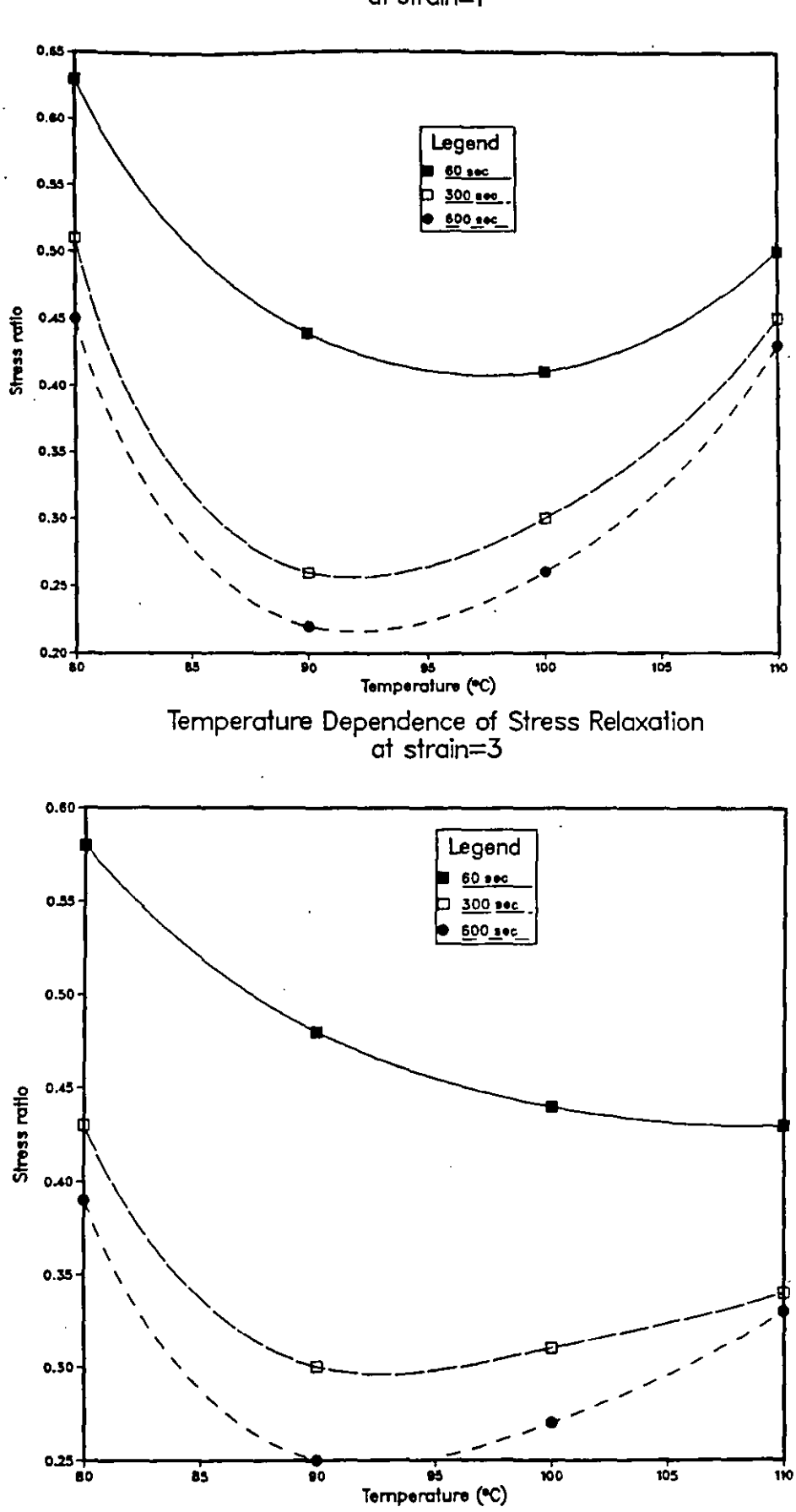

Figure 3.23 Temperature - Time dependence of stress ratio at constant strain

Table 3.4 also shows that relaxation rate increases with increasing temperature except at 80 °C which unexpectedly showed high relaxation rates. Increasing relaxation rate with temperature is due to enhancement of chain mobility..

The Maxwell model was used in calculating the relaxation rate of part 'b' of the curves presented in table 3.5. There is no clear trend from the values obtained. This is similar to stress-relaxation indices obtained from the continuous tensile relaxation. This may be due to the complications with respect to contributions from strain and thermally induced crystallization which are responsible for change in relaxation rate (part 'b').

In the stress-strain analysis earlier discussed, the deformation of PETP was described as rubber like especially at moderate strains. Thus the deformed PETP could be regarded as a stretched rubber like network with physical entanglements. The network points serve as temporary cross links. The kinetic theory of rubber elasticity predicts that the stress produced by uniaxial strain ε_o as

$$\sigma_o = N_o k T [\varepsilon_o - 1/(\varepsilon_o)^2] \quad \text{(ref 125)} \qquad \text{----------3.17}$$

where σ_o = stress at time t = o

ε_o = strain at t = o

k = Boltzman's constant

T = Absolute temperature (°K)

N_o = Number of network chains per unit volume of polymer

If the network chains break without reforming then N_o decreases to N, therefore the stress needed to maintain strain ε_o is given by :

$$\sigma_c = N k T (\varepsilon_o - 1/(\varepsilon_o)^2) \qquad \text{----------3.18}$$

Dividing equation 3.18 by 3.17

$$N = N_o (\sigma/\sigma_o) \qquad \text{----------3.19}$$

Thus, the number of network chains at any time t > 0 is directly proportional to the stress at that time. The exact way in which N changes with time is a function of the mechanism involved [126]. In PETP, the relaxation mechanism is constrained by strain induced and thermally induced crystallinity. The stress decay is due mainly to chain disentanglement within the network structure. If the rate of disentanglement is constant then stress relaxation obeys the decay law [127].

$$\sigma_t / \sigma_o = \exp(-k't) \qquad \text{----------3.20}$$

where k' = rate constant

t = time

Table 3.6 shows vividly that the change in N depends on the mechanism of deformation. At the lower strains (1and 2) N_o decreases but from a strain of 3 where strain-induced crystallization occurs N_o increases, at lower temperatures significantly. The loss of entanglements at the lower strain levels (strains 1 and 2) is responsible for reduction in N_o values. However at higher strains ($\varepsilon > 2$), the loss of entanglement points is replaced by nuclei for the formation of crystallites which form semi-permanent cross links; and increase with strain because of strain and thermally induced crystallinity. Therefore, the kinetic theory is valid below the strain hardening regime ($\varepsilon < 2$). At higher temperatures the chain mobility is enhanced, thus the reduction of N_o with strain. This also shows that the effect of strain-induced crystallinity decreases with increasing temperature. At 110 °C, the crystallization mechanism is highly influenced by thermal effects. This gave rise to the third segment 'c' which is due to constrained shrinkage (ie induction of tensile force at constant strain) under stress relaxation conditions.

Temperature °C	80		90		100		110	
Strain	$N_o.10^{26}$	$N.10^{26}$	$N_o.10^{26}$	$N.10^{26}$	$N_o.10^{26}$	$N.10^{26}$	$N_o.10^{26}$	$N.10^{26}$
1	4.27	1.92	2.49	0.65	2.63	0.97	2.12	1.00
2	2.43	0.88	1.50	0.39	1.61	0.69	1.14	0.60
3	4.46	1.74	2.07	0.52	1.14	0.43	0.91	0.35
4	13.80	9.28	4.41	2.69	1.01	0.49	1.06	0.69

Table 3.6 Change in number of network chains per unit volume (cm^3) (part 'a')

The temperature dependence of k' in equation 3.20 has been found to be expressed by the Arrhenius equation [128].

$$k' = A \exp(-E/RT) \qquad \text{----------3.21}$$

where A = frequency factor

E = Activation energy

R = gas constant

T = Absolute temperature

Because there are changes with temperature and strain in microcrystalline structure and in the stress-bearing mechanisms, the simple time-temperature superposition that is valid for amorphous polymers is not valid for strain crystallizable polymers like PETP. The fact that the curves are not parallel does not allow horizontal displacement along the log-time axis due to change in the rate of molecular motions with temperature. In addition, vertical shifts along the stress decay axis are not possible. Therefore, PETP does not obey Arrhenius equation especially at the lower strains (1 and 2). However, at engineering strain of 3, the relaxation curves between 90 to 110 °C are parallel. As shown in fig 3.21 (c) a horizontal line with the decay curves at the various temperatures gave the time for which $k' = 1/t^{129)}$. A plot of log k' vs 1/T gave a straight line (see fig 3.24). The activation energy calculated from the slope = E/R was 12.74 J/mol.

How do the stress relaxation results relate to thermoforming? The results shows that in order to reduce the relaxation effect, PETP should be deformed at lower processing temperatures where strain-induced crystallization inhibit molecular motions. Also, the time to effect thermally induced crystallization at the higher temperatures is rather long and will not provide an efficient cycle time during thermoforming process. Also, high cooling rate will be required; vacuum would have to be maintained whilst cooling takes place to prevent relaxation.

In conclusion, stress relaxation behaviour of PETP at the thermoforming temperatures.

(i) Could be described as rubber-elastic at moderate strains (below strain of 2) and obeys the kinetic theory of rubber-elasticity.

(ii) is influenced by strain and thermally induced crystallinity beyond strain of 2

(iii) exhibit discontinuity due to the effect of the strain and thermally induced crystallinity.

At the lower temperatures, relaxation is dominated by strain hardening effects while at the higher temperatures relaxation is increasingly dominated by thermally induced crystallization.

3.3.3.3 Density Measurement

Fig 3.25 shows density as a function of strain at each test temperature. The density increases with increasing strain and decreases with increasing temperature. Although it has been reported that orientation may increase the density of amorphous PETP [121], this was however, based on samples drawn at much lower strain rates compared to those employed in this work. Other workers [78,85] have reported presence

of crystallinity beyond 100 % elongation, which was verified by x-ray patterns and light micrographs.

Assuming a direct relationship between density and degree of crystallinity, the levels of crystallinity increases with strain but decreases with temperature.

Fig 3.26 shows the density of unoriented samples as a function of temperature (soaked for 10 minutes). The small differences in density with increasing temperature show that at the thermoforming temperatures the rate of crytallization is very slow in isotropic PETP; there was no significant crystallinity in the samples before they were deformed. Therefore, the crystallinity detected in the samples after deformation is due to strain induced crystallinity.

3.3.3.4 Wide Angle X-ray Diffraction

A series of x-ray diffraction patterns are shown in fig (3.27). Pattern A is from an amorphous unoriented sample and is included for reference. Patterns B to F are samples drawn from engineering strains between 1 to 5. The patterns show progressive increase in intensity of diffuse lobe in the equatorial direction, which is indicative of presence of imperfect crystals. The orientation of the lobes suggests a preferred orientation of crystals in the direction of stretch. Similar observations have been reported by Misra and Stein [93] and by Spruiell et al [92].

The evidence of density measurement and x-ray diffraction patterns confirm that the reinforcing mechanism in PETP during tensile drawing (and therefore thermoforming) above T_g is due to development of crystallinity.

3.3.3.5 Birefringence Measurements

The birefringence was calculated as stated in equation 3.12 at room temperature. It was measured as a function of stretch temperature, strain, strain rate and deformation stress.

Birefringence is a measure of the degree of molecular orientation in an oriented polymer, whether amorphous or (semi) crystalline.

The effect of strain on birefringence is shown in fig 3.28 (a - e) for all the strain rates employed. The birefringence (Δn) varies approximately linearly with engineering strain which is very similar to the behaviour of a physical network defined by permanent entanglement points [85, 86]. The development of birefringence is due to gradual alignment of the polymer chains parallel to the direction of stretch. In the 'natural draw' regime ε^N, characterised by uniform deformation stress, there is an increase in molecular orientation with strain. This could be explained in terms of breakdown of a limited number of network points in such a way that, although all chain still contribute towards birefringence, some cease to be effective in supporting

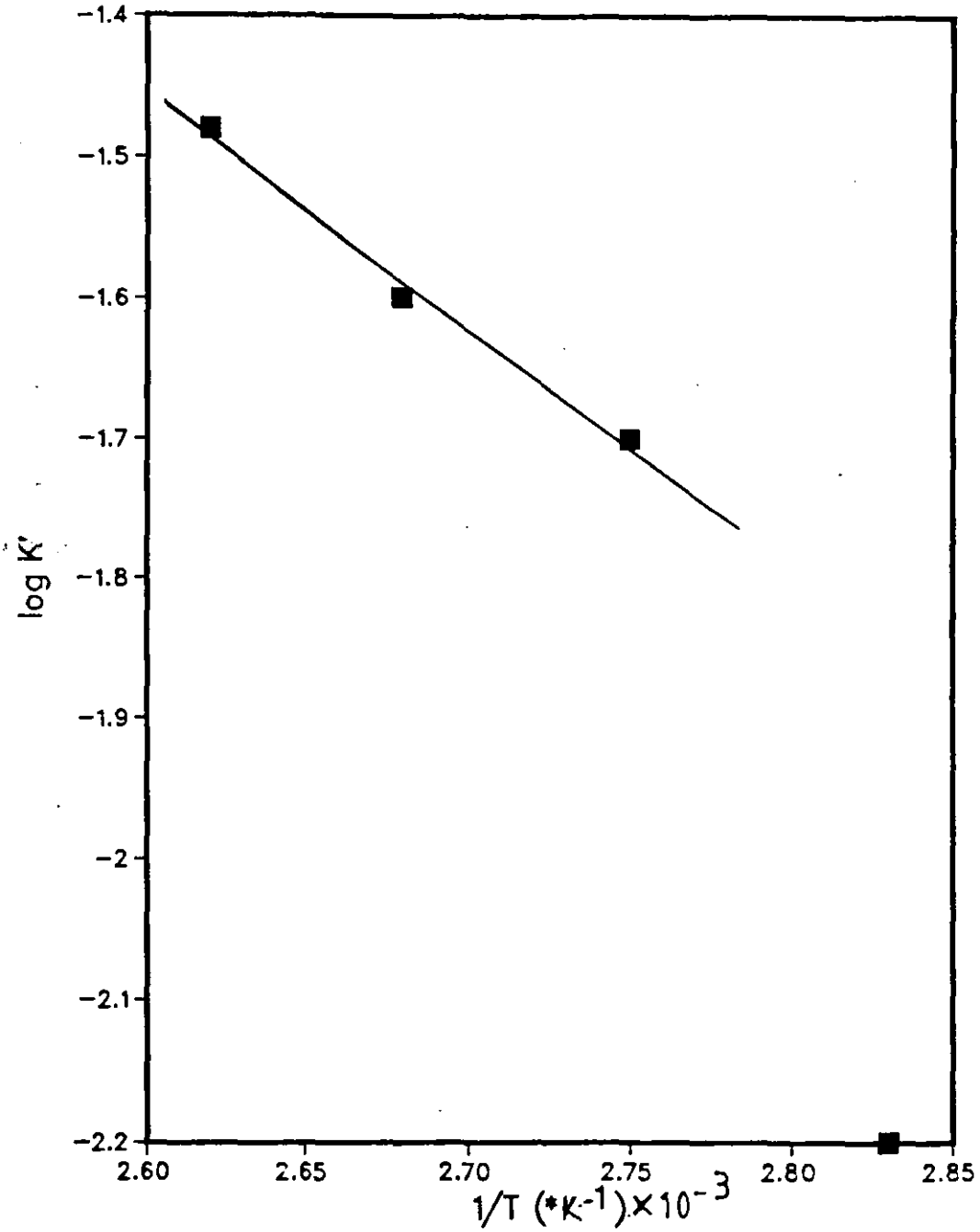

Figure 3.24 Temperature dependence of stress relaxation rate in PETP

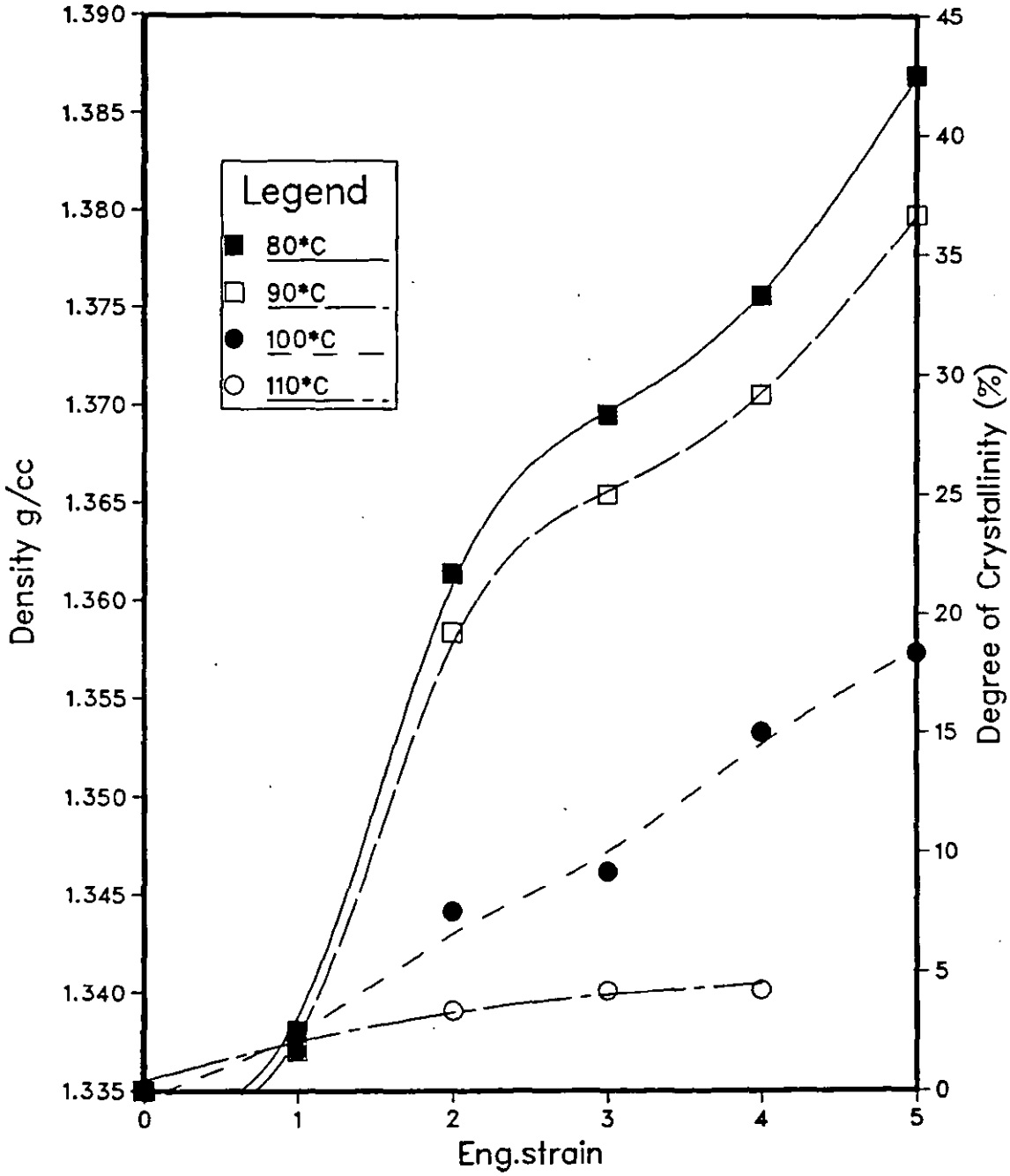

Figure 3.25 Density of strained samples at the thermoforming temperatures

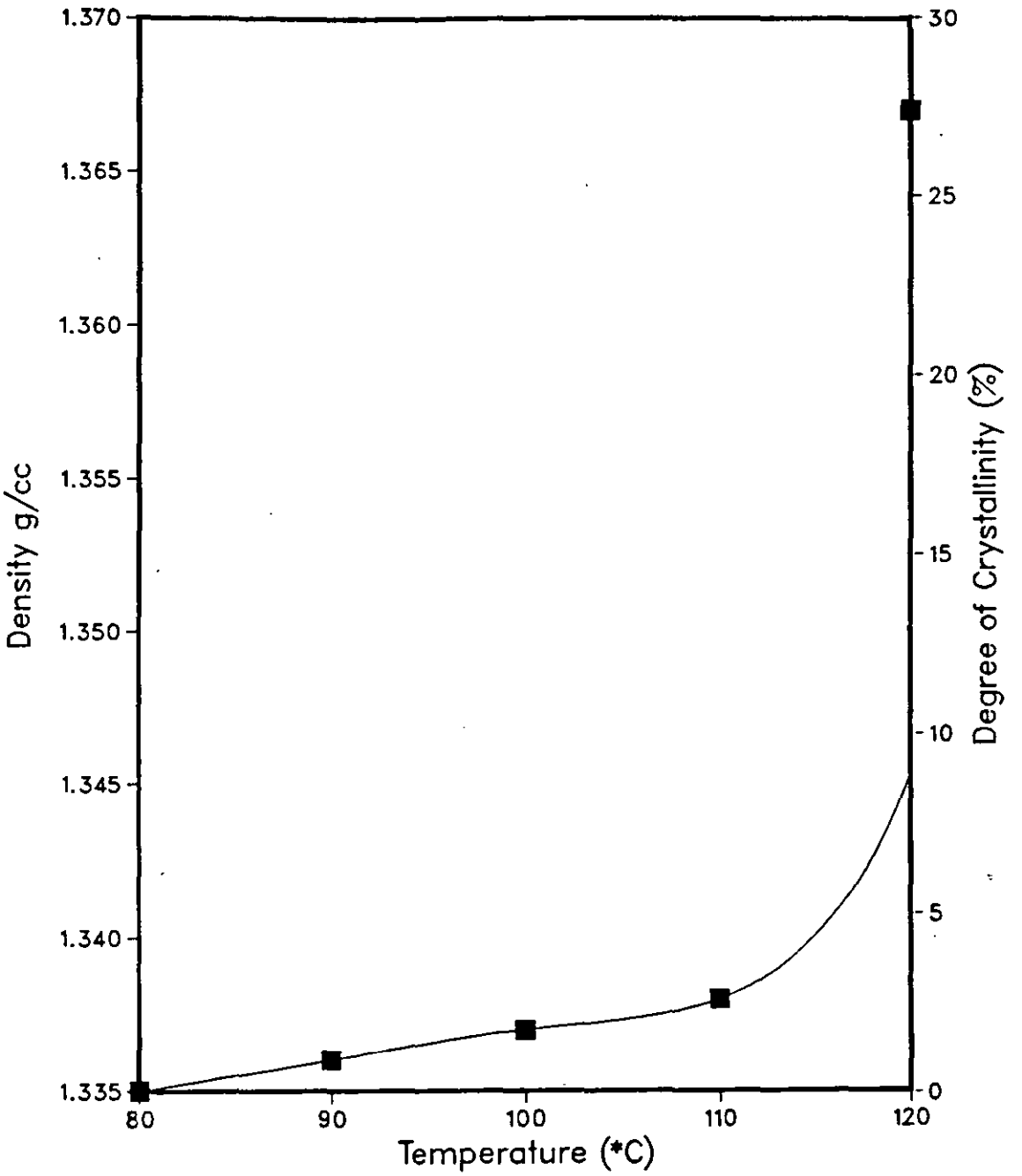

Figure 3.26 Density as a function of temperature of exposure

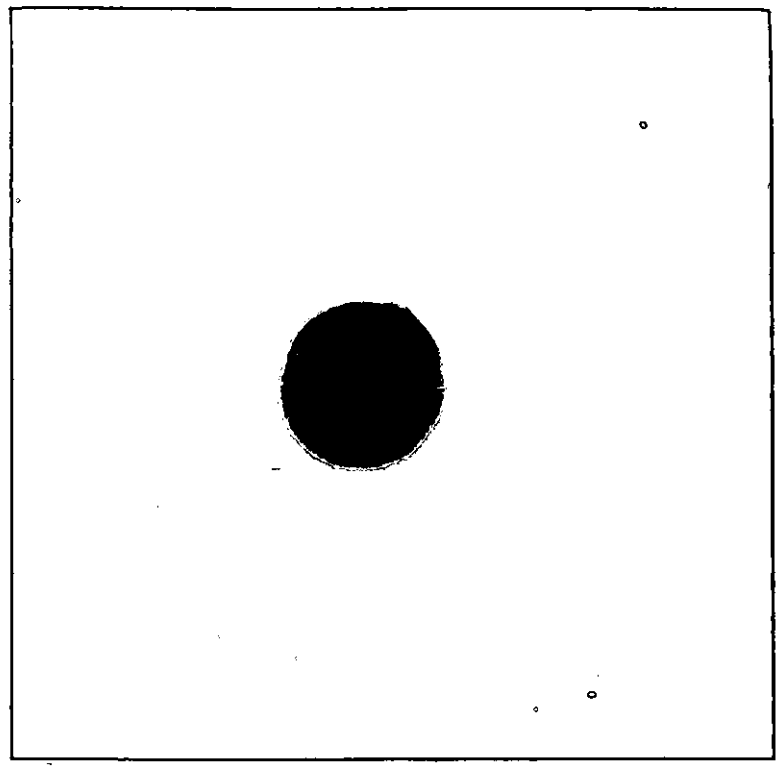

A

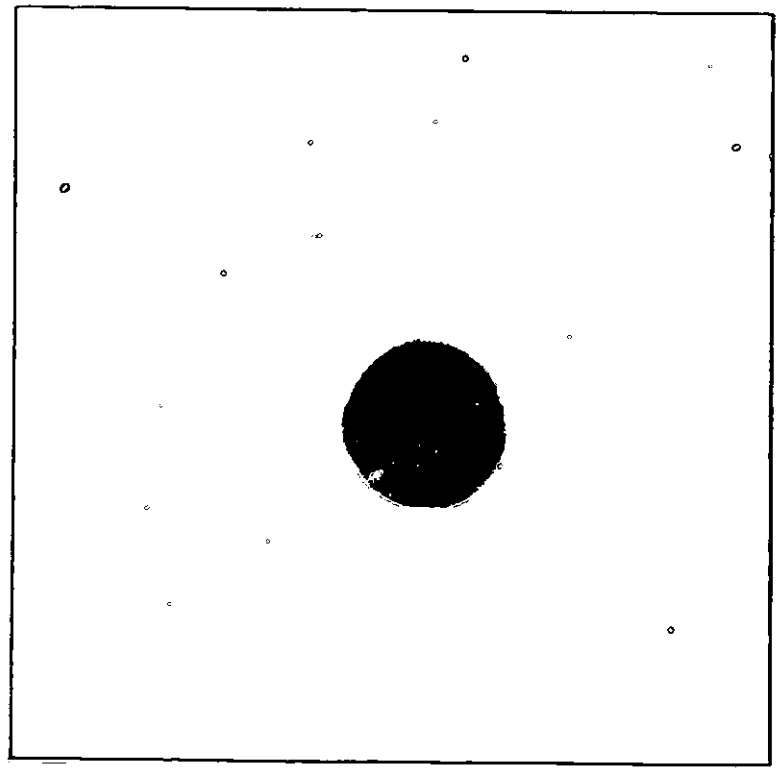

B

Figure 3.27 *Wide-angle X-ray diffraction pattern for PETP at different strain levels (A) = 0 ; (B) = 1 ; (C) = 2 ; (D) = 3 ; (E) = 4 ; (F) = 5.*

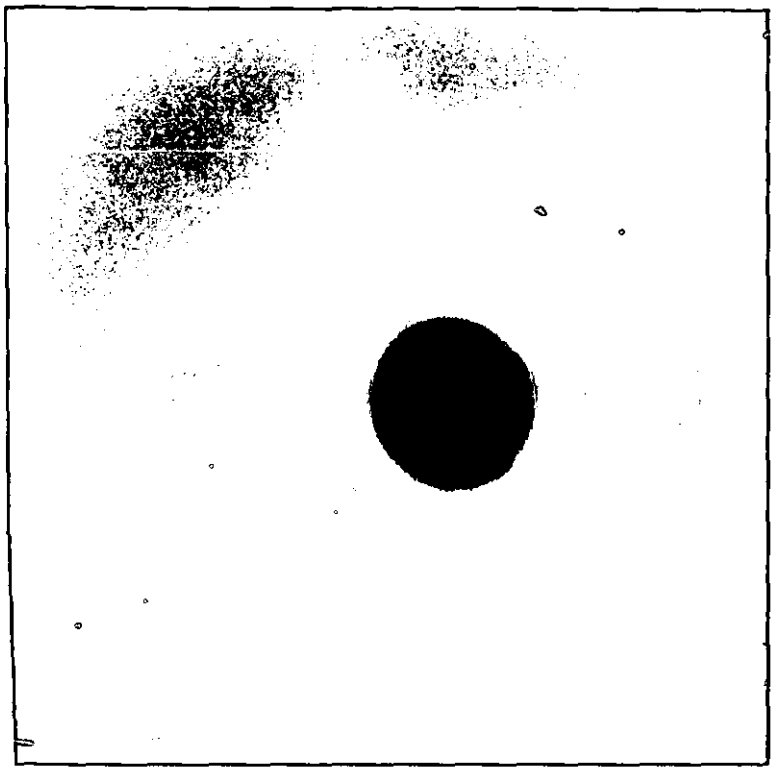

C

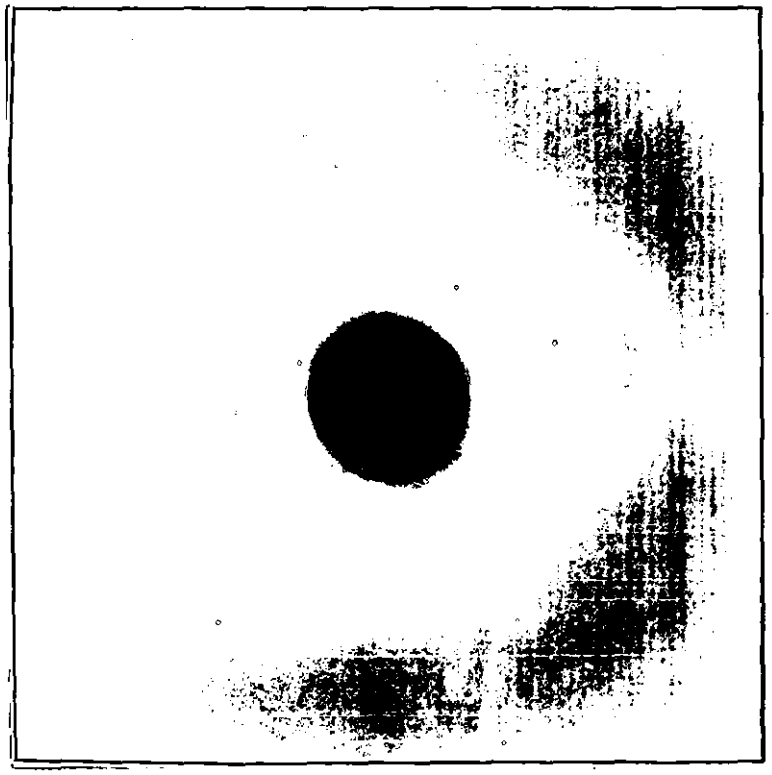

D

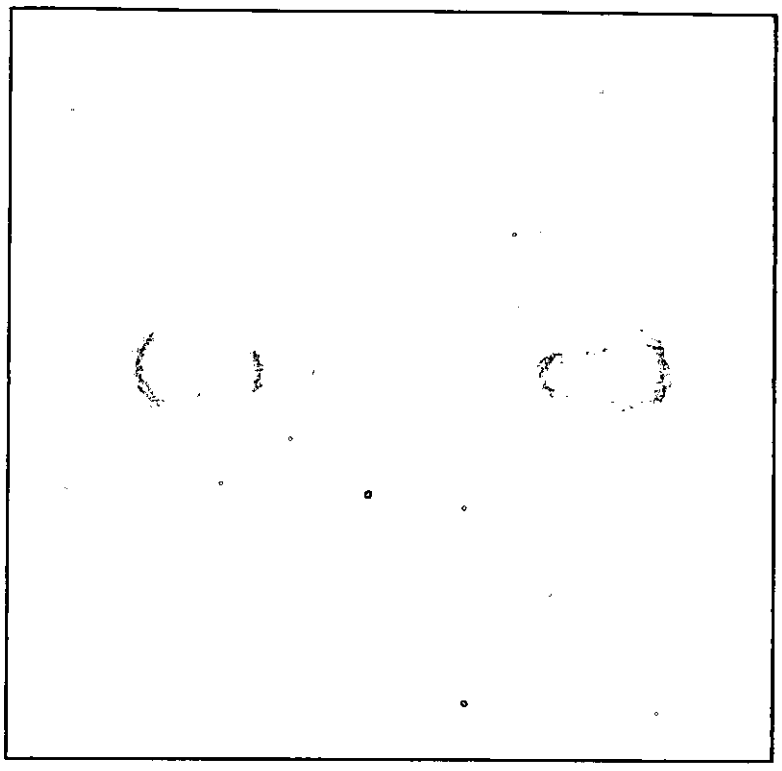

E

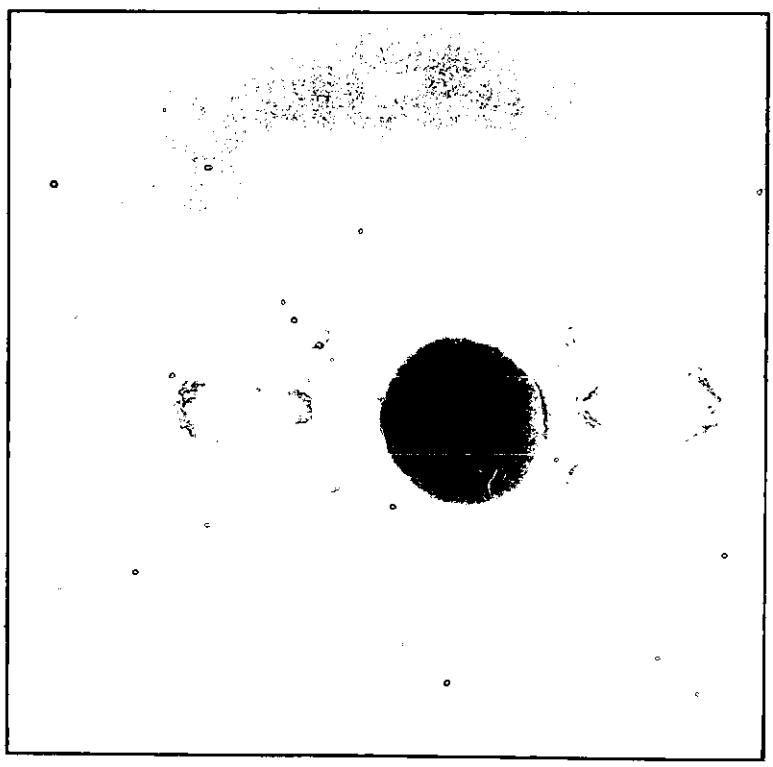

F

stress[85]. At higher strain levels where there is onset of strain induced crystallization, as shown by the density and x-ray diffraction patterns, the crystallization serves as semi permanent crosslinks which increases the orientation efficiency. However, the rate of increase of Δn with engineering strain decreases with increasing temperature. This is due to increase in relaxation process because of enhancement of chain mobility with increasing temperature.

The influence of strain rate on orientation is presented in fig 3.29 (a - d). Birefringence increases with increasing strain rate. The influence of strain rate is highly significant at higher temperatures where the degree of orientation is small when stretching is at low strain rates fig 3.30. This is due to simultaneous relaxation processes taking effect. At high temperatures and slow stretching speeds, the rate of relaxation of chains to their random conformation is faster then the rate of chain alignment. At sufficiently high strain rate, the chain alignment overcomes the rate of relaxation. Therefore, the elongation process at low strain rate could be explained in terms of chain slippage with consequent low orientation maintained. Whereas at the lower temperatures, the process of chain alignment is due to uncoiling of the molecular chains because of limited chain mobility with resultant high degree of orientation.

The relationship between degree of orientation and mechanical properties is plotted as tensile stress against the corresponding birefringence for increasing strain rate at each temperature is recorded for varying strains (fig 3.31). There is a simple relationship between deformation stress and birefringence especially at strains beyond the 'natural draw' ε^N regime. At the lower strains within ε^N, the correlation is not very good. This is not surprising as earlier explained. This is due to loss of some physical network which does not contribute to deformation resistance. Similar simple relationships between mechanical properties and birefringence have been reported by others [78, 82, 86, 89].

The results discussed show that the degree of orientation which determines the level of physical properties of a polymer is influenced by amount of extension (strain), strain rate and stretch temperature. In addition, the strain level is not enough to specify degree of orientation because for the same degree of stretch, various levels of physical properties can be obtained depending on stretch temperature and strain rate. In view of different correlations between degree of orientation and strain on one hand and mechanical properties on the other, the physical properties of orientated PETP are best specified by birefringence [95]. However, this does not distinguish between amorphous and semi-crystalline PETP.

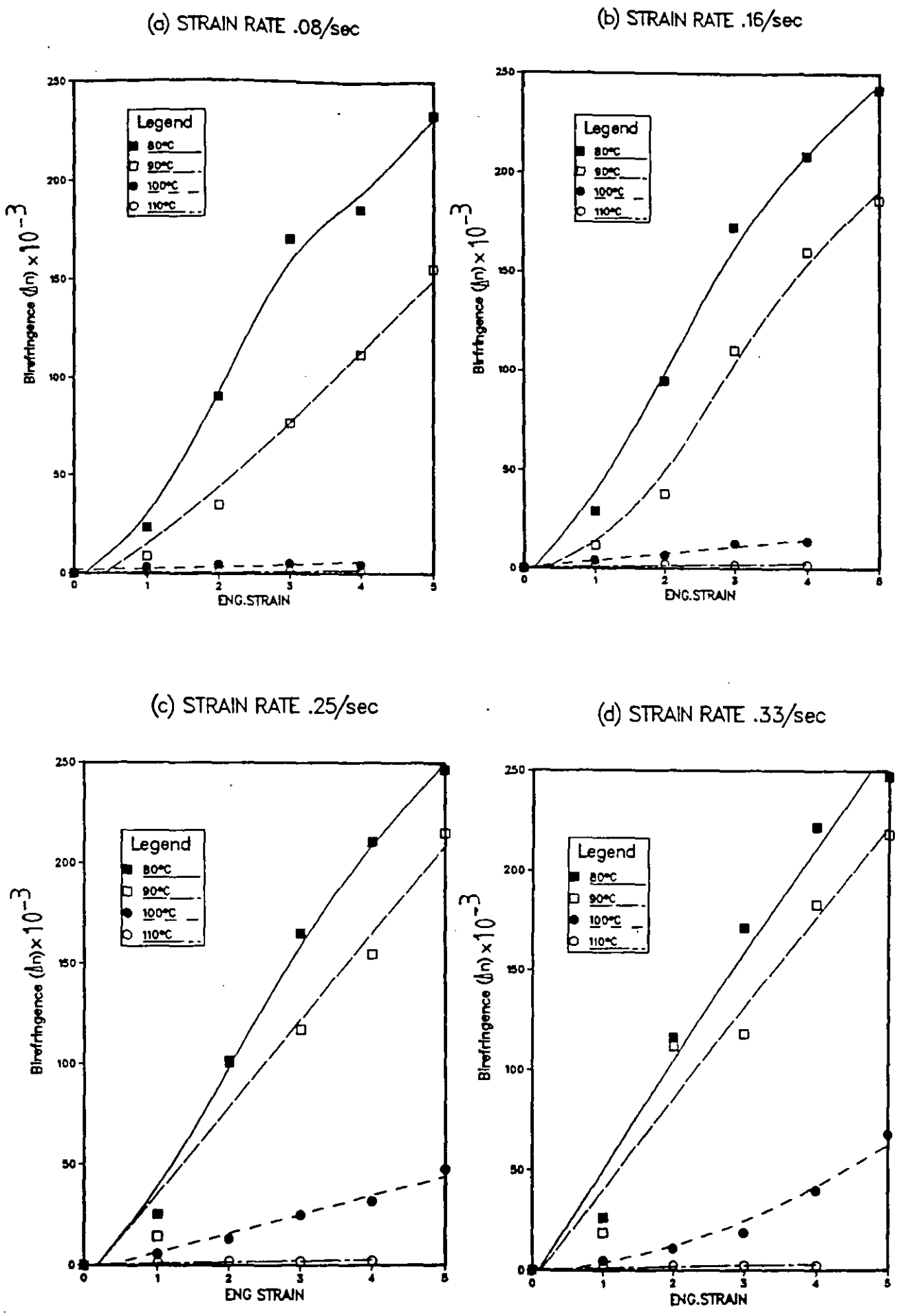

Figure 3.28 Birefringence as a function of strain at different temperatures

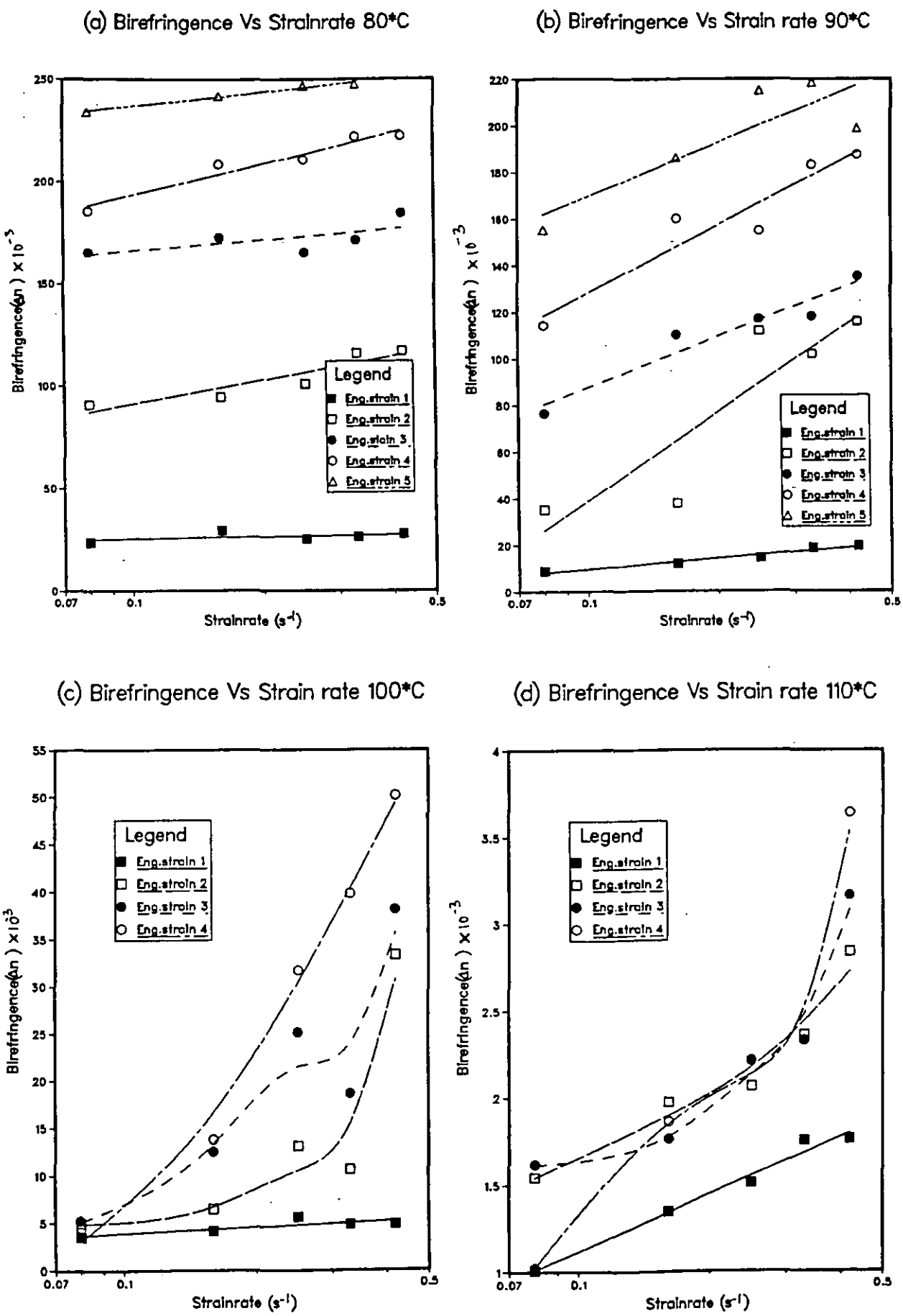

Figure 3.29 Birefringence as a function of strain rate at different strain levels

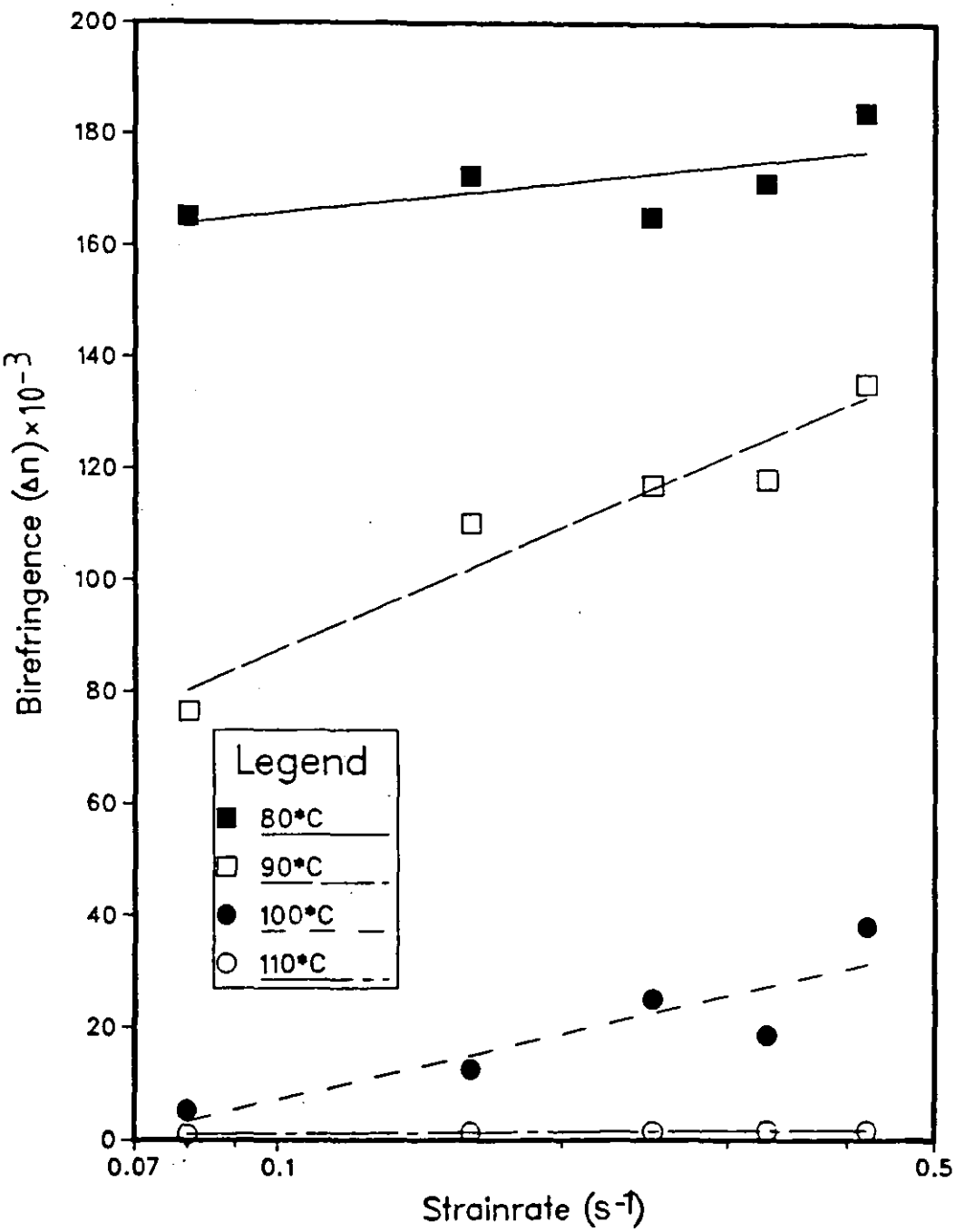

Figure 3.30 *Temperature dependence of Birefringence.*

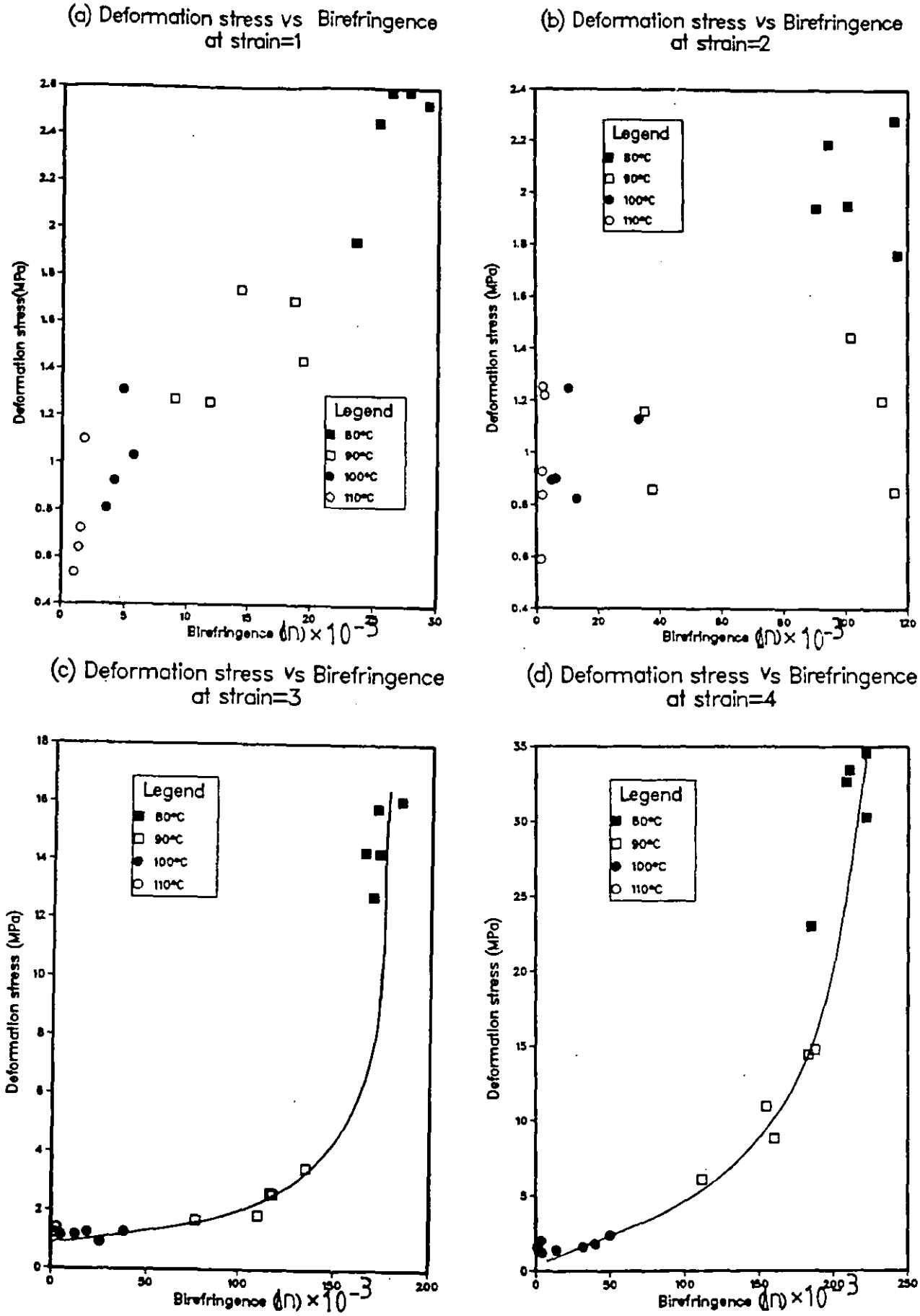

Figure 3.31 Variation of deformation stress with Birefringence at different temperatures for PETP

3.4 Conclusions - Physical Properties of amorphous PETP

Studies of tensile drawing behaviour of PETP within the thermoforming temperatures (ie $T_g < T < T_c$) as a function of strain and strain rate show that PETP sheet exhibits homogeneous deformation and goes through three regimes: (i) yield, (ii) deformation at uniform stress (ε^N) and (iii) strain hardening.

The strain hardening effect is exhibited beyond the critical strain of 2. It is independent of strain rate but is critically temperature-dependent.

A strain hardening equation $\sigma_t = K (\varepsilon_t)^n$ describes the strain hardening regime. It is proposed that the strain hardening index 'n' is related to PETP thermoformability. A high strain hardening index ensures uniform thickness in formed parts.

Stress relaxation in tension of PETP at the thermoforming temperatures exhibits discontinuities: three independent zones of response are proposed. These are the

(i) Normal chain relaxation (Maxwell model)

(ii) Strain hardening effects and

(iii) crystallization effects.

The kinetic theory of rubber elasticity is only valid below the strain hardening regime ($\varepsilon < 2$) of the stress-strain curve.

The loss of temporary cross links (chain entanglements) is compensated by permanent cross links due to strain and thermal induced crystallization which slows the rate of chain relaxation.

Evidence from density and wide angle x-ray diffraction shows that strain hardening in PETP is due to strain-induced crytallization.

Tensile drawing of PETP influences the degree of molecular orientation which in turn is likely to determine the physical properties of formed products.

The rate of increase of molecular orientation with strain decreases with increasing temperature and decreasing strain rate, due to increasing relaxation rates.

Overall, the degree of orientation is dependent on strain, strain rate and deformation temperature.

Chapter 4

Thermoforming Process

4.1 Introduction

In chapter 2, the thermoforming processing condition for PETP sheet was determined. In chapter 3, the thermoforming behaviour of PETP sheet was simulated. This chapter forms the beginning of the second part of this study. The next step is the assessment of formability of PETP sheet at the processing conditions established from consideration of the tensile tests. Before thermoforming PETP sheet, it is essential to familiarise the reader with the thermoforming process.

Thermoforming is a general term encompassing many processes and techniques for forming thermoplastic sheets into discrete articles [26]. It basically refers to heating of thermoplastic sheet to its softening point or rubbery state and pneumatically/mechanically stretching the hot and pliable sheet against the contours of a mould.

The use of plastic sheet as the basis distinguishes thermoforming from other types of processes such as blow moulding, injection moulding and compression moulding.

Early developments in thermoforming were with cast cellulose nitrate sheet in the late 1860's [26]. Perhaps this lead McConnel [136] to refer to thermoforming as 'the oldest infant'. However, it was restricted to a few applications and of little importance compared to other plastics processing methods.

The rapid growth of thermoforming, particularly in the packaging industry, is due primarily to the development of the screw extruder and extruder dies in the late 1940's and development in the 1950's. Also the improvement of machinery and the introduction of new plastics contributed to the growth of thermoforming [138].

4.2 Applications

The earliest commercial applications of thermoforming were developed during the last World War when glass in windscreens of high-performance aircraft was found to be unsuitable. Cast acrylic sheets, heated and formed over male moulds, were used in the United Kingdom and USA. The illuminated sign industry also used the cell-cast acrylic sheets after the war. Presently, the packaging industry, dominates the thermoforming industry because of the development in high speed packaging machines. This has been confirmed in Child's [138] report in 1969 and in Modern Plastics [5] in 1977.

Notable successes in non-packaging industries [140] include appliances such as refrigerator door liners and defroster trays; automotive components like headliners, compartment liners, inner door liners and bumper liners; light fitting housing; festive decorations; counter displays such as jewellery trays; industrial applications include, tote boxes, machine enclosures and guards, it is widely used for making toys and household goods such as baths, bath mats, picture frames, picnic basket liners, flower pots etc.

4.3 Thermoforming Machines

Thermoforming machinery generally is that which has the ability to apply heat to one or more plastic sheets, and induce a pressure against the sheet to force it against either a male or female mould until the shape produced is frozen.

Industrial thermoforming machines are as varied as the products they are designed to make. They range from relatively simple manually controlled equipment to the complex, computer-controlled rotary and in-line machines designed for mass production and efficiency

Any thermoforming machine must provide the following: [140, 141]

(1) A heating station where the plastic is heated to its forming temperature.
(2) A clamping frame to hold the sheet for heating and positioning for forming.
(3) A device to raise or lower the clamped sheet or to move the clamped sheet over the mould.
(4) A vacuum system
(5) An air pressure system
(6) Controls for the various operations and
(7) safety devices

Classification of the machines is often based on the number of operations they perform.

(1) Single-stage, sheet-fed Machines:

A single-stage machine can perform only one operation at a time and its total cycle is the sum of the times required for the whole forming operations including unloading of the formed article.

These types of machines are usually manually operated or semi-automatic. In semi-automatic machines, the clamping and removal of the formed sheet are done manually. All other operations are preset and carried out automatically. The machines are equipped with cycling controls and timers which allow each individual operation to be completed before the next one can start.

(2) Multi-stage, sheet-fed Machines:

These machines are designed for higher output and to utilise electric heating better. For instance, a two-stage machine can perform two operations simultaneously. It usually consists of two forming stations and a bank heater which move from one to the other. Machines with three or more stages are usually built on a horizontal circular frame called **Rotaries.** The rotary operates like a merry-go-round, indexing through the various stations at an angle after each operation depending on the number of stages on the machines (120 ° for 3 and 90 ° for 4 stage machine). These machines are usually semi-automatic and only need one operation to load and unload.

(3) In-line, sheet-fed Machines:

In contrast to the general purpose machines, where cut sheets are formed, these machines are designed to handle rolls of flexible plastics. The sheet is clamped in a frame which travels into the heating station, then indexes through the forming station and on to the unloading station where the part is removed by the operator.

This machine reduces manpower by eliminating handling of sheet. This makes the process cost effective. Speed of forming is variable depending upon the type of sheet material being used and its thickness. Often, the machine is dedicated to mass produce one item.

(4) Continuous Machines:

The continuous forming operation takes the material directly from the extruder to a forming machine which moves with the web of plastic emerging from the die, utilizing some of the heat from the extruded material up to the forming temperature.

The combined extrusion and thermoforming machine is employed primarily for high production runs. Its disadvantages are that

(a) a high degree of control and synchronisation is required

(b) hot sheeting cannot be pre-printed conveniently

(c) the rate of extrusion is generally lower then the capacity of a modern thermoformer.

Its advantages are

(a) lower heating cost

(b) uniformly heated sheets

(c) reduced material handling cost

(d) elimination of intervals when the mould is idle.

These machines are usually dedicated to one product or material.

(5) Packaging Machines:

Although most of the equipment already discussed can be used to form plastic packages, there are several machines which have been adapted to combine the forming operations with other packaging functions. Such machines are for skin or contour packaging and blister packaging. In skin packaging, no mould is employed, the transparent packaging film is drawn directly over the article to be packaged. In blister packaging, the film or sheeting is vacuum formed over or into a mould of the shape of the article to be packaged. There is another called snap packaging, where the thermoplastic sheet is formed with a lip by a sliding ring so that it can be snapped as a protection above the article [142].

Generally, machines operate with intermittent or continuous feed of roll stock and the various functions are performed simultaneously at a sequence of stations in line.

4.4 Methods of Forming

There are four main methods of thermoforming [141,142]; match-mould forming, slip forming, air blowing (or pressure forming) and vacuum forming. All the methods rely on three basic steps:

(a) heating a flat sheet to a forming temperature

(b) stretching the sheet into a suitable form and

(c) cooling it so that it retains the mould form

The extra steps for each of the methods are supposed to improve the wall thickness distribution of the sheet as it is stretched or deformed into the mould form.

(A) Match-mould Forming: is the process in which a thermoplastic sheet is clamped into a frame and heated to its forming temperature. A male mould is positioned on the top or bottom platen with a matched female mould mounted on the other. The mould is then closed, forcing the plastic to the contours of both moulds fig 4.1A. Trapped air is allowed to escape through vent holes drilled into the moulds.

This method was originally employed by the metal stamping industry. The plastics industry has replaced metals with thermoplastics for industrial applications. Matched-mould forming offers excellent reproduction of mould detail and dimensional accuracy. Variations of this method include, single-mould and plug-and-ring formings.

(B) Slip Forming: involves forming a hot thermoplastic sheet around a male mould mechanically. It requires a pneumatic press with an upper and lower cylinder fig 4.1 B. Various types of clamping methods have been devised to control the slippage and to prevent the clamps from chilling the sheet. Slip forming is used to avoid excessive thinning when forming articles with deep draws.

(C) Air Blowing or Pressure Forming: is the procedure in which positive air pressure is applied against the top of a hot thermoplastic sheet in a female mould fig 4.1C. Compressed and pre-heated air up to 500 psi (35 kg/cm^2) [140] is commonly used. The mould has vent holes to allow air entrapped below the sheet to escape. This process may be combined with mechanical or vacuum drawing. Compared to vacuum forming, pressure forming offers a faster production cycle (the sheet can be formed at a lower sheet temperature), greater part definition, and better dimensional control. Variations of pressure forming include, straight air blowing, free blowing, plug-assist blowing and trapped sheet forming.

(D) Vacuum Forming: consists of clamping a thermoplastic sheet in a frame around its periphery only, heated to forming temperature, and then it is brought into contact with the edge of the mould. This creates a seal which makes it possible to evacuate the air between the hot plastic sheet and the mould by applying the vacuum to force the hot plastic against the mould, fig 4.1 D.

Vacuum forming generally is the least expensive method because the mould employed is of light construction and has to withstand only atmospheric pressure. Variations of vacuum forming include, simple vacuum forming, free vacuum forming (ie without mould), vacuum snap-back forming, vacuum plug-assist forming, vacuum air-slip forming etc. Simple vacuum forming and vacuum plug-assist forming have been used in this work.

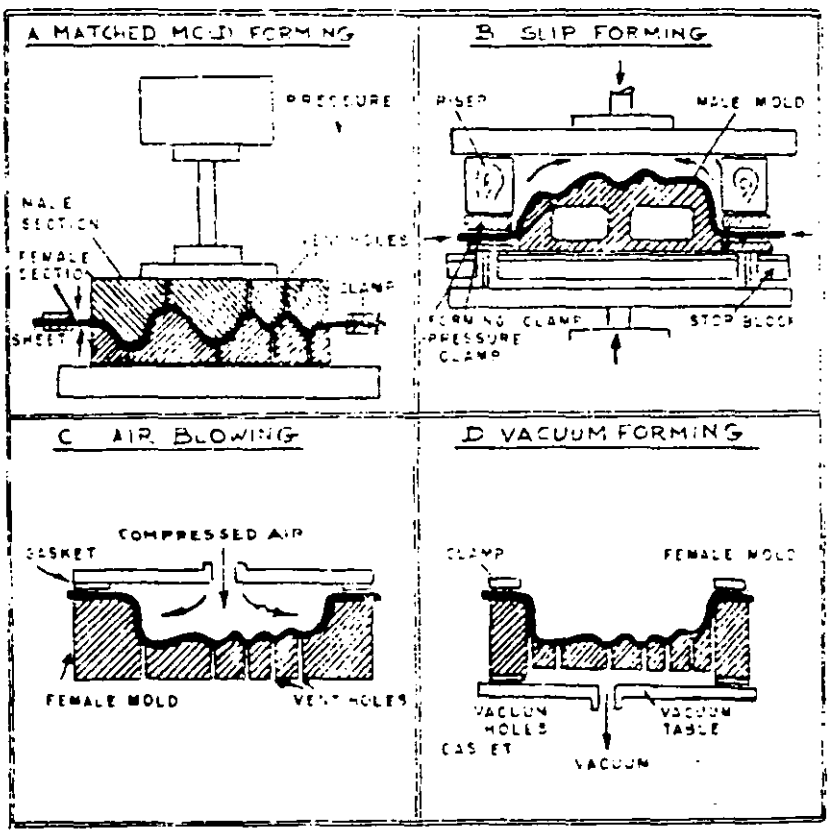

Figure 4.1[140] *The four basic methods of thermoplastic sheet forming*

4.5 Heating the Thermoplastic sheet

There are three main methods of heat transfer, conduction, convection and radiation.

Direct conduction is the most efficient way of transferring energy to the plastic sheet but it is rarely used[26] due to difficulties with:

(i) ensuring intimate contact without compressing the plastic sheet
(ii) heating the sheet without sticking to the plates and
(iii) transferring the sheet from the heater to the mould

As a result, much effort has been given to improving convection and radiant heating.

Convection is usually reserved for heating large heavy and thermally sensitive sheet stock used in batch type presses. The sheets are racked on horizontal table in a large oven, and heated air is forced around and between the sheets. The controlling factor is the convective heat transfer coefficient between the moving air and the plastic sheet surface. On attaining the desired temperature, the sheet is transferred to the forming station. Although, convection heating is relatively easy to apply to the sheet, the longer cycle times normally makes it economically unattractive for all but special cases.

Radiant heating is the most popular and economical mode of heating plastic sheet. An analysis of radiant heating and absorption by polymers has been reported by Throne et al [144]. They showed that radiant heating is at least twice as efficient as convection heating, even at relatively low heater temperature.

An important step to efficient thermoforming is the ability to bring the plastic sheet to a uniform and even forming temperature. If there are hot spots in a plastic sheet, there would be variation in strength at the hot and cool spots. The plastic will stretch more (or less) at there points of temperature variation.

There are several alternatives to moderating this extreme temperature differences within a sheet. The most obvious is to reduce heater temperature. Another way described by Platzer [141] is the use of shield screens. Progelholf et al [144] suggested 'on-off cycle' of the heaters. This has been found to be limited to the continuous sheet forming process. Thus the heat 'soak' during its residence time in the 'heat off' region, allowing the temperature profile partially to equilibrate.

Forming Temperatures [142]

All thermoplastic materials have specific processing temperatures. Basically, these ranges apply regardless of how the material is processed.

(i) Set Temperature: The temperature at which the part may be removed from the mould without warpage. It is usually below the softening point of the plastic.

(ii) Lower Processing Limit: This represents the lowest temperature that the material can be formed without creating processing difficulties. Materials processed below this limit may have excessive molecular orientation (unidirectional) which later could cause warpage, brittleness or other physical changes in the finished article.

(iii) Normal Forming Temperature: Temperature at which the sheet should be formed under normal operation. This temperature should be uniform throughout the sheet.

(iv) Upper Limit: The temperature point where the thermoplastic sheet begins to degrade or becomes too fluid to thermoform.

4.6 Process Variables

The thermoforming process has many variables which affect the appearance, quality, size, and material distribution in the formed part.

Variation in Plastic Sheet Feed Stock

(a) Sheet Thickness: Thickness variation in plastic sheet could result in non-uniformity in heat distribution, consequent non-uniformity in thickness in the formed part. When variations in thickness are found within a blank, a slower, and longer heating cycle, allowing heat to soak through the thick and thin spots is undertaken in practice. Good finish is improved with uniformity in temperature throughout the sheet.

(b) Sheet Viscosity or Melt index: Wide variation in molecular weight of the sheet from batch to batch leads to variation in melt viscosity which can create forming problems. This is particularly true of polyolefins [140]. In general, high molecular weight requires higher forming temperature (long forming cycles). Increasing molecular weight reduces crystallization rate in crystallizing polymers, but it improves impact strength, stiffness, and, increases moulding shrinkage. Changes in Mw of PETP will lead to different rates of crystallisation.

(c) Sheet Density: Increasing density of an amorphous material increases tensile strength, hardness and stiffness by reducing the free-volume proportion. In crystallizable polymers, increasing density implies increasing crystalline content in the sheet. This increases the forming temperatures and the tendency for sagging and general heating difficulties.

(d) Sheet Orientation: Some orientation is usually imparted to a sheet during extrusion or calendering which affects forming operations since orientation may relax (sheet will shrink) when $T > T_g$. Generally, some orientation in the product is desirable, but orientation in the pre-formed sheet should be minimised. With orientation, close tolerance parts can be produced, as long as the strain remains consistent from batch to batch. Orientation in polymer materials improve tensile strength and in strain crystallizable polymers, it improves the barrier properties. Because of the improved properties thinner films can be used to provide a rigid part. A good example is biaxially oriented PETP film used in packaging.

(e) Sheet Temperature: To achieve the fastest cycle, the sheet is formed on the lower side of the forming range for the particular material.

The choice of forming temperature is influenced by the type of draw. For simple draws, the lower forming temperature is chosen, where fast vacuum is used. Normal to deep draws, require temperatures between the normal and upper forming temperature of the particular sheet being shaped.

Mould Variables

Several different materials are employed in making thermoforming moulds, as discussed later. The various elements of the mould that affect forming characteristics are discussed here.

(a) Vacuum holes: proper air evacuation assists material deformation in the desired direction and uniform wall thickness. In vacuum forming, fast mould evacuation enhances uniform thickness in the formed part [141]. Slow evacuation causes the sheet first contacting the mould to chill faster than the balance of the sheet; producing thin sections or incompletely formed parts.

In general, deep corners require accelerated evacuation (ie close spacing of vacuum holes) to ensure the draw of material into corners. The diameter of the vacuum holes should be .25 - .6 mm for PE sheeting for instance, .6 - 1 mm for other thin gauge material and may increase to 1.5 mm for heavier rigid materials which are unlikely to be drawn into the holes. Where fine detail is needed, vacuum hole separation is as close as 5 mm.

(b) Mould Surface. In thermoforming, the finished parts acquire the details of the mould surface. A matte finished mould yields dull finish to the part. A highly polished mould gives a glossy part and improves ejection of finished article.

(c) Mould Temperature: The temperature of the mould surfaces plays an important role in thermoforming. Normally, mould temperatures are just below the 'set' temperature or the heat distortion point/T_g of the material.

Mould temperature affects the appearance of the formed part, and length of the forming cycle and mould definition of the finished part. Increasing mould temperature increases part shrinkage and cycle time of the forming technique (ie decrease cooling rate).

(d) Radii and Angles: Items with sharp corners can be made but are usually avoided because of excessive thinning in the part. In order to reduce excessive thinning at the corners, a generous radius is allowed for within the design limit of the shape desired.

Plug Variables

'Plugging' involves the use of 'plug-assist' to carry sheet material into a mould cavity and/or to stretch the portions of the sheet which forms the sides of the finished part.

(a) Plug Shape: The plug generally conforms closely to the mould shape but is smaller in size. Also generous radii are allowed at the plug corners. This facilitates stretching of sheet on the surface of the plug.

(b) Plug Material: The choice of material depends on the type of sheet material to be formed. If the plug is to be heated, aluminium is usually used because of its high thermal conductivity; however, if the plug is not to be heated, a wooden plug coated or covered with flannel is used.

(c) Plug Temperature: Surface temperature is maintained at or just below the temperature of the sheet being formed. Although the plug temperature is usually not critical as is the mould, too low a plug temperature will cause 'chill' marks and thick sections on the finished part. Coating the plug surface with PTFE avoids sticking and assists slippage.

(d) Plug Speed and Amount of Vacuum: Normally, vacuum bleed in the mould begins when the plug first touches the sheet (bubble). Plug speed must balance the rate of evacuation. If the plug speeds exceeds the vacuum bleed, air compression in the mould cavity is increased. A 'roll of material' follows the plug into the mould cavity, thus keeping the sheet from touching the relatively cold mould until the plug reaches the extremity of the mould.

Chapter 5

Assessment of Formability

5.1 Introduction

The tensile drawing behaviour of PETP over a range of thermoforming temperatures has been discussed in Chapter 3; the strain hardening indices were related to formability. This chapter assesses the formability of PETP sheet at the chosen temperature in the vacuum forming mode.

A brief description of thermoforming tools is given including the guidelines for selection of material and design of moulds.

5.2 Thermoforming Moulds

One of the most attractive features of the thermoforming process is its low tooling cost, because of the low pressures involved compared to other methods of processing plastics [142, 146].

Several types of materials have been used as moulds for thermoforming. The choice of material depends primarily upon the quantity and quality of formed items to be produced.

The most common mould materials are plaster, wood, cast phenolics, epoxies and urethane resins, sprayed metal, cast aluminium and machined metals (eg steel).

Wood and plaster moulds are often used for experimental, prototyping or short runs. They are perhaps the cheapest because of the ease of fabrication, they also require little or no finishing. However, wood and plaster tend to distort or shrink in service because of heat, and can be fragile[146].

Cast phenolics and epoxy resins have been used for medium runs. They exhibit good dimensional stability and good abrasion resistance and they may have high polished surfaces. Heating and cooling channels could be made behind the finished surface during mould preparation[147].

For production runs, metals or metal-surfaced moulds are used. They have the advantage of dimensional stability, good surface finish, abrasion resistance and very durable. Unfortunately, they require relatively lengthy and costly manufacturing time. The most common metal mould used is cast aluminium. It provides a good combination of durability, light-weight and thermal conductivity as, well as ease of fabrication. Cooling or heating lines, can be located relatively far apart because of the high thermal conductivity.

Before choosing the material for the mould, the role of the mould must be considered. Its primary function is that of the form into or onto which the sheet is drawn. In addition, it serves to remove heat from the sheet. The primary objective of

mould cooling is not necessarily to reduce sheet to room temperature. The mould must remove enough heat from the sheet to cause the sheet to retain the mould form when it is removed. In general, the thermal capacity of a mould is very large when compared with that of the sheet, and thus the mould remains nearly isothermal during the cooling stage. However, for continuous runs, the slow cooling of plaster, wood, plastic and similar poorly conductive materials requires that such moulds be cooled by cold air or similar means.

The shape and details required in a formed article influence the type of mould used. The location of fine detail often determines whether a male or female mould is used.

In general, female moulds provide easier release, are less likely to get scratched, (or damaged), produce thicker and stronger rims in containers, require smaller sheet blanks and provide the sharpest definition on the outside of the objects. Female moulds suffer from the disadvantage that they produce containers with excessive thinning at the corners; however, good plug-assist design can largely eliminate this problem.

Male moulds are used for reproducing find details on the inside of formed containers or articles. They are generally cheaper to produce. Male moulds are unsuitable for multicavity mouldings; female moulds are usually preferred. Formings on male moulds are difficult to release.

All thermoforming moulds used with vacuum or air pressure techniques require holes or channels or ducts for the evacuation of air or the buildup of pressure. The holes or slits diameter range between .2 - 1mm to avoid visible marks on the surface of parts [141]. Careful placement of the holes is required for fast, efficient air flow during the forming operation.

5.3 Mould Design

The main aim in this part of the work is to thermoform containers of volume range 200-500cm^3 similar to cans for carbonated drinks. Since the fine details are required on the outside of such containers, the female mould design was chosen. The limited supply of PETP sheet (restricted range of sheet gauge) further justified the choice since it is the more economical in terms of material usage. Figs 5.1 and 5.2 are the sketches of the female mould and plug used in this work.

The mould was machined from cast aluminium and designed to have three detachable sections so that different draw ratios could be formed as shown in fig 5.1. Although the extension ratio obtained at the thermoforming temperatures from the tensile test is in excess of 5 before failure, a limit of forming draw ratio of 2:1 was considered in order to avoid excessive thinning in formed parts. The first segment of the mould form a 1:2 draw ratio, segments 1 and 2 give 1:1 draw ratio whilst the three segments together produce 2:1 draw ratio. The details of the design are described later.

To maintain constant mould temperature during the forming operations, fluid heating channels were drilled into the mould. It is essential to heat the mould in order to reduce the 'chill' effect on the PETP sheet being drawn. Heating channels were also drilled into the plug (fig 5.2) head only, because it is the part of the plug that comes into direct contact with the sheet. The length of the plug was adjustable to conform to the draw ratio desired.

A simple conical shape of 2.5^o draft angle was chosen for easy fabrication and analysis to determine formability of PETP sheet. The dimensions of each segment of the mould is given in table 5.1. Base diameter was 70 mm.

Segment No	Depth (mm)	Rim Diameter (mm)	Draw Ratio
1	35	73	1:2
2	70	76	1:1
3	140	82	2:1

Table 5.1 Dimensions of the female mould

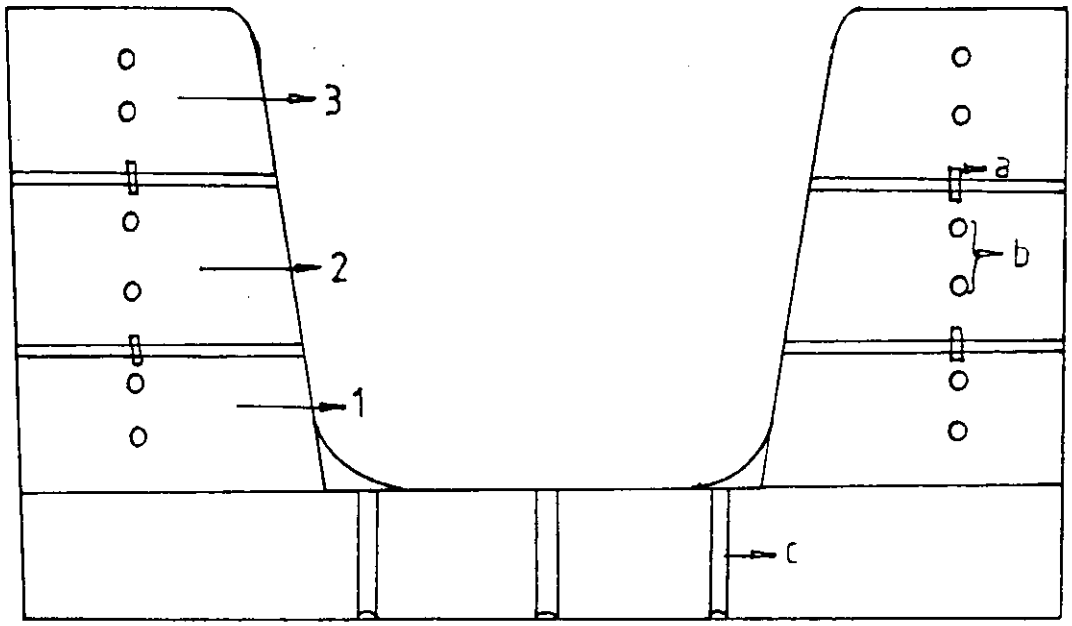

Figure 5.1 *Schematic view of the female mould*
1,2,3 - segment numbers ; a: screw fastener ;
b: heating channels ; c: vacuum channels

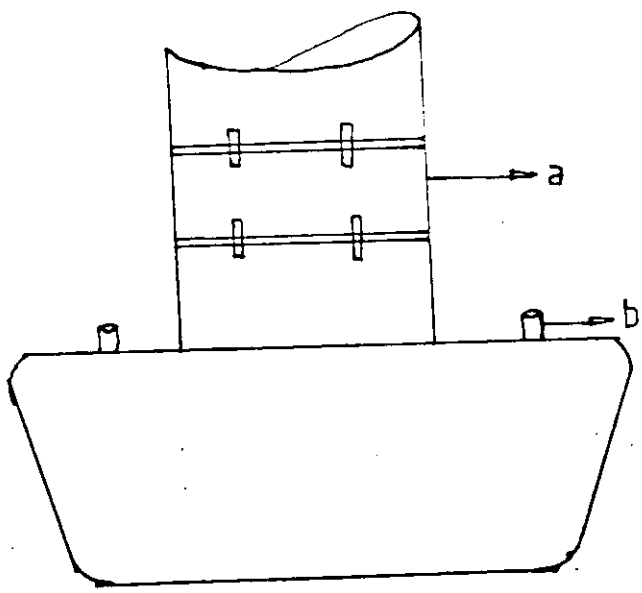

Figure 5.2 *Schematic view of the plug -assist*
a: plunger ; b: heating channel

5.4 Brief Description of the Thermoformer Used

The 'Hanwood' thermoformer, a semi automatic machine, was used; push buttons are available so that the set-up and various time cycles for the specific forming can be tested manually. After the process has been smoothed out, the machine can be switched to automatic control.

The heating system consist of 'sandwich radiant heaters' which heat both sides of the PETP sheet simultaneously. They reciprocate into position when the sheet is clamped and the equipment activated. The top heater was divided into three zones as shown in fig 5.3 below.

The power output of the heater banks in each zone can be controlled separately, a similar facility was not available for the bottom heater. In addition there are reflectors at the edges of the top heater plates to reduce heat loss. A close control of the sheet temperature was achieved.

Between the pump and the mould, there is a tank which is kept evacuated so that the suction required comes from the tank rather than directly from the pump.

The plug position is controlled pneumatically, while the forming table is controlled by hydraulics.

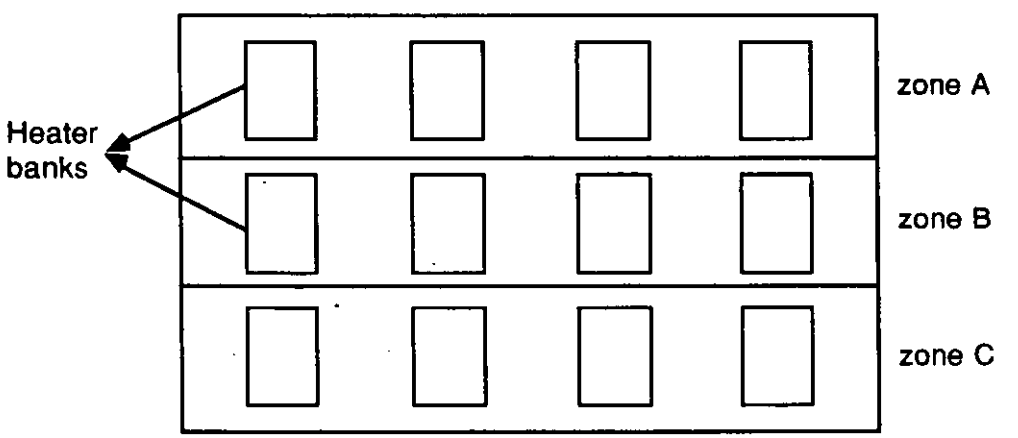

Figure 5.3 Heater banks arrangement in 'Hanwood' Thermoformer

5.5 Experimental

Exploratory formings were made in the simple vacuum forming mode into a female mould, (fig 5.1). Two draw ratios (draw ratio is defined in terms of ratio of the depth (h) to the minimum width (w) of the container) of 1:1 and 2:1 were investigated for PETP sheet.

Two main criteria were considered before determining the mould temperature:

(i) it must be high enough to prevent chill marks on the forming; and

(ii) at the same time low enough for the sheet to set and retain the mould form.

Since PETP T_g is 70 °C, mould temperatures at 60 °C was considered appropriate.

'Conair' circulating water heater with temperature regulator was used in heating the mould through the heating channels drilled into the aluminium mould.

In order to minimise friction, the inside of the mould was smeared with a thin film of silicone grease. This was necessary because PETP sheet has a tendency to stick to surfaces at elevated temperatures.

To determine the temperature-time profile of the sheet, chromel-alumel (Cr.Al) thermocouples were embedded on both surfaces of the sheet and connected to a voltage-time recorder.

The radiant heaters were adjusted to emit uniform heat. The voltage-time profile of the sheet during heating was recorded for 60 seconds. A voltage-temperature conversion chart was used to determine the temperature with time. The temperature-time profile determined three times is shown in fig 5.4. Time to attain selected thermoforming temperatures derived from the profile is shown in table 5.2.

Sheet Temperature °C	Time sec
80	25.5
90	30.0
100	36.0
110	41.0
120	48.0

Table 5.2 Time To Attain Forming Temperature

Rectangular sheets of approximately 120 x 140 mm were pre-printed with the pattern shown in fig 5.5 using a black ink with a specially designed rubber stamp. Radii of the concentric circles divided into quadrants are given in table 5.3. the grid was used in determining the biaxial deformation in the plane of the sheet. Using axial symmetry as shown in fig 5.6, the principal deformation ratios are defined as follows:

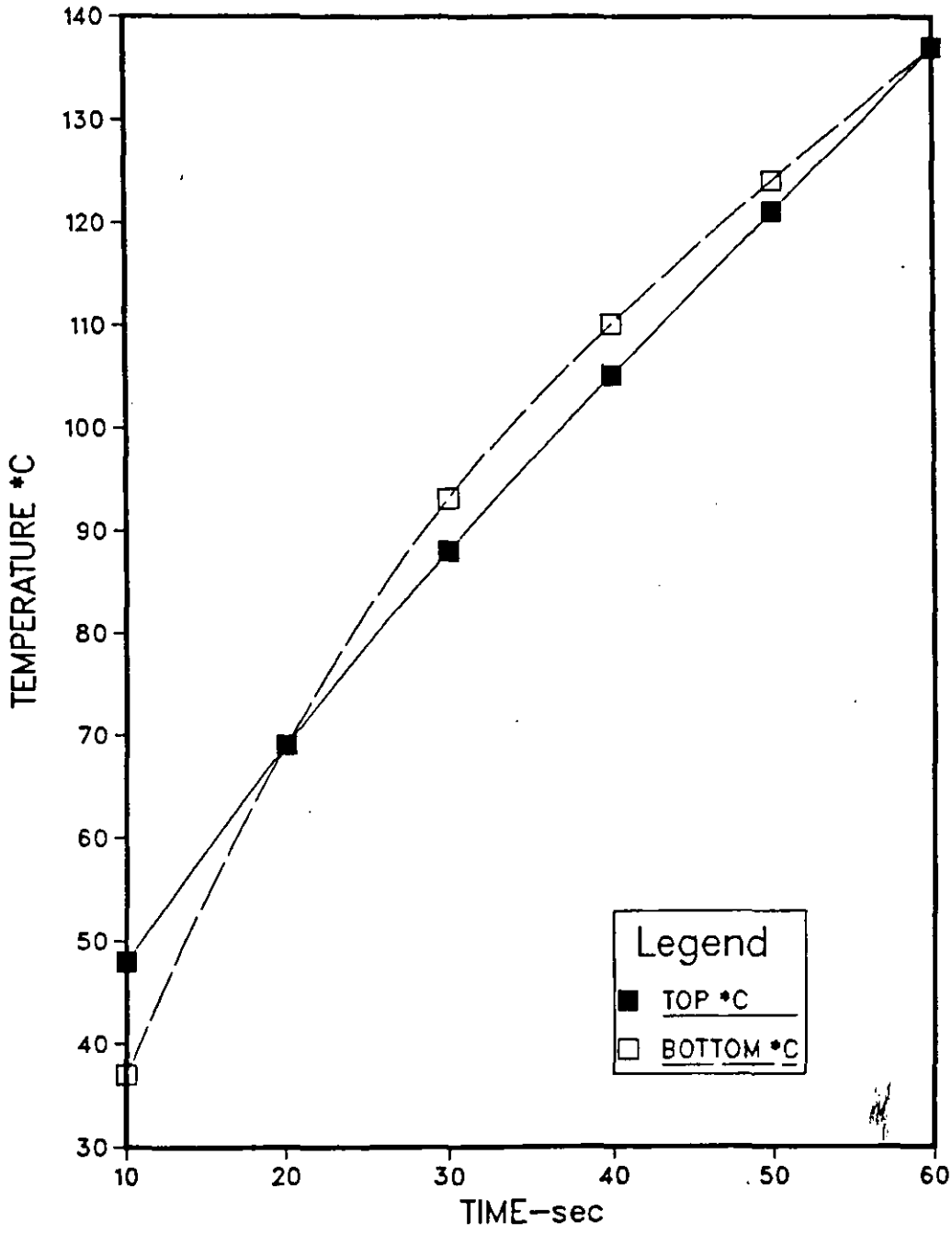

Figure 5.4 *Temperature profile of the top and bottom of the PETP sheet exposed to 'sandwich heaters'*

$$\text{Extension ratio, } \lambda_l = ds / dr_o = dr / dr_o \sqrt{1+(dw/dr)^2} = l/l_o \quad \text{---5.1}$$

where l_o = 5 mm, the separation between the concentric circles

l = the separation between concentric circles on the containers.

$$\text{Hoop strain, } \lambda_h = r/r_o \quad \text{----------5.2}$$

where r_o = initial radius of each concentric circle

r = final radius of each concentric circle in the containers.

$$\text{Reduced thickness, } \lambda_t = t / t_o \quad \text{----------5.3}$$

(strain perpendicular to the two directions)

where t_o = blank thickness

t = forming wall thickness

For equal biaxial deformation $\lambda_l = \lambda_h$.

The average thickness of PETP sheet was 1.45 mm ± 0.02. Average thickness of each segment of concentric circles on the containers was measured. Table 5.3 lists the numbers of radii of the circles from the centre. The relative position of each circle on the formings, assuming uniform deformation, is defined as "Designated Location" (see figs 5.7) on the containers.

The distance between consecutive circles was measured at the four points where the quadrants divide each circle and the average was recorded in order to determine extension ratio `(equation 5.1).

The average thickness in each forming assuming a perfectly uniform deformation is as follows:

$$t = \frac{\text{sheet volume (assuming constant volume)}}{\text{Total surface area of the mould}} \quad \text{---------- 5.4}$$

The mould was taken as Frustum of a cone:

$$\text{Total surface area} = \pi \left[R_2^2 + (R_1 + R_2) \sqrt{(R_1 - R_2)^2 + h^2} \right] \quad \text{——— 5.5}$$

where R_1 = Radius of the mould cavity

R_2 = Radius of mould base

h = Depth of the mould

sheet volume = $\pi R^2 t_b$ ---------- 5.6

where R = Effective clamping radius over the mould cavity
t_b = blank sheet thickness

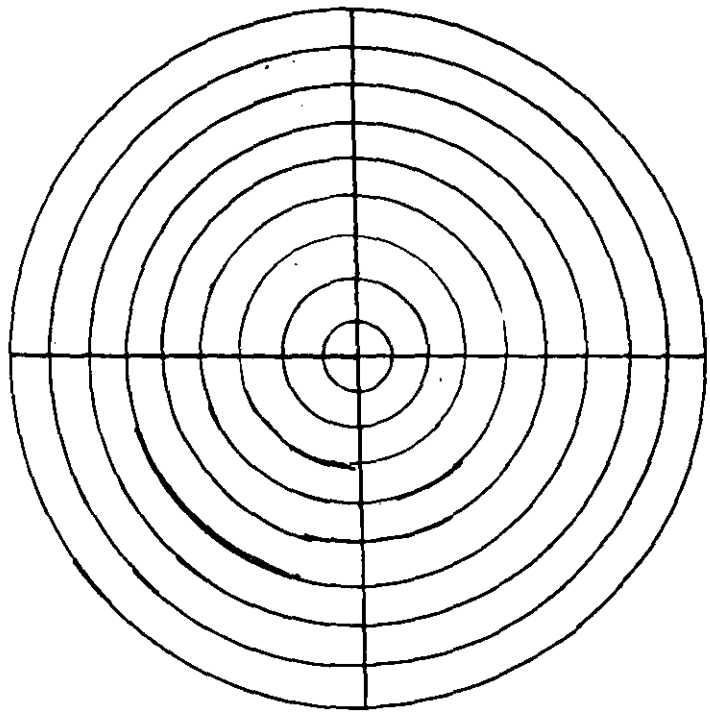

Figure 5.5 Printed pattern on the rectangular sheet

Circle number	Radius (mm)
1	5
2	10
3	15
4	20
5	25
6	30
7	35
8	40
9	45

Table 5.3 Radius of each ring from the centre outwards

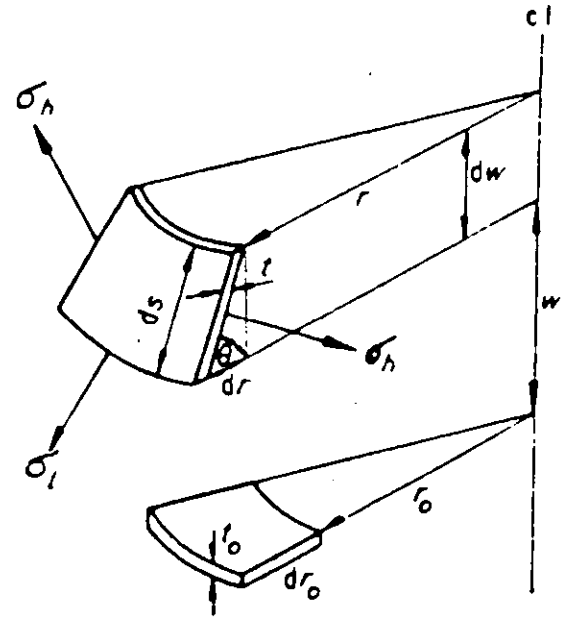

Figure 5.6 Axial symmetry of vacuum forming

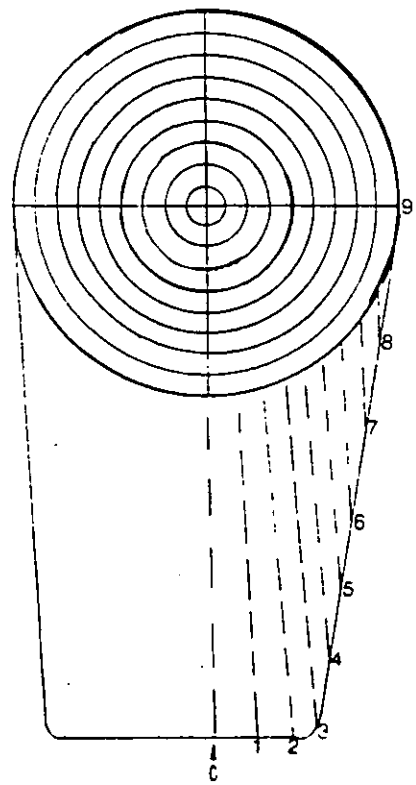

Figure 5.7 Designated location of the concentric rings assuming uniform deformation

5.6 Results

The deformation pattern of the sheet at the draw ratios considered (ie 1:1 and 2:1) is presented in term of reduced thickness (t/t_o) distribution and the extension ratio (l/l_o) distribution as a function of Designated Location of the concentric circles on the formings. Unfortunately, the deformation of PETP was not perfectly symmetrical, thus, the "Designated Location" of each circle does not represent their actual position on the containers. As a general guide, the first two circles (1 and 2) form the base of the containers while the remaining circles (3 - 9) form the wall of the containers.

Fig 5.8 shows that reduced thickness decreases sharply towards the centre (bottom) of the shallow formings at all the temperatures. The extension ratio (l/l_o) fig 5.9, gives a better illustration of the effect of sheet temperature on the deformation pattern. The extension ratio at the centre of the sheet (ie circle 1) increases with increasing temperature. There is no visual difference in the appearance or shape of the formings at the varying sheet temperatures shown in fig 5.10.

Fig 5.11 is a plot of thickness (t) as a function of the depth into the shallow containers. The thickness distribution is generally poor; up to 20 mm into the mould, the thickness distribution at all the temperatures is the same, however beyond this point thickness distribution is influenced by the sheet temperature. The variation in thickness increases with increasing sheet temperature.

The deformation behaviour in deep containers is shown in figs 5.12 and 5.13. Reduced thickness distribution in fig 5.12 shows that at the lower temperatures (80 and 90°C), there is a gradual thickness reduction especially within the first 6 segments of the concentric circles. With increasing temperature, the reduced thickness distribution deteriorates. The longitudinal strain distribution, fig 5.13, show the influence of sheet temperature much more clearly. At the lower temperatures, there is even deformation of the sheet where nearly even extension ratio values are recorded, except near the rim where the extension ratio decreases. As observed previously, the deformation pattern deteriorates with increasing sheet temperature. Fig 5.14 show the visual effect of sheet temperature on the forming characteristics. At the lower temperatures (eg 80 °C), the container is not completely drawn, but at the higher temperatures the container is fully deformed. The plot of thickness (t) as a function of depth into the deep containers is presented in fig 5.15. The effect of temperature on thickness distribution is as earlier observed.

The average thickness for the shallow containers determined by equation 5.4 is 0.28 mm while the average thickness for deep containers is 0.21. These values are reflected in figures 5.11 and fig 5.15 by the horizontal line which represents the theoretical level for uniform thickness in formings.

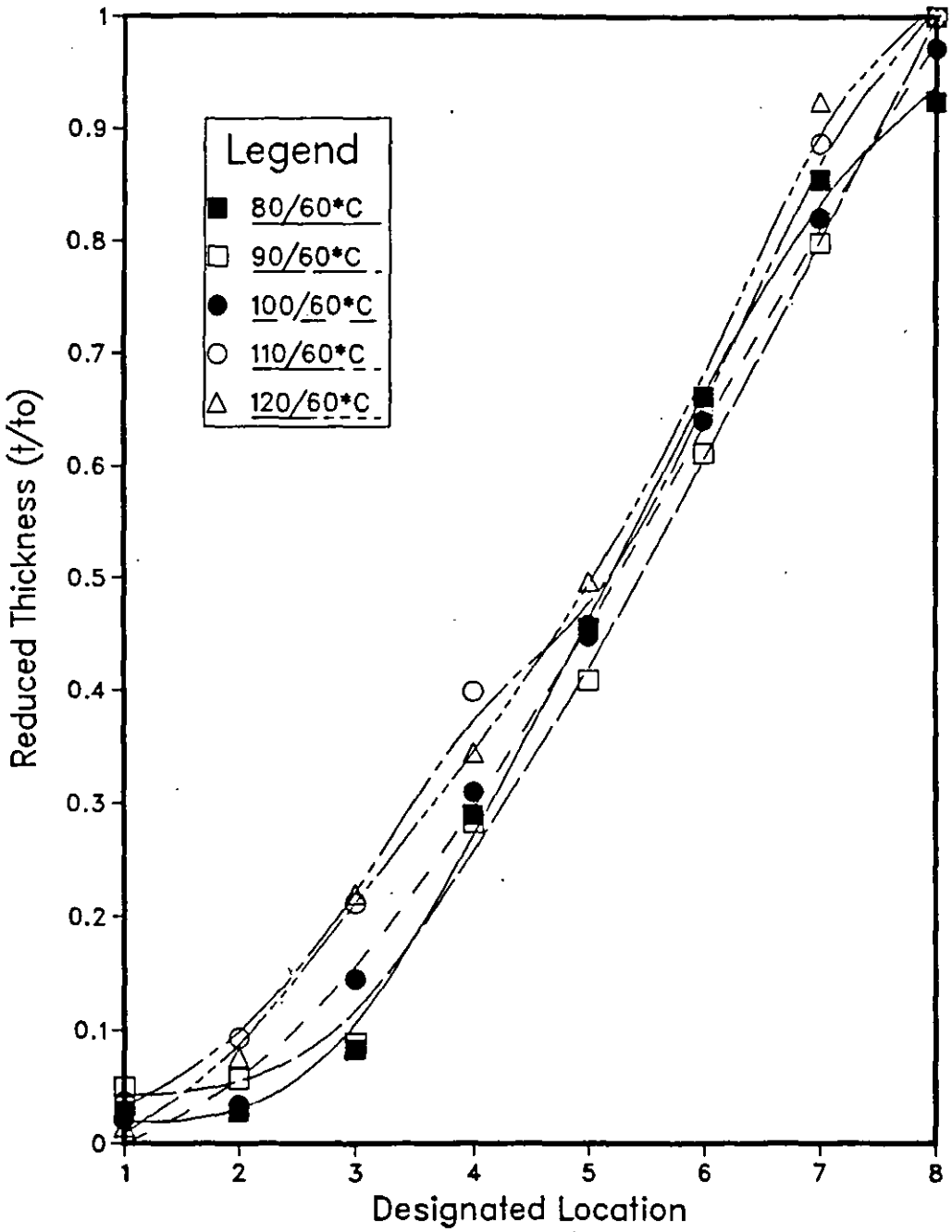

Figure 5.8 *Reduced thickness distribution in shallow containers as a function of 'Designated location' of the rings*
Legend:sheet / mould temperatures

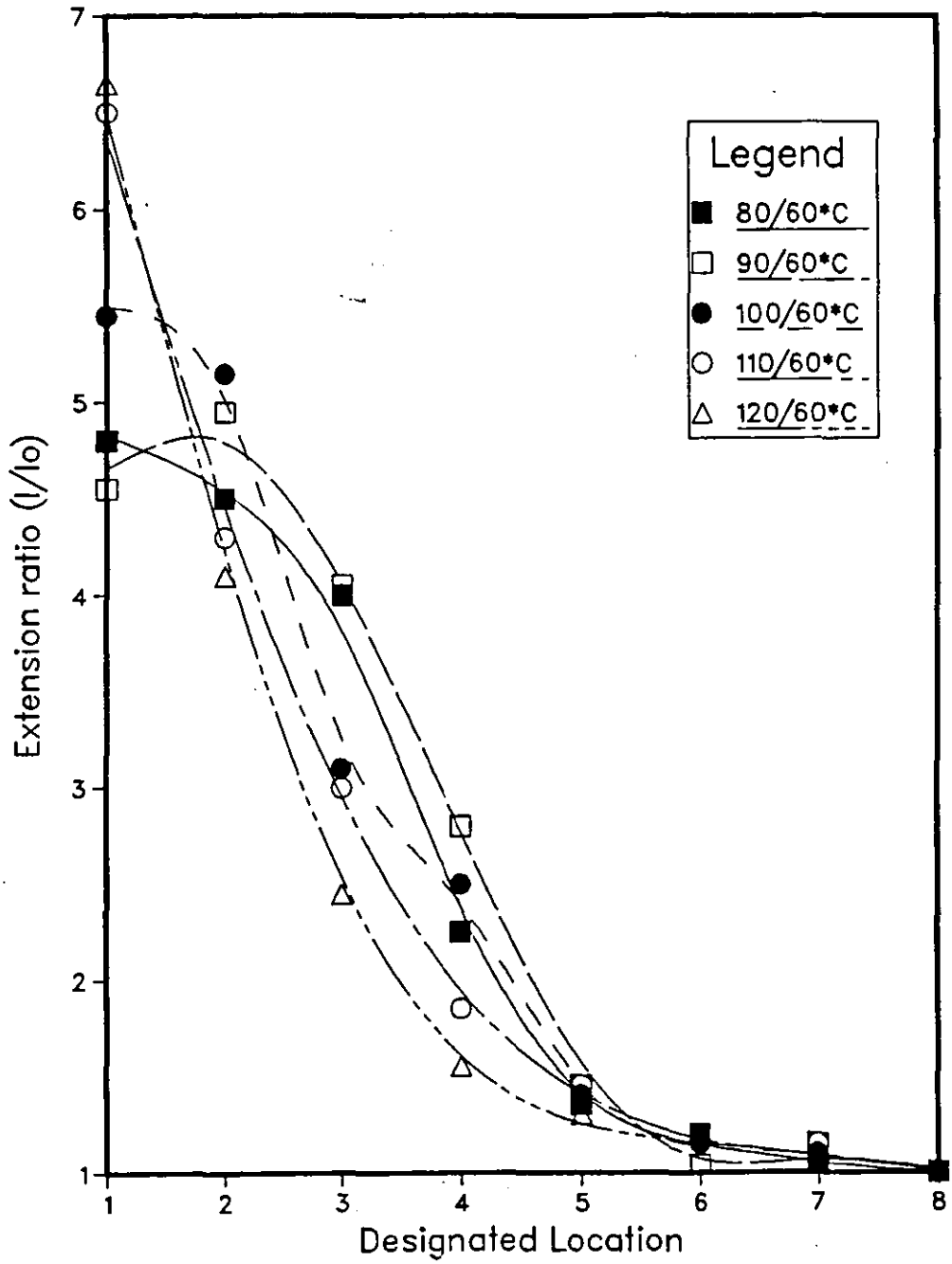

Figure 5.9 *Extension ratio distribution in shallow containers as a function of designated location' of the rings. Legend: sheet/mould temperatures*

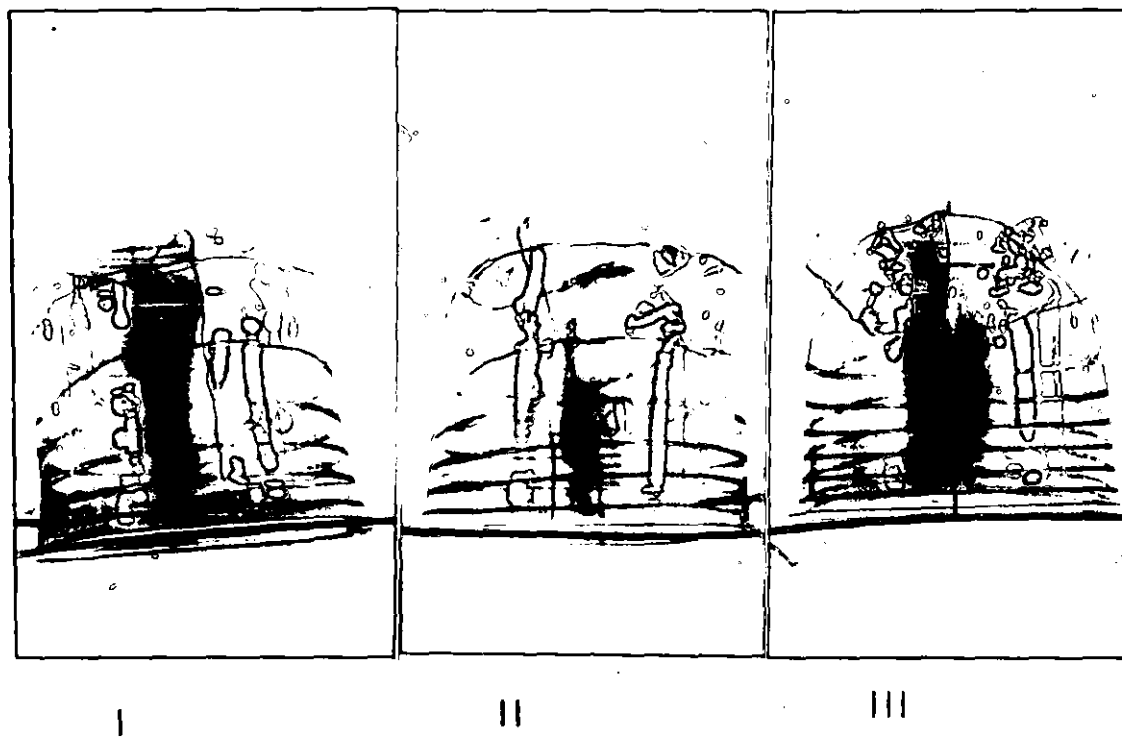

Figure 5.10 *Photograph of some shallow vacuum formed containers*
I = 80°C ; II = 100°C ; III = 120°C

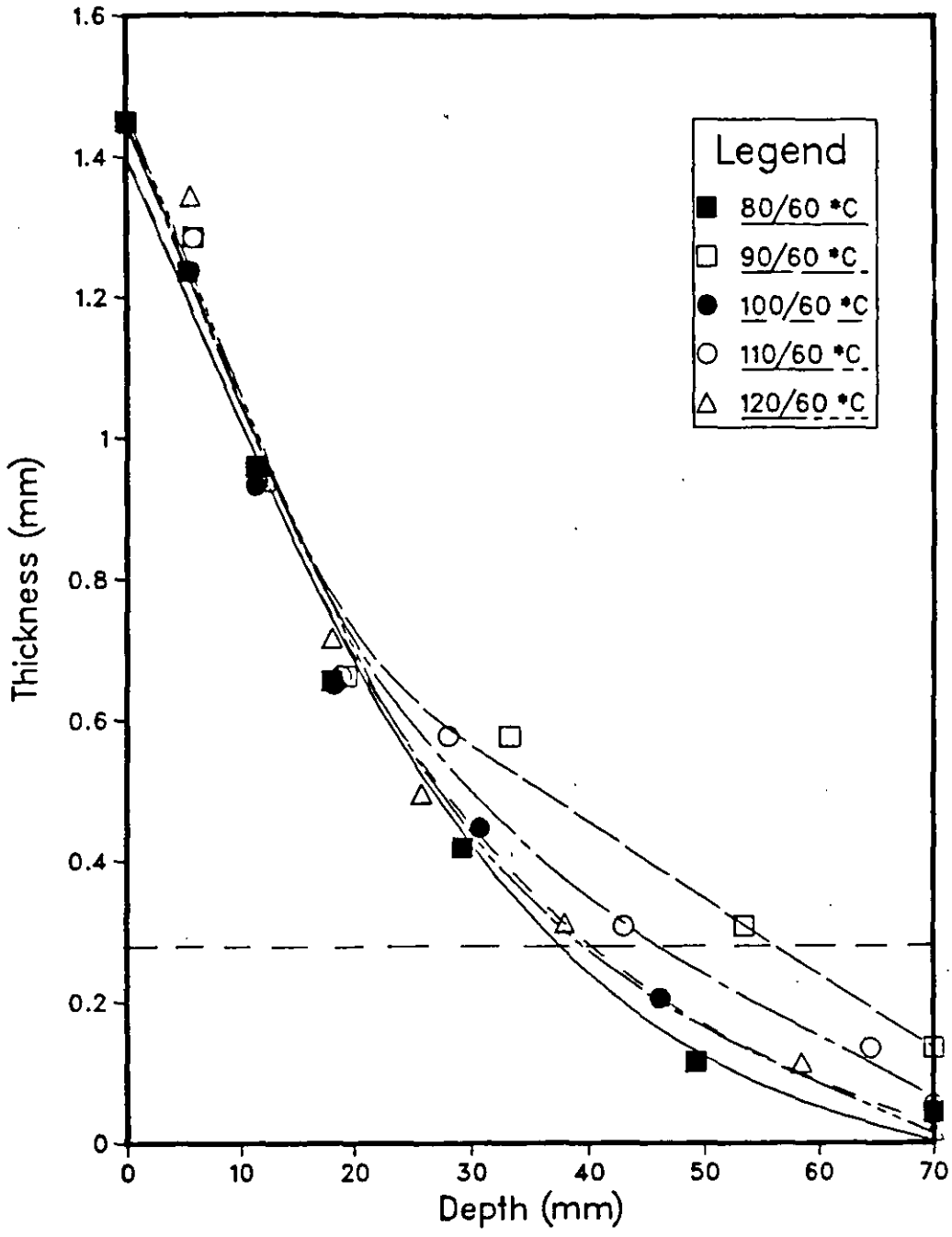

Figure 5.11 *Thickness distribution (shallow containers) as a function of depth. Legend: sheet/mould temperatures*

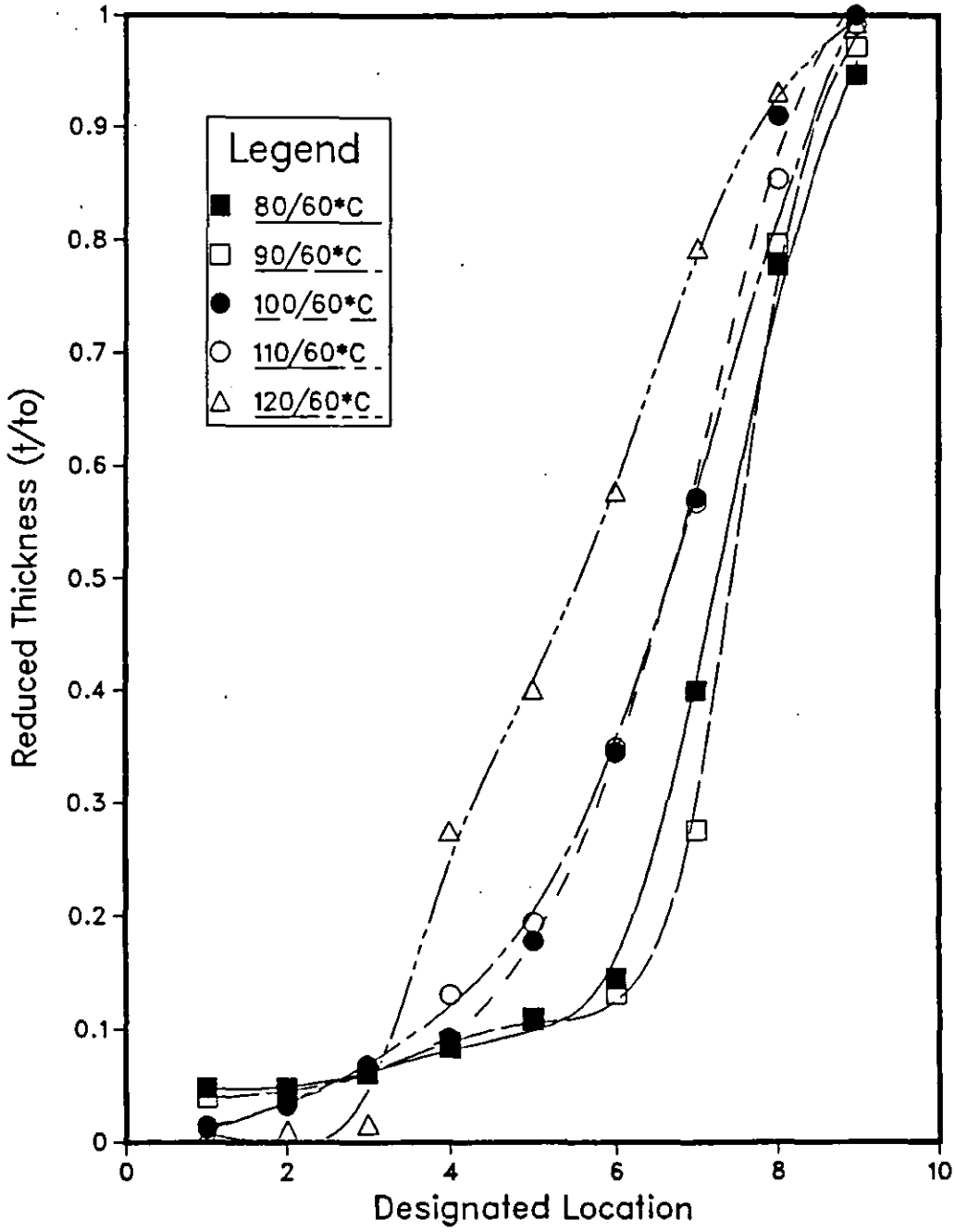

Figure 5.12 *Reduced thickness distribution (deep containers) as a function of 'Designated location' of the rings.*
Legend: sheet/mould temperatures

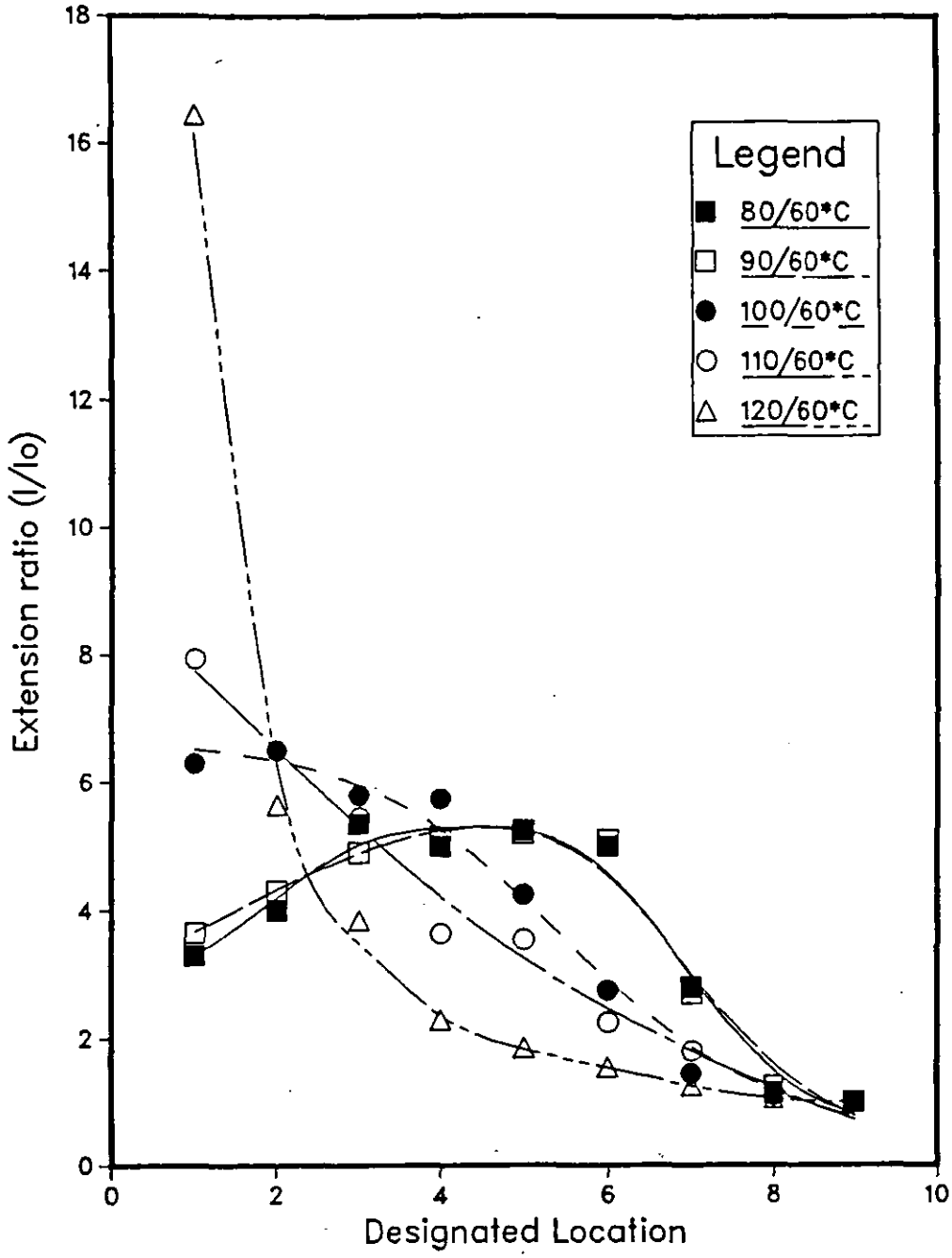

Figure 5.13 *Extension ratio distribution (deep containers) as a function of 'Designated location' of the rings.*
Legend: sheet/mould temperatures

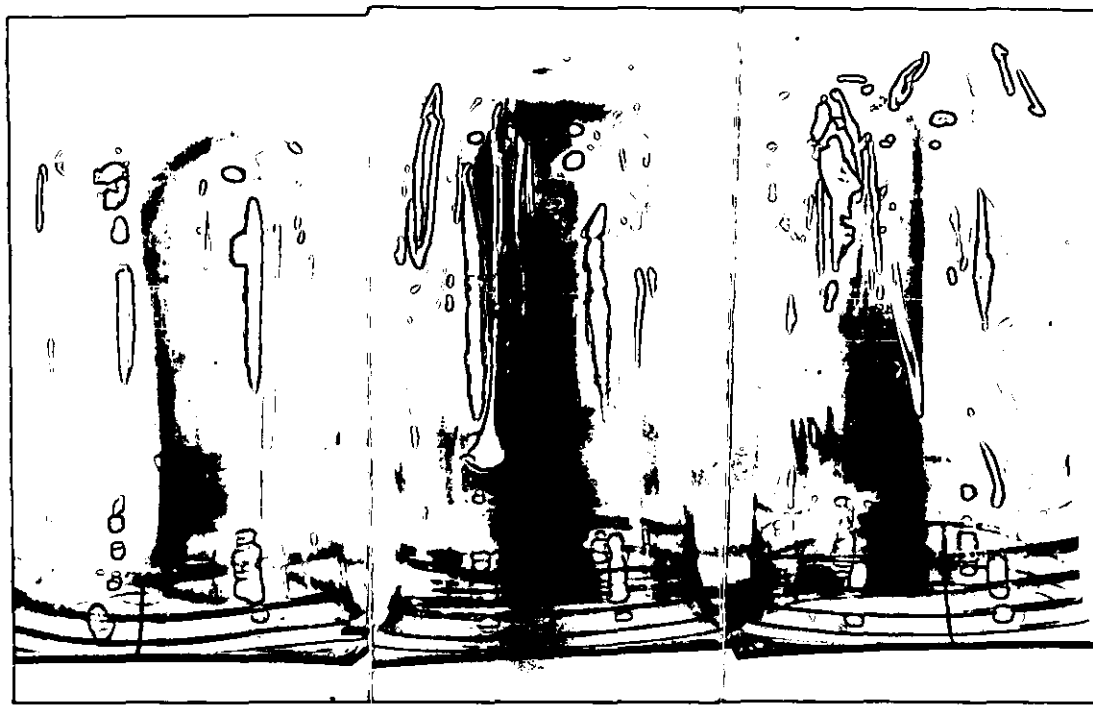

Figure 5.14 *Photographs of some deep vacuum formed containers*
I = 80°C
II = 100°C
III = 110°C

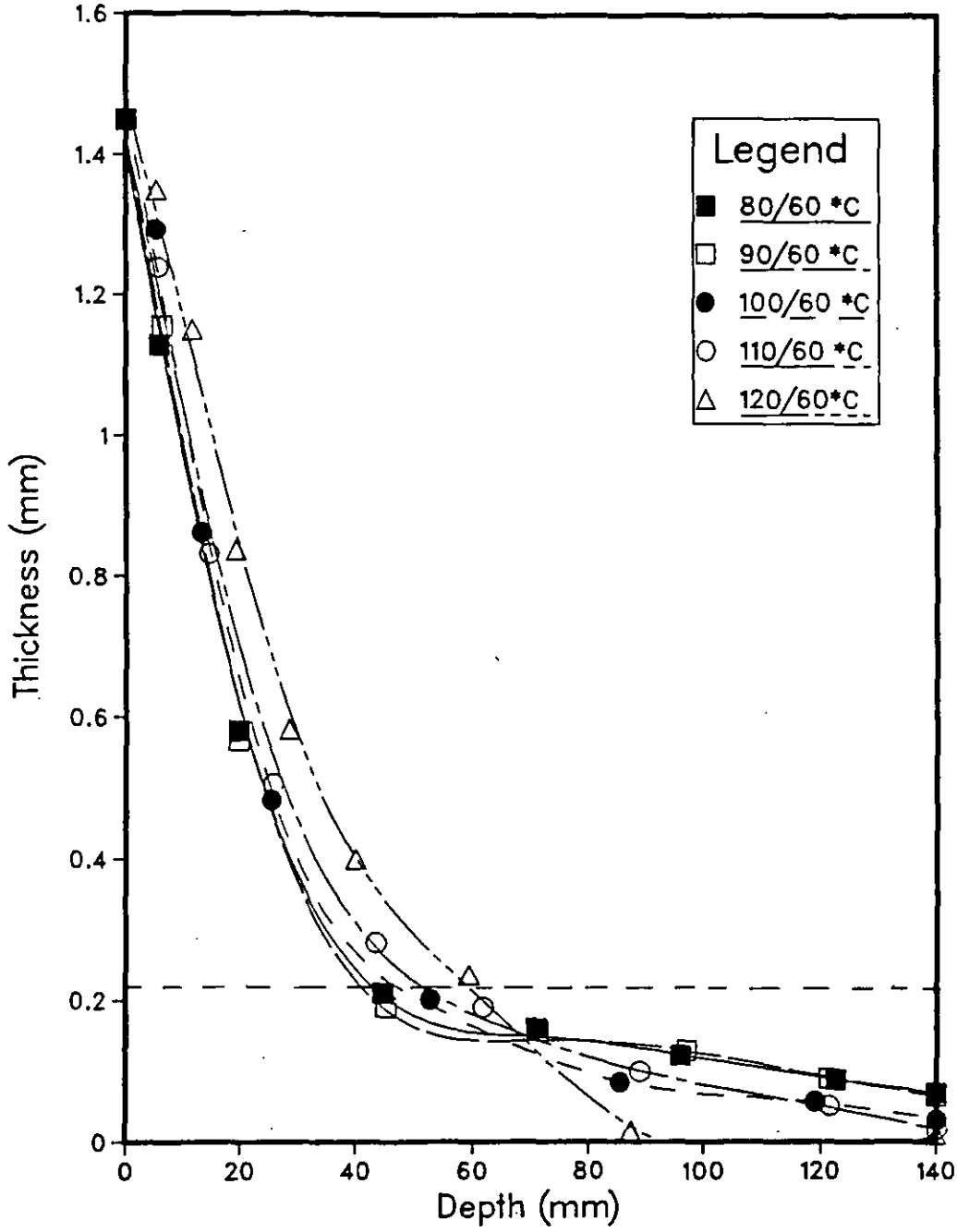

Figure 5.15 *Thickness distribution (deep containers) as a function of depth. Legend: sheet/mould temperatures*

5.7 Discussion

It must be stated that the essence of this part of the work is to relate forming characteristics to the stress-strain behaviour of PETP in the forming region (chapter 3). In calculating the strain during vacuum forming biaxial deformation is assumed. Thus, the average strain in vacuum forming may be conveniently defined as the ratio of the total surface area generated to the original surface area of the sheet over the mould cavity:

$$\varepsilon_{vf} = A - A_o / A_o \qquad \text{----------5.7}$$

where A = Total surface area of the mould

A_o = Total surface area of the blank sheet over the mould cavity

This definition is comparable to the one for uniaxial tensile strain ie $\varepsilon = l\text{-}l_o/l_o$

where l = final elongation

l_o = gauge length

For the shallow draw, the average strain (with respect to total surface area of the mould) is 1.10 and for deep draw container the average strain (with respect to total surface area of the mould) is 2.40 assuming uniform deformation of the entire sheet.

The results show that thickness and strain distribution in shallow draws is poor while at deep draws, the thickness and strain distributions are improved.From the analysis given above, the average strain in shallow draws is within the 'natural draw' (ε^N) regime of the stress-strain curve, while the average strain in deep draws is within the strain hardening regime. Therefore, the results confirm that strain hardening promotes uniform thickness in formed parts as predicted from the stress-strain analysis of PETP in chapter 3. In addition, for uniform deformation in formings, the average strain distribution must exceed the critical engineering strain of 2 for strain hardening effect.

Furthermore, the results show that forming within the temperature range 80 - 120 °C is possible at the selected draw ratios.In the shallow draws ,the sheet temperature seems not to have a great effect on thickness and extension ratio distributions. This is because the draw ratio is within the the natural draw regime where the behaviour of the PETP sheet is rubber-like and less temperature sensitive. However, increasing sheet temperature leads to poorer thickness and extension ratio distributions in the deep draws. This also proves that increasing temperature reduces the strain hardening effect (ie decreasing strain hardening indices with increasing temperature) thus uniform thickness is not promoted at the higher temperatures. The worst thickness distribution was obtained at 120 °C sheet temperature, because of loss of integrity in the sheet during deformationin deep draws. Therefore formings at the

lower temperatures (80 - 90 °C) exhibit high strain hardening effect which promote uniform strain and thickness in formed parts.

Figures 5.10 and 5.14 show the visual effect of sheet temperature on forming characteristics for some of the shallow and deep containers respectively. The incompletely filled mould at the lower temperatures (80 - 90 °C) for deep draws could be attributed to high stiffness (and high strain hardening indices) of PETP at these temperatures. Whereas, at the high temperatures where the sheet exhibits low strain hardening indices, complete formings were made. Therefore, higher stresses are required at the lower temperatures to produce fully formed containers.

The contrast between the theoretical horizontal line for uniform thickness over an entire forming and experimental results shown in figs 5.11 and 5.15 is due to inherent characteristic of vacuum forming: where the sheet is constrained at the rim and differential stress and strain are experienced from the clamping position to the middle of the sheet. At the deep draws there is a close correlation especially at the lower forming temperatures from about 40 mm into the mould. This is due to influence of the strain hardening effect,which promote uniform thickness in formed parts.

The above discussions have shown how sheet temperature affects thickness distribution in formings but we have not been able to assess the influence of mould temperature and its interaction with sheet temperature. In addition, we are not sure how much relaxation occurs as the material is stretched. Therefore, in the next chapter, the influence of thermoforming conditions on forming characteristics and properties will be investigated.

5.8 Conclusions

The practical evaluation of PETP formability has confirmed the proposals made after the simulation tests in Chapter 3, as follows:

(i) that PETP sheet can be thermoformed within the temperature range 80 - 110 °C.

(ii) that formings at draw ratios which correspond to average strain within the 'natural draw' regime of stress-strain curves will exhibit uneven thickness in formed parts; shallow draw containers exhibit poor thickness distribution at all the temperatures.

(iii) that formings at draw ratios which correspond to an average strain within the strain hardening regime of the stress-strain curve will exhibit more uniform thickness in formed parts. The results show that strain hardening promotes thickness uniformity in deep drawn (2:1) parts.

(iv) strain hardening equation ($\sigma = K\varepsilon^n$) is related to thermoformability of PETP. High strain hardening indices obtained at the lower temperatures (80 °C 'n' - 7.7, 90 °C 'n' = 7.0) promote thickness uniformity whilst low strain hardening indices obtained at the higher temperatures (3.3 and 3.1 for 100 °C and 110 °C respectively) reduce thickness uniformity in parts. Therefore, thermoforming of PETP is desirable at the lower temperatures (80 - 90 °C),especially for deep-drawn containers.

Chapter 6

Planning of Thermoforming Experiments

6.1 Introduction

The main thermoforming variables were discussed in Chapter 4; it is expected that different combinations of the variables will influence forming characteristics in different ways. Experiments on thermoforming have historically been on a trial and error basis; sheet temperature was regarded as the most critical factor. This procedure was followed in the exploratory work in Chapter 5, which confirmed the temperature sensitivity of PETP to deformation but failed to show the contribution of mould temperature to forming characteristics.

This report needs the study of the effect of thermoforming variables on forming characteristics of PETP. This is very important since most reports in the literature are on wholly amorphous plastics and little is known about thermoforming properties of crystallizable polymers such as PETP. In addition, the diversity of applications and market potential of thermoformed PETP makes a careful study desirable.

In classical research, each variable is inspected individually by holding the others stationary, varying each one in turn. This type of experiment can be very inefficient in terms of time and materials. This is especially important in this study because of limited supply of material. Furthermore, it can only provide a limited amount of information since it ignores interaction of variables.

A number of statistical techniques are available for co-ordinated planning of experiments. The choice of an appropriate design in this work was guided by the following objectives:

(i) Efficient use of experimental material.
(ii) Ability to determine quickly the effect of each factor.
(iii) Effect of interactions between separate factors.
(iv) Ability to evaluate the range of validity of the conclusions.

In the literature, there are relatively few reports that evaluate plastic processing by statistical methods. However, there are reports on statistical methods for optimizing compounding ingredients in rubbers [150-151] and PVC [152] Recently in our own laboratories, statistical analysis was used to optimize injection moulding conditions for polycarbonate [153].

The above criteria for the selection of statistical experimental procedures for thermoforming is satisfied by factorial experimental design, which is discussed in the first

part of this report .

In addition, the theories available for predicting thickness distribution in thermoformed parts will be explored, with the aim to explain the deformation processes during forming in the second part of the chapter.

Finally, the biaxial distortion of a 'printed on' grid and properties of the formings were investigated.

6.2 Choice of Factorial Experimental Design

An experimental design is a formalised experimental procedure. Each independent variable is called a factor and the number of possible forms of a factor is called the number of levels of the factor [154]. In this plan, each factor level is predetermined. A particular combination of one level from each factor determines a treatment. The experiment is called a **factorial experiment** when all or nearly all the factor combinations of interest are used.

A variety of designs exist ranging from the full factorial to a number of special purpose designs. The criteria for a good design include accuracy, reliability of the results, continuity of the result field, the importance of interactions, and ease of computational analysis.

The Rotatable Centre Composite Factorial Design (RCCFD) was selected from a set of standard methods. The selection was based on:

(i) successful application by other investigators in Institute of Polymer Technology LUT [150 - 153].

and (ii) its advantages over other designs (shown later).

The RCCFD is constructed by adding further treatment combinations to those obtained from two level factorial (2^p) design. The 2^p factorial enables an estimation of the first-order effects and all the interactions of the second order.

To the appropriate complete 2^p factorial are added $(2p + 1)$ supplementary points; one at the centre and the remaining $2p$ in pairs along the coordinate axes at $\pm a_1 \pm a_2 -- \pm a_p$ respectively. This makes the design centrally composite (symmetrical)[154,155].

The $(2p + 1)$ supplementary points are called the star points; their combination enables an estimation of the quadratic effects or 'lack of fit' of the model.

The values of a's can be chosen so that an orthogonal design can be obtained or to minimise the bias it can create if the true form of the response is not quadratic or to give the design the property of being rotatable.

Replication of runs at the centre provides an estimate of the experimental error and the precision of estimate at and near the centre.

The design matrices used in this work are the 2^2 and 2^3 factorial designs, they are summarized in tables (6.1) and (6.2). The arrangement for each is shown in fig (6.1) and (6.2) respectively.

Each independent variable was treated at five levels, where O is the mid point. The levels are codes as:

- a, - 1, O, 1, a,

The values of ± a were determined from [156].

$a = \pm 2^{p/4}$ ---------- 6.1

where p = number of variables

For $p = 2$, $a = \pm \sqrt{2}$

For $p = 3$, $a = \pm 1.68$

Sheet Temperature	Mould Temperature	
- 1	- 1	
1	- 1	2^2 full
- 1	1	factorial design
1	1	
- a	0	
a	0	"star" points
0	- a	
0	a	
0	0	
0	0	centre points
0	0	
0	0	

$\pm a = \pm \sqrt{2} = 1.41$

Table 6.1 Central Composite Design For 2^2 Factorial Experiment

The absolute values of the levels are indicated in Section (6.5).

The greatest attraction for RCCFD is that it allows flexible handling of the experimental procedure [154, 157]. Where the estimate of the response can be generated quickly, the experiment can be conducted sequentially. Whereas, in experiments involving a long period of time for the treatments to produce their effects, it makes sense to discover the optimum combination at the end of a single large experiment. The present work follows the latter procedure. In order to prevent systematic error, the order of the runs was randomised (this procedure being rather time consuming, because it takes a long time to stabilise tool temperatures).

Sheet Temperature	Mould Temperature	Plug Temperature	
- 1	- 1	- 1	
1	- 1	- 1	
- 1	1	- 1	2^3 full
1	1	- 1	factorial
- 1	- 1	1	design
1	- 1	1	
- 1	1	1	
1	1	1	
- a	0	0	
a	0	0	
0	- a	0	"star" points
0	a	0	
0	0	- a	
0	0	a	
0	0	0	
0	0	0	
0	0	0	centre point
0	0	0	
0	0	0	
0	0	0	

± a = 1.68

Table 6.2 *Central Composite Design for 2^3 Factorial Experiment*

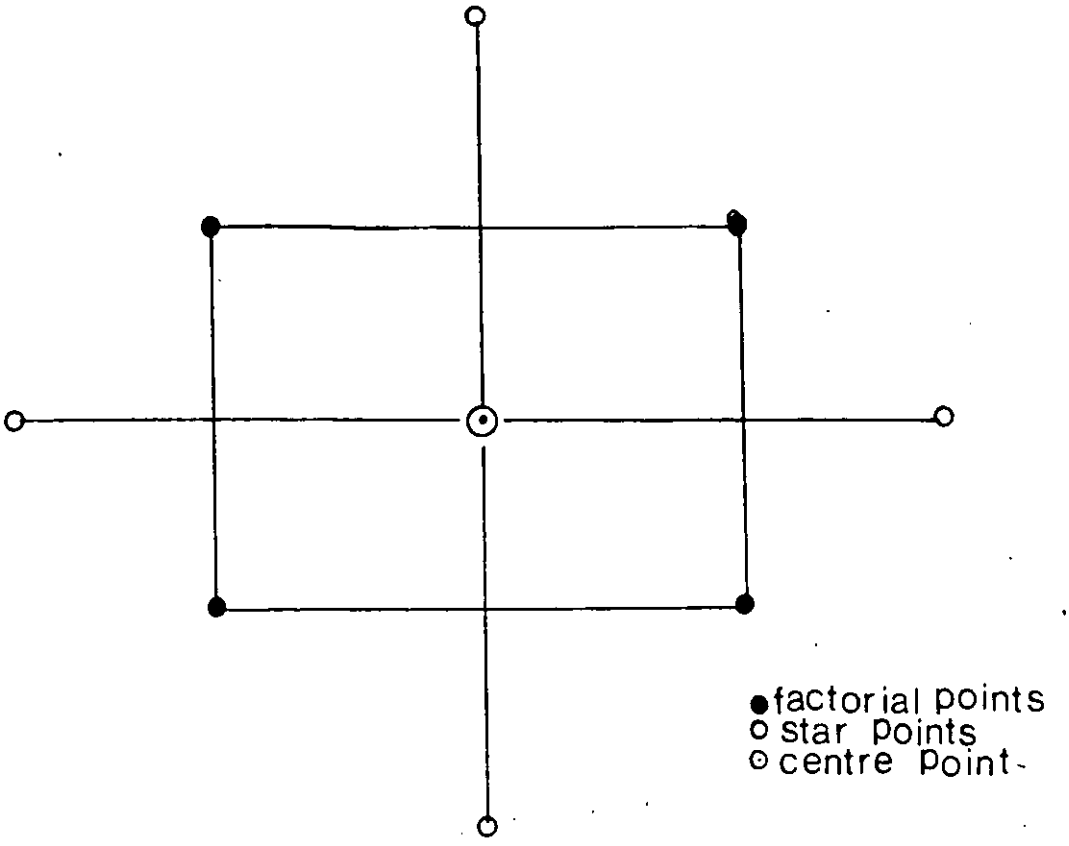

Figure 6.1 Arrangement of 2^2 composite Factorial Experiment

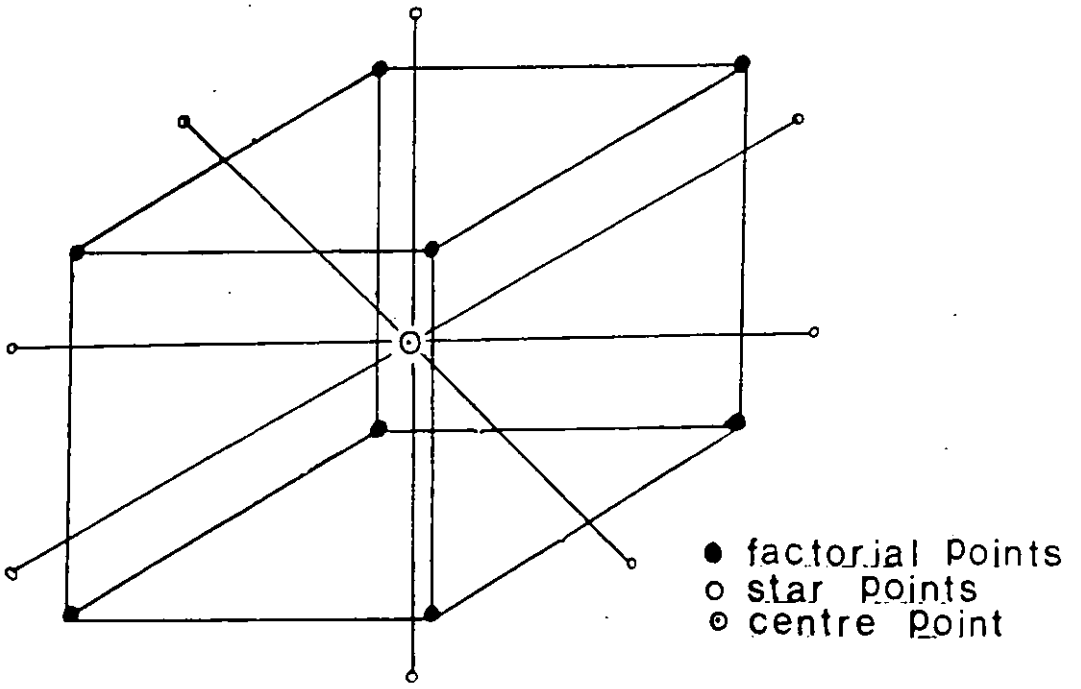

Figure 6.2 Arrangement of 2^3 composite factorial Experiment

6.3 Model Fitting and Assessment

The statistical approach to experimentation lends itself to mathematical representation. There are two main models; mechanistic and empirical models [155]. The mechanistic approach attempts to reflect the structure of the mechanism of the process. This would be useful in a situation where there is a clear understanding of an underlying trend. The empirical model specifies generalised mathematical relationships between the independent variables and measured properties (the dependent variables or responses) of such a process.

The empirical model has been used in this work because it is sufficiently flexible to describe a wide range of different types of behaviour, whereas the underlying mechanism of the thermoforming process is not fully known. The only limitation is that the response is only valid over limited ranges of the experimental data. With this in mind a polynominal model allowing for first order effect (main effect), second order effect (interaction effect) and curvature in the relationship between controls and response was chosen [158 159]. It has the general from:

$$Y = \beta_o + \Sigma \beta_i X_i + \Sigma \beta_{ii} X_i^2 + \Sigma \beta_{ij} X_i X_j \quad \text{---------- 6.2}$$

where Y = response
β_o = indpendent coefficient
β_i = linear coefficient (main effect)
β_{ii} = quadratic coefficient (characterizes the lack of fit)
β_{ij} = interaction effect of factors

For 2 variables the equation above becomes

$$Y = \beta_o + \beta_1 x_1 + \beta_2 x_2 + \beta_{11} x_1^2 + \beta_{22} x_2^2 + \beta_{12} x_1 x_2 \quad \text{-------6.3}$$

For 3 variables equation 6.2 becomes

$$Y = \beta_o + \beta_1 x_1 + \beta_2 x_2 + \beta_3 x_3 + \beta_{11} x_1^2 + \beta_{22} x_2^2 + \beta_{33} x_3^2 + \beta_{12} x_1 x_2 + \beta_{23} x_2 x_3 + \beta_{13} x_1 x_3 \text{ --- 6.4}$$

In general, for P independent variables, the corresponding equation contains n coefficients

where $n = 1/2 (P + 1) (P + 2)$ ---------- 6.5

The criterion used in fitting the model to the set of experimental data was Multivariate Regression Analysis Method (MVRA). This method is very useful for linear type models. There are a number of computer packages commercially available for fitting linear models. One of the best currently available is the Generalised Linear

Interactive Modelling (GLIM) package (release 3) which is available on the Multics computer in the LUT computer centre [160].

The program performs the MVRA on the result and fits a linear model which relates the individual response (dependent variables) to the independent variables, together with their quadratic and interaction terms. A normal distribution is assumed. The software gives the following information:

(i) The deviance of the model and the degree of freedom are displayed. The deviance is the sum of squares of the residuals and expresses the adequacy of the nominated model; for a perfect fit the deviance would be zero.
(ii) Estimates of the coefficients of the polynomial equation, together with their standard errors are also evaluated.

A ratio of estimate to standard error for each coefficient measures the effect of each coefficient. If the ratio is greater than 2, the term is taken as being statistically significant [156] [ie coefficient of significance > 95% (t - distribution tables)]

(iii) A table of the experimental and predicted values is constructed, including the residuals (the difference between the two).
(iv) Finally, the residuals are plotted against the predicted values. This allows a rapid assessment of adequacy of the model. If the points in the plot are randomly scattered the model is adequate: if the scatter is less random, the model is inadequate.

If the model is found to be inadequate a number of remedial steps can be taken;
(i) Simple removal of anomalous results.
(ii) re-run of particular treatments
(iii) another model may be developed, however, this may entail a change in initial objectives.
(iv) modify the model in order to better approximate the response. This could be achieved by [151]
    (a) adding new terms
    (b) transforming the data
    (c) adding high-order interactions
    (d) transforming the response variables, etc.

Finally, the occurrence of non-randomness can be prevented by randomisation or by a technique called 'blocking' [155]. The experiments in this work were run in random order to avoid drift in machine settings etc.

6.4 Optimization of the Thermoforming Processing Conditions

The next steps in the experimental program were determined by examining the form of the quadratic surface. Geometrical presentation of results is widely used to visualize the relation between a response and its independent variables. For single variable experiments, a two dimensional graph indicates the variation of the response over different levels of the variables. This technique can also be applied to mulitvariable experiments, simply by plotting the response versus one variable, holding the levels of the other independent variables constant. However, this method was found to be inefficient because it cannot detect interactive effects between the variables on the response [159]. In addition, the two dimensional presentation fails to show the maximum (or minimum) response value of multivariable function.

Alternatively, the relationship between a response and a number of independent variables may be represented by a three dimensional surface called the response surface. Response surface methodology [159] uses general type designs to study empirically the relationships between one or more measured responses, Y, and a number of independent variables x:

$$Y = f(x_1, x_2, x_3 \text{ ----- } x_j) \qquad \text{---------- 6.6}$$

It is then possible to construct a response surface if the predicted value as a function of the variables x.

This surface, commonly represented in the form of contours, can be studied visually to gain an appreciation of the relationship between the variables and the response.

Therefore, the response surface methods can be used to determine [158]

(i) how a particular response is affected by a set of variables within the experimental region of interest.

(ii) the level of variables that will give a product (forming) or process satisfying desirable specifications.

and (iii) operating conditions that should be maintained to obtain a maximum (or minimum) response and the local geography of the response surface near to this maximum (or minimum).

However, the response surface method has some limitations:

(a) The polynomial surface should be regarded only as an approximation to the function within the region covered by the experiment. Thus the result cannot be extrapolated to regions beyond the experimental space, defined by circular area of

radius $(1.414^2 + 1.414^2)^{1/2}$ for 2^2 factorial (see fig 6.3) [151] and $(1.68^2 + 1.68^2)^{1/2}$ for 2^3 factorial experiment.

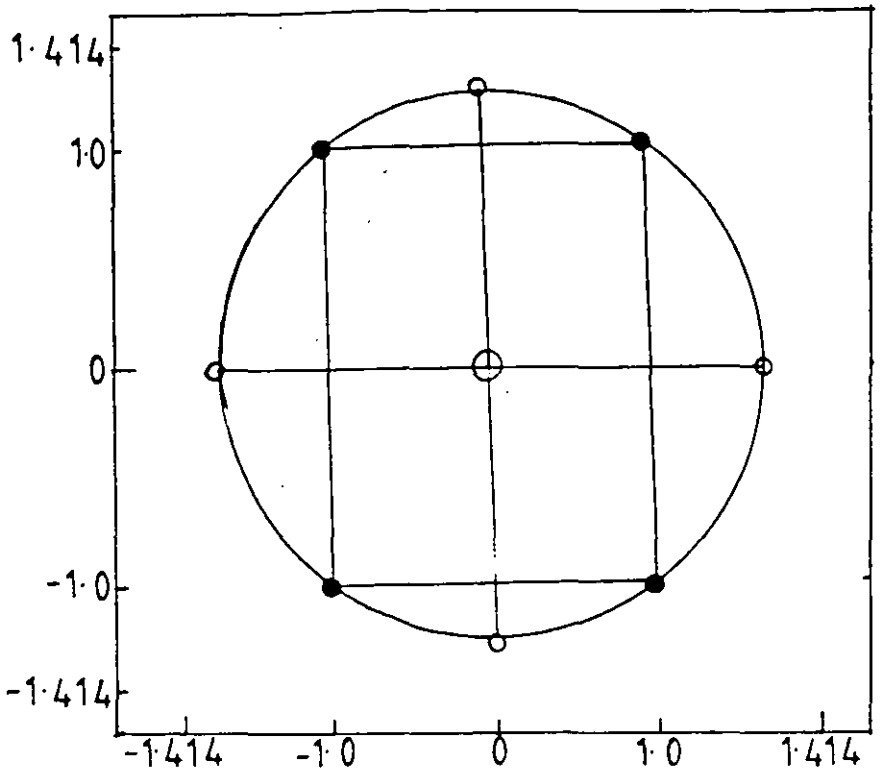

Figure 6.3 Extrapolated point in 2-variable central composite design

(b) Consequently the use of such models is only applicable to the equipment used in testing and cannot generally be transferred to other equipment. This also implies that data taken from laboratory equipment cannot be used to estimate operations on full scale processes.

The contour plots for the response surface were constructed by computer aided graphics in conjuction with suitable programs (see appendices I and II). Appendix I show the program that plots the response surface for 2^2 factorial (ie vacuum forming). Appendix II show the program for 2^3 Factorial (ie plug-assist forming). The basic features of the programs are:

(i) Reading the polynomial coefficients for each response.

(ii) For every response, one variable at any required code value is set (ie -1, 0, 1), and the other two variables (axial variables) are altered in turn.

(iii) The two axial independent variables are varied between (±)1.68 (for 2^3 factorial), and the response of each combination is then printed on each contour line of the contour plots.

The program for simple vacuum forming is limited to the first step, and a single plot shows the response for the two variables. However, for 2^3 factorial (ie plug-assist

forming) the number of contour plots resulting from all possible combinations was considerably larger, (>1000). The number of plots was reduced substantially by selecting only those variables associated with statistically significant coefficients.

6.5 Factorial Experiments

The forming procedures were as described in section 5.5. For simple vacuum forming, there are two main variables; these are sheet and mould temperature. Thus the process was represented by 2^2 composite factorial experimental design. With the addition of plug temperature for the plug-assist forming mode, 2^3 composite factorial design represents the experimental lay out. For each forming mode, two draw ratios (1:1 and 2:1) were made. The design of the experiments was based on experience gained from the exploratory work detailed in chapter 5. The relationship between the coded and the real values for the two factorial designs is shown in tables 6.3 and 6.4.

Vacuum Forming

	Real Values °C	
Code Values	Sheet	Mould
- 1.41	80	25
-1	86	35
0	100	60
1	114	85
1.41	120	95

Table 6.3: Coded and absolute values of 2^2 Factorial Variables

Plug-assist forming

	Real Values °C		
Code Values	Sheet	Mould	Plug
-1.68	80	25	80
-1	88	39	88
0	100	60	100
1	112	81	112
1.68	120	95	120

Table 6.4: Coded and absolute values of 2^3 Factorial Variables

Code Values		Real Values °C	
Sheet	Mould	Sheet	Mould
-1	-1	86	35
1	-1	114	35
-1	1	86	85
1	1	114	85
-1.41	0	80	60
1.412	0	120	60
0	-1.41	100	25
0	1.41	100	95
0	0	100	60

Table 6.5: Assignment of Real Values to central composite 2^2 Factorial Design - vacuum forming experiment

Code Values			Real Values °C		
sheet	mould	plug	sheet	mould	plug
-1	-1	-1	88	39	88
1	-1	-1	112	39	88
-1	1	-1	88	81	88
1	1	-1	112	81	88
-1	-1	1	88	39	112
1	-1	1	112	39	112
-1	1	1	88	81	112
1	1	1	112	81	112
-1.68	0	0	80	60	100
1.68	0	0	120	60	100
0	-1.68	0	100	25	100
0	1.68	0	100	95	100
0	0	-1.68	100	60	80
0	0	1.68	100	60	120
0	0	0	100	60	100

Table 6.6: Assignment of Real Values to central composite 2^3 Factorial Design - Plug-assist Forming Experiment

Assignment of the real values to the factorial designs is shown in tables 6.5 and 6.6 for 2^2 and 2^3 composite factorial designs respectively. The times to attain sheet forming temperatures are given in table 6.7 - as obtained in chapter 5.

Temperature °C	Time sec
80	25.5
86	27.5
88	29.0
100	36.0
112	42.5
114	44.0
120	48.0

Table 6.7: Times to Attain sheet forming Temperature

In order to be able to study the effect of processing conditions on the formings, it is essential to define parameters that measure quality of the product. These are: the thickness distribution coefficient and thermal stability (shrinkage) of the formings.

6.5.1 Determination of Thickness Distribution Coefficient

In Chapter 5,the thickness distribution in many of the formings was shown to be near exponential in shape ie. a linear-log plot of thickness versus depth (fig 6.4) gives a reasonable straight line.

Therfore, regression analysis of the thickness data for each processing condition (for each container) was performed to comply with a model of the form:

$$t = A e^{-Bh} \qquad \text{----------} \qquad 6.7$$

or $\ln t = \ln A - Bh$

where t = thickness (mm)

h = depth (mm) (along side of sample).

A,B = constant

The slope B was defined as a "coefficient of thickness distribution" in the formings. Whilst it is accepted that the exponential model is probably not the most accurate for all thickness distributions, it is convenient to handle in the statistical analysis and is more meaningful than spot values. Thickness (as a function of depth of draw) was measured as described in section 5.5.

Minitab linear regression analysis package (available in the L.U.T computer centre) was used to evaluate the constants (ie A and B) of the regression equation. In addition, Minitab presents analysis of variance of the data , and also a plot of the data for each container.

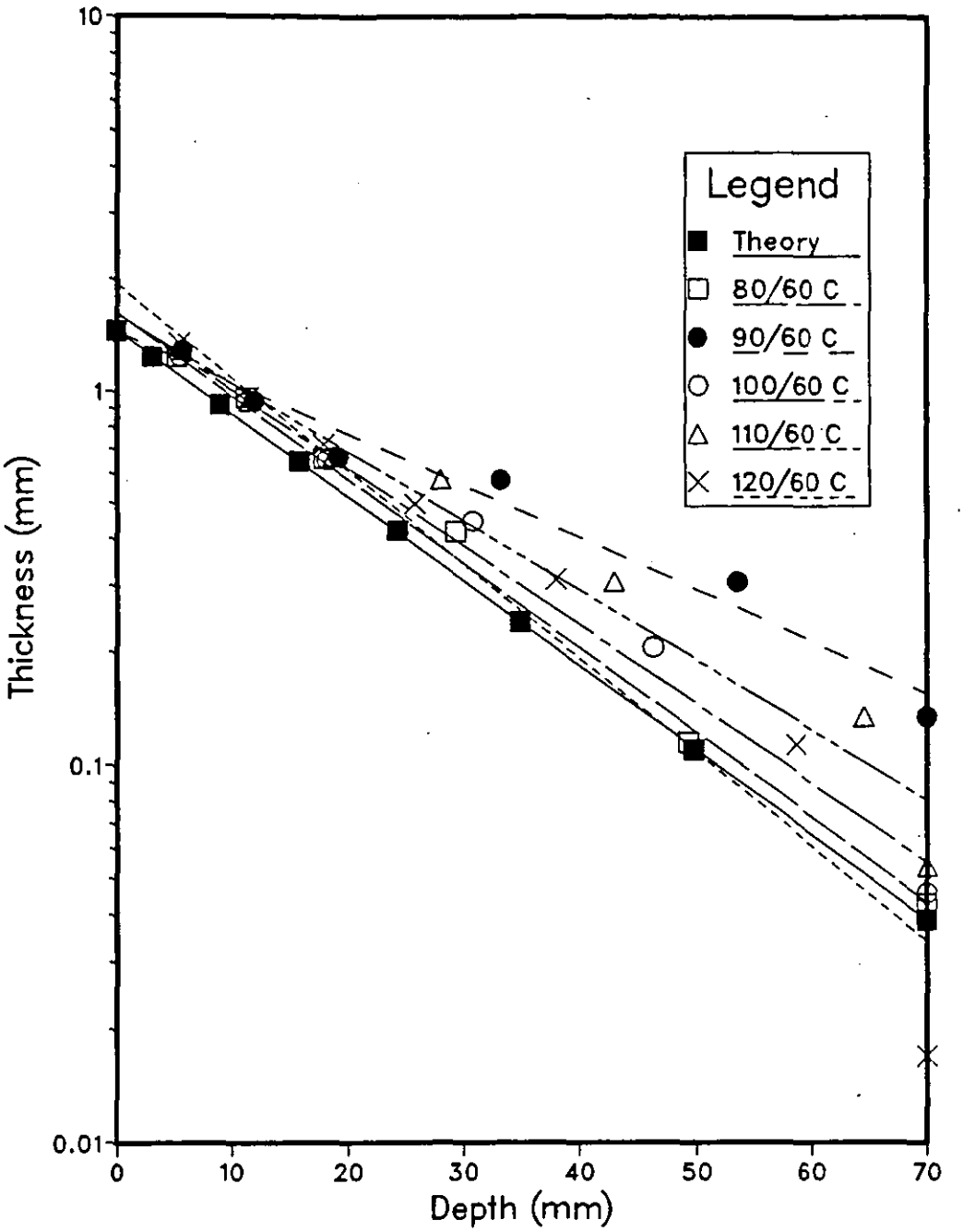

Figure 6.4 *Linear - log plot of thickness as a function of depth.*

6.5.2 Shrinkage

The effect of processing conditions on thermal stability of the containers was determined in terms of shrinkage (defined as change in total volumetric capacity). This was achieved by filling each container with water of determined volume, before and after exposure to a chosen temperature for 20 minutes. Care was taken to prevent deformation of the containers during the filling operation. This was achieved by clamping the containers at the rim and supporting the base on a platform.

The change in volume was determined by difference in volume of water to fill the container. The cumulative difference in volume by successive exposures to increasing temperature gives the change in volume as a function of temperature. The shrinkage, measured as volume change (%) was determined between 50 - 80°C for each container as follows:

$$\% \text{ volume change} = \frac{V_o - V}{V_o} \times 100 \qquad \text{---------- 6.8}$$

where V_o = Initial volume of water to fill a container before exposure to specified temperature.

V = Volume of water to fill the container after exposure to specified temperature.

The new volume becomes the initial volume for the subsequent experiment. Therefore, the change in volume determined is the cumulative shrinkage over the entire experiment. The change in volume capacity (or shrinkage) at 80 °C for each container was used to determine the effects of processing conditions.

The shrinkage measurement determines the suitability of thermoformed amorphous PETP for hot-filling applications.

6.6 Results and Analysis of the Factorial Experiments

6.6.1 Thickness Distribution

Table 6.8 shows the data for coefficient of thickness variation for shallow and deep vacuum formed containers at different processing conditions (at their code values). The real values of the processing conditions are given in table 6.5. Also, table 6.9 shows the data for coefficient of thickness variations in Plug-assist formed containers at the various combinations of the processing conditions in their code values. The real values are presented in table 6.6.

All the results were analysed in terms of the Multivariate Regression Analysis (MVRA) using the GLIM [160] package. The estimates of the coefficients and their significance for the polynomial model used for simple vacuum forming are presented in Table 6.10 and 6.11 for shallow and deep draws respectively. The table of polynomial coefficients can be interpreted as follows:

(i) a positive value of the estimate indicates deterioration in thickness distribution with increasing value of the variable (eg sheet temperature)

(ii) a negative value of the estimate indicates improvement in thickness distribution with increasing value of the variable

(iii) the statistical significance of each variable is determined from the ratio of the estimate and the standard error (the ratio is significant when it is ≥ 2)[156]

The adequacy of the model was evaluated from the plot of residuals against the fitted values presented in fig 6.5 and 6.6 for shallow and deep draws respectively.

Code Values		Draw ratio	
Sheet	Mould	1:1	2:1
-1	-1	.0534	.0196
1	-1	.0680	.0223
-1	1	.0521	.0206
1	1	.0696	.0290
-1.41	0	.0518	.0208
1.41	0	.0577	.0400
0	-1.41	.0521	.0248
0	1.41	.0470	.0276
0	0	.0484	.0272
0	0	.0577	.0287
0	0	.0331	.0258
0	0	.0470	.0244

Table 6.8 Degree of Thickness Variation in vacuum formed containers

Code Values			Draw Ratio	
Sheet	Mould	Plug	1:1	2:1
-1	-1	-1	.0216	.0183
1	-1	-1	.0285	.0137
-1	1	-1	.0159	.0211
1	1	-1	.0198	.0101
-1	-1	1	.0158	.0141
1	-1	1	.0169	.0100
-1	1	1	.0176	.0156
1	1	1	.0114	.0107
-1.68	0	0	.0157	.0157
1.68	0	0	.0185	.0153
0	-1.68	0	.0155	.0113
0	1.68	0	.0123	.0128
0	0	-1.68	.0249	.0151
0	0	1.68	.0156	.0128
0	0	0	.0200	.0136
0	0	0	.0214	.0135
0	0	0	.0212	.0140
0	0	0	.0211	.0094
0	0	0	.0229	.0133
0	0	0	.0221	.0143

Table 6.9: Degree of Thickness Variation in Plug-assist formed containers

Polynomial Terms		Estimate	Standard Error	Estimate / Std Error
B_o	(Grand Mean)	0.4765×10^{-1}	0.5306×10^{-2}	-
B_1	(S)	0.5067×10^{-2}	0.2657×10^{-2}	1.91 +
B_2	(M)	-0.8639×10^{-3}	0.2657×10^{-2}	- 0.33
B_{11}	(SS)	0.5734×10^{-2}	0.3523×10^{-2}	1.63 +
B_{22}	(MM)	0.3119×10^{-2}	0.3523×10^{-2}	0.89
B_{12}	(SM)	0.7250×10^{-3}	0.3752×10^{-2}	0.19

Table 6.10 Table of polynomial Coefficients for Thickness Distribution in shallow vacuum formed containers

polynomial terms		Estimate	Standard Error	Estimate / Std Error
B_o	(Grand mean)	0.2798×10^{-1}	0.3425×10^{-2}	-
B_1	(S)	0.4786×10^{-2}	0.1715×10^{-2}	2.79 *
B_2	(M)	0.1460×10^{-2}	0.17115×10^{-2}	0.85
B_{11}	(SS)	-0.1487×10^{-3}	0.2274×10^{-2}	- 0.07
B_{22}	(MM)	-0.2261×10^{-2}	0.2274×10^{-2}	- 0.99
B_{12}	(SM)	0.1425×10^{-2}	0.2422×10^{-2}	0.59

Table 6.11 *Table of Polynomial Coefficients for Thickness Distribution in Deep Vacuum Formed containers*

where S = sheet temperature coefficient]
M = Mould
SS = Quadratic coefficient for sheet temperature
MM = Quadratic coefficient for mould temperature
SM = Interaction effect between sheet and mould temperatures

* Indicates significant effect (>95% in t distribution)

+ Indicates near significant effect.

Tables 6.12 and 6.13 show the estimate of the coefficients and their significance in plug-assist forming, shallow and deep draws respectively. The adequacy of the polynomial model was evaluated from figs 6.7 and 6.8 for shallow and deep draws respectively.

The response surfaces for thickness distribution in shallow and deep vacuum formed containers are presented in figs 6.9 and 6.10 while figs 6.11 and 6.12 present the response surface (thickness distribution) for shallow and deep plug-assist formed containers respectively.

polynomial terms		Estimate	Standard Error	Estimate / Std Error
B_o	(Grand mean)	0.2798×10^{-1}	0.3425×10^{-2}	-
B_1	(S)	0.4786×10^{-2}	0.1715×10^{-2}	2.79 *
B_2	(M)	0.1460×10^{-2}	0.17115×10^{-2}	0.85
B_{11}	(SS)	-0.1487×10^{-3}	0.2274×10^{-2}	- 0.07
B_{22}	(MM)	-0.2261×10^{-2}	0.2274×10^{-2}	- 0.99
B_{12}	(SM)	0.1425×10^{-2}	0.2422×10^{-2}	0.59

Table 6.11 Table of Polynomial Coefficients for Thickness Distribution in Deep Vacuum Formed containers

where S = sheet temperature coefficient]
M = Mould
SS = Quadratic coefficient for sheet temperature
MM = Quadratic coefficient for mould temperature
SM = Interaction effect between sheet and mould temperatures

* Indicates significant effect (>95% in t distribution)

Tables 6.12 and 6.13 show the estimate of the coefficients and their significance in plug-assist forming, shallow and deep draws respectively. The adequacy of the polynomial model was evaluated from figs 6.7 and 6.8 for shallow and deep draws respectively.

The response surfaces for thickness distribution in shallow and deep vacuum formed containers are presented in figs 6.9 and 6.10 while figs 6.11 and 6.12 present the response surface (thickness distribution) for shallow and deep plug-assist formed containers respectively.

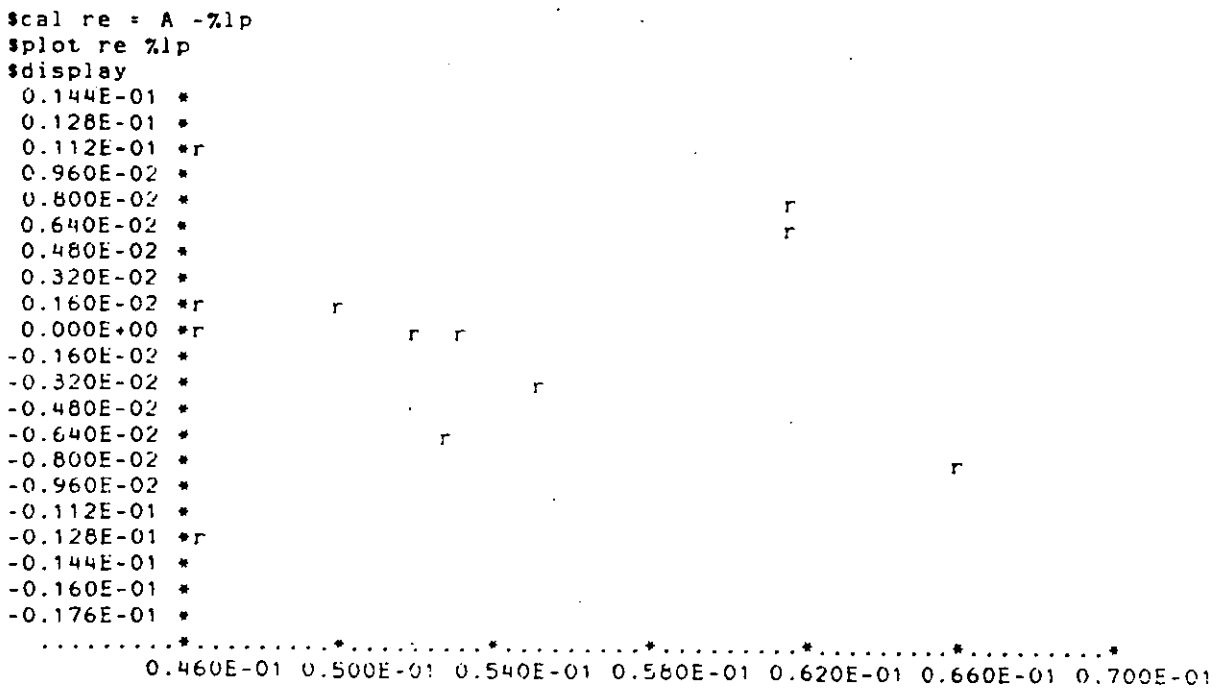

Figure 6.5 *Residuals vs fitted values for coefficient of thickness distribution (shallow vacuum drawn containers)*

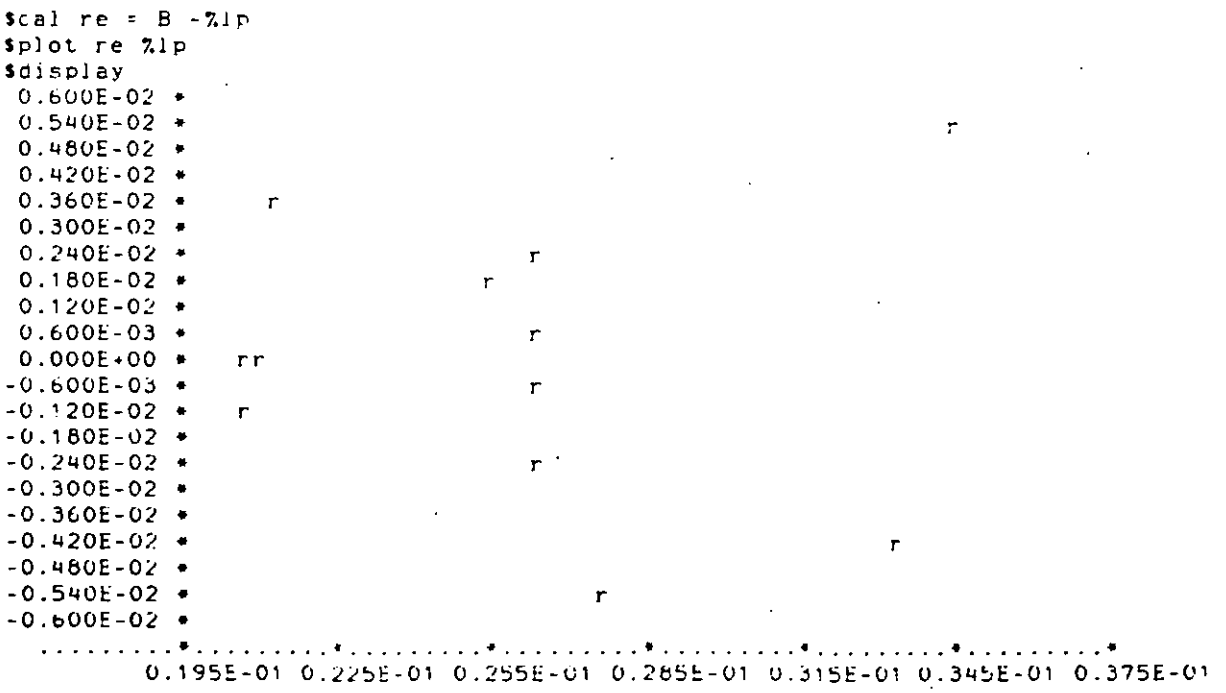

Figure 6.6 *Residuals vs fitted values for coefficient of thickness distribution (deep vacuum drawn containers)*

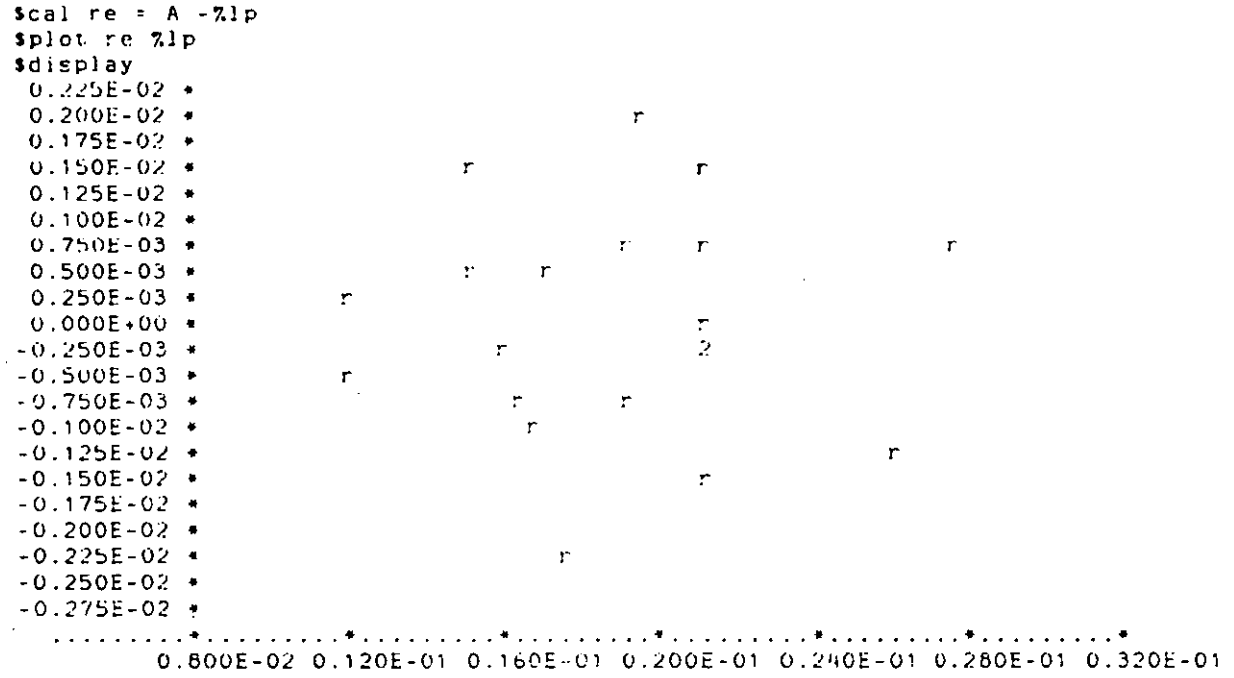

Figure 6.7 Residuals vs fitted values for coefficient of thickness distribution (shallow plug-assist formed containers)

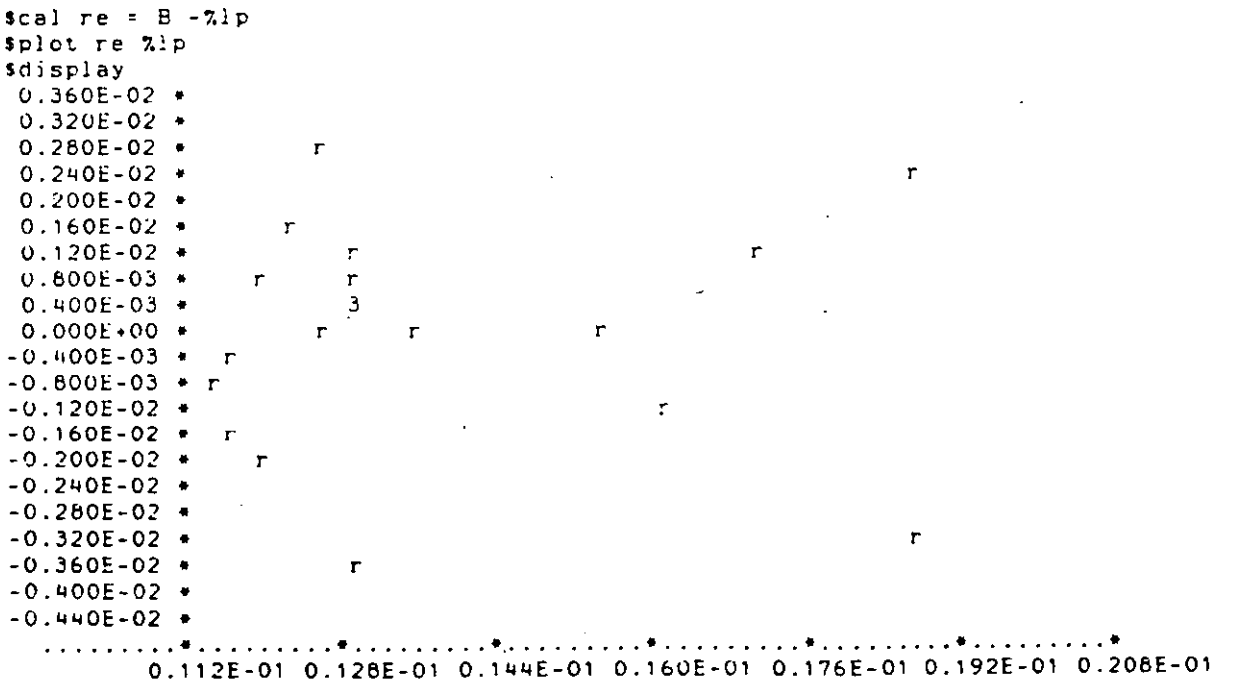

Figure 6.8 Residuals vs fitted values for coefficient of thickness distribution (deep plug-assist formed containers)

Polynomial terms		Estimate	Standard Error	Estimate / Std Error
B_o(Grand Mean)		0.2140×10^{-1}	0.5980×10^{-3}	-
B_1	(S)	0.7625×10^{-3}	0.3970×10^{-3}	1.92 +
B_2	(M)	-0.1721×10^{-2}	0.3970×10^{-3}	-4.34 *
B_3	(P)	-0.2911×10^{-2}	0.3970×10^{-3}	-7.33 *
B_{11}	(SS)	-0.1196×10^{-3}	0.3869×10^{-3}	-3.09 *
B_{22}	(MM)	-0.2330×10^{-2}	0.3869×10^{-3}	-6.02 *
B_{33}	(PP)	-0.8023×10^{-4}	0.3869×10^{-3}	-0.21
B_{12}	(SM)	-0.1287×10^{-2}	0.5185×10^{-3}	-2.48 *
B_{13}	(SP)	-0.1987×10^{-2}	0.5185×10^{-3}	-3.83 *
B_{23}	(MP)	0.1338×10^{-2}	0.5185×10^{-3}	2.58 *

Table 6.12 Table of polynomial coefficients for thickness distribution in shallow Plug-assist formed containers

* Indicates coefficient significance (> 95 % in t - distribution)

+ Indicates near significant effect

Polynomial terms		Estimate	Standard Error	Estimate / Std Error
B_o(Grand Mean)		0.1298×10^{-1}	0.9596×10^{-3}	-
B_1	(S)	-0.1852×10^{-2}	0.6370×10^{-3}	-2.91 *
B_2	(M)	0.2873×10^{-3}	0.6370×10^{-3}	0.45
B_3	(P)	-0.1849×10^{-2}	0.6370×10^{-3}	-2.90 *
B_{11}	(SS)	0.1138×10^{-2}	0.6208×10^{-3}	1.83
B_{22}	(MM)	-0.8442×10^{-4}	0.6208×10^{-3}	-0.14
B_{33}	(PP)	-0.3147×10^{-3}	0.6208×10^{-3}	-0.51
B_{12}	(SM)	-0.9000×10^{-3}	0.8319×10^{-3}	-1.08
B_{13}	(SP)	0.8250×10^{-3}	0.8319×10^{-3}	0.99
B_{23}	(MP)	0.3750×10^{-3}	0.8319×10^{-3}	0.45

Table 6.13: Table of Polynomial coefficients for Thickness Distribution in deep Plug-assist formed containers

* Indicates significant coefficient (> 95 % in t - distribution)

+ Indicates near significant effect

where S = sheet temperature coefficient
M = mould temperature coefficient
P = plug temperature coefficient
SS = quadratic coefficient for sheet temperature
MM = quadratic coefficient for mould temperature
PP = quadratic coefficient for plug temperature
SM = interaction coefficient for sheet and mould temperatures
SP = interaction coefficient for sheet and plug temperatures
MP = interaction coefficient for mould and plug temperatures

In the plug-assist formed containers, the response surface was investigated only at variables (processing condition) that showed statistical significance from the GLIM [160] analysis.

Figs 6.5 and 6.6 show that the Polynomial nominated (equation 6.3) for vacuum forming (ie 2^2 factorial)is adequate. The relationship between the equation and forming variables presented in the GLIM analysis is as follows:

Polynomial Model - $Y = B_o + B_1 x_1 + B_2 x_2 + B_{11} x^2 + B_{22} x_{22} + B_{12} x_1 x_2$

where Y = t = thickness distribution
B_o = grand mean
B_1 = S = sheet temperature
B_2 = M = mould temperature
B_{11} = SS = quadratic effect of sheet temperature
B_{22} = MM = quadratic effect of mould temperature
B_{12} = SM = Interaction between sheet and mould temperature
x = level of each variable

In addition, equation 6.4, the nominated polynomial for plug-assist forming (2^3 factorial) is adequate as shown in figs 6.7 and 6.8.

ie the polynomial $Y = B_o + B_1 x_1 + B_2 x_2 + B_3 x_3 + B_{11} x^2_1 + B_{22} x^2_2 + B_{33} x^2_3 + B_{12} x_1 x_2 + B_{13} x_1 x_3 + B_{23} x_2 x_3$

where

Y	= t	=	the thickness
B_o	=		grand mean
B_1	= S	=	sheet temperature
B_2	= M	=	mould temperature
B_3	= P	=	plug
B_{11}	= SS	=	quadratic effect of sheet temperature
B_{22}	= MM	=	quadratic effect of mould temperature
B_{33}	= PP	=	quadratic effect of plug temperature
B_{12}	= SM	=	interaction between sheet and mould temperature
B_{13}	= SP	=	interaction between sheet and plug temperature
B_{23}	= MP	=	interaction between mould and plug temperature
x	=		level of variable at desired combinations

The analysis of the coefficients from the GLIM package for simple vacuum forming indicates that sheet temperaure is the main variable that influences thickness distribution in the containers.

The information obtainable from the response surface profile is quite vast, so analysis will be restricted to global trend, especially in the plug-assist mode, while laying emphasis on optimum region for processing containers with desirable properties.

Fig 6.9 represents the response surface for shallow formed containers. It shows that below 90°C and above 100°C, the thickness distribution deteriorates. Therfore, the best forming region is between 90-100°C sheet temperature (ie region of least thickness variation).

Fig 6.10 represents the response surface for deep vacuum formed containers. Thickness distribution deteriorates with increasing sheet temperature. A comparison of fig 6.9 and 6.10 indicate that thickness distribution is better in the deep draws than in the shallow draws (ie from the contour height values since minimum height indicate least thickness variation).

In the plug-assist forming, the shallow draw show that each forming variables has a significant effect on thickness distribution. And more importantly, there is significant interaction between them. Therefore, each variable was investigated at their -1, 0, 1 code values. However, in the deep plug-assist forming, sheet and plug temperatures have significant effects but no interaction between the variables was

observed (table 6.12). In this case, sheet and plug temperatures were varied at their -1, 0, 1 code values as explained in section 6.4.

Figs 6.11 and 6.12 represent the thickness variation in shallow and deep plug-assist drawn containers . The influence of varying processing conditions on the plug-assist formed containers is rather complex especially where there is strong interaction effect between the variables. A close examination of fig 6.11 (graphs 1 - 9) which represents shallow plug-assist formed containers shows that:

(i) at constant sheet temperature, increasing mould temperature improves thickness distribution (graphs 2 and 3). However , at the lower sheet temperature (graph 1) increasing mould temperature causes deterioration in thickness distribution.

(ii) at constant mould temperature, increasing plug temperature causes deterioration in thickness distribution (graphs 4 - 6).

(iii) at constant plug temperature, increasing sheet temperature improves thickness distribution in the formings (graphs 7 - 9).

Overall, the least variation in thickness in shallow plug-assist formed containers was obtained at sheet/mould/plug temperatures 112/75/112°C.

Fig 6.12 (graphs 1 - 6) represents the response surface (thickness distribution) for deep plug-assist formed containers . The following can be deduced:

(i) graphs 1 - 3 show that mould temperature has very little effect on thickness distribution, but improved thickness distribution can be obtained between 90 - 112°C plug temperature.

(ii) graphs 4-6 shows that better thickness distribution can be obtained between 90 - 112°C sheet temperature.

The best forming conditions was obtained at sheet/mould/plug temperatures 88/75/112°C.

In both simple vacuum and plug-assist forming modes, better thickness distribution was obtained in the deep draws.

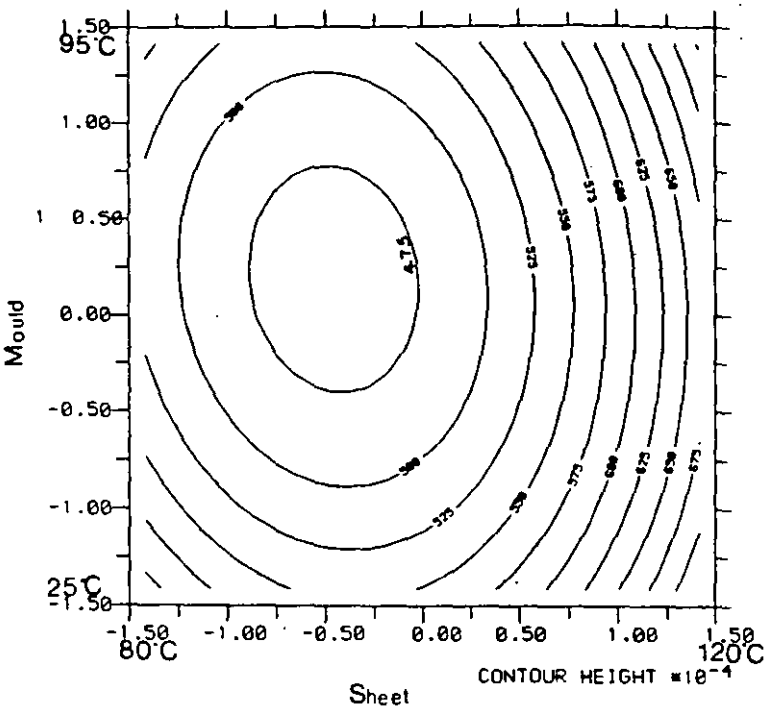

Figure 6.9 *Contour plot of thickness distribution (shallow vacuum drawn containers*

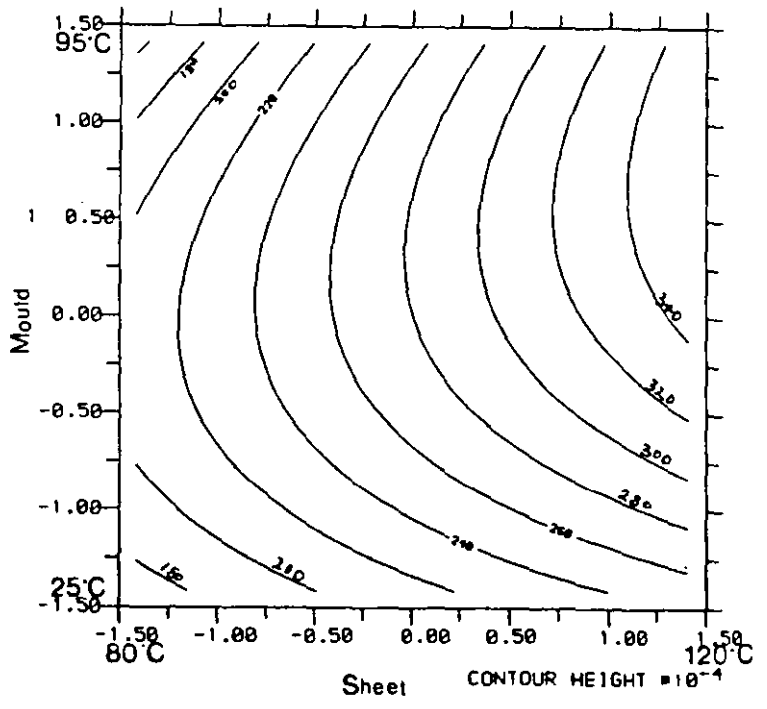

Figure 6.10 *Contour plot of thickness distribution (deep vacuum drawn containers)*

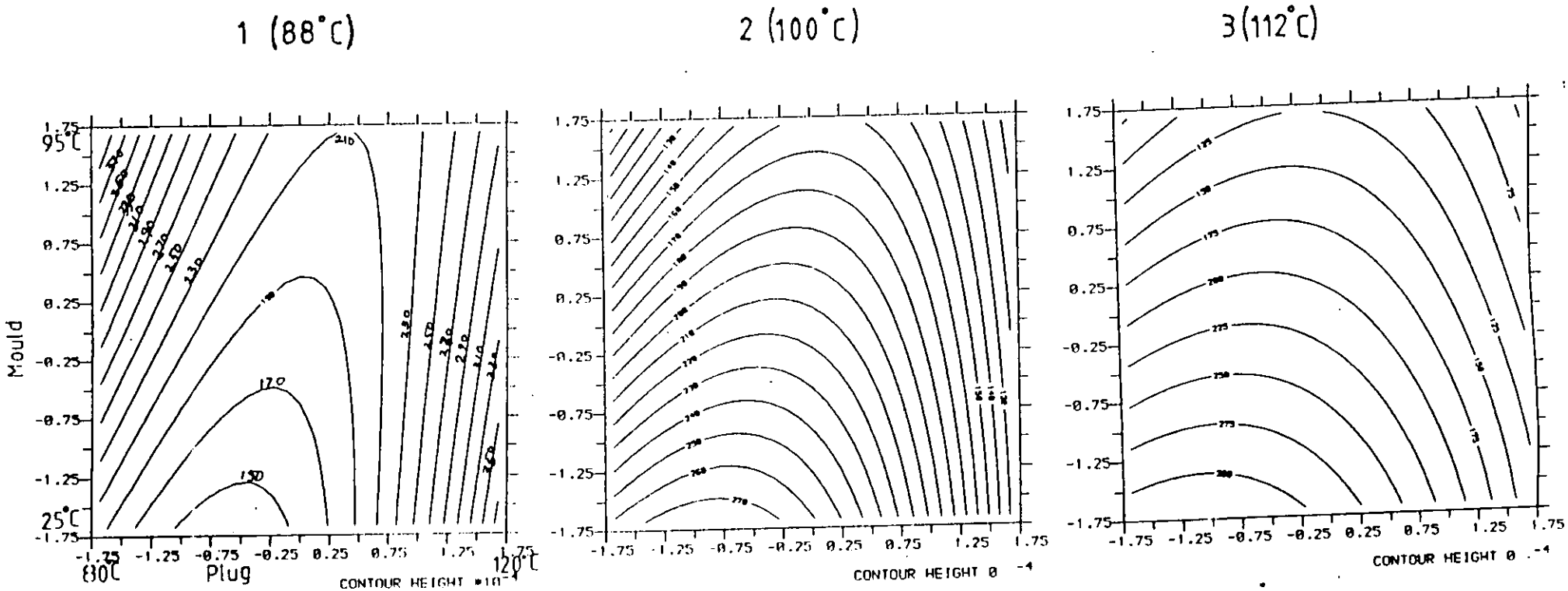

Figure 6.11 *Contour plot of thickness distribution (shallow plug-assist formed containers)*

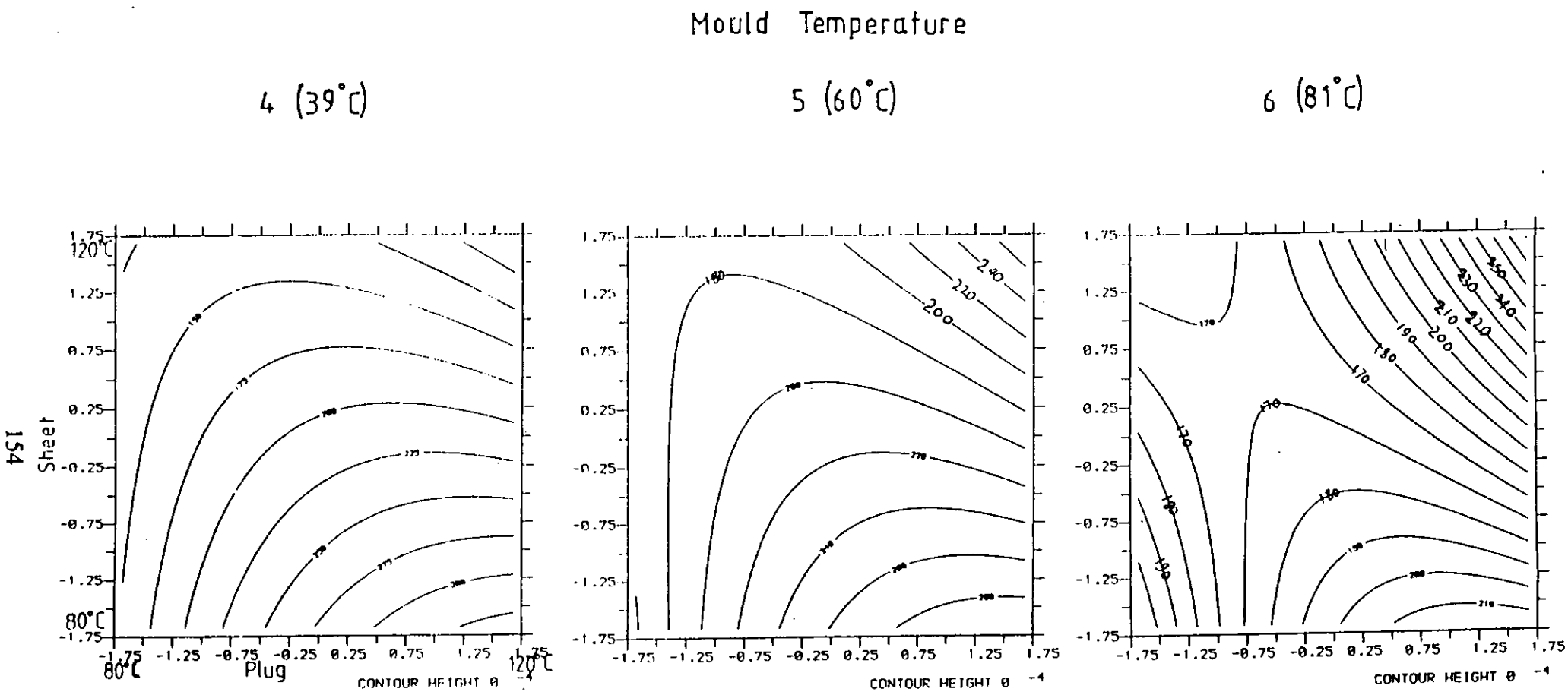

Figure 6.11 *Contour plot of thickness distribution (shallow plug-assist formed containers)*

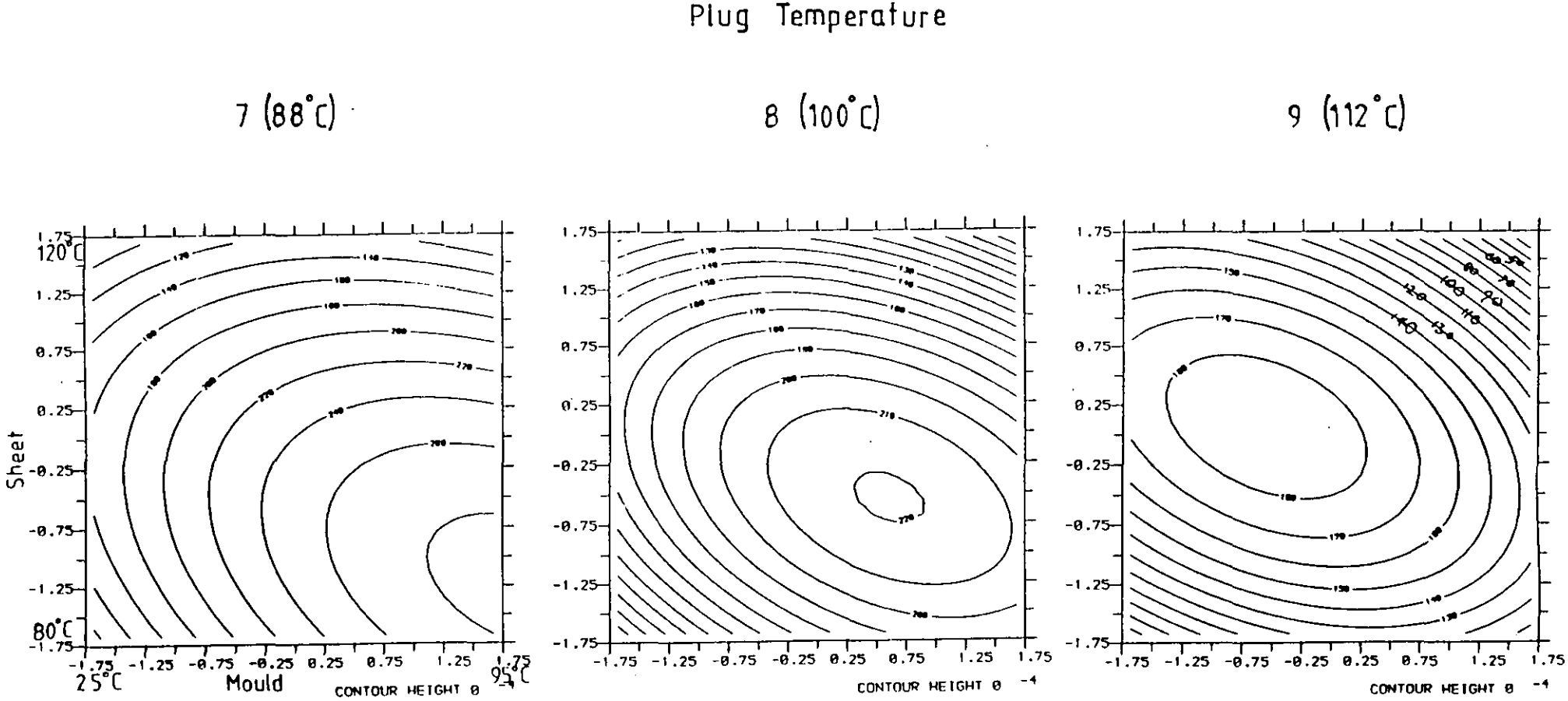

Figure 6.11 *Contour plot of thickness distribution (shallow plug-assist formed containers)*

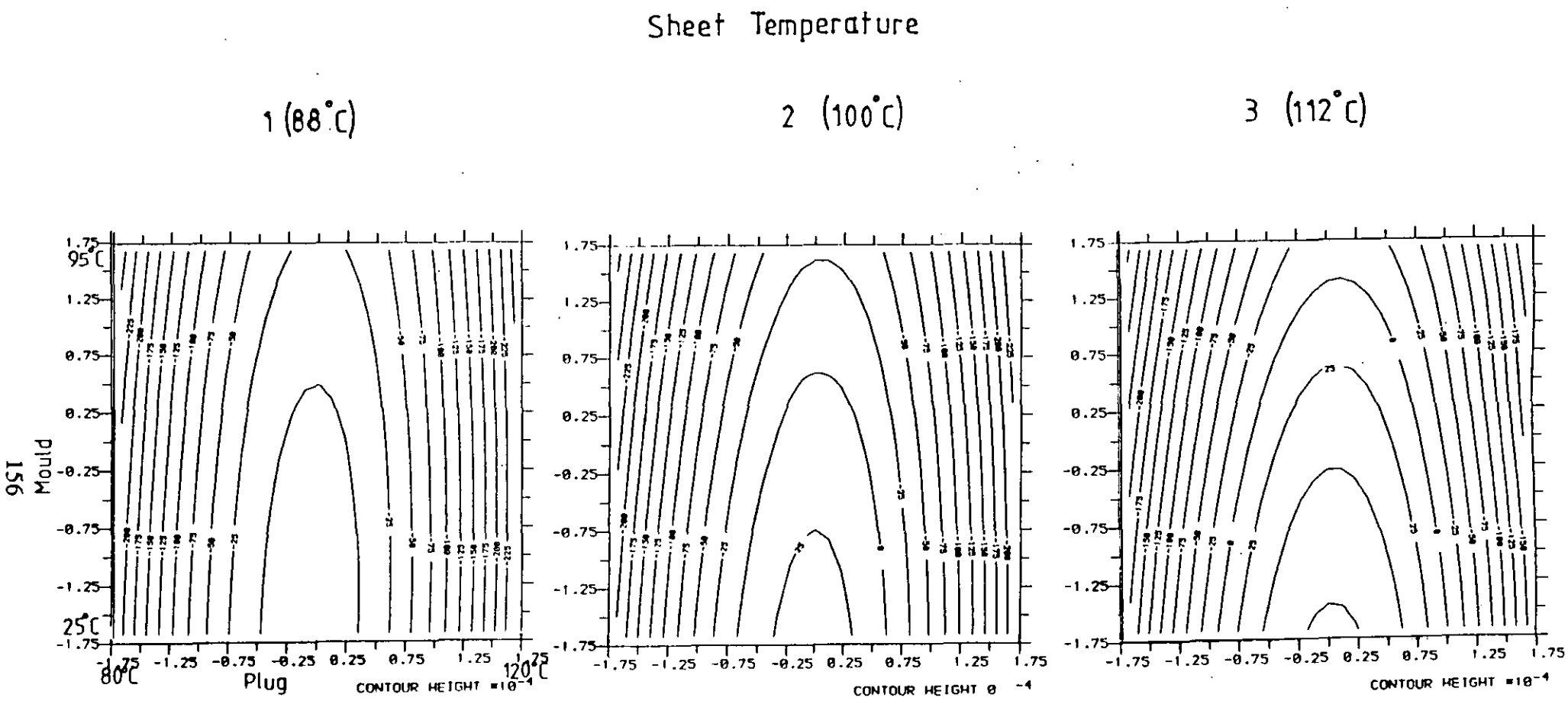

Figure 6.12 *Contour plot of thickness distribution (deep plug-assist formed containers)*

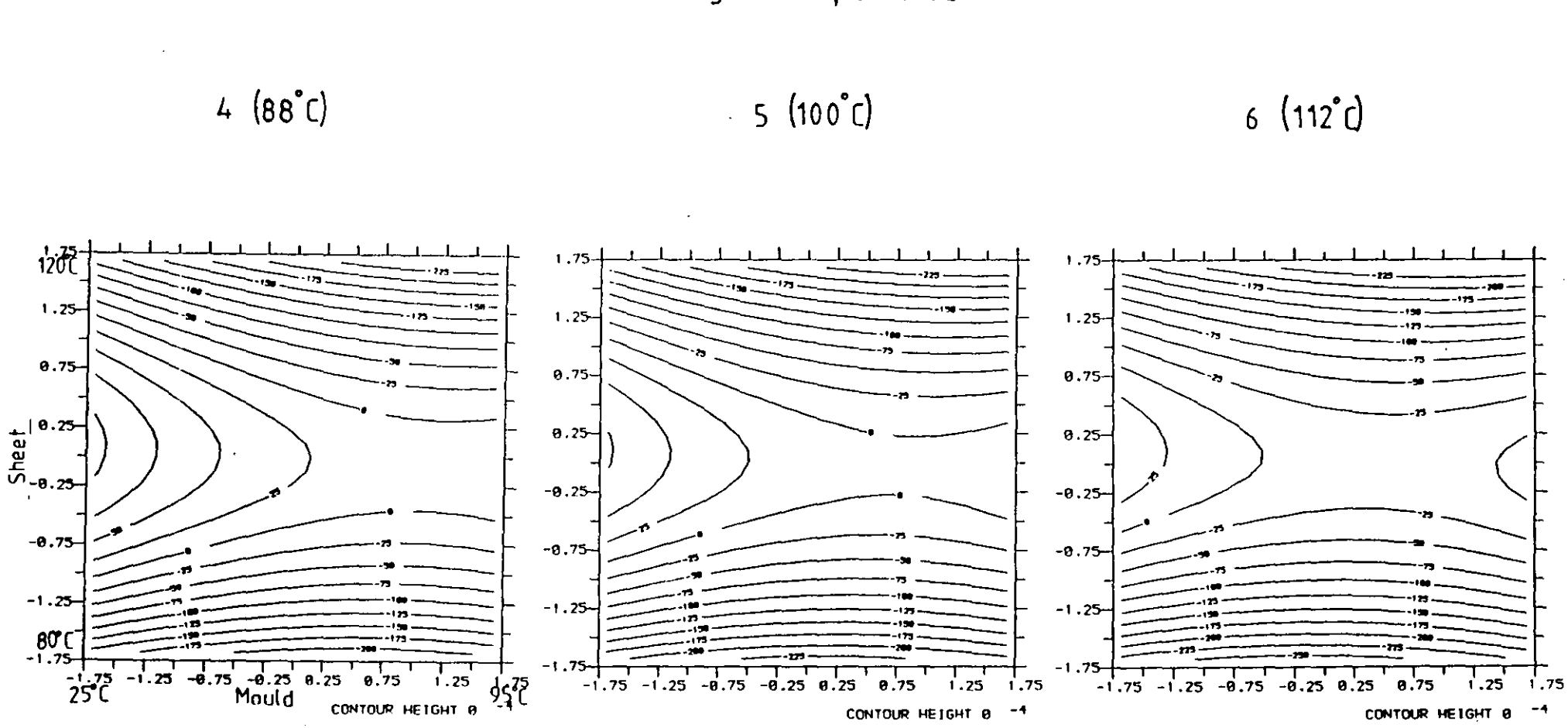

Figure 6.12 Contour plot of thickness distribution (deep plug-assist formed containers)

6.6.2 Shrinkage

Table 6.14 shows the data for thermal shrinkage in shallow and deep vacuum formed containers at different combinations of the processing conditions. Similarly table 6.15 presents the data for shrinkage in plug-assist formed containers at different processing conditions. The real values of the processing conditions are given in table 6.5, for vacuum forming, and table 6.6, for plug-assist forming.

The shrinkage data were analysed with the GLIM Package [160] on the computer. The estimates of the coefficients and their significance are found in tables 6.16 and 6.17 for shallow and deep vacuum formed containers; those for shallow and deep plug-assist formed containers are presented on tables 6.18 and 6.19 respectively.

Code Values		Draw ratio	
Sheet	Mould	1:1	2:1
-1	-1	38.89	48.78
1	-1	35.85	60.35
-1	1	23.40	3.77
1	1	29.17	19.56
-1.41	0	38.00	8.00
1.41	0	37.04	64.20
0	-1.41	39.62	51.72
0	1.41	14.59	1.79
0	0	35.85	21.05
0	0	35.92	21.28

Table 6.14: Change in volume capacity of the containers at 80 °C

Figs 6.13 and 6.14 (for shallow and deep vacuum forming) and also Figs 6.15 and 6.16 (for shallow and deep plug-assist forming respectively) show that the polynomial for each forming mode is adequate. In this case, the response Y in equations 6.3 and 6.4 is shrinkage. The response surface investigation was limited to variables with significant effects, especially in plug-assist forming.

In vacuum forming, the shallow draw showSa significant effect of mould temperature and a slight interaction between sheet and mould temperatures (table 6.16. However in the deep draw (table 6.17) sheet and mould temperatures have significant effect but no significant interaction was observed. Fig 6.17 show that shrinkage decreases with increasing mould temperature in the shallow vacuum formed containers.

Code Values			Draw ratio	
Sheet	Mould	Plug	1:1	2:1
-1	-1	-1	32.0	15.46
1	-1	-1	59.62	45.54
-1	1	-1	20.83	11.22
1	1	1	17.31	9.62
1	-1	1	16.00	12.28
-1	1	1	9.09	4.12
1	1	1	8.70	11.71
-1.68	0	0	17.39	7.41
1.68	0	0	16.67	40.35
0	-1.68	0	20.00	16.07
0	1.68	0	4.55	2.94
0	0	-1.68	28.00	46.67
0	0	1.68	17.39	6.60
0	0	0	20.00	12.15
0	0	0	21.25	12.62

Table 6.15 Change in volume capacity of plug-assist formed containers.

Polynomial terms		Estimate	Standard Error	Estimate / Std Error
B_o	(Grand Mean)	35.8900	1.7560	-
B_1	(S)	0.12726	0.8794	0.20
B_2	(M)	-7.2040	0.8794	-8.19 *
B_{11}	(SS)	0.7044	1.1660	0.60
B_{22}	(MM)	-4.5340	1.1660	-3.89 *
B_{12}	(SM)	2.2020	1.2420	1.77 +

Table 6.16 Table of polynomial coefficients for shrinkage in the shallow vacuum formed containers

Polynomial terms		Estimate	Standard Error	Estimate / Std Error
B_0	(Grand Mean)	21.160	6.845	-
B_1	(S)	13.370	3.428	3.90 *
B_2	(M)	- 19.580	3.428	-5.71 *
B_{11}	(SS)	7.926	4.454	1.74 +
B_{22}	(MM)	3.226	4.545	0.71
B_{12}	(SM)	1.055	4.840	0.22

Table 6.17 Table of Polynomial coefficients for shrinkage in the deep vacuum formed containers

* Indicates significant effect (> 95% in t - distribution)

\+ near significant effect

Polynomial terms		Estimate	Standard Error	Estimate / Std Error
B_0	(Grand Mean)	19.7700	7.447	-
B_1	(S)	3.4920	3.055	1.14
B_2	(M)	-5.0200	3.055	-1.64 +
B_3	(P)	-8.0400	3.139	-2.56 *
B_{11}	(SS)	0.7406	3.512	0.21
B_{22}	(MM)	-0.9441	3.512	-0.27
B_{33}	(PP)	2.7480	3.512	0.78
B_{12}	(SM)	-0.6667	4.339	-0.15
B_{13}	(SP)	-4.6800	4.161	-1.12
B_{23}	(MP)	3.2900	4.161	0.79

Table 6.18 Table of polynomial coefficients for shrinkage in the shallow plug-assist formed containers

Polynomial terms		Estimate	Standard Error	Estimate Std Error
B_0(Grand Mean)		12.830	3.030	-
B_1	(S)	8.970	1.243	7.22 *
B_2	(M)	-2.929	1.243	-2.36 *
B_3	(P)	-10.380	1.277	-8.13 *
B_{11}	(SS)	3.016	1.429	2.11 *
B_{22}	(MM)	-2.077	1.429	-1.45
B_{33}	(PP)	3.992	1.429	2.79 *
B_{12}	(SM)	-2.313	1.765	-1.31
B_{13}	(SP)	-3.546	1.693	-2.09 *
B_{23}	(MP)	2.994	1.693	1.77 +

Table 6.19 *Table of Polynomial coefficients for shrinkage in the deep plug-assist formed containers*

* Indicates significant effect (>95% in t distribution)

\+ Indicates near significant effect

In the deep draws, the shrinkage also decreases with increasing mould temperature (fig 6.18). The plug temperature is the most significant variable that affects shrinkage in shallow plug-assist formed parts (Table 6.18). Fig 6.19 (Graphs1 - 3) shows that shrinkage decreases with increasing plug temperature. Deep plug-assist formed containers show that each variable has significant effect, and also there is significant interaction between sheet and plug temperatures (Table 6.19). Fig 6.20 (Graphs 1 - 3) show that shrinkage is reduced at the lower sheet temperatures. In contrast increasing mould temperature as shown in graphs 4 - 6 causes decrease in shrinkage in the formings; while high plug temperatures reduce shrinkage (Graphs 7-9).

All these data are discussed, and related to other parts of the thesis, in the following section.

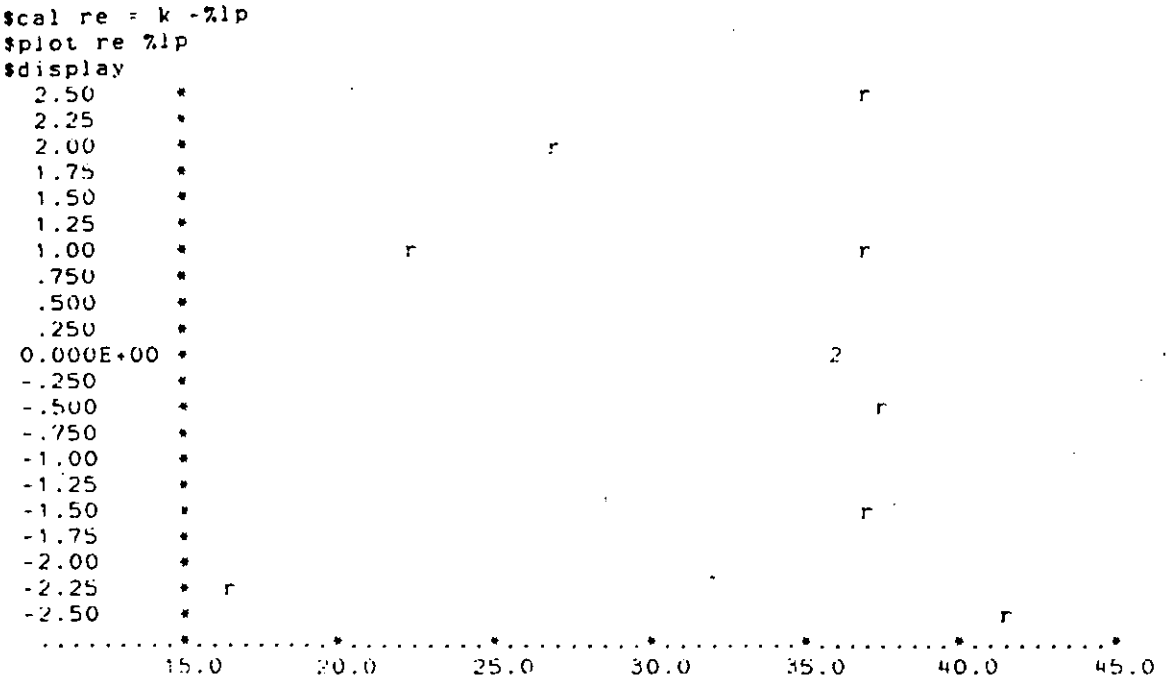

Figure 6.13 Residuals Vs fitted values of shrinkage (shallow vacuum drawn containers

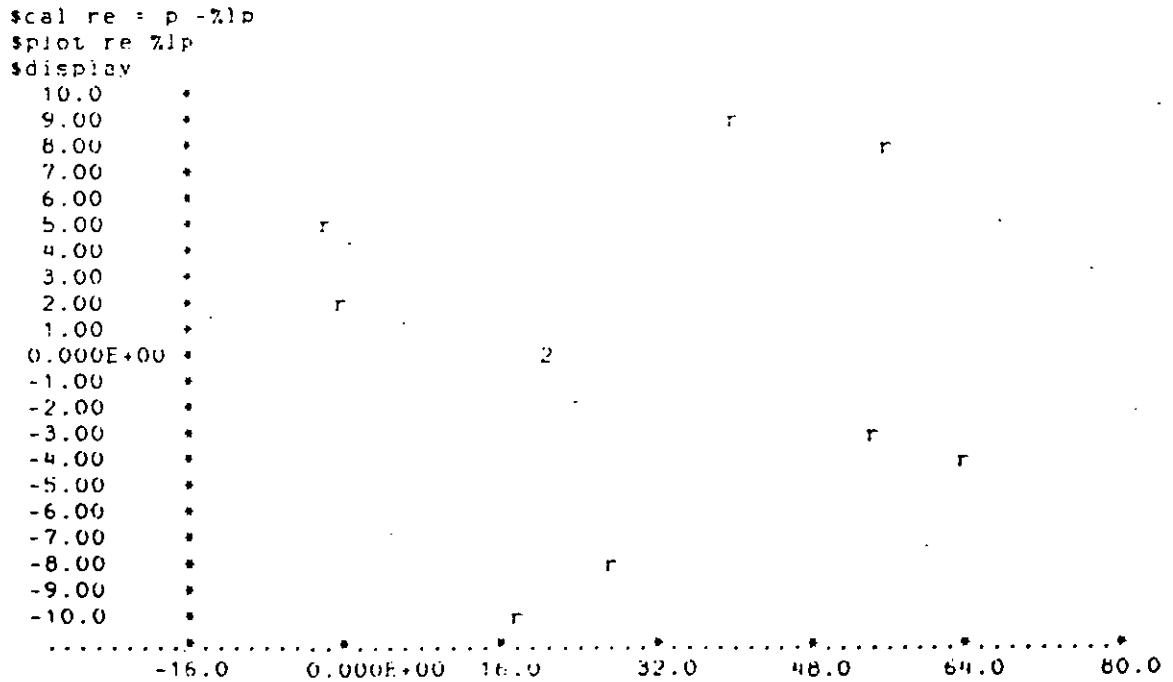

Figure 6.14 Residuals Vs fitted values for shrinkage (deep vacuum drawn containers)

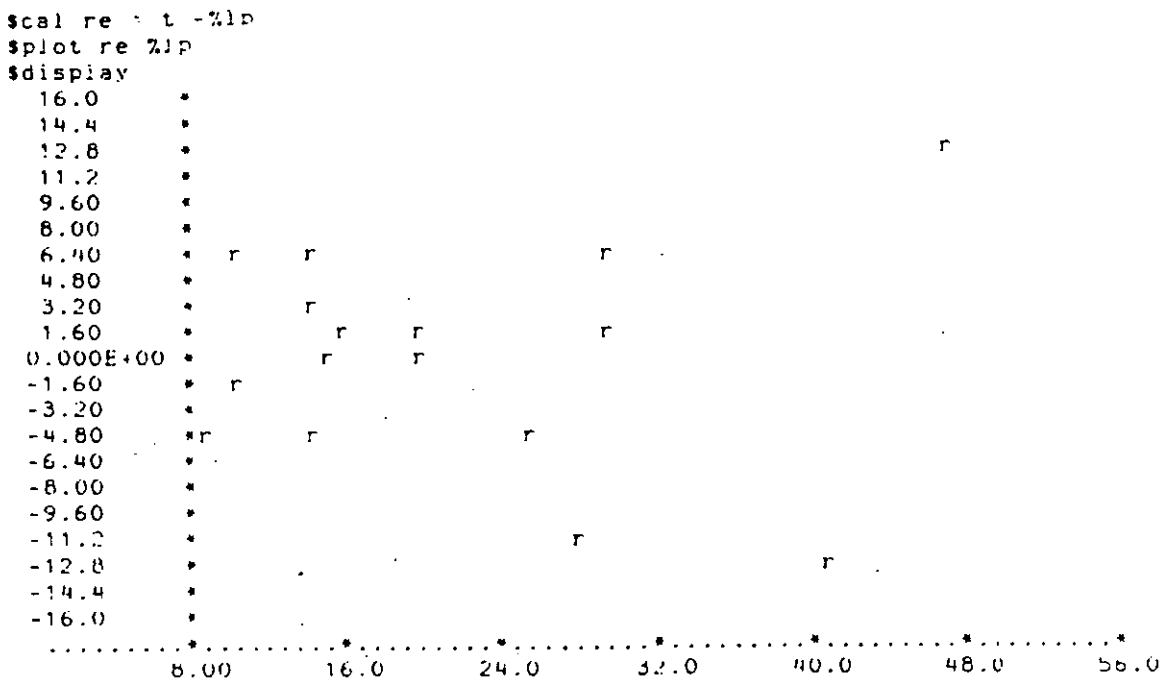

Figure 6.15 Residuals Vs fitted values for shrinkage (shallow plug-assist formed containers

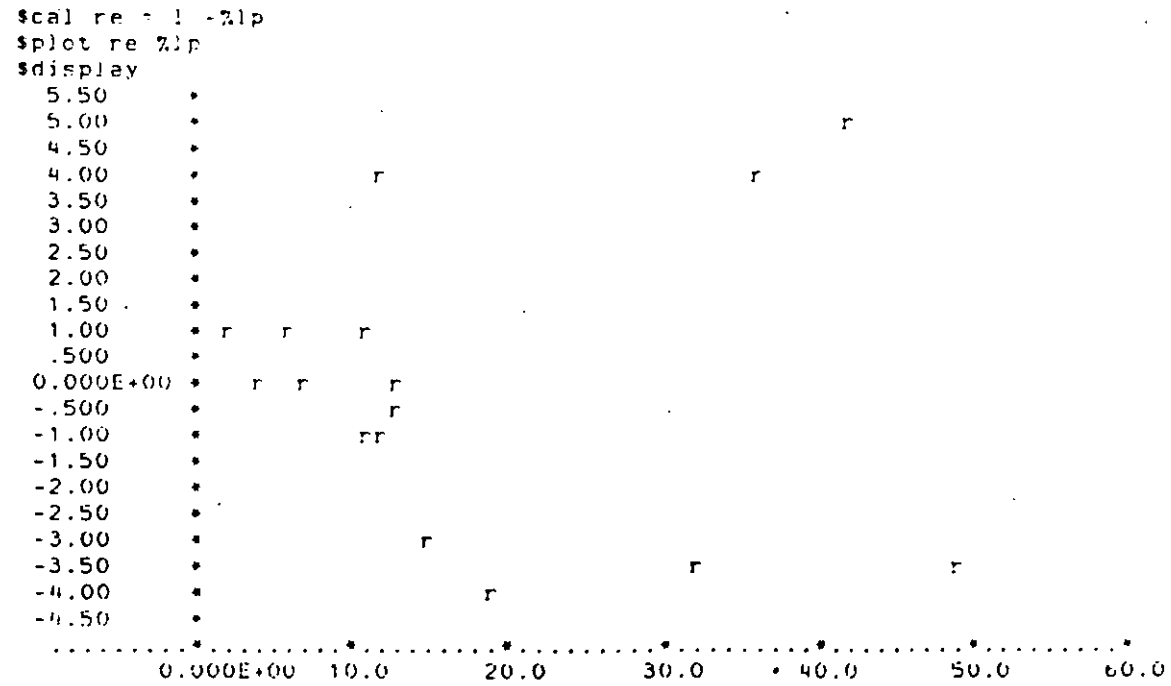

Figure 6.16 Residuals Vs fitted values for shrinkage (deep plug-assist formed containers)

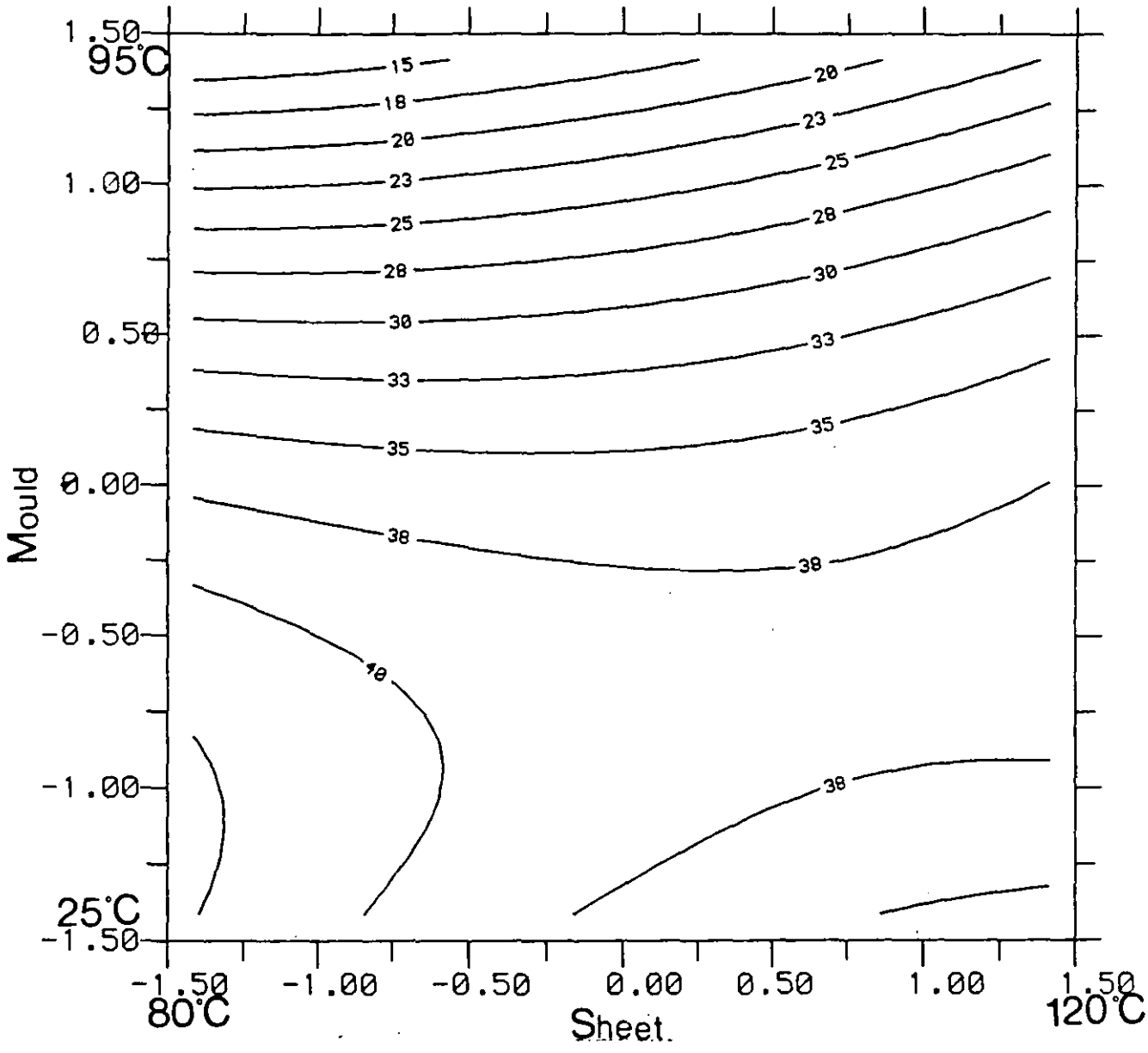

Figure 6.17 *Contour plot of shrinkage variation (shallow vacuum formed containers)*

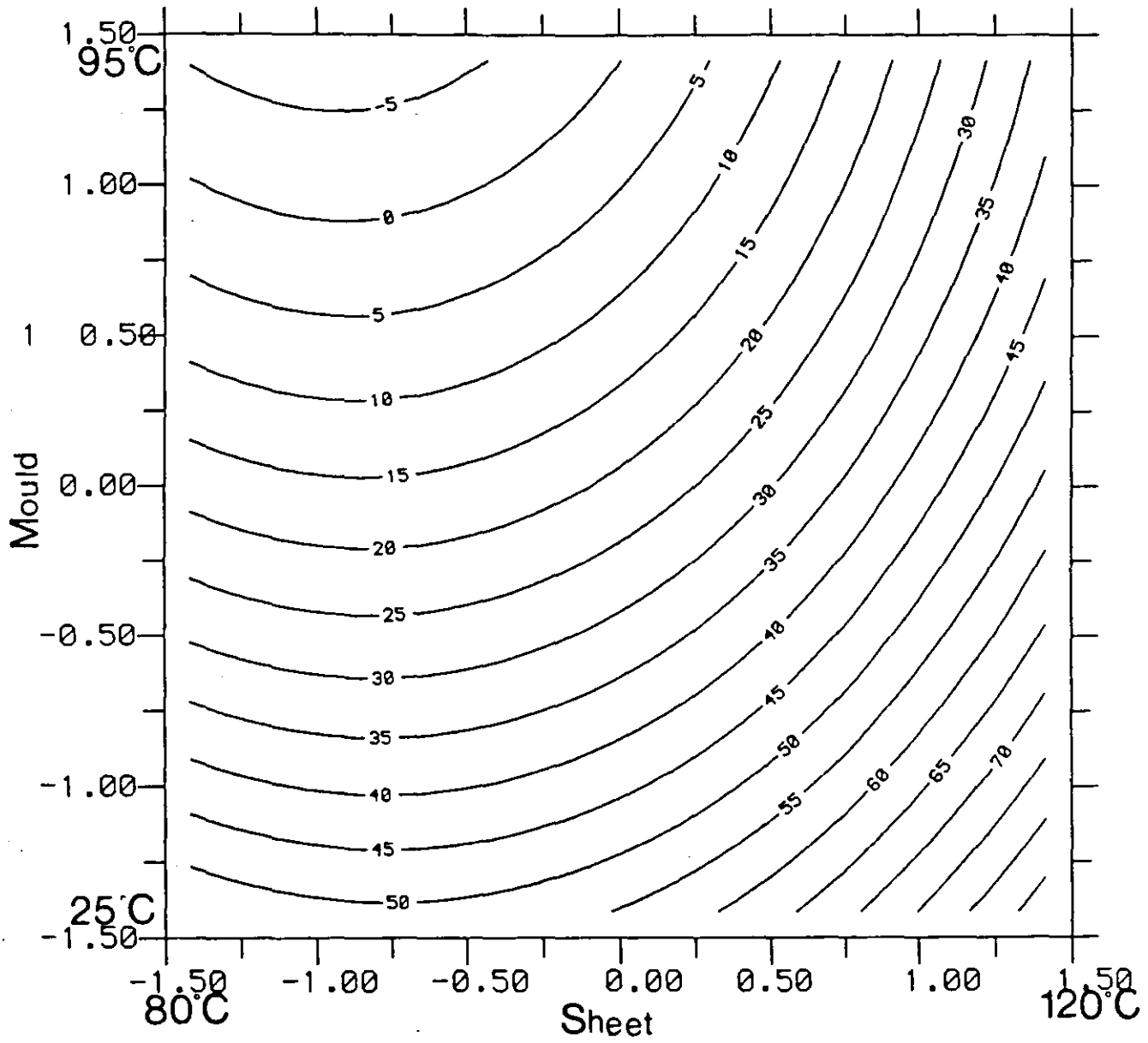

Figure 6.18 *Contour plot of shrinkage variation (deep vacuum formed containers)*

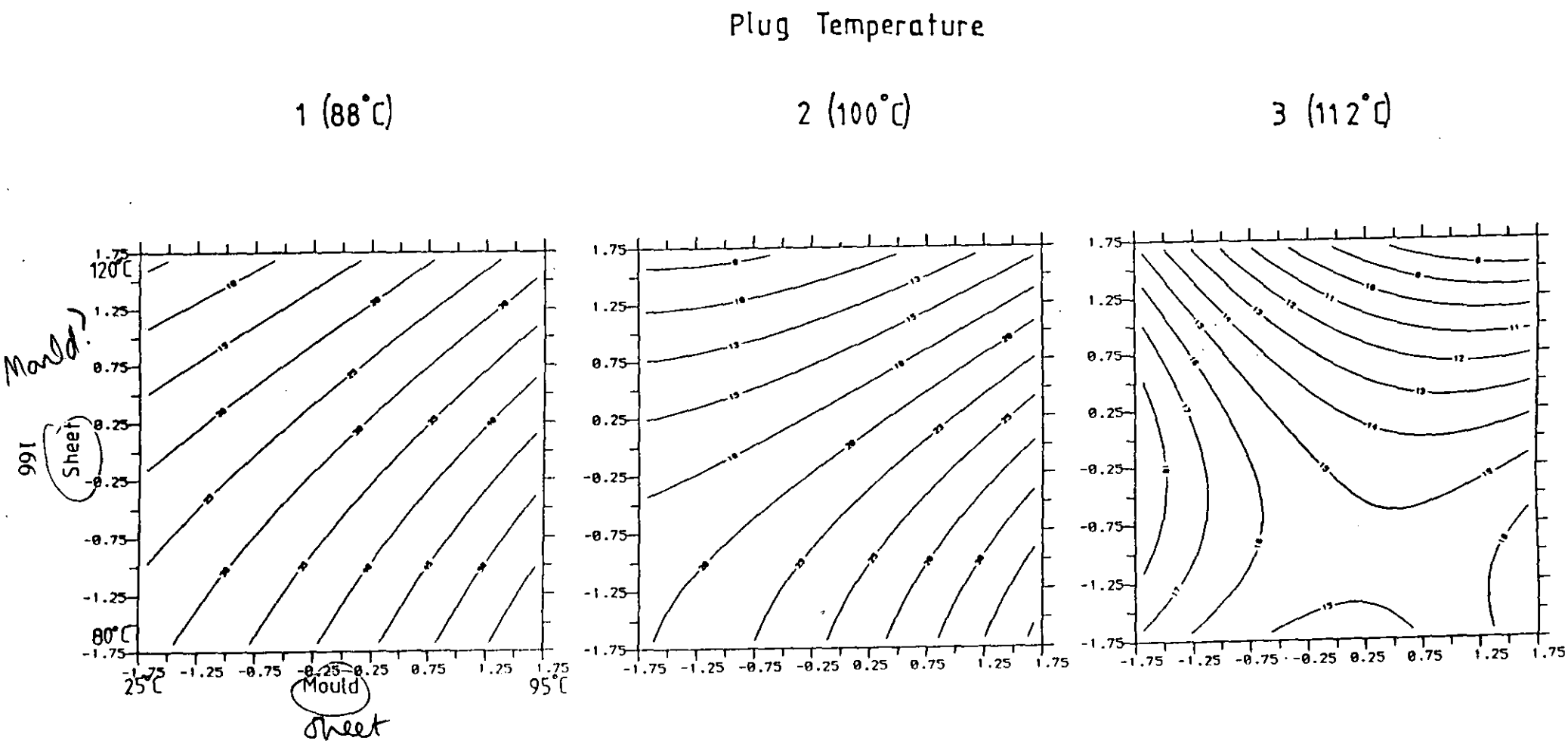

Figure 6.19 Co: .ntour plot of shrinkage variation (shallow vplug-assist formed containers)

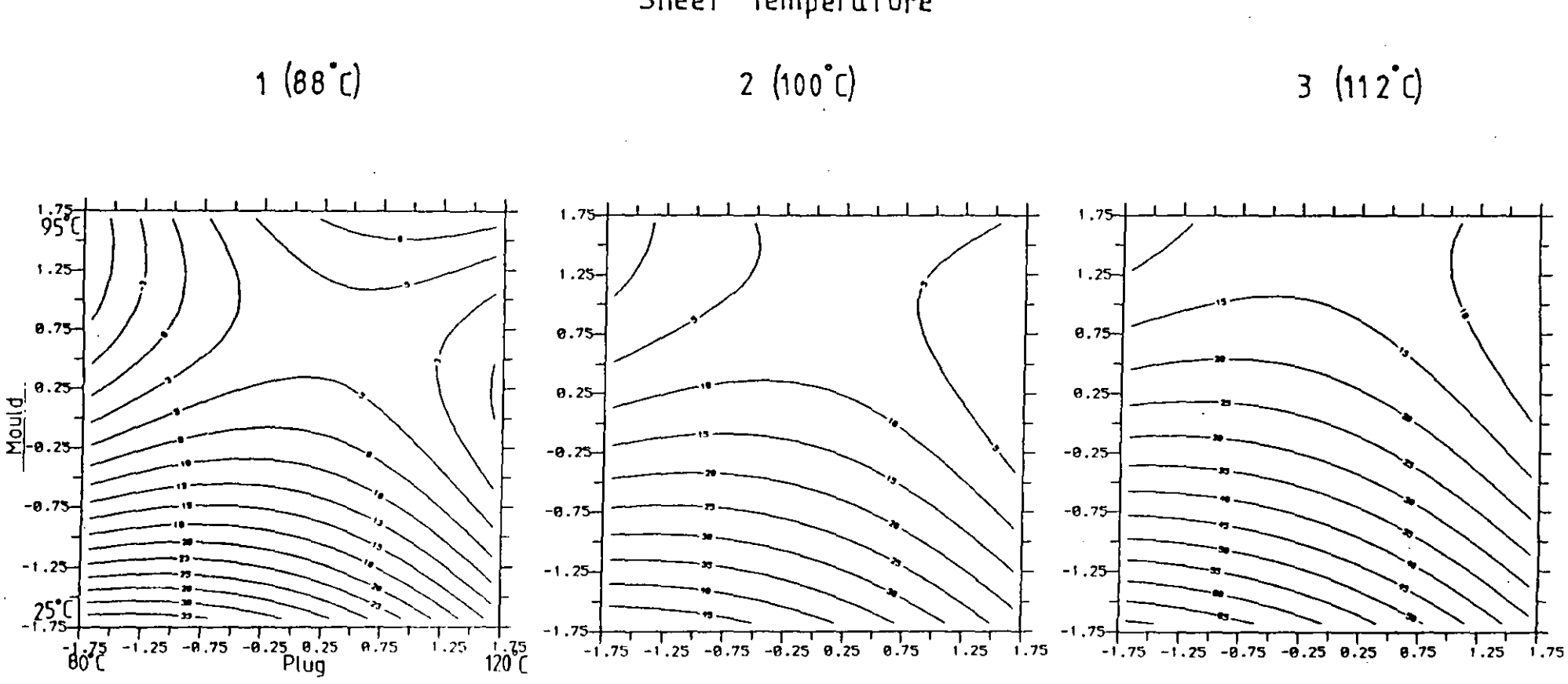

Figure 6.20 *Co. ntour plot of shrinkage variation (deep plug-assist formed containers)*

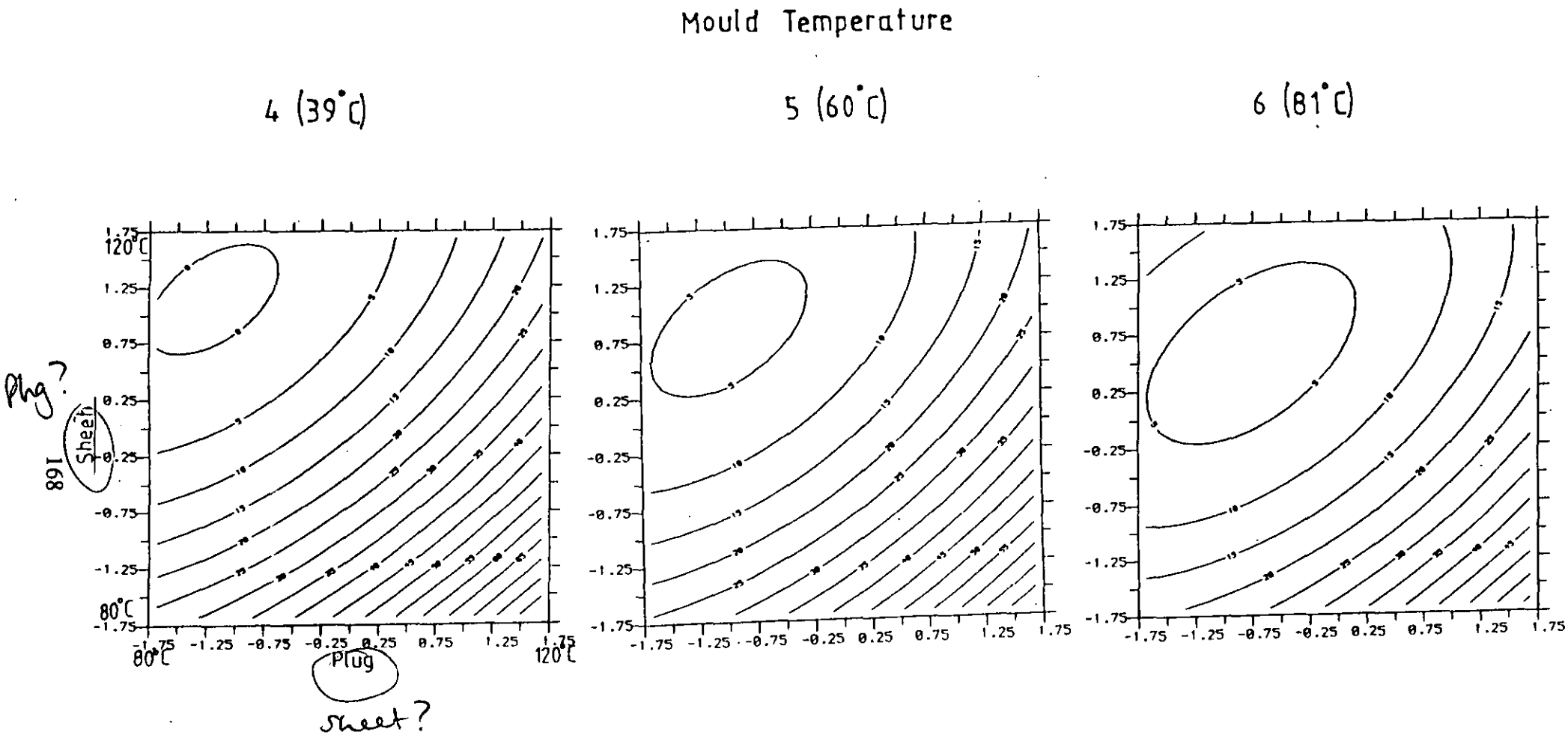

Figure 6.20 *Co. ntour plot of shrinkage variation (deep plug-assist formed containers)*

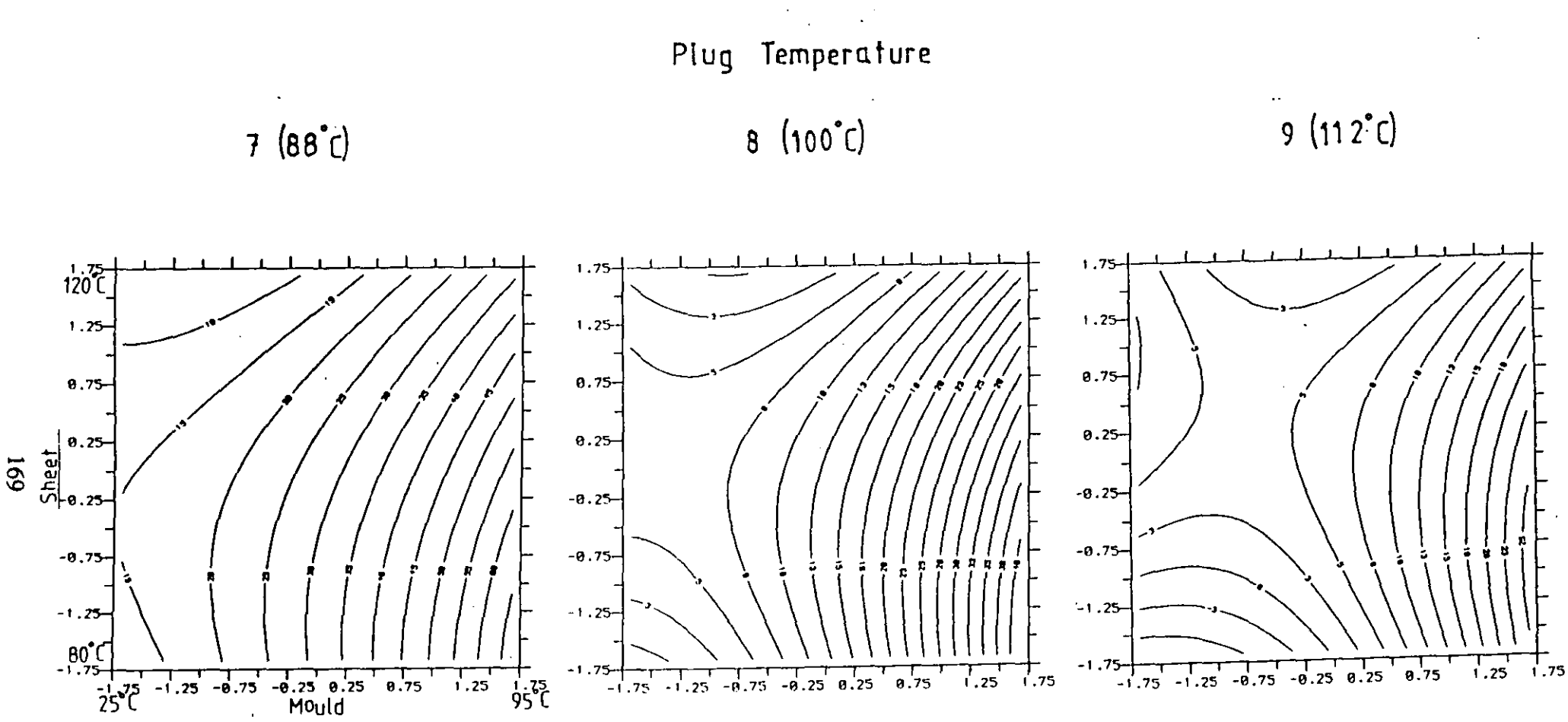

Figure 6.20 Co ntour plot of shrinkage variation (deep plug-assist formed containers)

6.6.3 Discussion

(A) Thickness Distribution

The statistical analysis of the thickness distribution and shrinkage in the formings has shown that, sheet temperature is not the only critical variable in thermoforming as is often generally perceived.

(i) **Vacuum Formed Containers**

In the exploratory formings (Chapter 5) the results suggest that thickness distribution in shallow draws was not highly temperature sensitive . The statistical experimental approach has ensured the determination of the best processing conditions to obtain containers of least thickness variation. Better thickness distribution was obtained between 90-100oC (Fig 6.9) for shallow vacuum containers because

(a) PETP exhibit typical rubber-elastic properties at these temperatures and

(b) the draw ratio is within the 'natural draw' regime defined in the stress-strain curve (Chapter 3).

In contrast, for the deep draws (Fig 6.10), the draw ratio is within the strain hardening regime which has been shown to discourage local thinning (or necking), thus enhancing thickness uniformity in formed parts. Since the stain hardening effect decreases with increasing temperature in PETP, it is not surprising that thickness distribution deteriorates with increasing sheet temperature.

(ii) **Plug-assist Formed Containers**

In the plug-assist formed containers , the complex interaction between the variables makes concise interpretation of the response surface difficult. The high processing condition values which promote uniform thickness in shallow plug-assist formed containers can be attributed to enhancement of chain mobility (ie less resistance to deformation) which is required at shallow draws as explained for vacuum forming mode. This satisfies the rubber-elastic properties of PETP at draw ratio within the 'natural draw' regime.

On the other hand, in the deep draws, lower sheet temperatures ensure uniform thickness. This is because PETP exhibit high strain hardening effect at these temperatures (80-90°C) where it has been shown to promote thickness uniformity. However, the relationship between plug temperature and thickness distribution is complex. At the lower plug temperatures, the increasing deterioration in thickness distribution could be attributed to increasing sliding friction between the plug surface and the PETP sheet. The two situations restricts stretching with consequent excessive wall thinning. The influence of plug temperature on the shallow draws is limited because stretching from the plug surface is very small with resultant limited effect on

the thickness distribution. Therefore, better thickness distribution obtained between 90-100°C plug temperature ensures chain mobility (within the sheet) and low sliding friction between the sheet and plug surface.Effect of friction will be further explored in the later part of the analysis in this work.

Overall,the thickness distribution results confirm that uniform thickness is promoted at the lower forming sheet temperture where PETP exhibits high strain hardening behaviour, especially in the deep draws. Since thickness distribution in deep draws is superior to shallow draws, proof is derived to show that draw ratio must exceed the 'natural draw' regime defined in the stress-strain curve (Chapter 3).

Therefore best forming temperatures to obtain containers of least variation in thickness is as follows:

Vacuum Forming	Temperatures°C	
Draw ratio	Sheet	Mould
1:1	90-100	55-70
2:1	80-90	70-90

Plug-assit Forming		Temperatures°C	
Draw ratio	Sheet	Mould	Plug
1:1	100-112	75-85	100-112
2:1	80-90	70-80	100-112

(B) Shrinkage Distribution

The shrinkage data showed the contribution of the tool temperatures to formed containers, high mould temperatures are required to reduce shrinkage, especially in the shallow draws. This is because the deformation is within the rubber-elastic region; thus it relies on thermally induced crystallization to reduce shrinkage. Perhaps, the orientation may simply relax-out at high mould temperatures. In the deep draw however, both strain and thermally induced crystallinity appear to contribute to thermal stability in the formings.

In the plug-assist formed containers, the plug temperature plays a prominent role. High plug temperatures 'heat set' the orientation, induce crystallinity in the sheet, especially in the deep draws. The higher shrinkage values in the shallow draws is because deformation is within the rubber-elastic region, thus recoverable. Whereas, in the deep draws, there is combined effect of strain and thermally induced crystallinity which reduced the chain mobility as shown in the stress relaxation results (Chapter 3).

It was expected that the shrinkage in the plug-assist formed containers (where deformation is more unidirectional) will be greater than the shrinkage in the vacuum formed containers (where there is an element of biaxial deformation). This was not reflected in the results; perhaps due to thermal induced crystallinity enhanced by additional heating of the sheet by the plug.

From the contour plots the best forming conditions to manufacture thermally stable PETP containers are as follows:

Vacuum forming	Temperatures °C	
for both 1:1 and 2:1	Sheet	Mould
draw ratios	80 - 90	90 - 95

Plug-assist forming	Temperatures °C		
Draw ratio	Sheet	Mould	Plug
1:1	100 - 112	70 - 95	100 - 112
2:1	80 - 90	30 - 65	100 - 112

Therefore, it is concluded that thermoformed PETP can be used for hot fillable applications, at least up to 80 °C, at the specified conditions.

6.7 Theories Predicting Thickness Distribution of Thermoformed Parts

Early investigation of the analysis of forming was on biaxial deformation of warmed thermoplastics. Schmidt and Carley [165] studied biaxial deformation of a number of amorphous plastics about their T_g by blowing a bubble. They expressed the principal extension ratios in terms of cylindrical coordinates as shown in fig 6.21

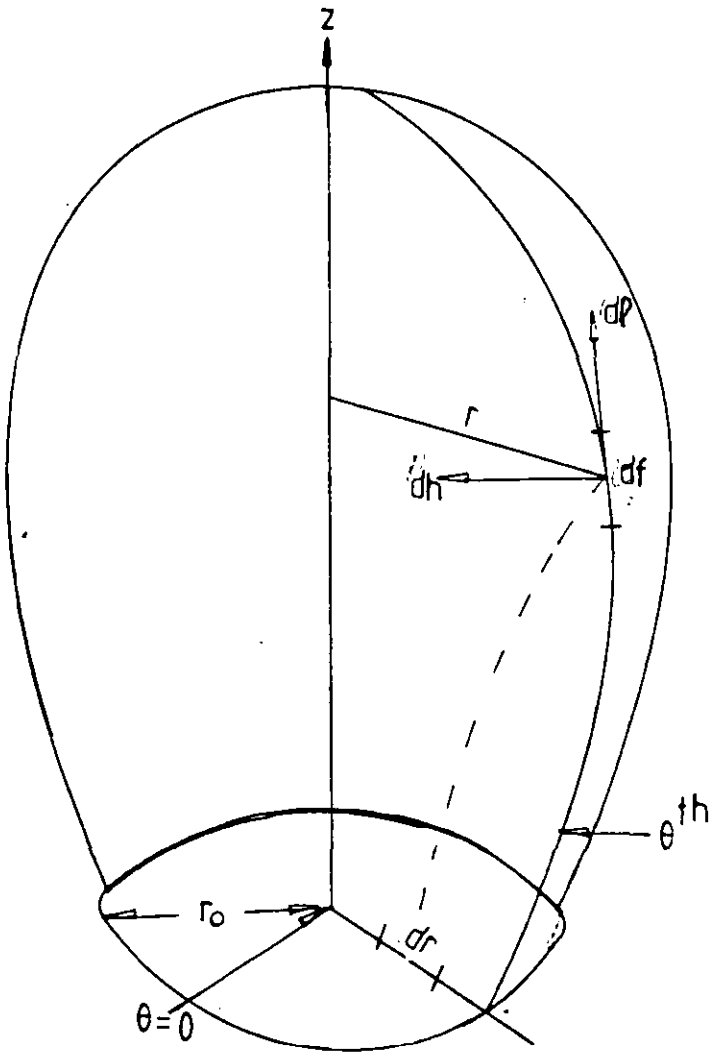

Figure 6.21 Cylindrical coordinate system used in the analysis of idealized axisymmetric deformation of a bubble

$$\lambda_l = df/d\rho \qquad \text{----------6.9}$$

(the extension ratio in the longitudinal direction)

$$\lambda_h = \frac{2\pi r}{2\pi r_o} \qquad \text{---------- 6.10}$$

(extension ratio in the latitudinal/hoop direction ie perpendicular to λ_l)

$$\lambda_t = \frac{t}{t_b} \qquad \text{---------- 6.11}$$

(t_b is the initial sheet thickness, t is the thickness of deformed element:extension ratio perpendicular to the others)

r_o is the radius of a given circle on the original sheet, and f is the arc length measured along a meridian from the pole of the deformed middle surface to a point (r,θ,Z). λ_L was obtained from the continuity equation:

$$\lambda_l = 1/\lambda_2\lambda_3 \qquad \text{----------6.12}$$

The profile of the bubble from the extension ratios was assumed to relate to conventional thermoforming of the plastics investigated. Similar analysis have been carried out by other researchers [166 - 171].

However, the deformation of a bubble is applicable to the early stages of thermoforming (to the point where mould contact is made) regardless of the forming technique adopted (except for straight drape forming).

In conventional vacuum forming, as the sheet is drawn into the mould it contacts the mould first at the rim, then the walls of the mould. If the bubble was stopped from drawing at the instant it touches the rim, the sheet wall thickness would be very similar to that given by Schmidt and Carley [165].

This has been pointed out by Williams [166] in his study of vacuum forming of PMMA sheet into conical moulds. Using similar geometry to that given in Fig 5.4 the principal extension ratios were determined as follows:

$$\lambda_l = dh/dr_o = (dr/dr_o)1/\cos\alpha \qquad \text{----------6.13}$$

α = the angle of the conical wall

$$\lambda_h = \frac{r}{r_o} \qquad \text{---------- 6.14}$$

$\lambda_l = \lambda_h$ for equal biaxial deformation with boundary condition that $r = r_o = a$

$r = a\,(r_o/_a)\cos\alpha$

a = mould rim radius

The wall thickness was shown to vary with depth of draw according to

$$\lambda_t = t/t_b = \{r/a\}^{2[(1/\cos\alpha) - 1]} \qquad \text{----------6.15}$$

For vertical wall $\alpha = \pi/_2$

$$t / t_b = \exp(-2h/a) \qquad \text{----------6.16}$$

Where h = the distance down the wall of the mould.

Williams [166] applied thin shell deformation theory to determine relationships between applied force and draw ratios as follows:

$$P = 2F_o \sin\alpha/r\{1 - [\sin^6\alpha/8(1 - \cos^3\alpha)]\} \qquad \text{----------6.17}$$

and for vertical wall (cylinder)

$$P = (2F_o/a)\{(1 - 1/8 \exp[-6h/a])\} \qquad \text{----------6.18}$$

where P = Forming Pressure

F_o = Force per unit length

$F_o = \varnothing t_o$, $\varnothing$ = material property obtained from stress-strain data

$$\sigma\lambda = \varnothing\left[\lambda^2 - \frac{1}{\lambda^4}\right] \qquad \text{---------- 6.19}$$

σ = stress and λ = extension ratio.

A fair correlation between the predicted thickness distribution and experiment was obtained for PMMA.

A similar solution to that of Williams [166] was derived by Ragab [167] working with super plastic metals. He went further to derive solutions for estimating the forming time [168] to attain a given depth of moulding in amorphous plastics (fig 6.22).

$$T = (PR/\varnothing t)^{-1/\varepsilon^*} \; (\gamma/R) \int_c^R [C/R]^{\{-\gamma-(\gamma+1)\varepsilon^*+1\}} - \{(C/R)^{3\gamma-(\gamma+1)(\varepsilon^*+1)}\}^{1/\varepsilon^*} dc \quad \text{--- 6.20}$$

where T = forming time

P = Forming pressure

R = Radius of curvature of free bubble

t = thickness at the given depth

c = Radius of curvature of sheet after contact with mould walls

$\varnothing, \varepsilon^*$ = material constants

$\gamma = [2 \cot \beta - (\pi - 2\beta)]/(\pi - 2\beta)$

β = semi angle of the conical mould

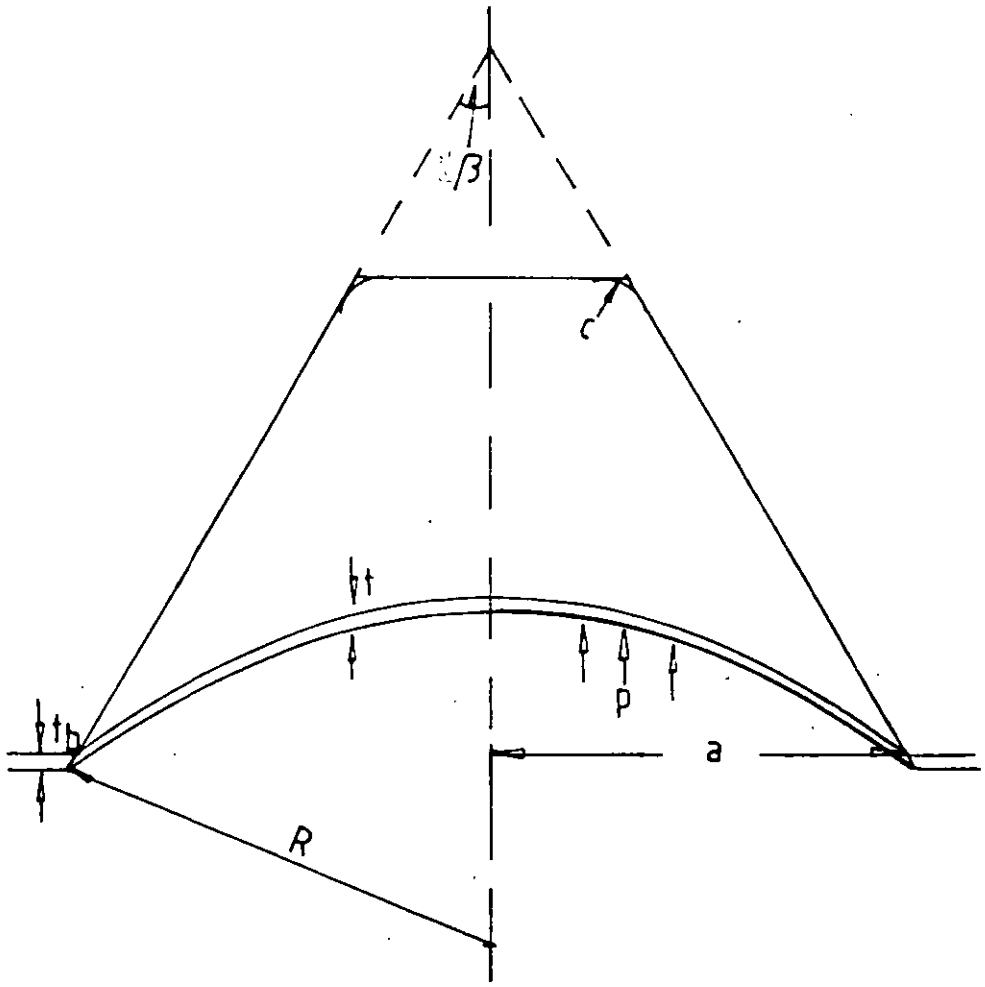

Figure 6.22 Geometry of forming a conical mould

Fair agreement was found between theory and experiment for acrylic sheet.

It should be realised the above theories were based on geometrical factors. This was further extended by Tadmor et al [169] in their model for predicting thickness distribution profile for truncated formings. They divided the forming process into three sections. The first being the free bubble generation stage. Then the free bubbles comes into contact with the mould walls or the mould bottom depending on the depth of draw considered. They considered that the geometry of deformation changes when the sheet bottoms on the mould as shown in Figs 6.23 and 6.24 [169].

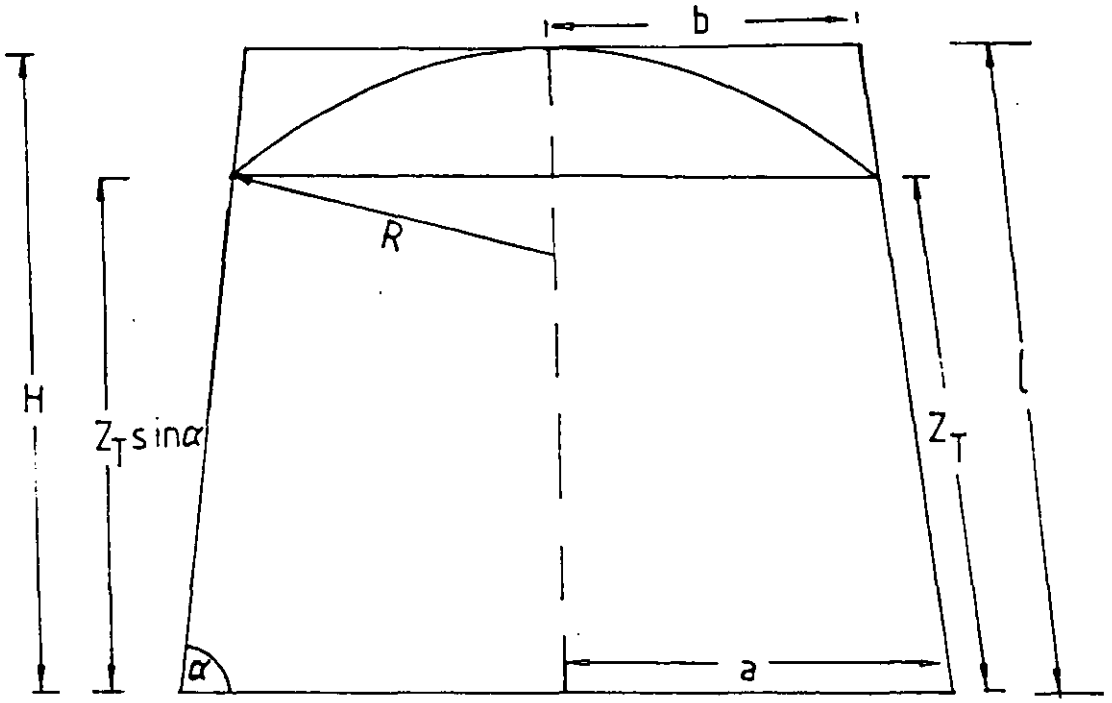

Figure 6.23 Geometry of forming in a deep conical mould

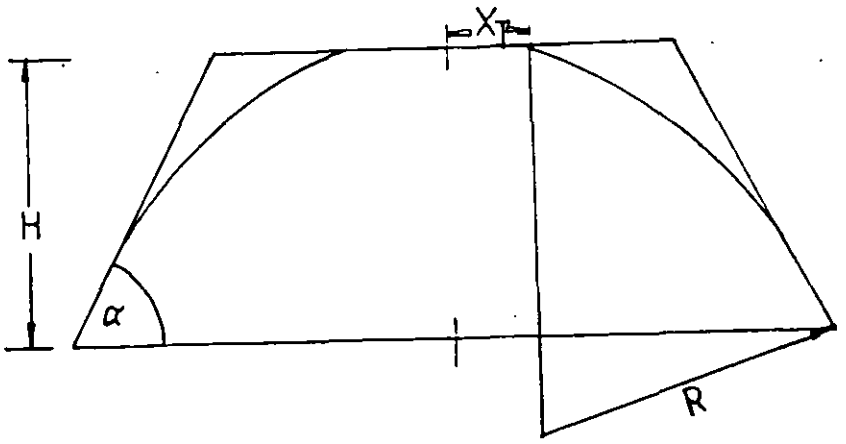

Figure 6.24 Geometry of forming in a shallow conical mould

The wall thickness distribution for conical mould was predicted by the equation 6.21

$$t = t_b (1 + \cos\alpha/2) [H - Z\sin\alpha/H]^{\sec\alpha - 1} \quad \text{----------6.21}$$

where H = height

Z = slant height of the mould displaced

α = conical angle

For details of change in geometry at the bottom of the mould, the reader is referred to reference [169]. The change in geometry at the bottom of the mould is not as complex as made out to be. In practice this is usually nullified by allowing for generous radii at the corners of the mould. In addition, the deformation at the bottom of the mould is governed by biaxial stretching, thus uniform thickness. The model for predicting wall thickness distribution is the same with that given by Crawford [170].

Tadmor et al's [169] equations were based on Sheryshev et al's [171] model in which they not only considered geometrical factors but recognised the effect of the technological parameters of the process on the variation in wall thickness in vacuum forming. For a conical mould the thickness variation was given by

$$t = t_o (1 - l / b\cos\alpha)^{-2 + kof} \quad \text{----------6.22}$$

for cylindrical article, $t = t_o \exp(-k_o H/b)$ ---------- 6.23

where $f = \sin^2\alpha / (1 - \cos\alpha)\cos\alpha$

$t_o = 1/2\ k_s\ m t_b$

for cylindrical article, $to = t_b k_s/2$

and $m = \sin^2\alpha/1 - \cos\alpha$ -------- 6.24

l = slant height of mould, H = height of mould

b = radius of the conical base

α = conical angle

k_o = cooling factor (characterises the degree of cooling by material being formed)

k_s = stretch factor of the material.

They assumed that:

$k_o < 1$ when part of the material is being drawn away from the conical region.

$k_o = 1$ when the drawing of material stops on contacting the mould wall (no slippage in the wall).

$k_o > 1$ when part of the spherical bubble is cooling during forming

Sheryshev et al [171] show that increasing mould temperature decreases variation in wall thickness.

All the above solutions for predicting wall thickness distribution assumed near-elastic behaviour of the plastic sheet above T_g. Also the following simplifying assumptions were made for the forming process:[169]

(1) The thermoformed sheet is isotropic (pre-orientation should therefore be avoided)
(2) The instantaneous free bubble is uniform in thickness and spherical in shape.
(3) The temperature of the free bubble is uniform and does not vary with time.
(4) Upon contact with the relatively cold mould surface the polymer is chilled ($T \ll T_g$) and there is no further deformation. The deformation is limited to free bubble which uniformly decreases in thickness.
(5) There is no polymer drawing about the clamping frame area.
(6) The polymer is incompressible.
(7) A circular symmetry is assumed for the mould.

The first assumption is fair, because even in situations in which the material is not perfectly isotropic, the heating process reduces the anisotropy in amorphous sheet before forming.

It is generally true that the free bubble is spherical in shape, however, the thickness is not uniform. Lai and Holt [103] and others [27,165] have demonstrated that the thickness varies from the pole of the bubble to the rim.

The temperatures across the spherical bubble is not uniform as shown by Schmidt et al [165]. They found that the temperature of the sheet drops rapidly at the centre of the bubble.

It is assumed that the friction effect between the mould surface and the formed sheet (due to chilling effect) is such that no slippage occurs. However, there are seemingly conflicting reports in the literature with respect to influence of mould

temperature on friction characteristics of polymers (HIPSin particular). Sheryshev et al [171] showed that increasing mould temperature improves thickness distribution in formed parts, thus the incorporation of a cooling factor into their model as a correction coefficient for the thickness profile prediction. In contrast , Tsai [172] showed that increasing mould temperatures increases the sliding friction of polystyrene sheets on the mould surface especially et high sheet temperatures. It was expected that the influence of temperature on thickness distribution in PETP formings would be highlighted in section 6.6.1. Unfortunately, the procedure was not sensitive enough to acknowledge the effect of mould temperature on thickness distribution in the formings; except in Fig 6.11 (Graph 4-6) where increasing mould temperature was found to improve thickness distribution in shallow plug-assist formed containers. The influence of tool temperatures on deformation characteristics of PETP sheet will be further investigated in the later section of this report.

In practice, heated material is partially drawn into the female mould from the space bounded by the clamping device but not directly over the female mould (and also beneath the clamping frame). Thus the assumption that drawing is limited to the material directly located over the mould cavity is not strictly correct. Sheryshev at al [171] accounted for this in their derivation by introducing a correction factor k_s (stretch factor of the material) into the equation for thickness change in the free bubble.

The assumptions of incompressibility of material and circular symmetry are valid and essential to obtain solutions to the equation.

The main drawback of female vacuum forming is that the thickness decreases from the rim to the bottom of the forming. To over come this problem plug-assist is usually employed as earlier stated in Chapter 4. Plug-assist promotes wall thickness uniformity.

Very few researchers have attempted to analyse plug-assist forming Williams[166] considered a conical mould of radius 'a' and plug of radius 'b' and found a relationship between the displacement 'h' from the rim of the mould and the local radius of the sheet(fig 6.25).

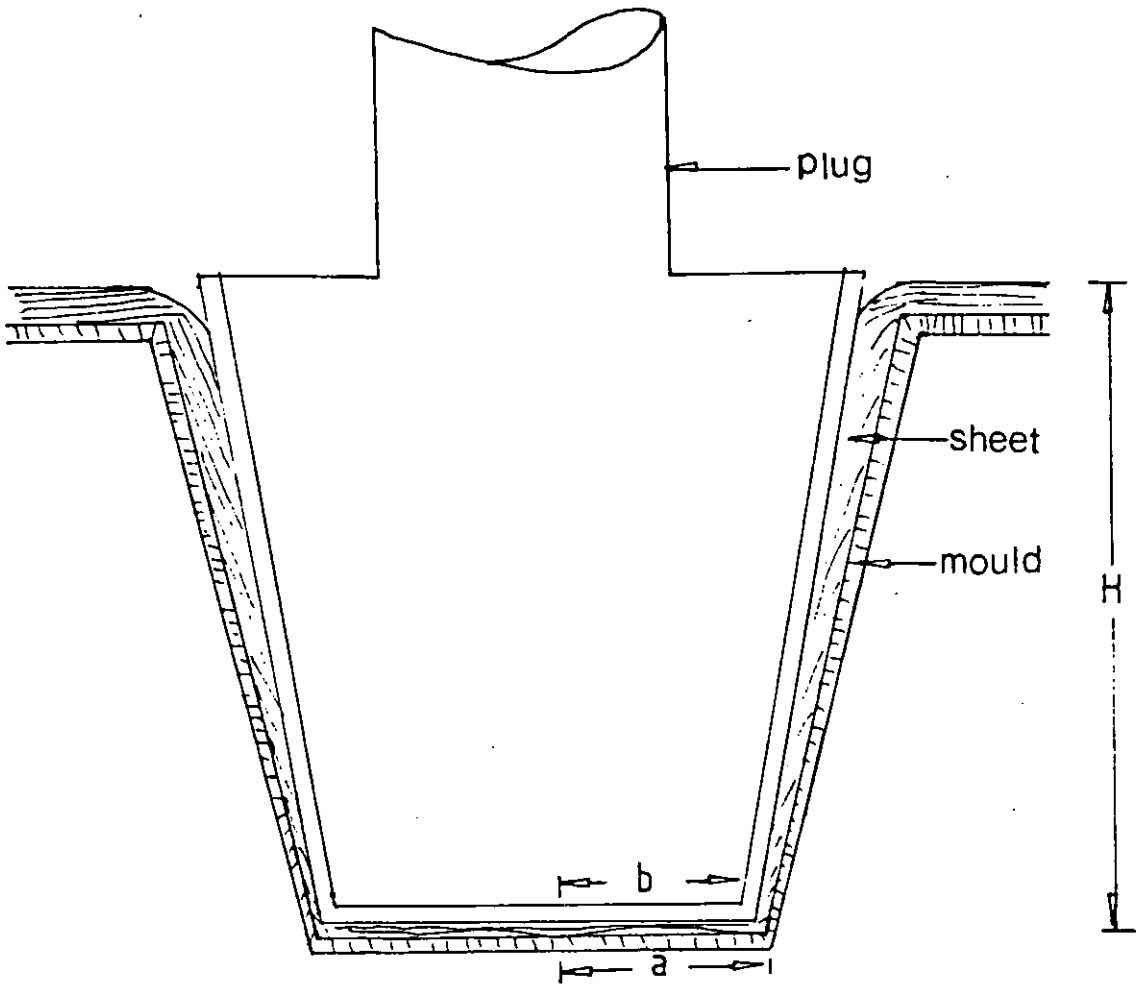

Figure 6.25 Geometry of forming in plug-assist mode

$$h = \frac{H\,(a - r)}{a - b} \qquad \text{---------- 6.25}$$

where $0 \leq h \leq H$

a = mould base radius

b = plug radius

r = local radius of formed sheet

The reduced thickness of the stretched sheet was given as:

$$t / t_b = 1/(1 + \sqrt{[\,H / r \ln \{a/b\}]^2}\,) \qquad \text{----------6.26}$$

The ratio of deflection of plug height is given as:

$$h/H = [\ln (a/r)] / [\ln (a/b)] \quad \text{----------6.27}$$

However, the analysis given by Williams failed to take into consideration additional surface area generated by the plug action [148,173]. Throne [148] suggested simple modification to the equation to account for the extra surface area generated which reduces the ultimate h/a. He replaced the plug radius (a) with an effective plug radius which included the new surface area as follows:

$$A = \pi [\sqrt{(H^2 - (a - b)^2}](a + b) + \pi b^2/4 \quad \text{---------- 6.28}$$

A = surface area

a was replaced with

$$a_{eff} = \sqrt{4A/\pi} \quad \text{---------- 6.29}$$

Sheryshev et al (173) in their analysis of plug assist forming allowed an increase in surface area of plastic sheet due to plug action. In addition they incorporated correction coefficients due to processing parameters which affect the wall thickness distribution. The wall thickness at any point on a conical article Fig 6.8 with plug-assist was given as:

$$t = (2/\pi)\, k^c_s\, k^P_s\, t_b \exp(-h/n) \quad \text{----------6.30}$$

$$\text{where } n = \frac{a^2 - b^2}{4 (K^m_o a + K^P_o b)}$$

t_b = blank thickness

a = mould base radius

b = plug base radius

h = displaced height from the rim

k_s^c = stretch factor of the material from under the clamping frame

k_s^p = stretch factor of the material from the part of the surface of the blank situated at the plug nose

k_o^m = cooling factor of plastic sheet in contact with mould surface

k_o^p = cooling factor of plastic sheet surface in contact with plug

Sheryshev et al [173] assumed that $k_o^p = k_o^m$

when (i) constant temperature is maintained on the plug and mould during forming by means of a fluid.

and (ii) plug and mould are made from materials of the same thermophysical properties.

Assuming k_s^c is negligible, since the clamping device usually secures the plastic sheet, k_s^p was calculated as follows:

$$t = (2/\pi)\, k^p_s k^c_s t_b \exp(-h/n)$$

Therefore, Plot of ln t vs h gives a straight line where - 1/n = slope

and $\ln (2/\pi)\, k^p_s k^c_s t_b$ =intercept of the straight line

As shown above, this equation is more of a tool to investigate the influence of processing conditions on wall thickness distribution rather than to predict thickness variation in formings.

In this part of the work, Williams' models predictions are compared with thickness distrubution for PETP containers for both vacuum and plug-assist modes of thermoforming. Also Sheryshev's models are used to evaluate the effect of processing conditons on deformation processes.

6.7.1 Comparision of Experimental Thickness Distribution with that of Williams' model

The thickness profile (as a function of depth) of the shallow vacuum formed containers is shown in Fig 6.26. The predicted thickness distribution is represented by the 'Theory Curve' (William's model [166]). There is a good agreement between the experimental thickness distributions and that predicted by the model. The agreement between the model prediction and experiment appears to improve at the lower mould temperatures. This is shown particularly at process conditons sheet/mould temperatures. 80/35 °C and 100/25 °C. This behaviour agrees with the hypothesis of model; that is, the sheet freezes onto the mould wall on coming into contact; whereas, at higher temperatures, the experimental thickness distribution deviates from the model prediction. This is not surprising, since the model does not account for influence of processing conditions on thickness distribution in formed parts. Increasing mould temperature may change the frictional characteristics between polymer and the mould wall.

Fig 6.27 illustrates the relationship between experimental thickness distribution and model prediction for deep (2:1) vacuum formed containers. There is a reasonable agreement between the model and experiment up to 20 mm into the mould. Beyond this point, there is a deviation from the model prediction. This is due to strain crystallization behaviour by PETP, since the model was developed for amorphous plastics (PMMA) which do not exhibit strain crystallization behaviour. The effect of strain hardening is significant at the lower temperatures where the formings exhibit uniform thickness from about 40 mm into the mould (see sheet/mould 86/85 °C, 86/35°C and 80/60 °C (fig 6.27). The agreement between the model and experimental thickness distribution improves with increasing difference between the sheet and mould temperatures. As observed for shallow vacuum formed containers, this agrees with the working hypothesis of the model. At the lower sheet temperatures (80 - 100 °C) and higher mould temperatures (85 - 95 °C) which encourage wall slippage, also promote near-isothermal and uniform deformation. Also it encourages strain hardening which promotes uniformed thickness in formed parts. Therefore, as observed for shallow draws, deviation from the model is due to the fact that the model does not account for the effect of varying mould temperature on the behaviour of polymer being thermoformed.

The thickness distributions (as a function of depth) of the shallow plug-assist formed containers are shown in fig 6.28 for different forming conditions. Here, there is a lesser degree of agreement between William's model [165] and experimental results. However, the experiment showed smaller reduction in wall thickness compared to the model prediction. This is because the model assumed no sheet deformation on the plug

surface. Also, the model did not take into consideration, as pointed out by others [148, 173], additional surface area generated by the plug and vacuum action during the forming operation.

However, the model predicts a sharp reduction in thickness around the rim of the container, which was obtained in practice. Also, the main objective of plug assistance was achieved; formings of better structural integrity (lesser reduction in wall thickness) compared to vacuum formed containers of equivalent draw ratio.

From about 30 mm into the mould, there is increasing thickness towards the base of the containers especially at the high sheet and high plug temperatures. This resulted in deviation from model prediction. This is typified by sheet/mould/plug conditions 112/81/112 °C, 112/39/112 °C and 88/81/112 °C in fig 6.28. This could be attributed to two main reasons: (i) increasing frictional forces between the sheet and the plug surface at higher plug temperatures, which inhibits uniform stretching of sheet from the plug surface [173] and (ii) higher plug temperatures assists crystallinity development in PETP (increases time available for crystallisation), which further inhibits the 'extensibility' of the sheet. These effects were not considered in the model.

In deep drawn plug-assist formed containers (fig 6.29) there is a better correlation between the model prediction and the thickness distribution compared to shallow drawn similarly formed containers. The slight deviation from the model prediction from about 40 mm into the mould is due to effect of strainhardening as observed in vacuum formed deep containers. A better thickness distribution was obtained in practice especially at the lower sheet temperatures where higher strainhardening effect is exhibited.

In additon, as observed in shallow plug assist containers, thickness towards the base of the containers from about 80 mm into the mould increases especially at high sheet and plug temperatures.

Therefore, strainhardening behaviour at the lower sheet temperatures, high frictional forces between the sheet and plug at high temperatures and thermal induction of crystallinity are responsible for the slight deviation of experimental results from model prediction.

In conclusion, the William's model [166] requires some refinements in order to predict accurately thickness distribution of thermoformed PETP parts. These include the effect of processing conditions (eg the requirements of near-isothermal condition for uniform deformation which encourage slippage on the mould wall), the effect of strain-induced crystallization in crystallizable polymer like PETP which improve thickness distribution in formed parts.

(a) Thickness Distribution 1:1V

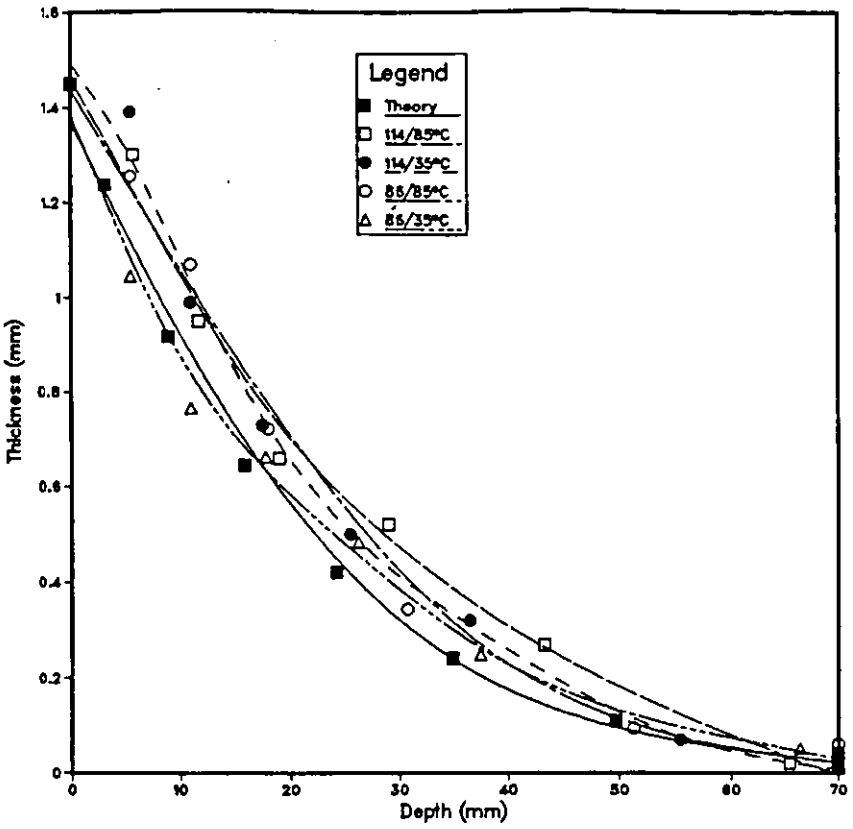

(b) Thickness Distribution 1:1V

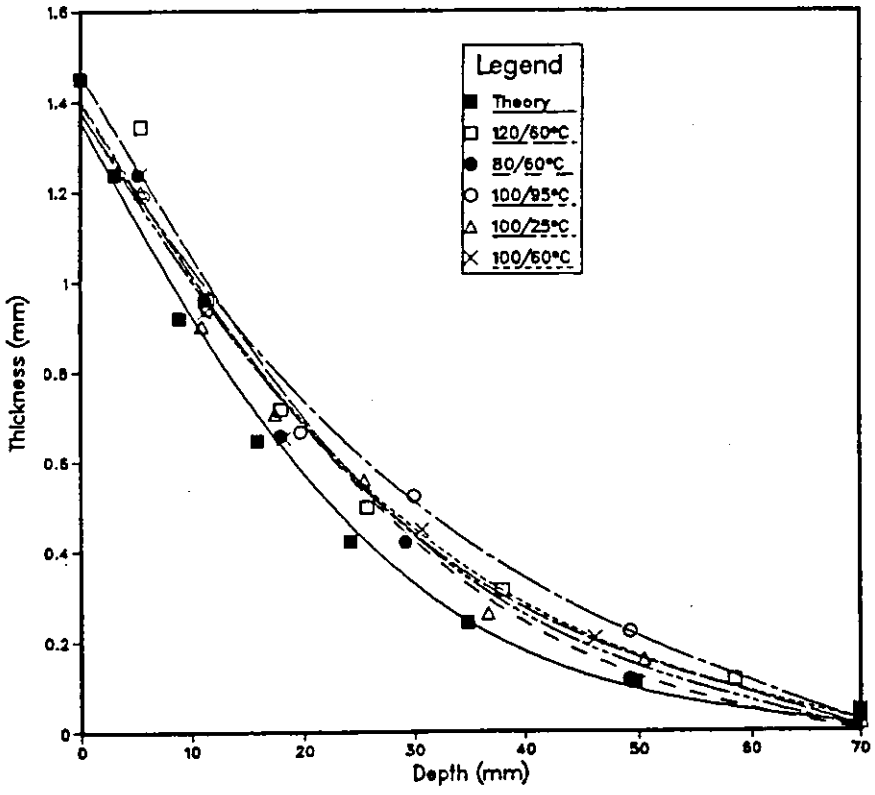

Figure 6.26 Comparison of experimental thickness distribution with prediction from Williams model (shallow vacuum draw). Legend: sheet/mould temperatures

(a) Thickness Distribution 2:1V

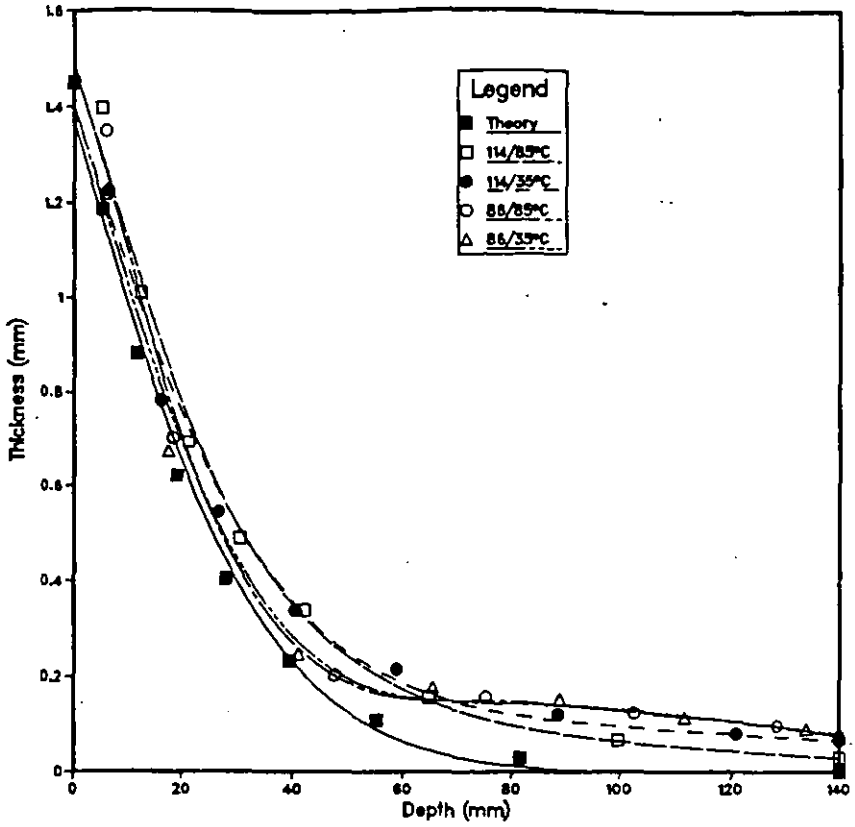

(b) Thickness Distribution 2:1V

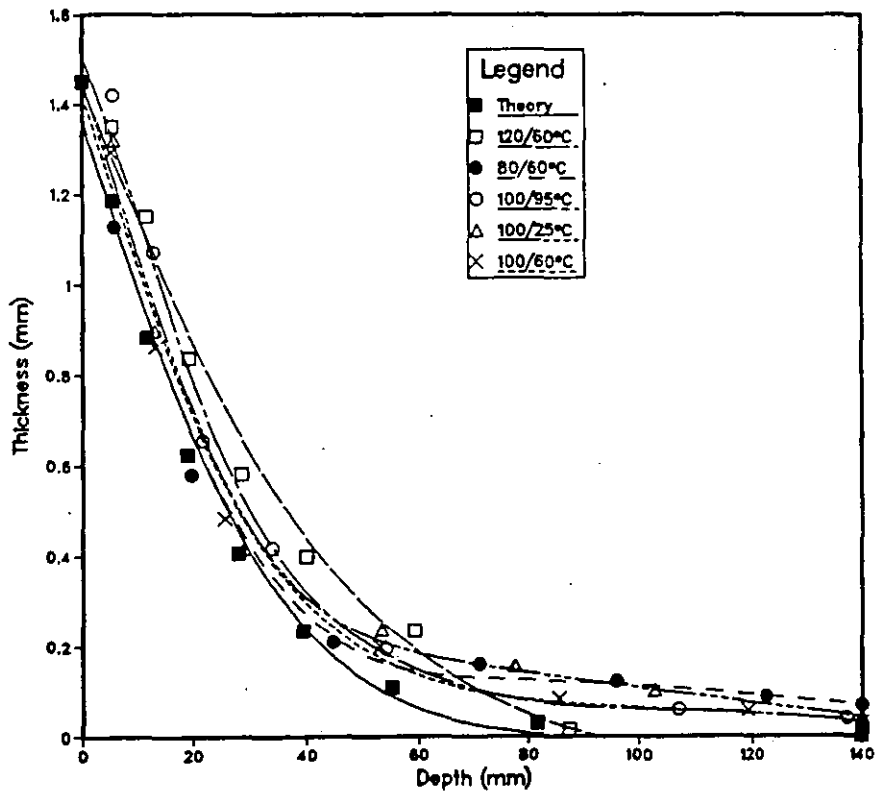

Figure 6.27 *Comparison of experimental thickness distribution with prediction from Wlliams model (deep vacuum draw). Legend: sheet/mould temperatures*

(a) Thickness Distribution 1:1P

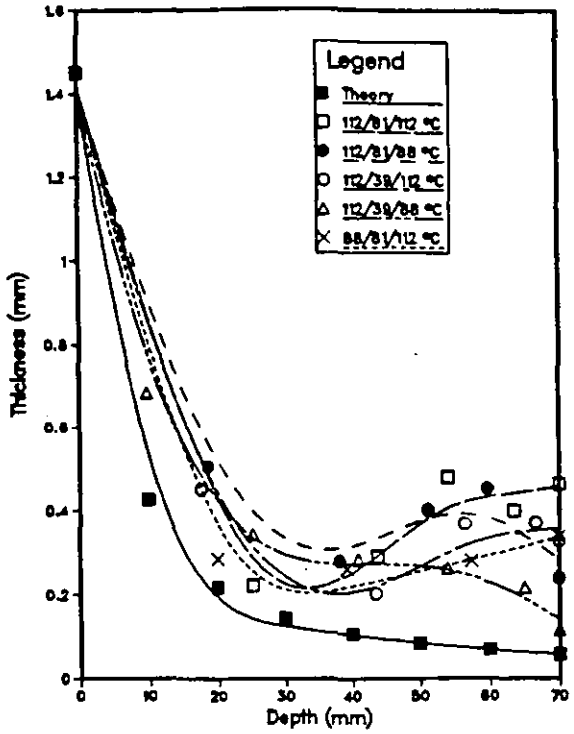

(b) Thickness Distribution 1:1P

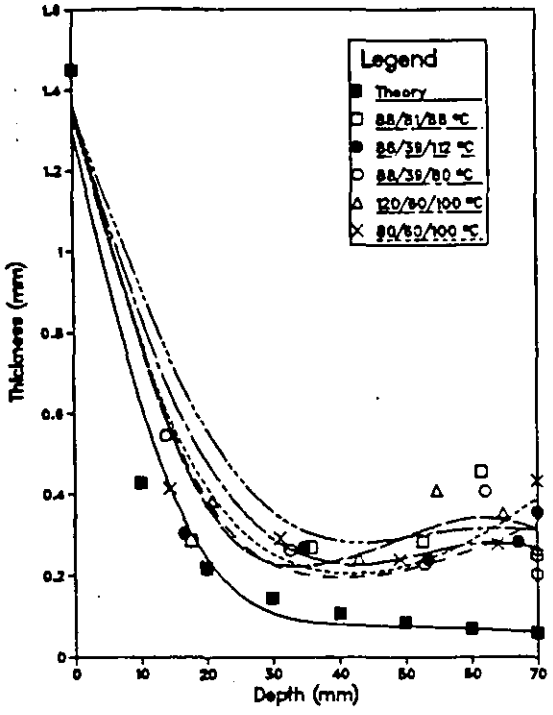

(c) Thickness Distribution 1:1P

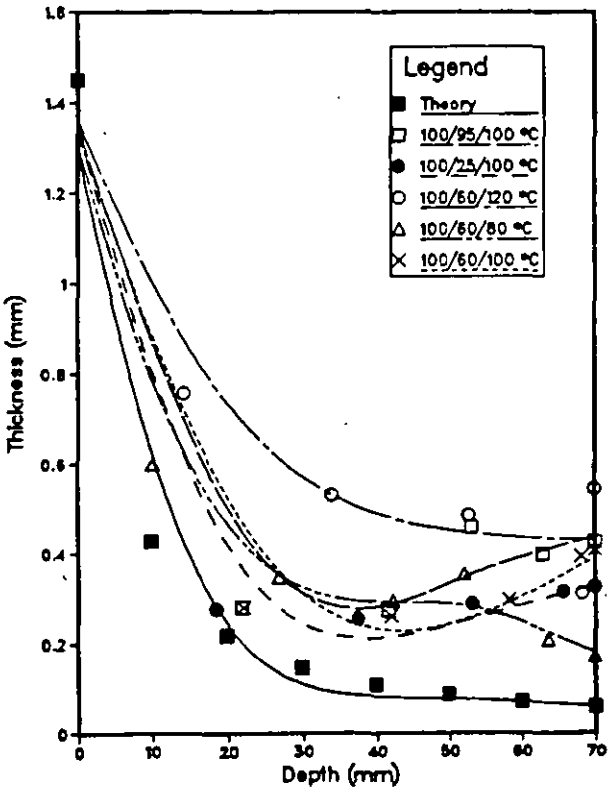

Figure 6.28 *Comparison of experimental thickness distribution with prediction from Williams model (shallow plug-assist). Legend: sheet/mould/plug temperatures*

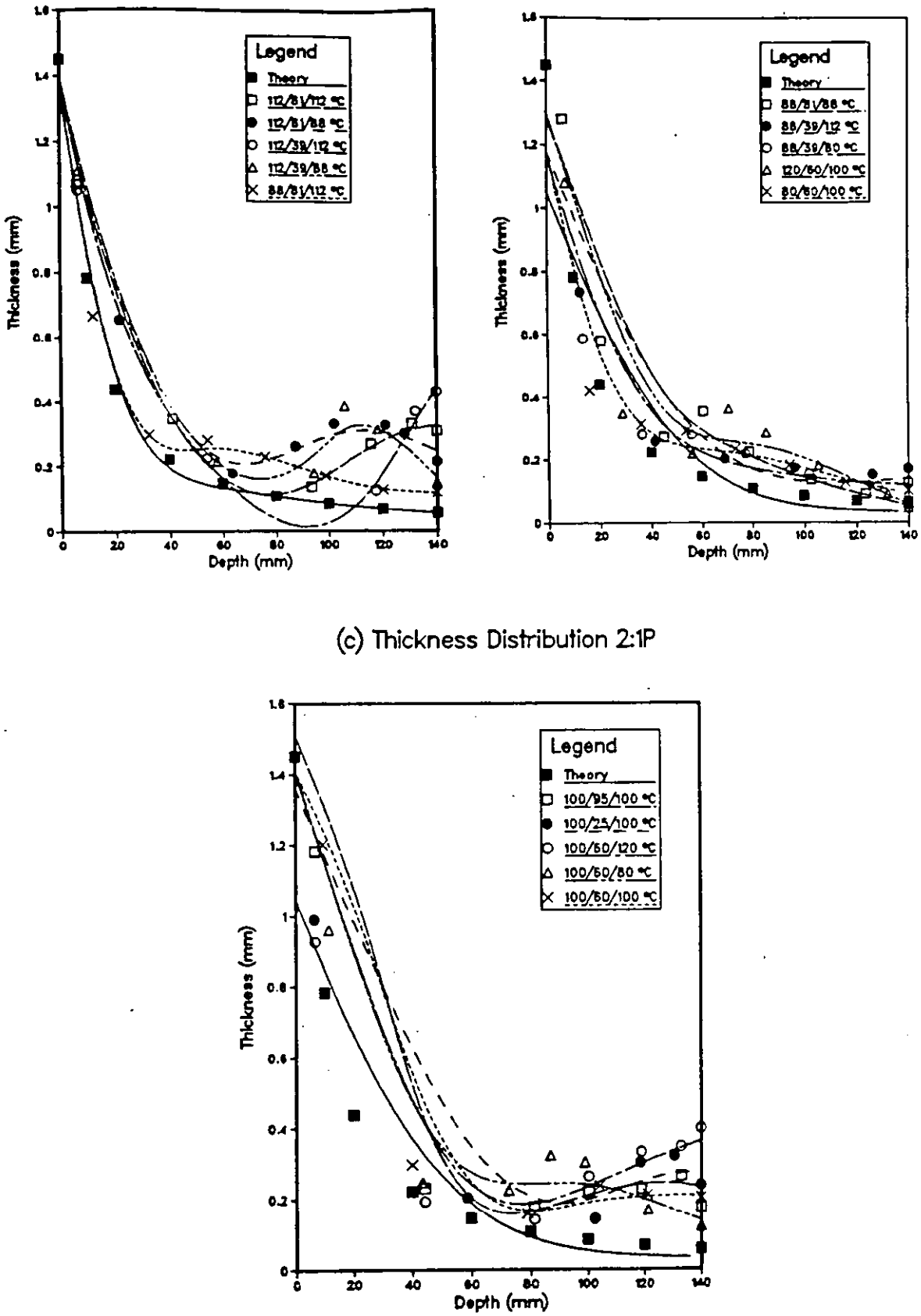

Figure 6.29 *Comparison of experimental thickness distribution with prediction from Williams model (deep plug-assist) Legend: sheet/mould/plug temperatures*

6.7.2 Comparision fo Sheryshev's Model Prediction with Experimental Results

The cooling and stretch factors [171,173] defined in equation 6.23 for vacuum forming, and equation 6.30 for plug-assist forming were determined for each combination of processing conditions employed. In order to gain knowledge of the deformation processes and the influence of each forming variable, data were analysed by the GLIM statistical Package [160] as used in section 6.5.

At this juncture, it is necessary to define the coefficients of the model. The cooling factor (k_o) characterises the degree of heat loss by the material being formed, with the assumptions that :

If $k_o < 1$ part of the material being formed slips on the mould wall.

$k_o = 1$ drawing of material stops on contacting the mould wall (ie no wall slippage)

$k_o > 1$ sections of the spherical bubble are cooling during forming.

The stretch factor (k_s) is a measure of sheet drawing from region beyond that situated above the mould cavity in vacuum forming whilst in plug-assist forming, it characterises drawing from the plug surface.

Table 6.20 gives the cooling (k_o) and stretch factor (k_s) values for shallow and deep vacuum formed containers; also the cooling (k_o) and stretch (k_s^p) factors for plug-assist formed containers are given in table 6.21

Tables 6.22 - 6.25 present the coefficients of the polynomial for cooling and stretch factors in vacuum drawn containers.

		Draw Ratio			
		1:1		2:1	
Code	Values	k_s	k_o	k_s	k_o
-1	-1	1.860	1.869	.984	.686
1	-1	2.986	2.100	1.142	.781
-1	1	2.074	1.824	1.101	.721
1	1	3.164	2.436	1.477	1.015
-1.41	0	1.966	1.813	.959	.728
1.41	0	2.492	2.020	2.2021	1.400
0	-1.41	2.074	1.824	1.277	.868
0	1.41	2.029	1.645	1.429	.966
0	0	1.966	1.694	1.230	1.005
0	0	2.349	2.020	1.193	.903
0	0	1.639	1.159	1.296	.854
0	0	1.915	1.645	1.083	.812

Table 6.20 Cooling and stretch factors in vacuum formed containers

Code Values			Draw Ratio 1:1		2:1	
			k_s^p	k_o	k_s^p	k_o
-1	-1	-1	.906	.0324	1.134	.0412
1	-1	-1	1.033	.0428	1.057	.0310
-1	1	-1	.717	.0239	1.154	.0475
1	1	-1	.995	.0297	.827	.0227
-1	-1	1	.690	.0237	.796	.0320
1	-1	1	.859	.0254	.912	.0225
-1	1	1	.754	.0264	.799	.0351
1	1	1	.713	.0171	.916	.0241
-1.68	0	0	.734	.0234	.749	.0353
1.68	0	0	.897	.0278	.677	.0344
0	-1.68	0	.697	.0233	.909	.0250
0	1.68	0	.740	.0185	.902	.0288
0	0	-1.68	.723	.0201	.990	.0340
0	0	1.68	1.131	.0234	.673	.0173
0	0	0	1.027	.0312	.910	.0306
0	0	0	1.044	.0321	.828	.0340
0	0	0	1.014	.0318	.879	.0320
0	0	0	.997	.0317	.549	.0212
0	0	0	1.060	.0344	.809	.0299
0	0	0	.992	.0332	.858	.0322

Table 6.21: Cooling and stretch factors for plug-assist formed containers

Polynomial terms		Estimate	Standard Error	Estimate / Std Error
B_o	(Grand Mean)	1.6290	0.1526	-
B_1	(S)	0.1423	0.1080	1.32
B_2	(M)	0.4841×10^{-2}	0.1080	0.04
B_{11}	(SS)	0.2027	0.1211	1.67 +
B_{22}	(MM)	0.1111	0.1211	0.92
B_{12}	(SM)	0.9525×10^{-1}	0.1526	0.62

Table 6.22: Table of Polynomical coefficients for cooling factor in shallow vacuum formed contatiners

Polynomial terms		Estimate	Standard Error	Estimate / Std Error
B_o(Grand Mean)		1.9660	0.1869	-
B_1	(S)	0.3708	0.1323	2.80 *
B_2	(M)	0.4119×10^{-1}	0.1323	0.31
B_{11}	(SS)	0.2277	0.1483	1.54 +
B_{22}	(MM)	0.1384	0.1483	0.93
B_{12}	(SM)	-0.9000×10^{-2}	0.1869	-0.05

Table 6.23: Table of polynomial coefficients for stretch factor in shallow vacuum formed containers

* Indicates significant coefficient

\+ Indicates near significant coefficient

Polynomical terms		Estimate	Standard Error	Estimate / Std Error
B_o(Grand Mean)		0.8941	0.7487×10^{-1}	-
B_1	(S)	0.1676	0.5302×10^{-1}	3.16 *
B_2	(M)	0.5105×10^{-1}	0.5302×10^{-1}	0.96
B_{11}	(SS)	0.3761×10^{-1}	0.5943×10^{-1}	0.63
B_{22}	(MM)	-0.3663×10^{-1}	0.5943×10^{-1}	-0.61
B_{12}	(SM)	0.4975×10^{-1}	0.7487×10^{-1}	0.66

Table 6.24 Table of polynomial coefficients for cooling factor in deep vacuum formed containers

Polynomial terms		Estimate	Standard Error	Estimate / Std Error
B_o(Grand Mean)		1.2010	0.1060	-
B_1	(S)	0.2547	0.7508×10^{-1}	3.39 *
B_2	(M)	0.8354×10^{-1}	0.7508×10^{-1}	1.11
B_{11}	(SS)	0.8317×10^{-1}	0.8417×10^{-1}	0.99
B_{22}	(MM)	0.1426×10^{-1}	0.8417×10^{-1}	0.17
B_{12}	(SM)	0.5450×10^{-1}	0.1060	0.51

Table 6.25: Table of polynomial coefficients for stretch factor in deep vacuum formed containers

Polynomial terms		Estimate	Standard Error	Estimate / Std Error
B_o(Grand Mean)		0.3222×10^{-1}	0.1926×10^{-2}	-
B_1	(S)	0.1172×10^{-2}	0.1279×10^{-2}	0.92
B_2	(M)	-0.2584×10^{-2}	0.1279×10^{-2}	-2.02 *
B_3	(P)	-0.2247×10^{-2}	0.1279×10^{-2}	-1.76 +
B_{11}	(SS)	-0.1238×10^{-2}	0.1246×10^{-1}	-0.99
B_{22}	(MM)	-0.2903×10^{-2}	0.1246×10^{-2}	-2.33 *
B_{33}	(PP)	-0.2602×10^{-2}	0.1246×10^{-2}	-2.09 *
B_{12}	(SM)	-0.1950×10^{-2}	0.1670×10^{-2}	-1.17
B_{13}	(SP)	-0.2975×10^{-2}	0.1670×10^{-2}	-1.78 +
B_{23}	(MP)	0.2000×10^{-2}	0.1670×10^{-2}	1.20

Table 6.26 Table of Polynomical coefficients for cooling factor in shallow plug-assist formed containers

Polynomial terms		Estimate	Standard Error	Estimate / Error
B_o(Grand Mean)		1.021	0.5242×10^{-1}	-
B_1	(S)	0.5913×10^{-1}	0.3480×10^{-1}	1.70 +
B_2	(M)	-0.1735×10^{-1}	0.3480×10^{-1}	-0.50
B_3	(P)	0.3697×10^{-2}	0.3480×10^{-1}	0.11
B_{11}	(SS)	-0.6783×10^{-1}	0.3391×10^{-1}	-2.00 *
B_{22}	(MM)	-0.1022	0.3391	-3.01 *
B_{33}	(PP)	-0.2832×10^{-1}	0.3391×10^{-1}	-0.84
B_{12}	(SM)	-0.7375×10^{-2}	0.4545×10^{-1}	-0.16
B_{13}	(SP)	-0.3463×10^{-1}	0.4545×10^{-1}	-0.76
B_{23}	(MP)	0.1813×10^{-1}	0.4545×10^{-1}	0.40

Table 6.27 Table of polynomial coefficients for stretch factor in shallow plug-assist formed containers

* Indicates significant coefficient

\+ Indicates near significant coefficient

Polynomial terms		Estimate	Standard Error	Estimate / Std Error
B_o(Grand Mean)		0.2989×10^{-1}	0.2260×10^{-2}	-
B_1	(S)	-0.4178×10^{-2}	0.1500×10^{-2}	-2.79 *
B_2	(M)	0.6657×10^{-3}	0.1500×10^{-2}	0.44
B_3	(P)	-0.4160×10^{-2}	0.1500×10^{-2}	-2.77 *
B_{11}	(SS)	0.2345×10^{-2}	0.1462×10^{-2}	1.60 +
B_{22}	(MM)	-0.4714×10^{-3}	0.1462×10^{-2}	-0.32
B_{33}	(PP)	-0.9143×10^{-3}	0.1462×10^{-2}	-0.63
B_{12}	(SM)	-0.2012×10^{-2}	0.1959×10^{-2}	-1.03
B_{13}	(SP)	0.1812×10^{-2}	0.1959×10^{-2}	0.92
B_{23}	(MP)	0.8375×10^{-3}	0.1959×10^{-2}	0.43

Table 6.28 *Table of polynomial coefficients for cooling factor in deep plug-assist formed containers*

Polynomial terms		Estimate	Standard Error	Estimate / Std Error
B_o(Grand Mean)		0.8011	0.5004×10^{-1}	-
B_1	(S)	-0.2140×10^{-1}	0.3322×10^{-1}	-0.64
B_2	(M)	-0.1574×10^{-1}	0.3322×10^{-1}	-0.47
B_3	(P)	-0.9392×10^{-1}	0.3322×10^{-1}	-2.83 *
B_{11}	(SS)	-0.4821×10^{-2}	0.3237×10^{-1}	-0.15
B_{22}	(MM)	0.6338×10^{-1}	0.3237×10^{-1}	1.96 +
B_{33}	(PP)	0.3716×10^{-1}	0.3237×10^{-1}	1.15
B_{12}	(SM)	-0.3112×10^{-1}	0.4338×10^{-1}	-0.72
B_{13}	(SP)	0.7963×10^{-1}	0.4338×10^{-1}	1.84 +
B_{23}	(MP)	0.2713×10^{-1}	0.4338×10^{-1}	0.63

Table 6.29: *Table of polynomial coefficients for stretch factor in deep plug-assist formed containers*

* Indicates significant coefficient

\+ Indicates near-significant coefficient

Also the coefficients of the polynomial for cooling and stretch factors for plug-assist formed containers are presented in tables 6.26- 6.29.

Figs 6.30 - 6.33 show that the polynomial for vacuum forming is adequate. Also figs 6.34 - 6.37 show that the polynomial for plug-assist forming is satisfactory.

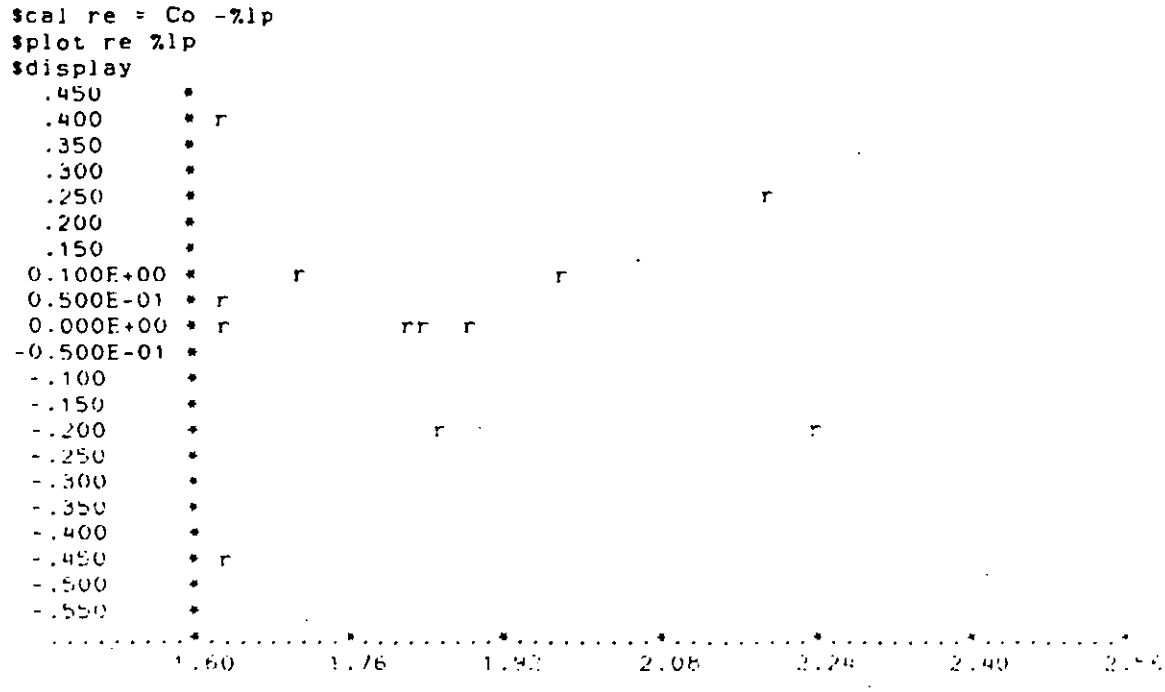

Figure 6.30 *Residuals Vs fitted values for cooling factor (shallow vacuum drawn containers*

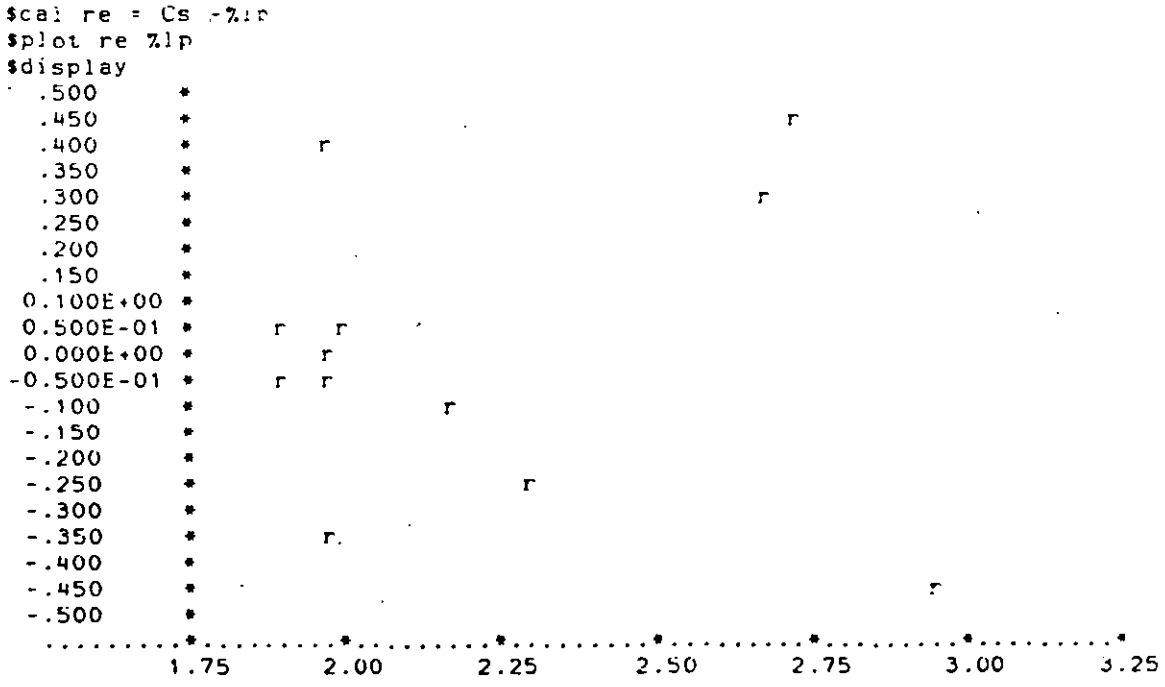

Figure 6.31 *Residuals Vs fitted values for stretch factor (shallow vacuum drawn containers)*

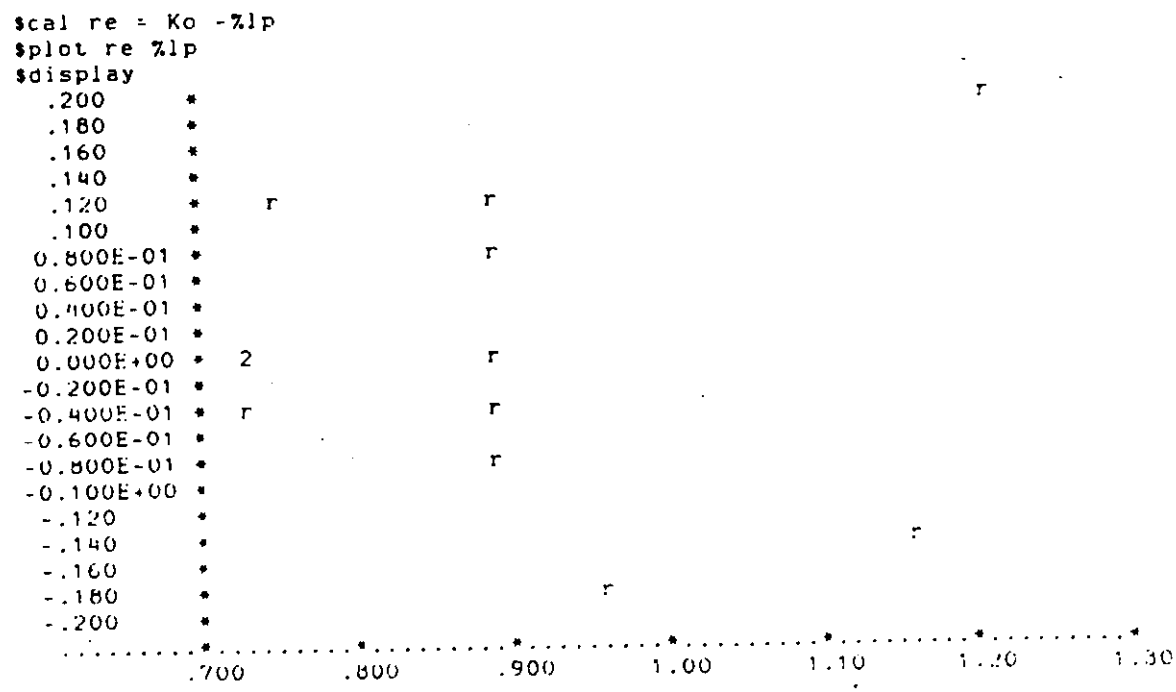

Figure 6.32 Residuals Vs fitted values for cooling factor (deep vacuum drawn containers

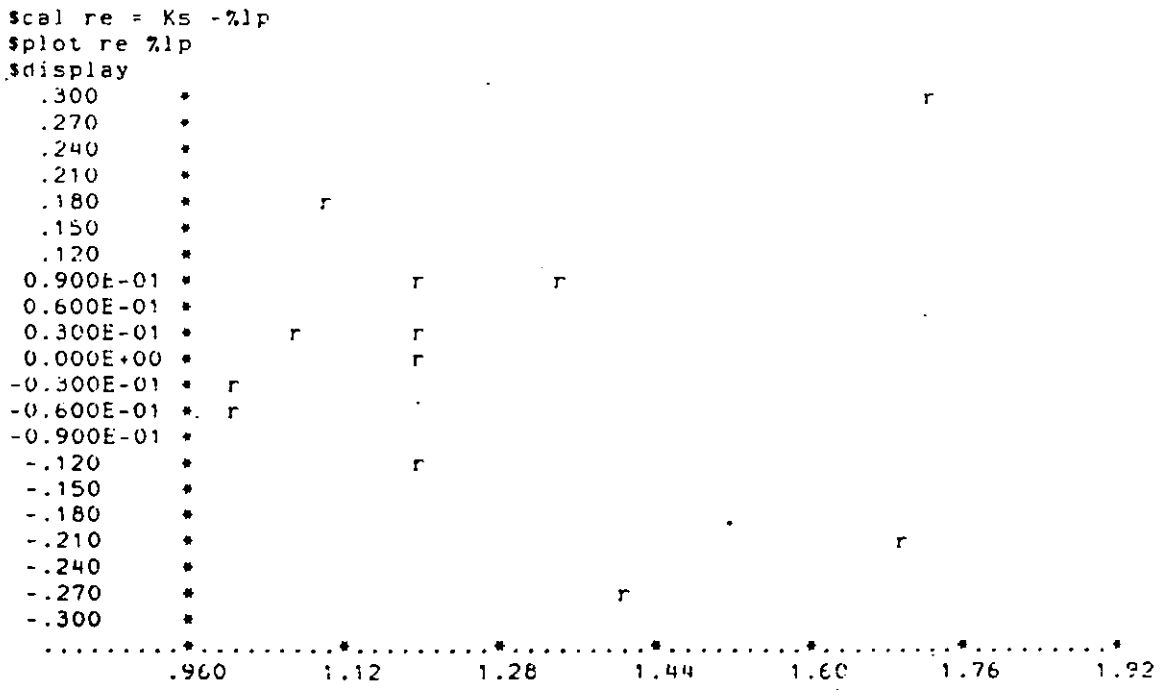

Figure 6.33. Residuals Vs fitted values for stretch factor (deep vacuum drawn containers)

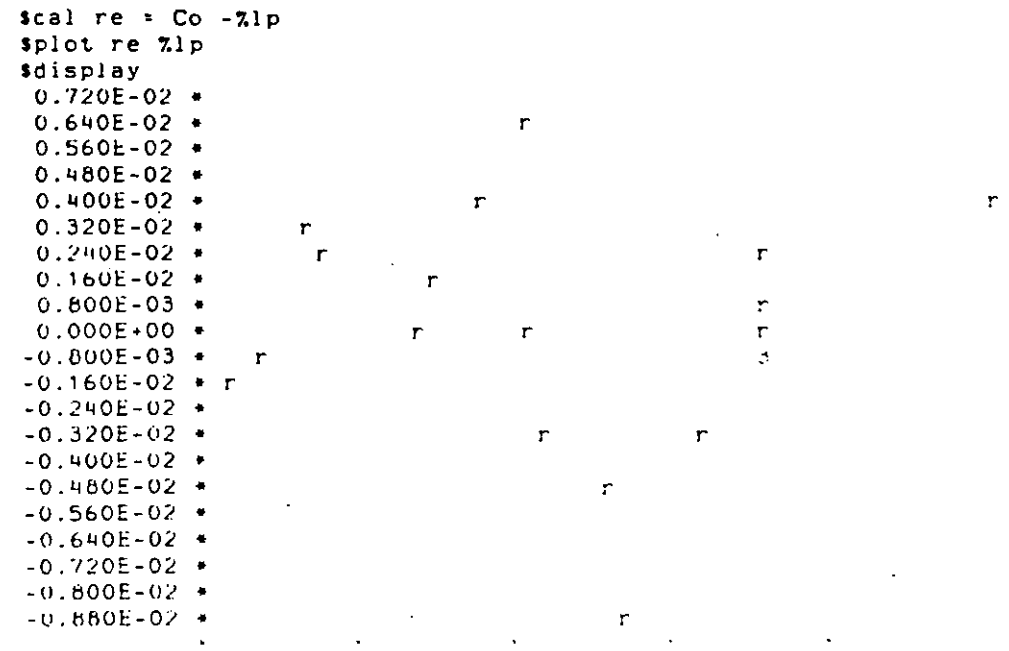

Figure 6.34 Residuals Vs fitted values for cooling factor (shallow plug-assist formed containers

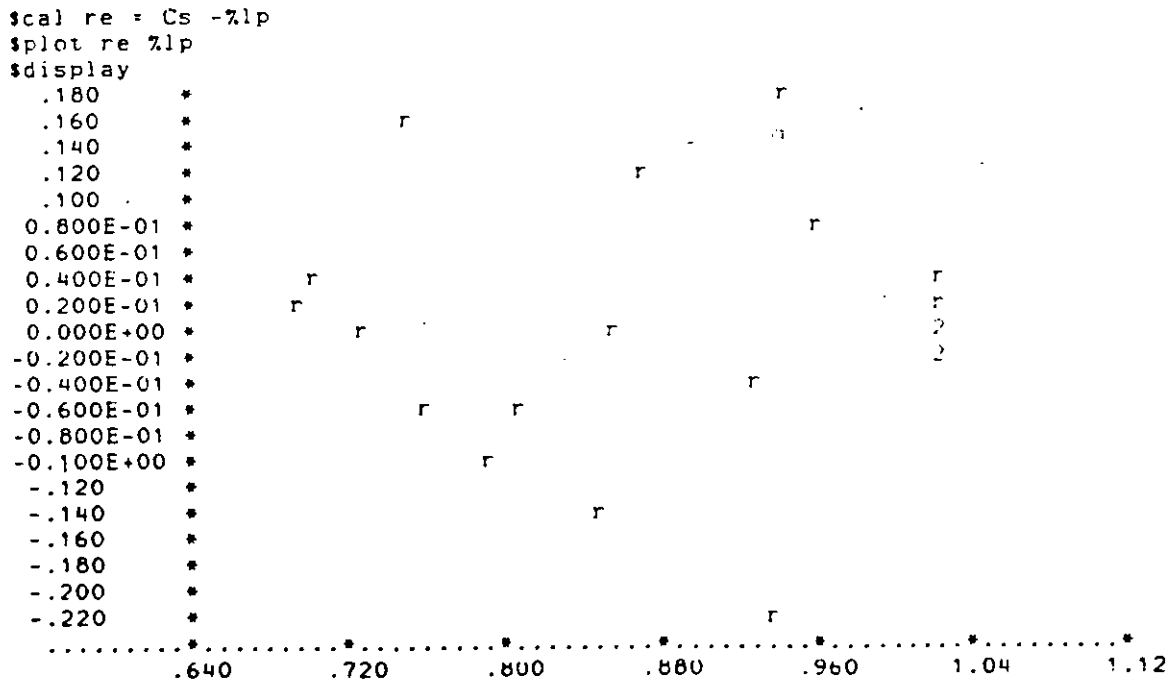

Figure 6.35 Residuals Vs fitted values for stretch factor (shallow plug-assist formed containers)

```
$cal re = Ko -%lp
$plot re %lp
$display
 0.720E-02 *
 0.640E-02 *          r
 0.560E-02 *
 0.480E-02 *                  r                              r
 0.400E-02 *                   r
 0.320E-02 *
 0.240E-02 *                   2     r             r
 0.160E-02 *
 0.800E-03 *                   r
 0.000E+00 *       r           r r       r
-0.800E-03 *                  r
-0.160E-02 *
-0.240E-02 *         r     r
-0.320E-02 *r
-0.400E-02 *              r
-0.480E-02 *
-0.560E-02 *
-0.640E-02 *
-0.720E-02 *
-0.800E-02 *                                                 r
-0.880E-02 *                   r
  .........*.........*.........*.........*.........*.........*.........*
         0.200E-01 0.250E-01 0.300E-01 0.350E-01 0.400E-01 0.450E-01 0.500E-01
```

Figure 6.36 Residuals Vs fitted values for cooling factor (deep plug-assist formed containers

```
$cal re = Ks -%lp
$plot re %lp
$display
   .120      *
   .100      r          r                  r
 0.800E-01   *          r    r                          r
 0.600E-01   *          r
 0.400E-01   *                    r                          r
 0.200E-01   *          rr r
 0.000E+00   *          r
-0.200E-01   *
-0.400E-01   *
-0.600E-01   *                               r
-0.800E-01   *     2       r                          r
-0.100E+00   *                                  r
  -.120      *
  -.140      *
  -.160      *
  -.180      *
  -.200      *
  -.220      *
  -.240      *
  -.260      *          r
  -.280      *
  .........*.........*.........*.........*.........*.........*.........*
          .700       .800       .900       1.00       1.10       1.20       1.30
```

Figure 6.37 Residuals Vs fitted values for stretch factor (deep plug-assist formed containers)

The response surface is limited to those variables with significant effects, especially for the plug-assist forming. In addition a global view of the information from the contour plot is presented.

The forming variables have no significant effect on the cooling factor in the shallow vacuum formed containers. Contour plot was not generated. However, sheet temperature has a significant effect on the stretch factor. Fig 6.38 shows that stretch factor decreases with decreasing sheet temperature. In the deep vacuum formed containers, the sheet temperature has a significant effect on the cooling and stretch factors (Tables 6.24 - 25). Figs 6.39 - 6.40 show that cooling and stretch factors respectively increase with increasing sheet temperature.

In the plug-assist forming, mould temperature has a significant effect on the cooling factor and only slight interaction between sheet and plug temperatures. (Table 6.26). However, there was no variable with significant effect on the stretch factor. Therefore, contour plots were not necessary. Sheet and plug temperature each influence the cooling factor in the deep draw. Also the plug temperature has a significant effect on the stretch factor in deep plug-assist draw containers.

The assumptions of Sheryshev's model discussed in section 6.7 are now used to explain the significance of the cooling and stretch factor in the deformation processes during forming.

The non-significance of the processing variables on the cooling factor in the shallow vacuum formed containers is an inherent characteristic of the deformation mechanism. Table 6.20 shows that the cooling factor values for shallow vacuum formings are greater than 1. This implies that part of the spherical bubble generated at the outset of vacuum forming was cooling. This is due to the fact the spherical bubble bottoms on the mould before stretching to the mould wall [169]. Therefore, the processing conditions cannot affect the rate of cooling for the shallow vacuum formed containers. This agrees with earlier deduction from the exploratory experiments (Chapter 5).. However, the stretch factor decreases with decreasing sheet temperature in fig 6.38. Also the degree of the stretch factor values across the varying processing condtion is very narrow. It should be remembered that the stretch factor (k_s) is a measure of drawing from beyond the region of the mould cavity. Therefore, the limited variation in k_s is because very little drawing takes place beyond the mould cavity.

In the case of deep vacuum drawn containers, figs 6.39 and 6.40, expressed the sheet temperature dependence of cooling and stretch factors respectively. The cooling factor (k_o) is below 1 at the lower sheet temperature, which suggests that there was drawing on the mould wall (ie slippage) during forming. At the higher sheet temperature the cooling factor is around 1. This implies that the sheet freezes on to the mould wall on contact. Thus the deformation of the sheet is limited to the spherical

bubble generated by the vacuum action. The stretch factor values increase with increasing sheet temperature fig 6.40. Higher stretch factors were obtained at the higher sheet temperatures because of limited drawing caused by increasing frictional forces between the sheet and forming platform [172]. At the lower sheet temperatures, lower stretch factor was obtained because of lower frictional forces between the sheet and the forming table, thus increased drawing from beyond the mould cavity (ie decreased fraction of sheet beyond the mould cavity). These results show a good agreement between the model and experiment for vacuum forming.

Fig 6.41 shows cooling factor values at different mould temperatures for shallow plug-assist formed containers. It shows that low cooling factor values are obtained at high mould temperatures. This is because the mould serves as heat sink during forming. Thus, the rate of heat loss (cooling factor) by the sheet to the mould wall decreases with increasing mould temperatures. This result shows that cooling factor is mould temperature-dependent. A close examination of table 6.27 shows that stretch factor in shallow plug-assist formed containers is slightly sheet temperature dependent. These observations agree with the hypothesis of the model [171,173].

Fig 6.42 represents the effect of processing conditions on cooling factor in deep plug-assist formed containers. Graphs (1-3), and Graphs (4-6) show that the cooling factor decreases with increasing sheet and plug temperatures respectively. The stretch factor, fig 6.43 Graphs (1 - 3), also decreases with increasing plug temperatures. The difference in the forming variable dependence of cooling factor in shallow and deep draws is due to difference in deformation processes in the two draw ratios. At the deep draws, there is significant stretching of the sheet from the plug surface whereas at the shallow draws, there is very little stretching of sheet from the plug surface.

A close examination of Fig 6.43 Graph 3 shows that at high plug temperature, increasing sheet temperature increases the sliding friction of PETP on the surface of the plug, resulting in increasing stretch factor values (ie reduced stretching from the plug surface). Also, the graph suggest that at mould temperatures above ~85 °C, the sliding friction of PETP on the mould surface increases [172], thus reducing the tendency for further stretching of the sheet on the mould wall. This may be responsible for excessive wall thinning in some of the deep plug-assist formed containers. At about sheet/mould/plug temperature combination of 85/60/100 °C, the sliding friction was a minimum, resulting in lower stretch factor values (ie low sliding friction between the tools and PETP). It must be pointed out that in Fig 6.43 Graphs 1 &2 , high stretch factor values were obtained at the lower plug and sheet temperatures, but the stretch factor values decrease with increasing sheet temperature between 50 - 60 °C mould temperature. Therefore, it seems there is a complex interaction between the sheet temperature and tool temperatures which influences the sliding friction.From the

evidence so far, it seems sliding friction between PETP and the plug surface increases sharply above 112 °C. Perhaps at this temperature the sheet crystallizes and shrinks on to the plug surface. At the low tool temperatures, limited drawing of the sheet is attributable to a chill effect.

The cooling factor values in plug-assist forming is below 1. This shows that the sheet was drawn on the mould wall, which was expected. Overall, there is a good agreement between the Sheryshev's model hypothesis and experiment for both simple vacuum and plug-assist forming. The slight deviation with respect to dependence of cooling factor on sheet and plug temperature can be attributed to strain hardending behaviour in PETP at deep draws. Whereas, in the shallow draws where deformation is within the rubber-elastic region (similar to behaviour of HIPS on which the assumptions were modelled) the cooling factor was mould temperature dependent.

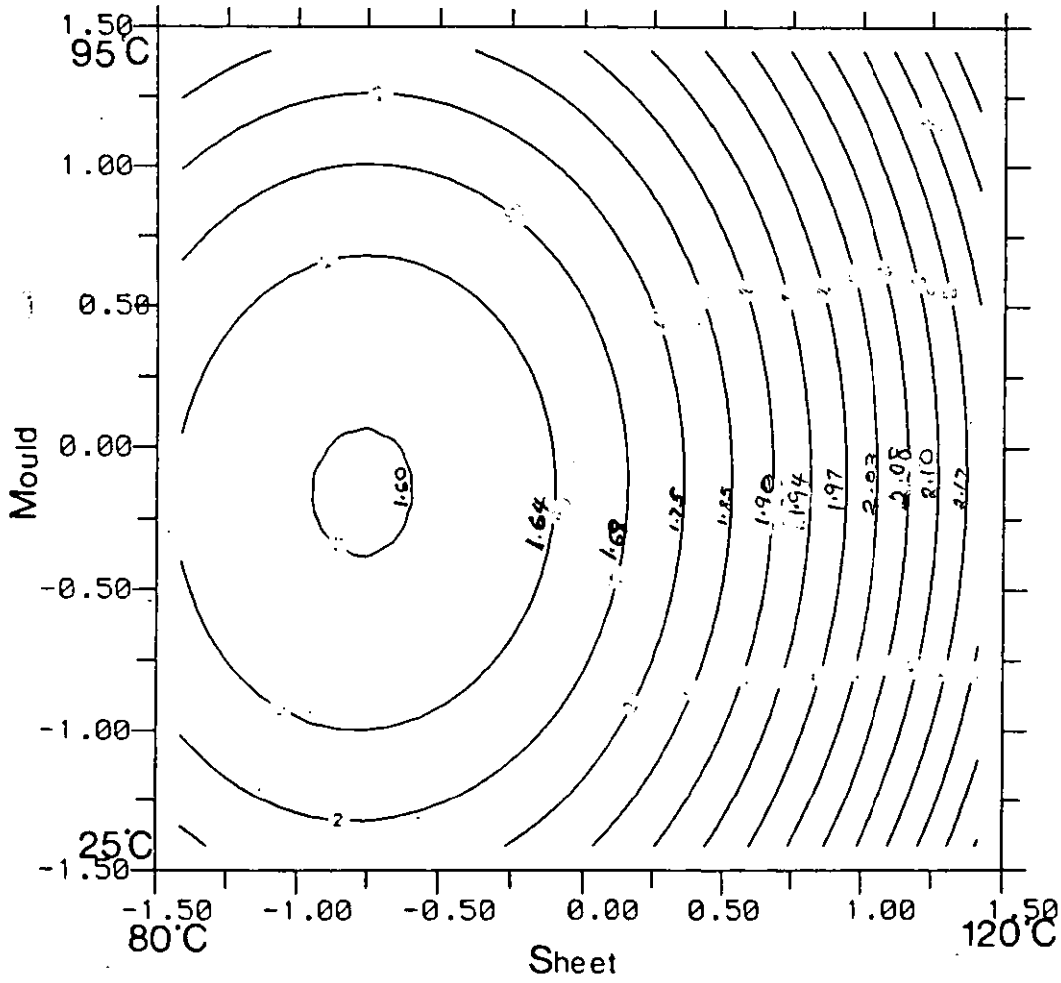

Figure 6.38 Contour plot of stretch factor variation (shallow vacuum formed containers)

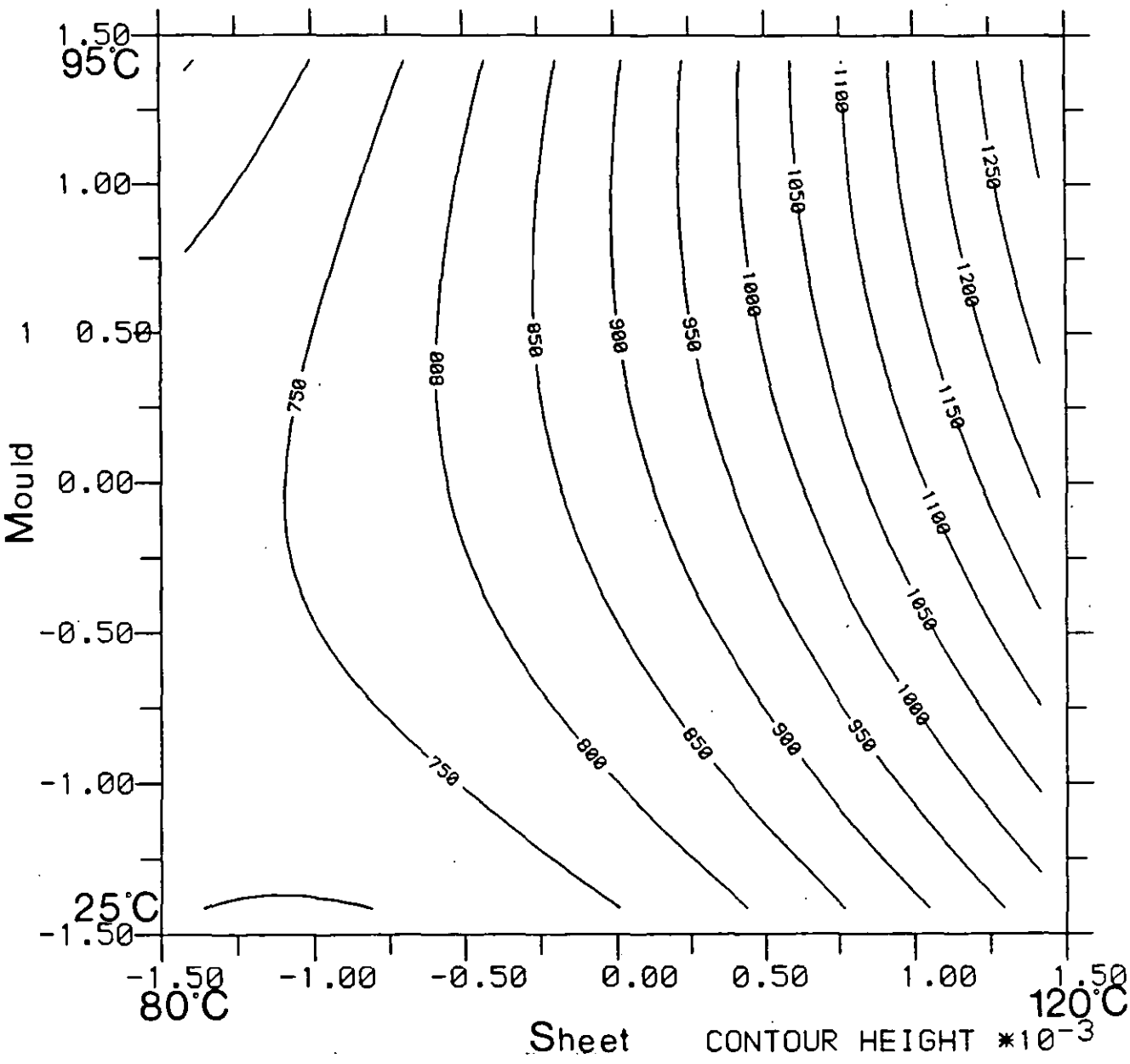

Figure 6.39 *Contour plot of cooling factor variation (deep vacuum formed containers)*

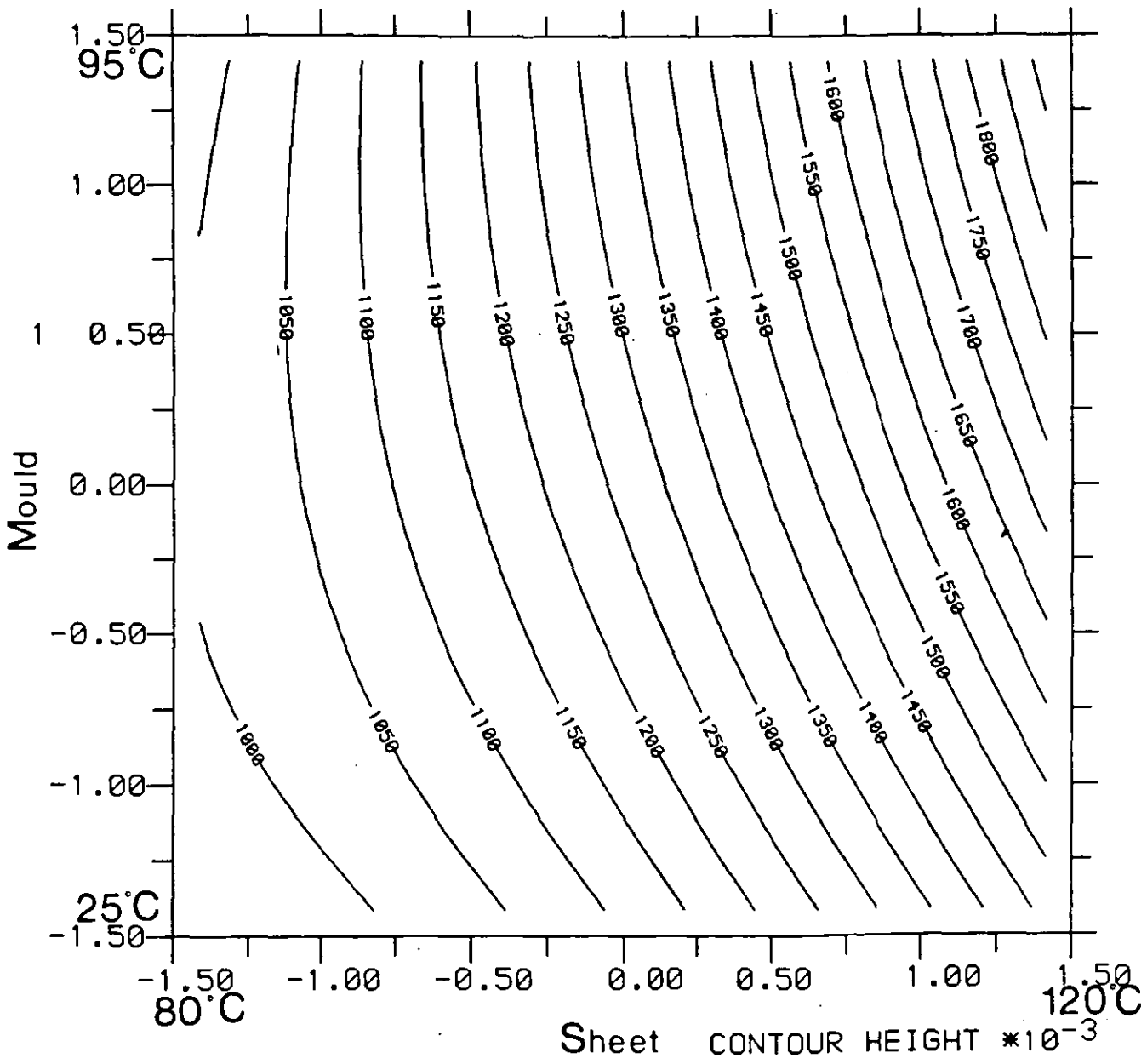

Figure 6.40 *Contour plot of stretch factor variation (deep vacuum formed containers)*

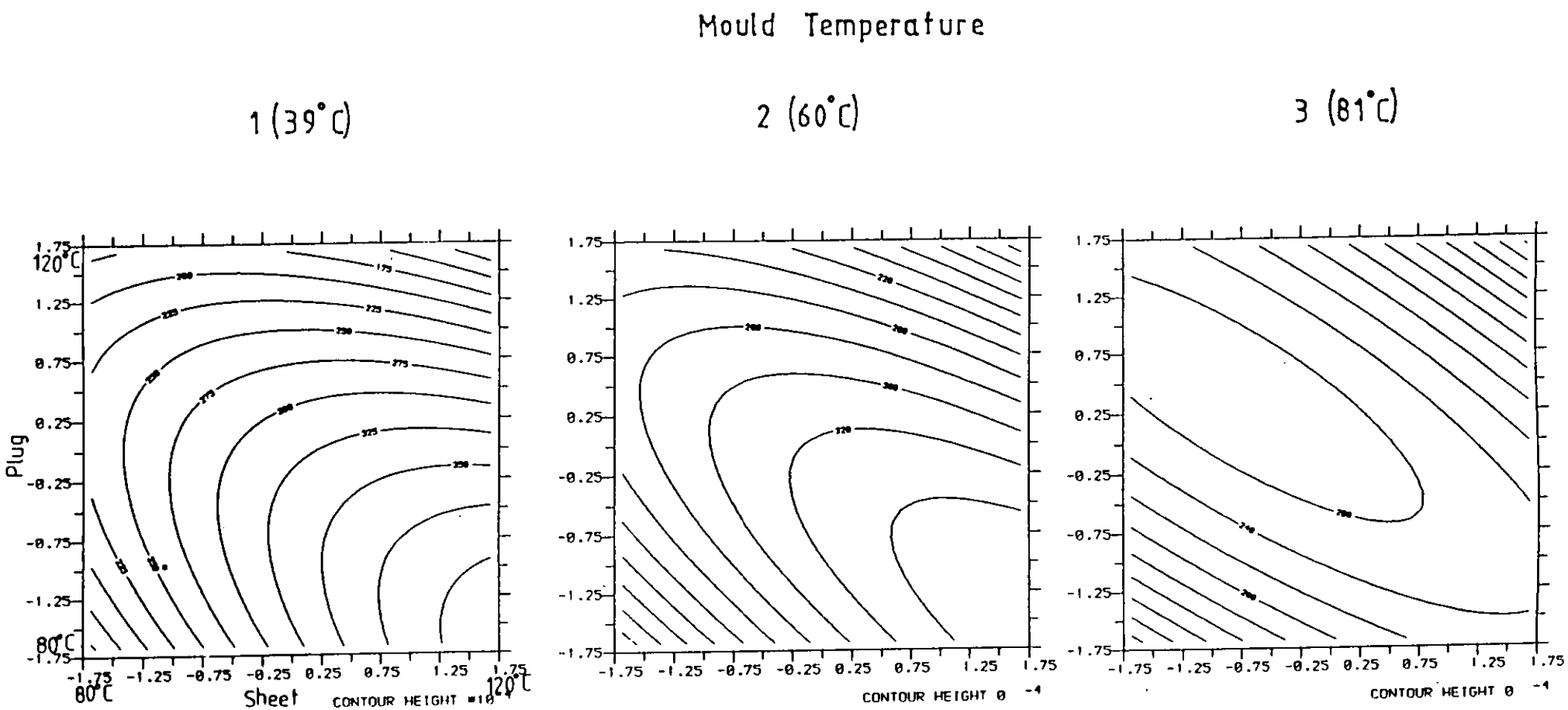

Figure 6.41 *Contour plot of cooling factor variation (shallow plug-assist formed containers)*

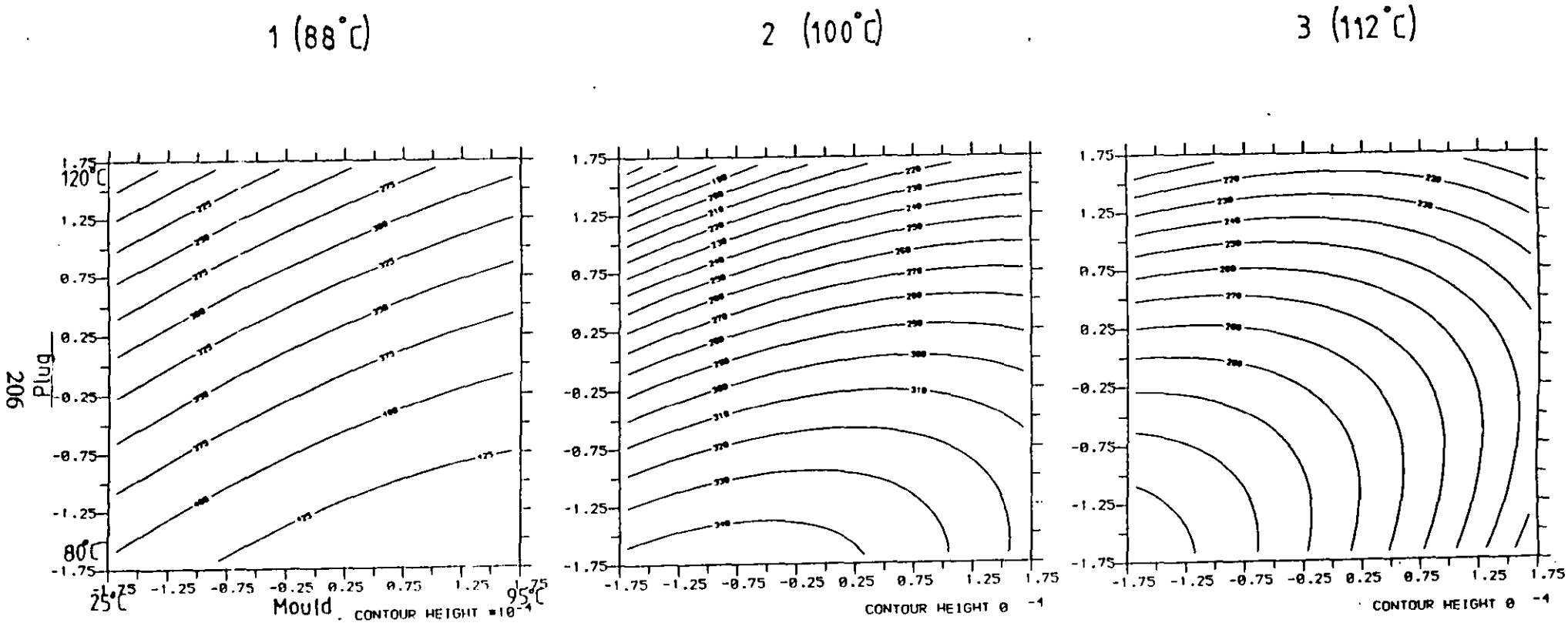

Figure 6.42 *Contour plot of cooling factor variation (deep plug-assist formed containers)*

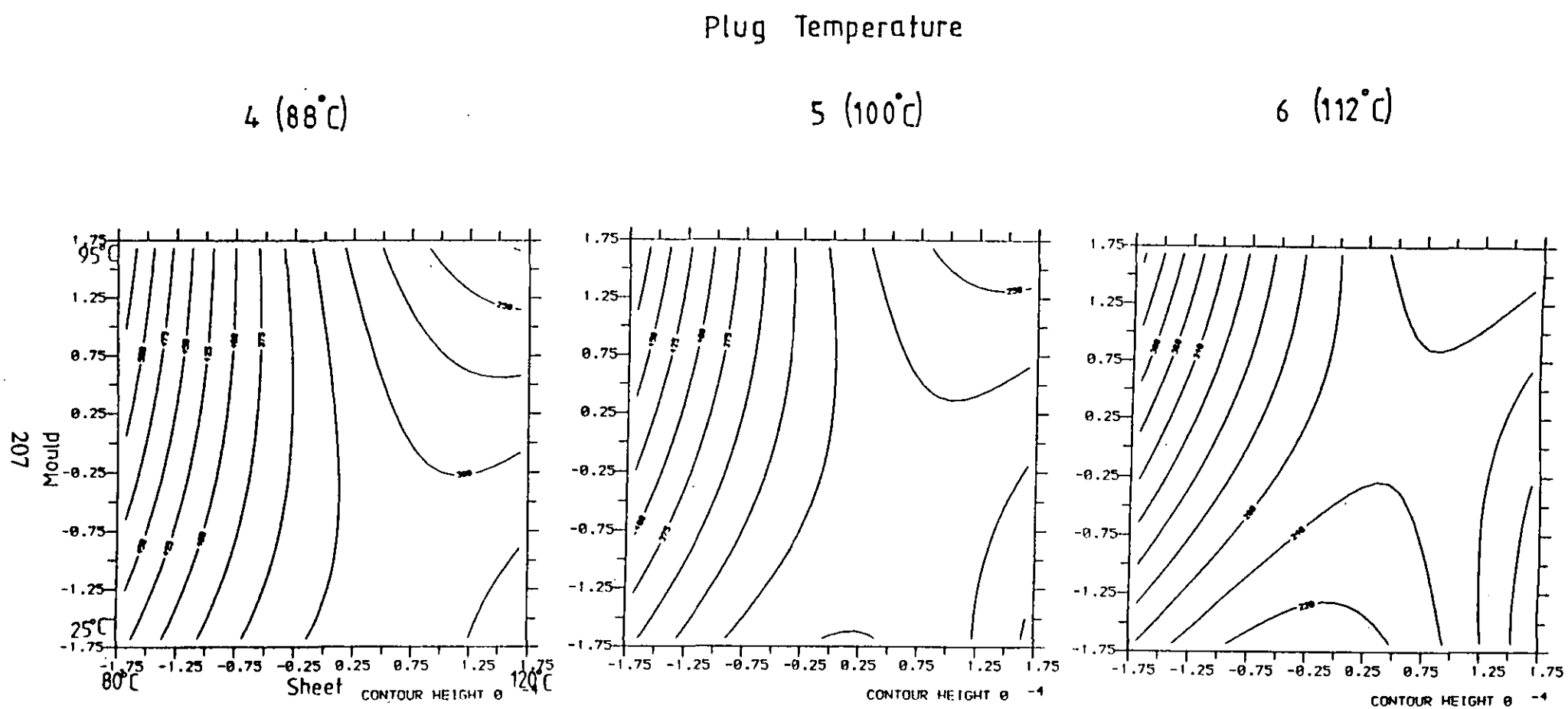

Figure 6.42 Contour plot of cooling factor variation (deep plug-assist formed containers)

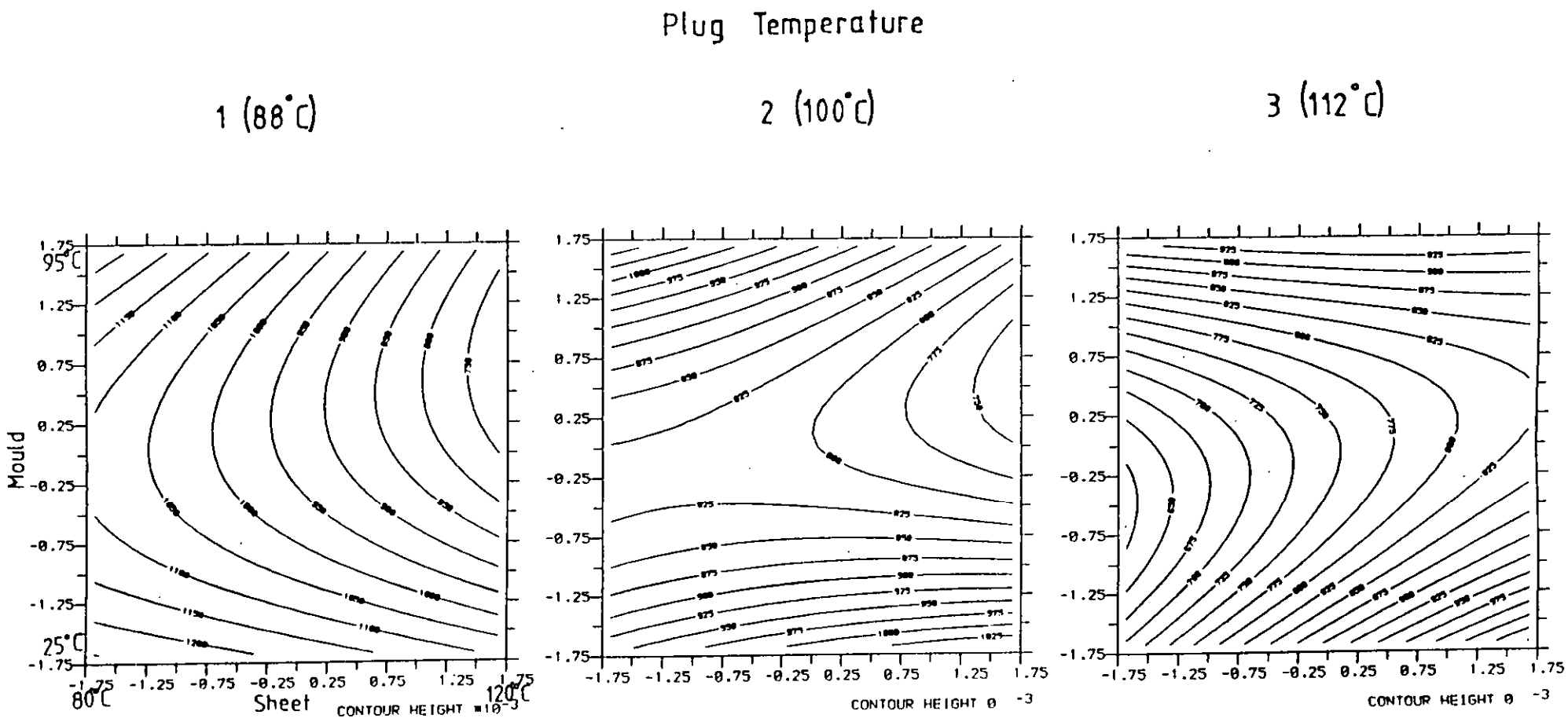

Figure 6.43 *Contour plot of stretch factor variation (deep plug-assist formed containers)*

6.8 Miscellaneous Properties of Containers

6.8.1 Grid Distortion

The biaxial grid distortions in the formings were measured in terms of extension ratio (l/l_o) defined in equation 5.1. The extension ratio was plotted against the designated position of the concentric rings defined in fig 5.7. The general influence of processing conditions was investigated. Circumferential strain is fixed by the contours of the mould.

6.8.1.2 Grid Distortion Results and Discussion

Fig 6.44 shows the extension ratio distribution in the shallow vacuum formed containers.

As previously observed in the exploratory experiments in Chapter 5, the influence of processing conditions is not immediately obvious. However a close examination of the results (ie Fig 6.44) shows that near-isothermal processing conditions improve extension ratio distribution (see for example 86/85 °C). In addition, much of the deformation is limited to concentric rings in the middle of the sheet. This shows that the spherical bubble bottoms on the mould before stretching to the mould wall [169] . This is explicitly revealed in Fig 6.45(VI) where the walls of the containers did not conform fully to the mould form due to chill effect.The grid pattern on the containers i n Fig 6.45 shows that the deformation of the sheet was symmetrical. It also confirms that near-isothermal processing conditions improve the extension distribution and appearance of the forming as shown in Fig 6.45 (III &V).

The extension ratio distribution in deep vacuum formed containers is presented in fig 6.46. Better extension ratio distribution was observed at the lower sheet temperatures. Also deep drawn containers exhibit better strain distribution compared to shallow drawn containers because the draw ratio is beyond the natural draw regime. The grid pattern on the formings in fig 6.47 show clearly the effect of processing conditions. It shows that for relatively cold moulds, the sheet freezes off on the mould wall resulting in excessive thinning of the deforming surface, especially at high sheet temperature Fig 6.47 (I -II); whereas at low sheet temperature the resistance of the sheet to deformation is higher resulting in incomplete formings (Fig 6.47 VI). But at near-isothermal conditions, there is uniform deformation with good forming characteristics (6.47 V).

The extension ratio distribution in shallow plug-assist formings is presented in fig 6.48. The plots show limited deformation on the plug surface (ie the first 3 rings from the middle) as explained by the stretch factor in Sheryshev's model. The bulk of deformation is limited to the toroidal surface, thus the extension ratio increases towards

the rim of the containers. Fig 6.49 shows that the influence of processing conditons on shallow plug-assist formings is minimal. However, a close examination of the formings reveal that at relatively high mould temperatures, the forming show dimensional instability especally towards the base as shown in fig 6,49 II, VI and XI. This is attributed to relaxation of orientation in the sheet since the draw ratio is within the rubber-elastic region. However, at the low mould temperature, the sheet freezes on the mould wall thus preventing relaxation of orientation in the sheet.

Extension ratio distribution in the deep plug-assist containers is presented in fig 6.50. Unlike the shallow plug-assist drawn containers , the influence of processing conditions is apparent in these products.At sheet temperatures between 80 - 100 °C and plug temperatures between 100 - 112 °C ,the extension ratio distribution is optimised. Tkis analysis is also supported by a close examination of the photographs of the formings in Fig 6.51. This observation enables a proper evaluation of the effect of PETP sheet temperatures on the sliding friction on the plug surface. Sheet temperatures above 100 °C and excessively high plug temprratures (eg. >112 °C) increases the sliding friction between PETP and Plug surface thus limiting stretching from the plug surface (Fig 6.51 I&II). At the lower plug temperatures (<100 °C) the low stretching from the plug surface could be attributed to chill effects or high resistance to deformation at the lower sheet temperatures (~80 °C) which has been demonstrated in the simulation tests (Chapter 3). The influence of mould temperature is not as significant as in simple vacuum as observed in the shallow plug-assist formed containers (Fig 6.51 VI,XI). This has been attributed to relaxation of orientation in the sheet.

Overall, the analysis of the results show that draw ratios should exceed the 'natural draw' defined in the stress-strain curve of PETP to obtain uniform strain distribution in the formings. Also near-isothermal conditions promote uniform strain distribution which is obtained at the following conditions:

Vacuum forming	Temperatures °C	
1:1 and 2:1	Sheet	Mould
draw ratios	80	60
	86	85

Plug-assist forming	Temperatures °C		
Draw ratio	Sheet	Mould	Plug
1:1	88	81	112
	80	60	100
2:1	88	81	112
	100	60	100
	80	60	100

Finally, the photographs of the grid patterns on the containers highlighted the influence of processing conditions, exemplified by the factorial experimental design. The extension ratio distribution obtained at sheet/mould temperatures 86/85 and 86/35 °C for vacuum formed containers (fig 6.46) are similar, however, the photographs in fig 6.47 show that low mould temperature (35 °C) increased the resistance of sheet to deformation due to rapid loss of heat from the sheet. While in the plug-assist, the influence of processing conditions on dimensional instability was shown in figs 6.49 and 6.51.

(a) Extension ratio Distribution 1:1v

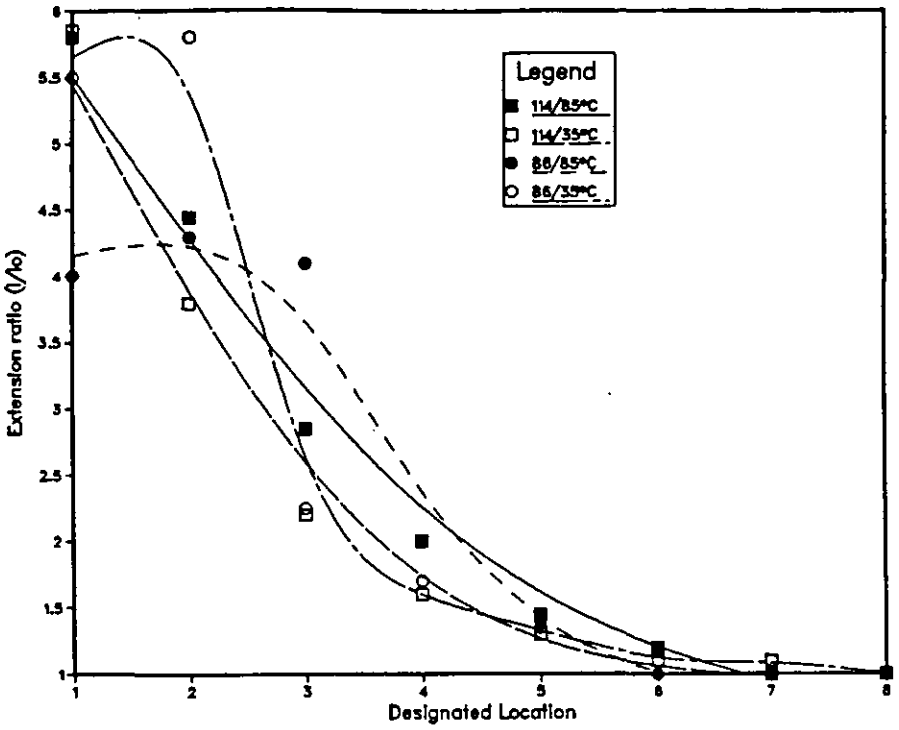

(b) Extension ratio Distribution 1:1V

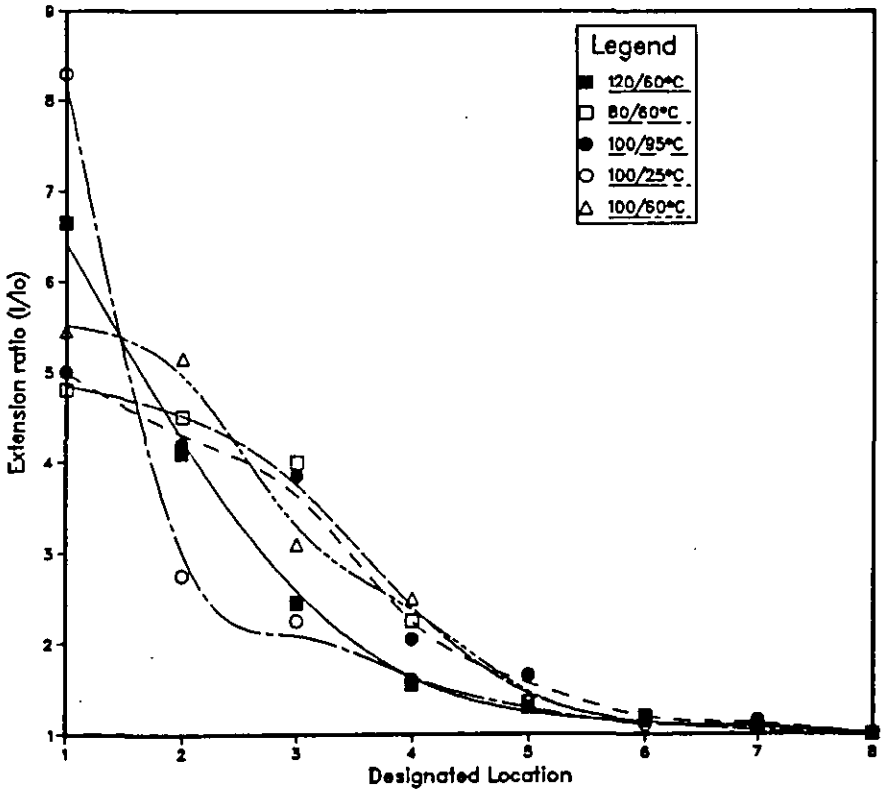

Figure 6.44 Extension ratio as a function of the rings (shallow vacuum formed containers)

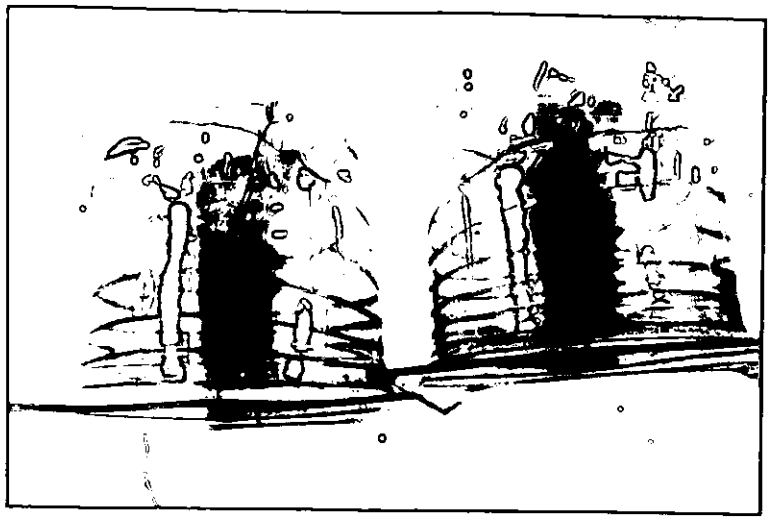

I II

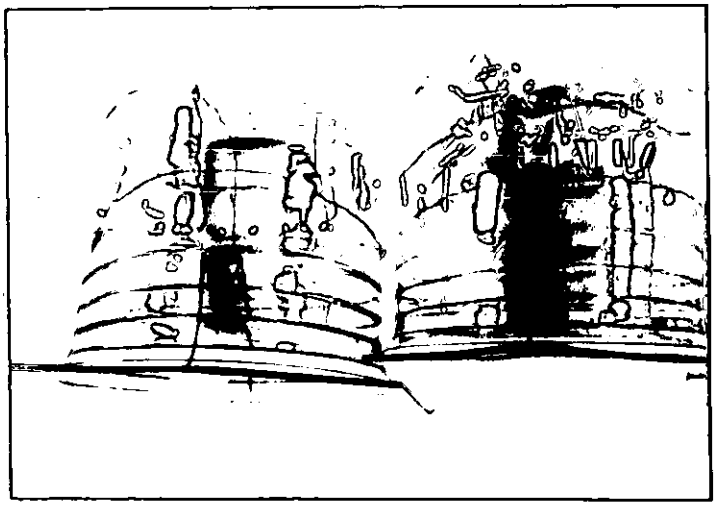

III IV

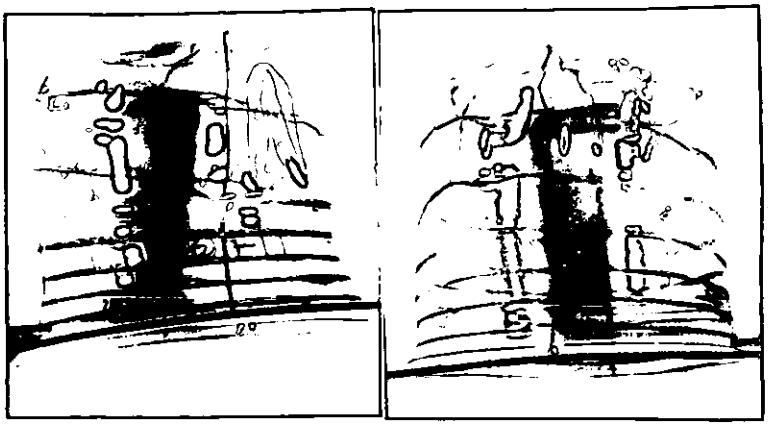

V VI

	Sheet T°C	Mould T°C
I	114	85
II	114	35
III	100	95
IV	100	25
V	86	85
VI	86	35

Figure 6.45 Photographs of shallow vacuum formed containers at different processing conditions

(a) Extension ratio Distribution 2:1V

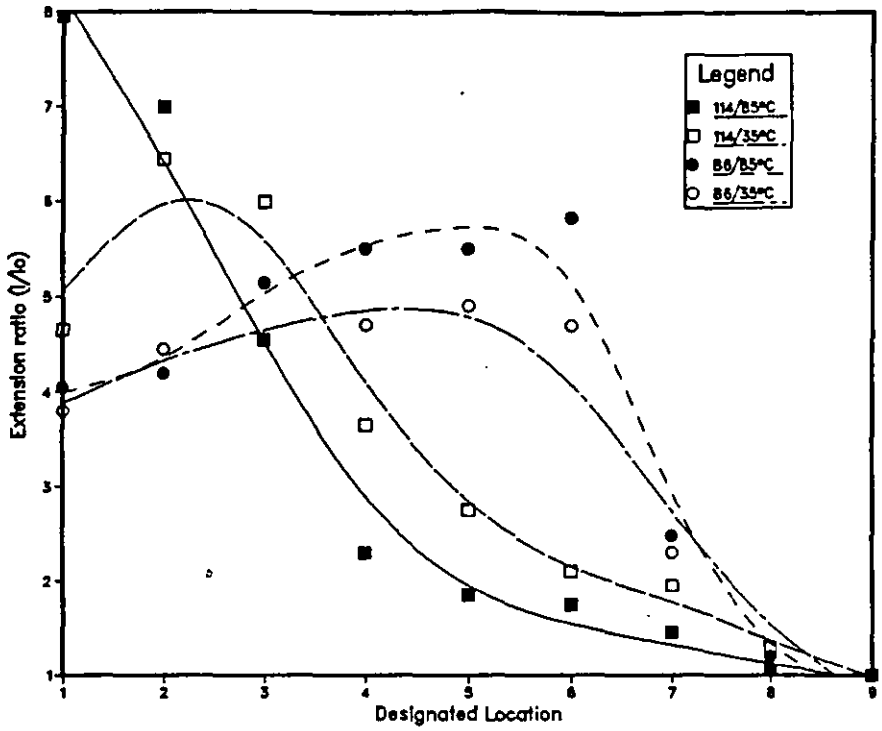

(b) Extension ratio Distribution 2:1V

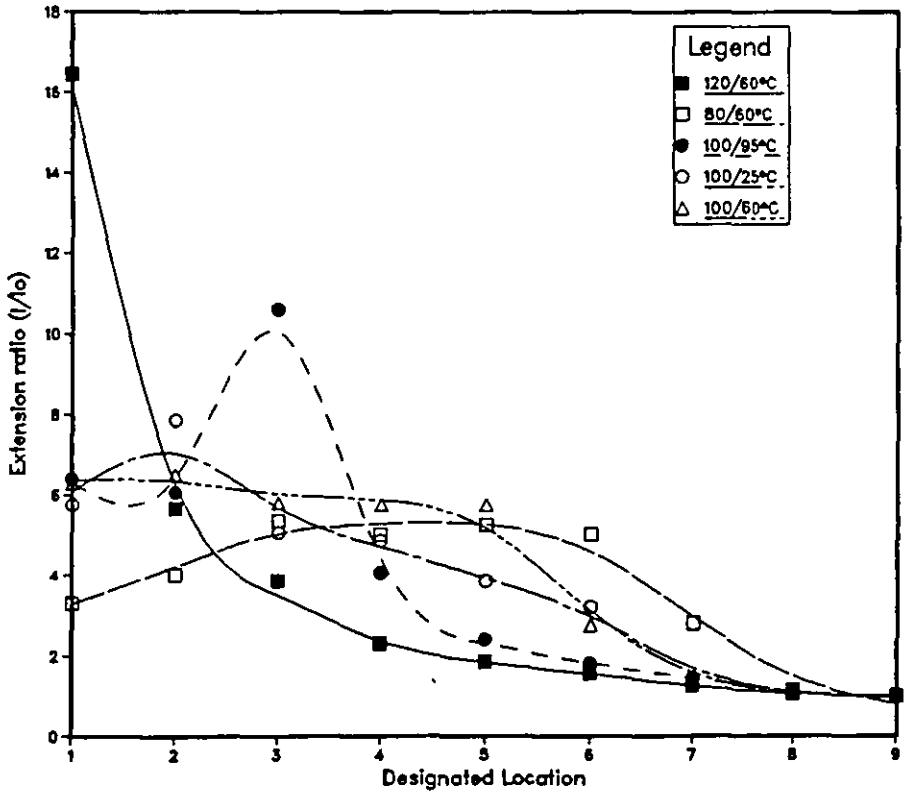

Figure 6.46 *Extension ratio as a function of 'Designated location of' the rings (shallow vacuum formed containers)*

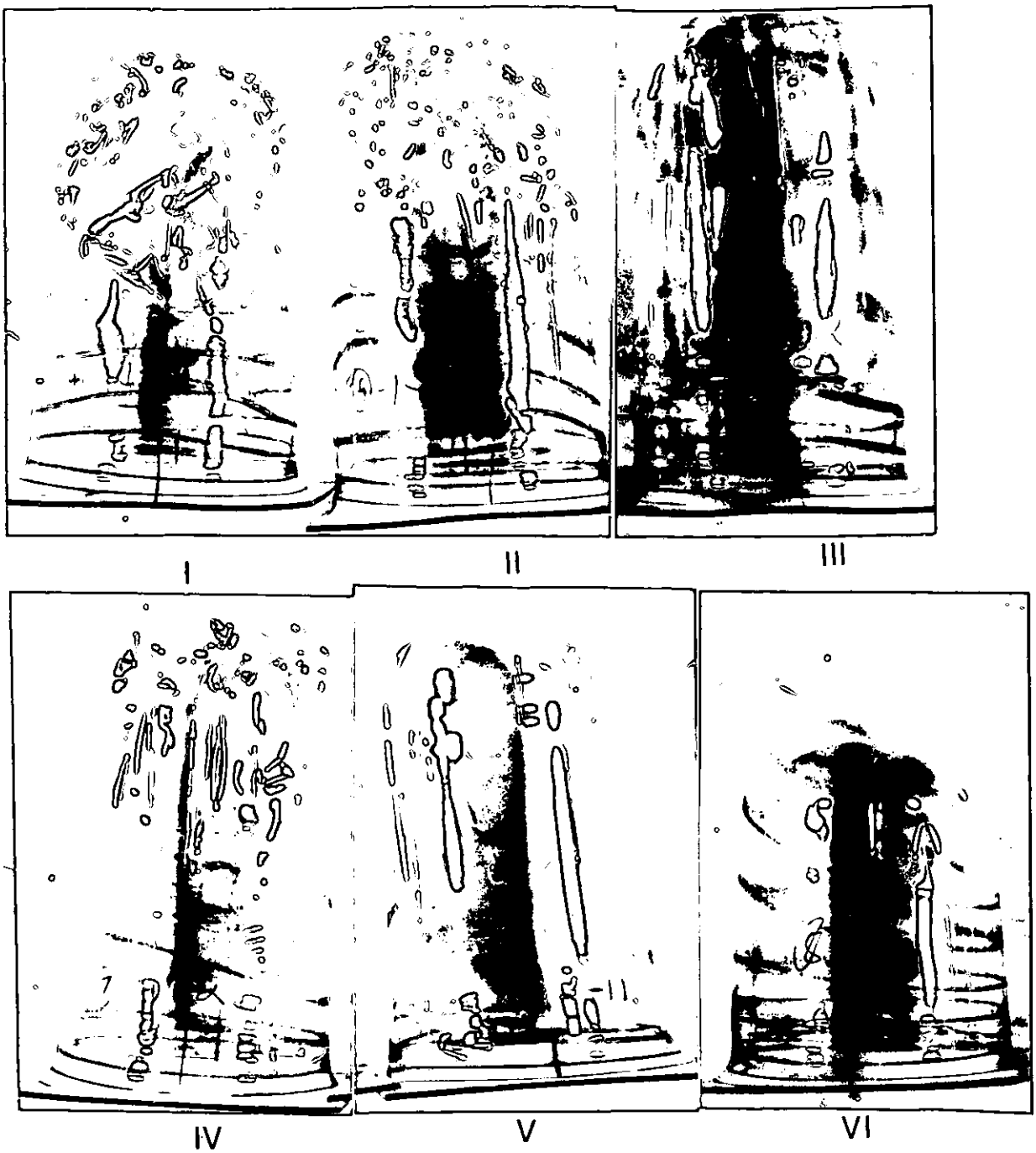

	Sheet T°C	Mould T°C
I	114	85
II	114	35
III	100	95
IV	100	25
V	86	85
VI	86	35

Figure 6.47 Photographs of deep vacuum formed containers at different processing conditions

(a) Extension ratio Distribution 1:1P

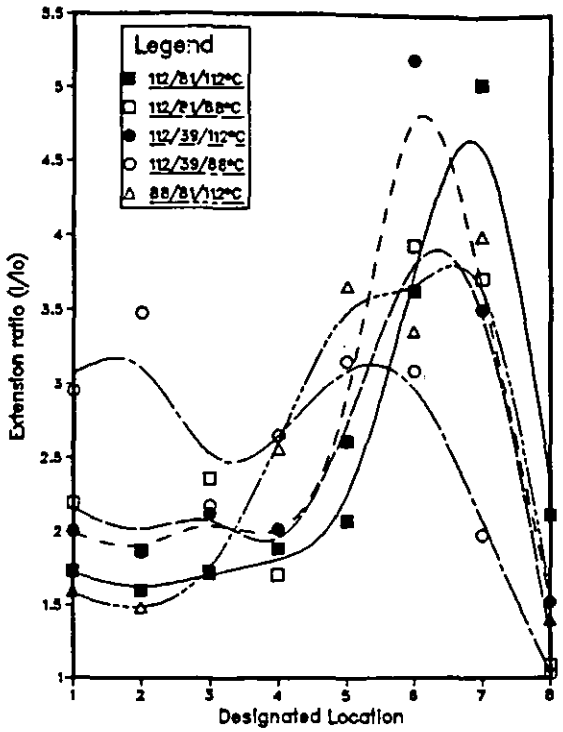

(b) Extension ratio Distribution 1:1P

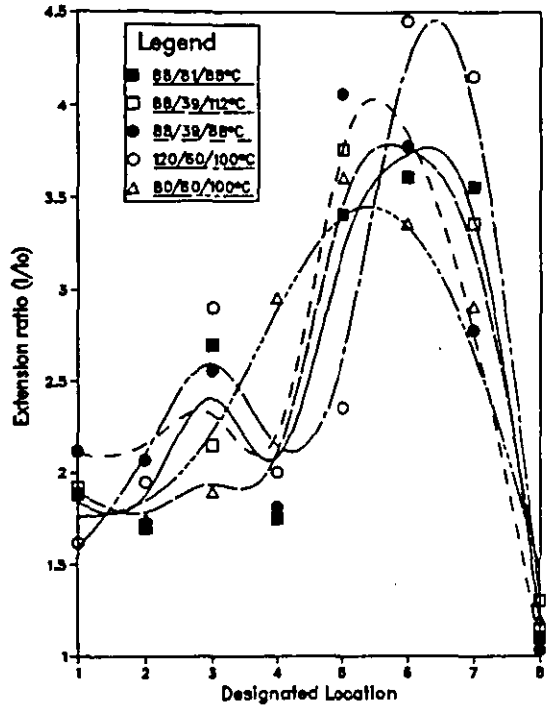

(c) Extension ratio Distribution 1:1P

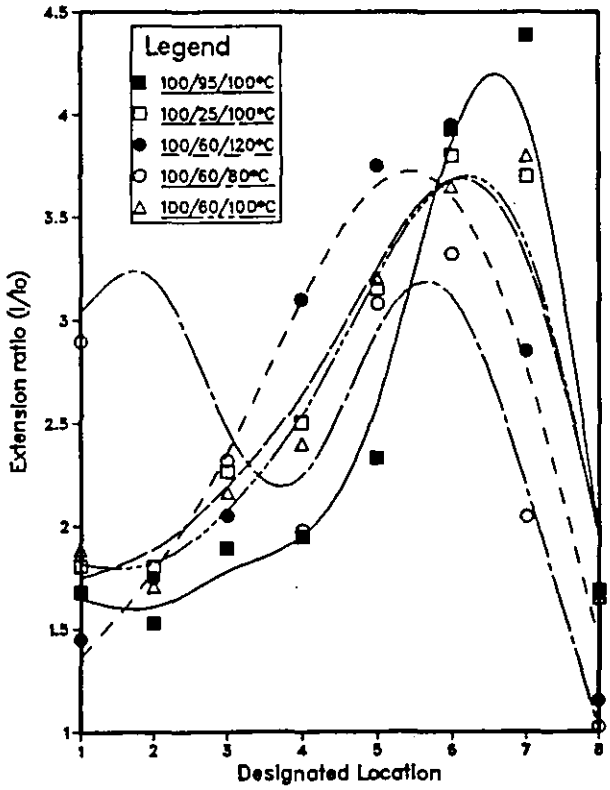

Figure 6.48 *Extension ratio as a function of 'Designated location of the rings (shallow plug-assist)*
Legend: sheet/mould/plug temperatures

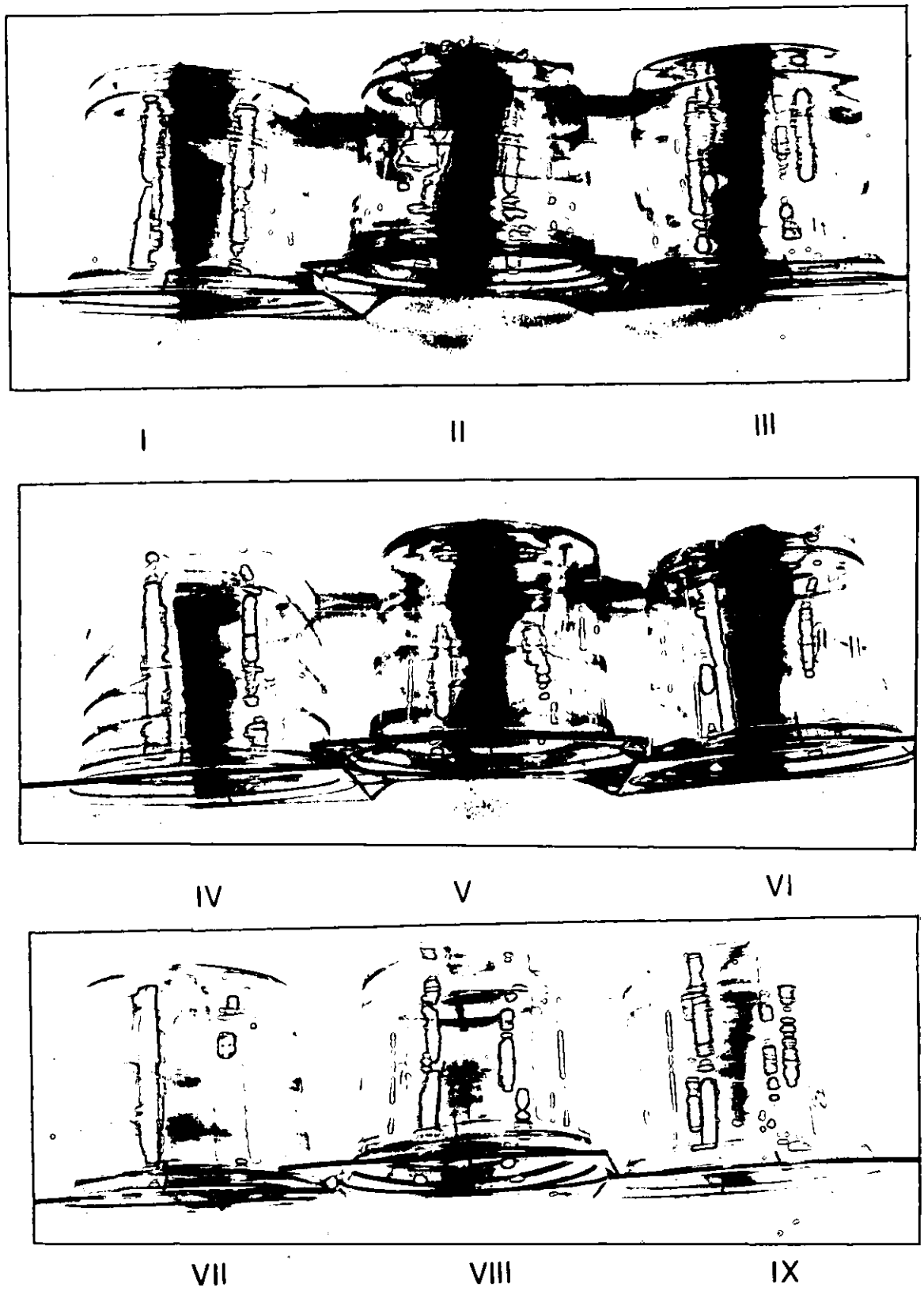

Figure 6.49 Photographs of shallow plug-assist formed containers at different processing conditions

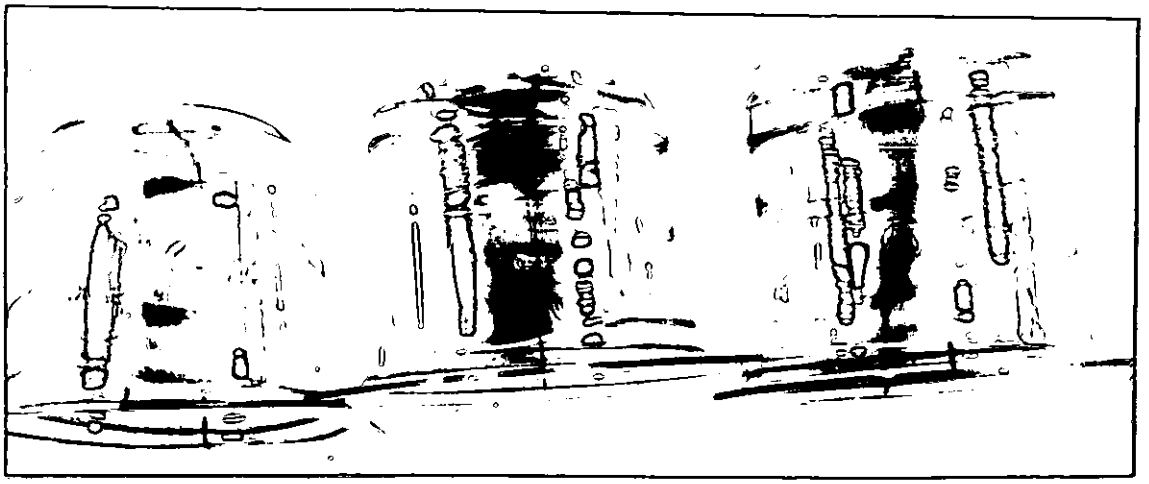

X XI XII

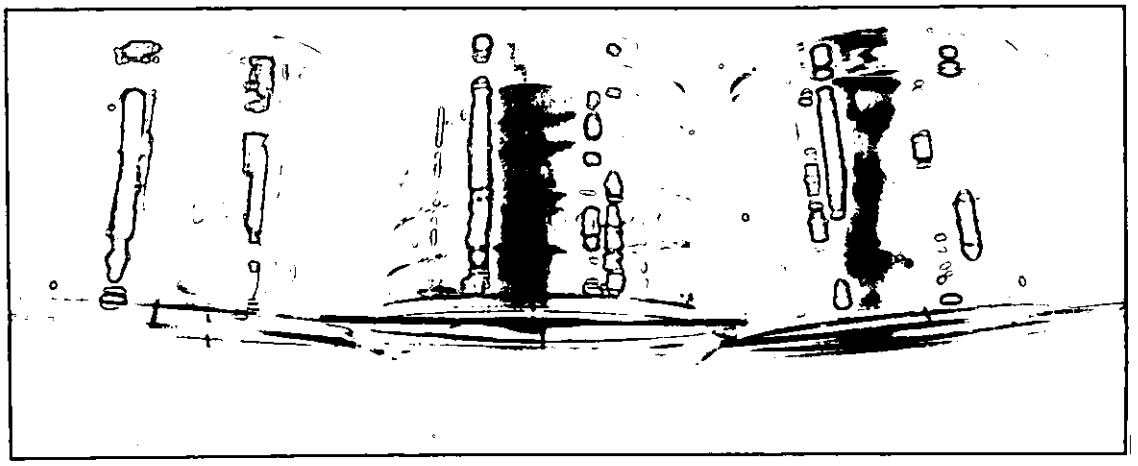

XIII XIV XV

Number	Processing Conditions S	M	P	Number	Processing Conditions S	M	P
I	112	81	112	IX	120	60	100
II	112	81	88	X	80	60	100
III	112	39	112	XI	100	95	100
IV	112	39	88	XII	100	25	100
V	88	81	112	XIII	100	60	120
VI	88	81	88	XIV	100	60	80
VII	88	39	112	XV	100	60	100
VIII	88	39	88				

S=sheet temp; M=mould temp ; P=plug temp

(a) Extension ratio Distribution 2:1P

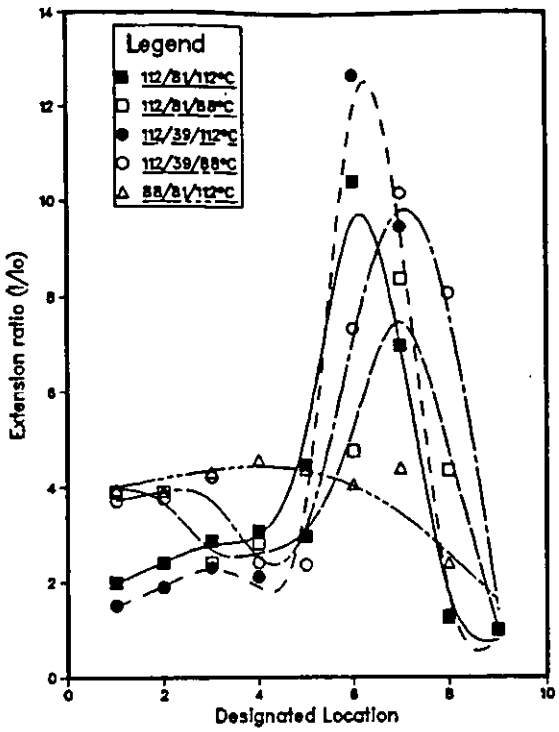

(b) Extension ratio Distribution 2:1P

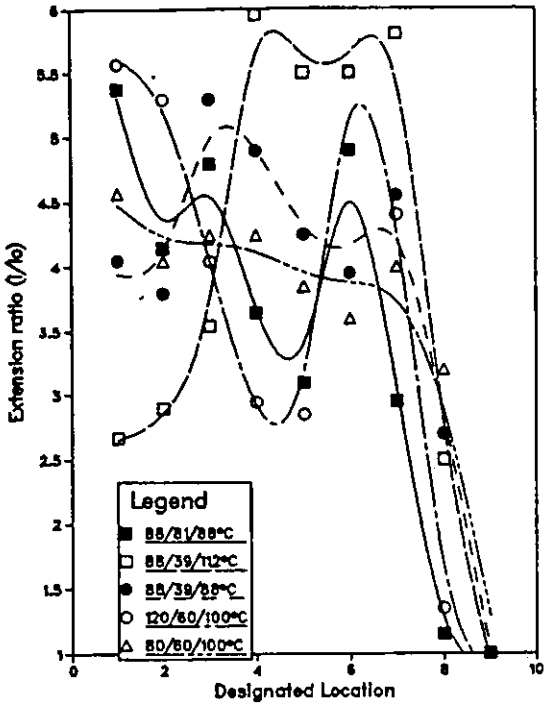

(c) Extension ratio Distribution 2:1P

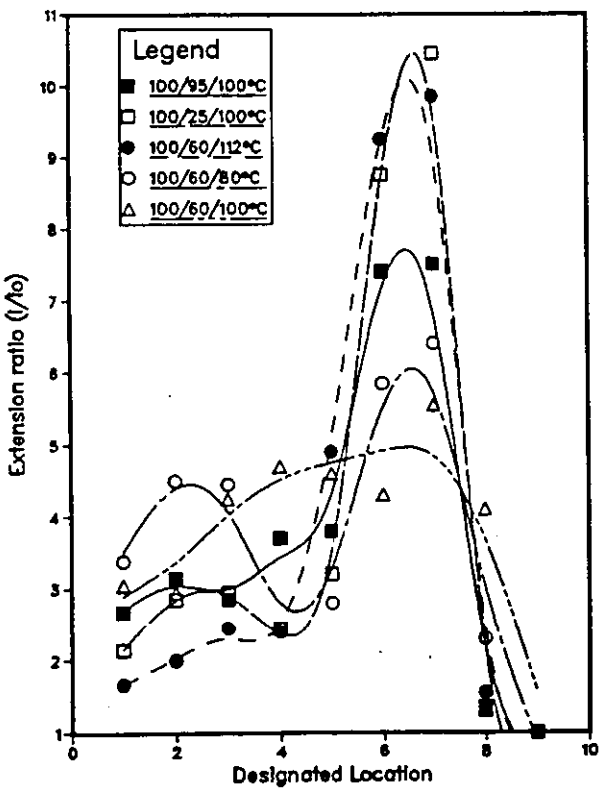

Figure 6.50 *Extension ratio as a function of 'Designated location' of the rings (deep plug-assist)*
Legend: sheet/mould/plug temperatures.

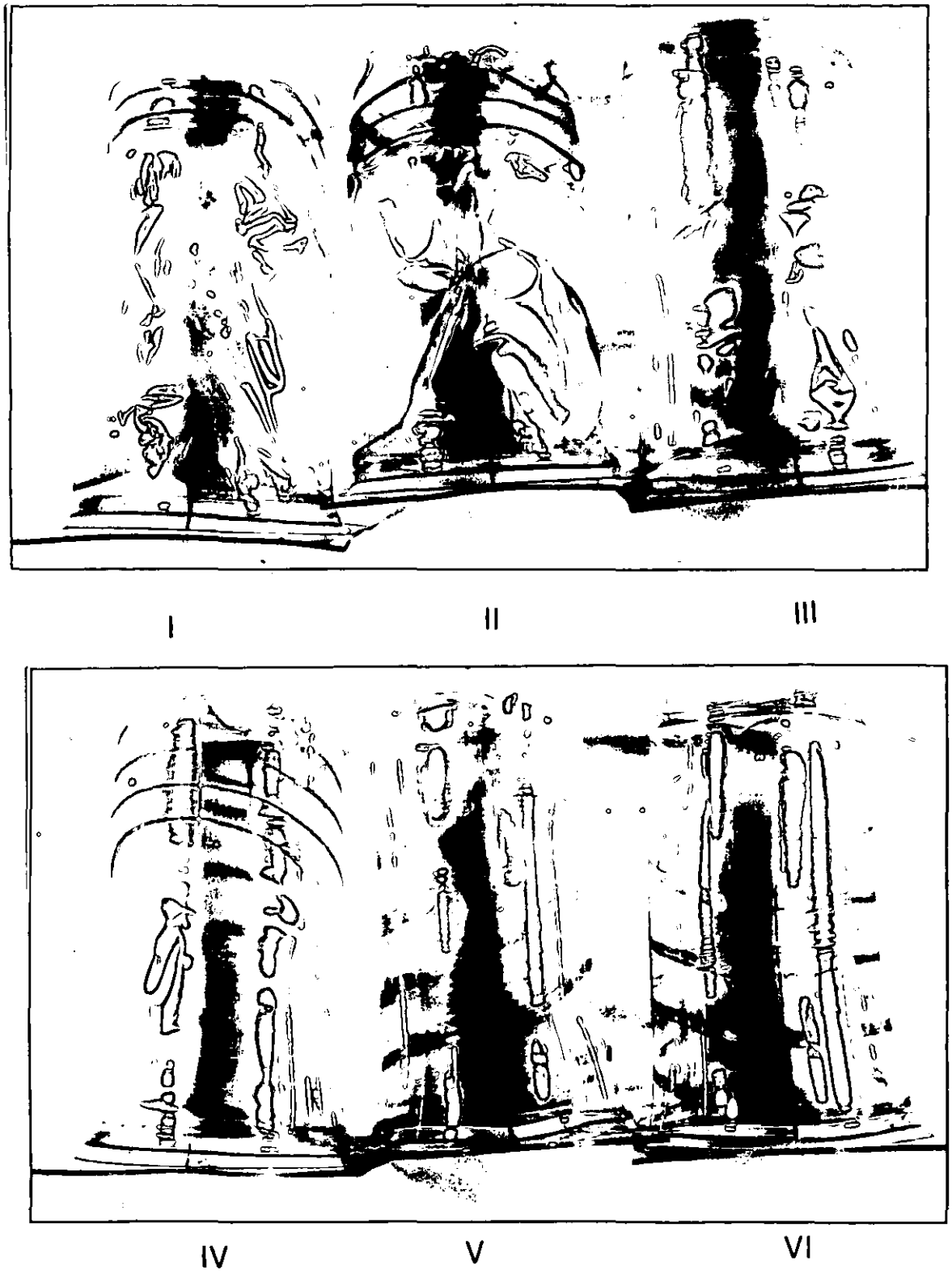

Figure 6.51 *Photographs of deep plug-assist formed containers at different processing conditions.*

VII VIII IX

X XI XII

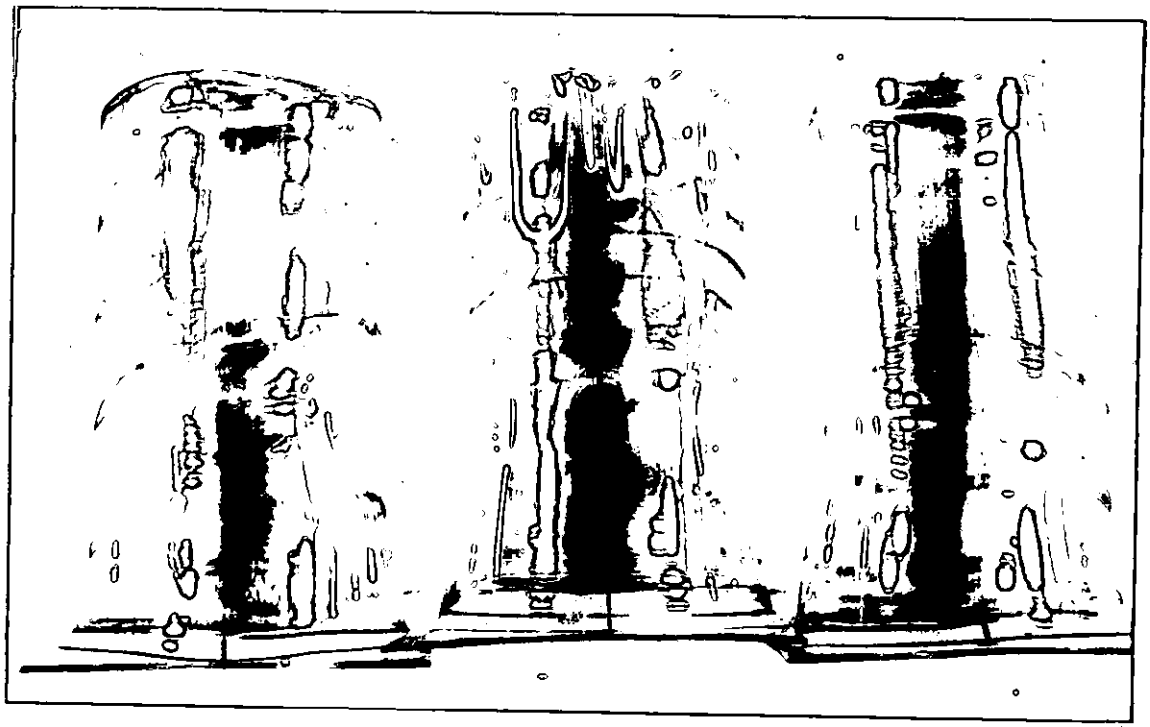

XIII XIV XV

Number	Processing Conditions S	M	P	Number	Processing Conditions S	M	P
I	112	81	112	IX	120	60	100
II	112	81	88	X	80	60	100
III	112	39	112	XI	100	95	100
IV	112	39	88	XII	100	25	100
V	88	81	112	XIII	100	60	120
VI	88	81	88	XIV	100	60	80
VII	88	39	112	XV	100	60	100
VIII	88	39	88				

S=sheet temp; M=mould temp ; P=plug temp

6.8.2 Tensile Properties (Hoop Direction)

Ring samples of 10 mm width were cut from the containers made at different processing conditions. The samples were prepared on a lathe in order to cut samples of uniform width. Three samples were cut from the deep drawn containers while two samples were cut from shallow drawn containers. Fig 6.52 illustrates the relative position of the samples on the containers.

A special ring sample holder illustrated in fig 6.53 was used in determining the tensile properties of the samples.

The surface of the sample holder was smeared with thin film of silicone oil in order to reduce friction and to ensure that the whole sample was subject to uniform deformation. Since the thickness across the cross-section of a sample is not uniform, the thickness of the thinnest position was recorded. This is because stresses are concentrated in regions of minimum thickness, which serve as weak points in the sample.

Tests could not be conducted on the longitudinal sections of the containers because of extreme thickness gradient from the rim to the base, which would render the data meaningless.

The hoop tensile tests were conducted at a nominal test speed of 10 mm/min and room temperature (23 °C) on the JJ Lloyd tensile testing equipment. The following parameters were determined: yield stress (σ_y) tensile strength at break (σ_B) and elongation to break (ε_B).

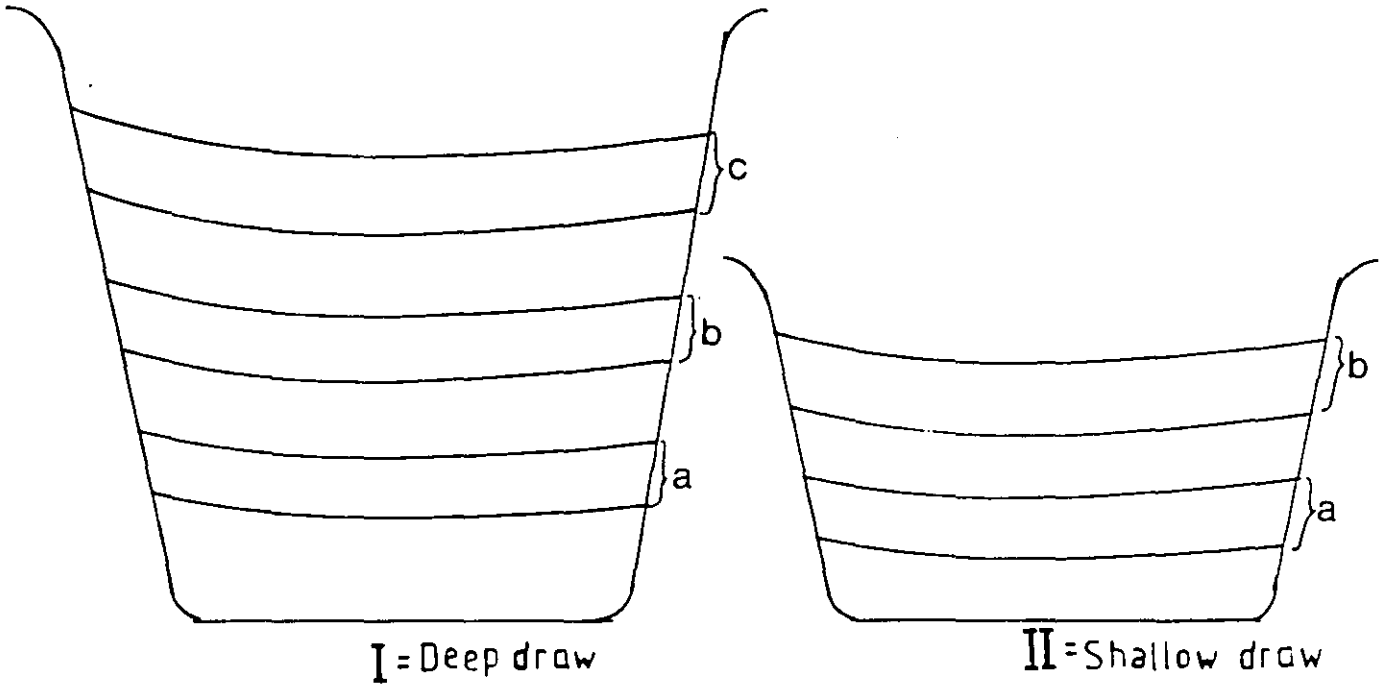

Figure 6.52 Relative positions of tensile ring samples on the containers

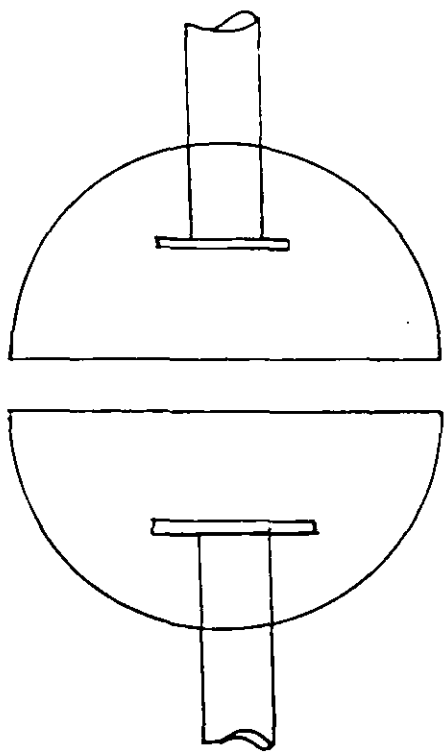

Figure 6.53 Schematic representation of ring sample holder

6.8.2.1 Tensile Properties Results and Discussion

The results of the tensile tests on samples cut from the containers are presented in tables 6.30 - 6.33. Typical (engineering) stress-strain curves for the samples cut from vacuum or plug-assist formed containers are shown in fig 6.54.

Curve I in fig 6.54 represents samples that exhibit ductile failure. This is typical of oriented amorphous plastics which yield before further deformation and eventual failure. Curve II is typical of undrawn amorphous glassy plastics.

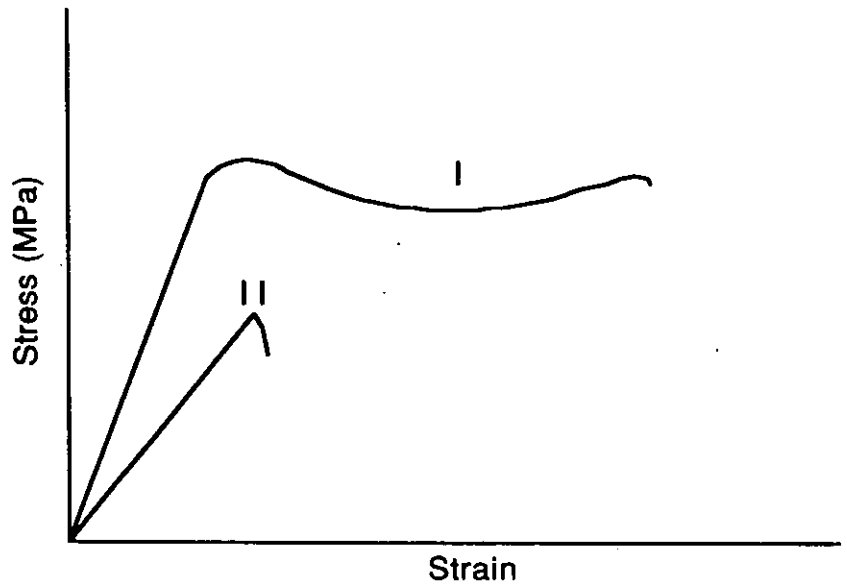

Figure 6.54 Typical stress-strain curve for samples cut from the containers

Process Condtions °C							
No	Sheet	Mould	Sample	Load(N)	Yield stress (MPa)	Tensile strength (MPa)	Elongation to break (%)
1	114	85	a	16	72.0	80	150
			b	920		167.27	13.3
2	114	35	a	29.6	52.14	52.86	45.3
			b	688		129.81	23.5
3	86	85	a	84	80.0	105.0	491.1
			b	50.0		89.13	15.6
4	86	35	a	30	77.33	100.0	196.4
			b	86.4		154.29	9.4
5	120	60	a	9.6	48.0	48.0	81.3
			b	744		161.04	10.0
6	80	60	a	60.4	84.29	86.29	150
			b	776		143.70	16.4
7	100	95	a	40	41.67	83.33	10.0
			b	1024		109.40	16.9
8	100	25	a	277.2	90.00	90.67	101.4
			b	832		143.45	8.2
9	100	60	a	68..8	182.00	172.0	60.0
			b	680		161.91	9.4
10	100	60	a	32	99.20	128.00	88.6
			b	812		169.17	10.0
11	100	60	a	40	87.11	88.89	76.7
			b	692		164.76	8.2
12	100	60	a	88	192.00	176.00	25.3
			b	808		149.63	10.6

Table 6.30 Tensile properties of shallow draw vacuum formed PETP containers

Process Conditions							
No	Sheet	Mould	Sample	Load(N)	Yield stress (MPa)	Tensile strength (MPa)	Elongation to break (%)
1	114	85	a	17.6	88	96.0	23.8
			b	36.0	180	174.0	26.3
			c	712.0		111.25	5.0
2	114	35	a	9.6	96.0	144.0	67.1
			b	48.0		60.0	5.00
			c	178.0		46.84	4.80
3	86	85	a	34		42.5	10.0
			b	216		154.29	12.3
			c	236		118.0	9.10
4	86	35	a	112	160	161.71	94.0
			b	128		85.33	5.50
			c	372		143.08	7.70
5	120	60	a	8.0	80.0	88.0	51.0
			b	190.0		76.0	7.80
			c	700.0		148	7.50
6	80	60	a	161.0	123.85	102.312	12.3
			b	196.0		150.77	13.30
			c	226.0		102.73	9.50
7	100	95	a	88.0	293.33	298.67	92.3
			b	94.0	117.50	105.00	13.7
			c	146.0		40.56	6.0
8	100	25	a	62.0	206.67	226.67	18.20
			b	154.0	70.0	70.91	22.6
			c	260.0		78.79	5.20
9	100	60	a	70.4	117.33	122.67	8.80
			b	99.2		124.0	5.50
			c	217.0		108.5	4.80
10	100	60	a	106.0		212	12.0
			b	138.0		138	6.7
			c	166.0	103.75	104.38	10.0
11	100	60	a	70.0	87.5	82.5	15.6
			b	140.0	107.69	92.31	11.9
			c	250.0		96.15	6.9
12	100	60	a	84		169.6	21.0
			b	122.4		111.27	7.10
			c	238.0		125.26	6.40

Table 6.31 Tensile Properties of Deep draw vacuum formed PETP containers

Sample 'a' in both shallow and deep vacuum formed containers exhibits ductile failure (table 6.9 and 6.10), due to high biaxial orientation in this part of the forming. It should be remembered that, the bases of the containers were formed from the spherical bubble generated by the vacuum action at the start of forming. The yield or necking behaviour exhibited can be attributed to stress softening [112] (geometrical changes in sample) exemplified by a load drop (material property)[174] during stretching.

Sample 'b' in shallow containers and test samples 'b' and 'c' in deep vacuum formed containers exhibit brittle failure. This is due to anisotropy and limited deformation in the section of the formings. In the shallow draws, there is limited deformation in the forming, while in deep containers, brittle failure in sample 'b' is due to anisotropy. There is more unidirectional deformation perpendicular to the direction of test (Hoop direction). Sample 'c' exhibits brittle failure because of limited or no deformation in that part of the containers. Therefore, the orientation in vacuum formed containers can be modelled as shown in fig 6.55

The higher tensile strength values obtained for sample 'a' in deep containers compared to shallow containers (see tables 6.30 and 6.31) is due to influence of strain-induced crystallinity. At deep draws, the sheet is drawn beyond the 'natural draw' ε^N regime of the stress-strain curve defined in Chapter 3. Therefore, orientation and strain hardening improves the toughness of the forming.

In the Plug-assist forming, the mode of deformation is different compared to straight vacuum forming. Here the deformation is more unidirectional (ie in the stretch direction). Therefore, because of anisotropic effect, the samples in plug-assist formed containers to a large extent exhibit brittle failure (curve II in fig 6.54) ie no yield, as shown in tables 6.32 and 6.33.

Process Conditions °C								
No	Sheet	Mould	Plug	Sample	Load(N)	Yield stress (MPa)	Tensile Strength (MPa)	Elongation tobreak(%
1	112	81	112	a	310		72.61	18.2
				b	164		149.09	1.0
2	112	81	88	a	318		133.57	14.5
				b	362		201	14.1
3	112	39	112	a	266		70.0	13.8
				b	73		152.0	8.8
4	112	39	88	a	279		62.0	10.0
				b	280		175.0	12.9
5	88	81	112	a	372		143.08	22.2
				b	432		154.29	16.7
6	88	81	88	a	254		115.45	18.2
				b	256		72.29	12.5
7	88	39	112	a	280		107.69	20.0
				b	440		146.67	18.8
8	88	39	88	a	282	117.5	100.83	61.5
				b	367		114.69	11.8
9	120	60	100	a	224		149.33	12.3
				b	315		121.15	12.3
10	80	60	100	a	376		134.29	22.7
				b	460		135.29	14.7
11	100	95	100	a	376		144.62	16.7
				b	382		136.43	22.2
12	100	25	100	a	350		106.06	15.4
				b	232		110.48	10.0
13	100	60	120	a	296		148.0	12.3
				b	392		135.17	14.1
14	100	60	80	a	318	122.31	94.23	133.3
				b	412		158.46	10.6
15	100	60	100	a	322		11.03	12.3
				b	260		113.04	12.3
16	100	60	100	a	316		126.4	16.4
				b	230		92.0	10.0
17	100	60	100	a	324		140.87	18.2
				b	402		184.8	18.6
18	100	60	100	a	360		171.43	15.0
				b	394		131.33	14.7
19.100		60	100	a	307		122.8	14.5
				b	344		98.29	14.3
20	100	60	100	a	396		184.35	19.2
				b	390		150.00	25.0

Table 6.32 Tensile Properties of Shallow Plug-assist Formed PETP Containers

Process Conditions °C								
No	Sheet	Mould	Plug	Sample	Load(N)	Yield stress (MPa)	Tensile strength (MPa)	Elongation tobreak(%
1	112	81	112	a	142	40.57	40.57	70.0
				b	12		17.14	16.7
				c	144		72.0	3.8
2	112	81	88	a	180		66.67	22.2
				b	154		118.46	8.3
				c	152		190.00	11.10
3	112	39	112	a	128		91.43	10.0
				b	10	50	50.0	9.5
				c	25	125	125.0	21.1
4	112	39	88	a	156		78.0	6.7
				b	250		80.65	6.7
				c	300		85.71	5.9
5	88	81	112	a	160		228.57	14.3
				b	318		167.37	20.8
				c	450		173.08	18.4
6	88	81	88	a	114	142.5	132.5	23.1
				b	344		127.41	18.2
				c	403		115.14	13.6
7	88	39	112	a	145	181.25	157.50	29.0
				b	282		134.29	18.0
				c	376		144.62	19.0
8	88	39	88	a	114		162.86	25.0
				b	272		151.11	15.0
				c	402		167.50	14.0
9	120	60	100	a	429		104.63	18.2
				b	8	30	40.00	10.9
				c	112		44.80	4.2
10	80	60	100	a	149	212.86	205.71	50.0
				b	332		166.0	16.0
				c	419		149.64	13.0
11	100	95	100	a	142		78.89	10.0
				b	209		149.29	13.6
				c	142		78.89	9.1
12	100	25	100	a	146		162.22	10.7
				b	66		82.50	8.3
				c	146		97.33	6.0
13	100	60	120	a	78		78.0	9.1
				b	102		56.67	6.3
				c	303		202.0	15.6
14	100	60	80	a	137		105.38	10.7
				b	224		140.00	8.3
				c	212		163.08	10.5
15	100	60	100	a	142		109.23	11.5
				b	226		86.92	11.5
				c	202		144.29	11.5
16	100	60	100	a	160		76.19	11.5
				b	149		64.78	7.7
				c	134		103	5.6
17	100	60	100	a	74		105.71	7.1
				b	110		220.0	8.3
				c	173		86.5	
18	100	60	100	a	154		192.5	12.5
				b	121		67.22	11.5
				c	212		212.0	12.5
19	100	60	100	a	146		132.73	13.6
				b	285		142.50	11.5
				c	332		127.69	10.7
20	100	60	100	a	112		86.15	11.5
				b	200		71.43	11.5
				c	266		95.0	10.7

Table 6.33 Tensile Properties of Deep draw Plug-assist formed PETP containers

The effect of anisotropy is pronounced in the elongation to failure. The vacuum formed containers exhibit higher elongation to failure compared to equivalent plug-assist containers of the same draw ratio. However, a comparative study of shallow and deep vacuum formed containers, show that sample 'a ' in shallow draws exhibits higher elongation to failure compared to equivalent samples in deep containers. This is due to the effect of strain-induced crystallization in deep drawn samples which inhibits stretching of the molecular chains. Whereas in the shallow drawn containers, there is no strain-induced crystallization since the draw ratio is within the 'natural draw' regime of the stress-strain curve. Also elongation to failure in shallow plug-assist formed containers is higher than in deep plug-assist formed containers. In both cases, the samples are being drawn perpendicular to direction of orientation in the samples. The influence of strain induced crystallization in deep draws as observed in vacuum draw containers reduces the elongation to failure.

It would be interesting to study the influence of processing conditions on the tensile properties of the PETP containers. However, because of limited material available, and at least 5 containers at each processing condition is needed to be tested for reliable results, the tensile results were not considered for factorial analysis.

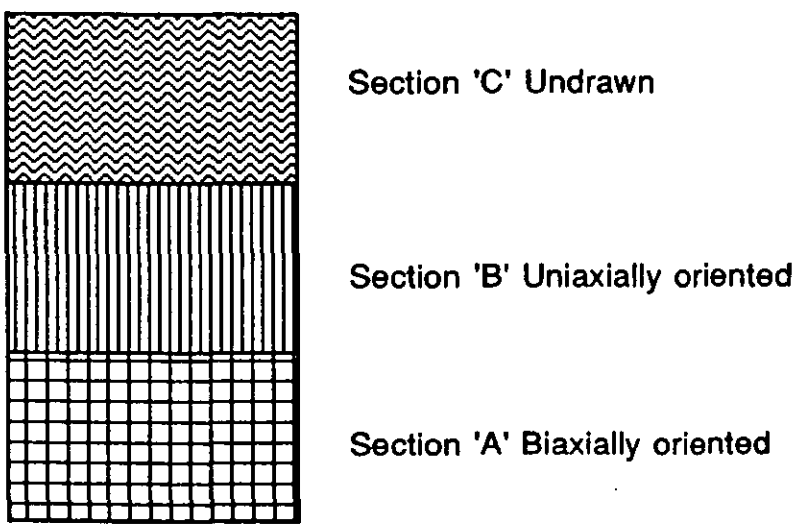

Figure 6.55 Schematic representation of orientation in vacuum formed PETP

6.8.3 Birefringence

The spectrophotometric technique [106] for measuring degree of molecular orientation (as explained in Chapter 3) was used. Planar birefringence as a function of the segment number on the containers was determined (fig 5.7).

The containers produced at the following processing conditions were analysed:

Vacuum Formed Containers	Temperatures °C	
	Sheet	Mould
2:1 draw ratio only	90	60
	100	60
	86	85

Plug-assist formed containers	Temperatures °C		
	Sheet	Mould	Plug
1:1 and 2:1 draw ratios	100	60	100
	88	39	112
	112	39	88
	80	60	100
	100	60	120

6.8.3.1 Birefringence Results and Discussion

Planar birefringence of the outside surface of the formings was determined. Optical extinction was observed in sections towards the base of the vacuum formed containers. This was expected since the spherical gap generated by vacuum action is essentially biaxially oriented.

In the shallow draw containers, the bulk of the forming was subjected to equi-biaxial deformation, thus no birefringence results were obtained. Towards the rim of the container, the orientation was so small that the spectrophotometric technique was not sensitive enough to measure the birefringence. Microscopic technique could not be used because of high level of dispersion in the samples.

In deep draw vacuum formed containers there was stretching on the walls of the mould during the forming process, thus difference in polarisability of the molecular chains in the principal extension ratios (ie hoop and longitudinal directions). Fig 6.56 shows that birefringence decreases with increasing segment number. This is because, stretching of the sheet increases towards the bottom of the container. Also it could be related to longitudinal strain distribution in the containers which decreases towards the rim. If there were no stretching on the mould wall during forming, each element of the forming would exhibit balanced orientation or extinction in every direction between crossed polars.

Fig 6.57 is a plot of birefringence vs segment number for plug-assist formed shallow containers. The birefringence values increase from the base to the rim of the containers. This is due to greater longitudinal strain imposed on the sheet by the plug action. There is less variability in the birefringence value due to uniform strain distribution. Similar observations were noted in plug assist deep draw containers Fig 6.58; greater birefringence values were obtained because of greater deformation involved at the larger draw ratio.

These results show that vacuum forming is essentially biaxial deformation, while plug-assist imposes unidirectional deformation on plastic sheet during forming processes.

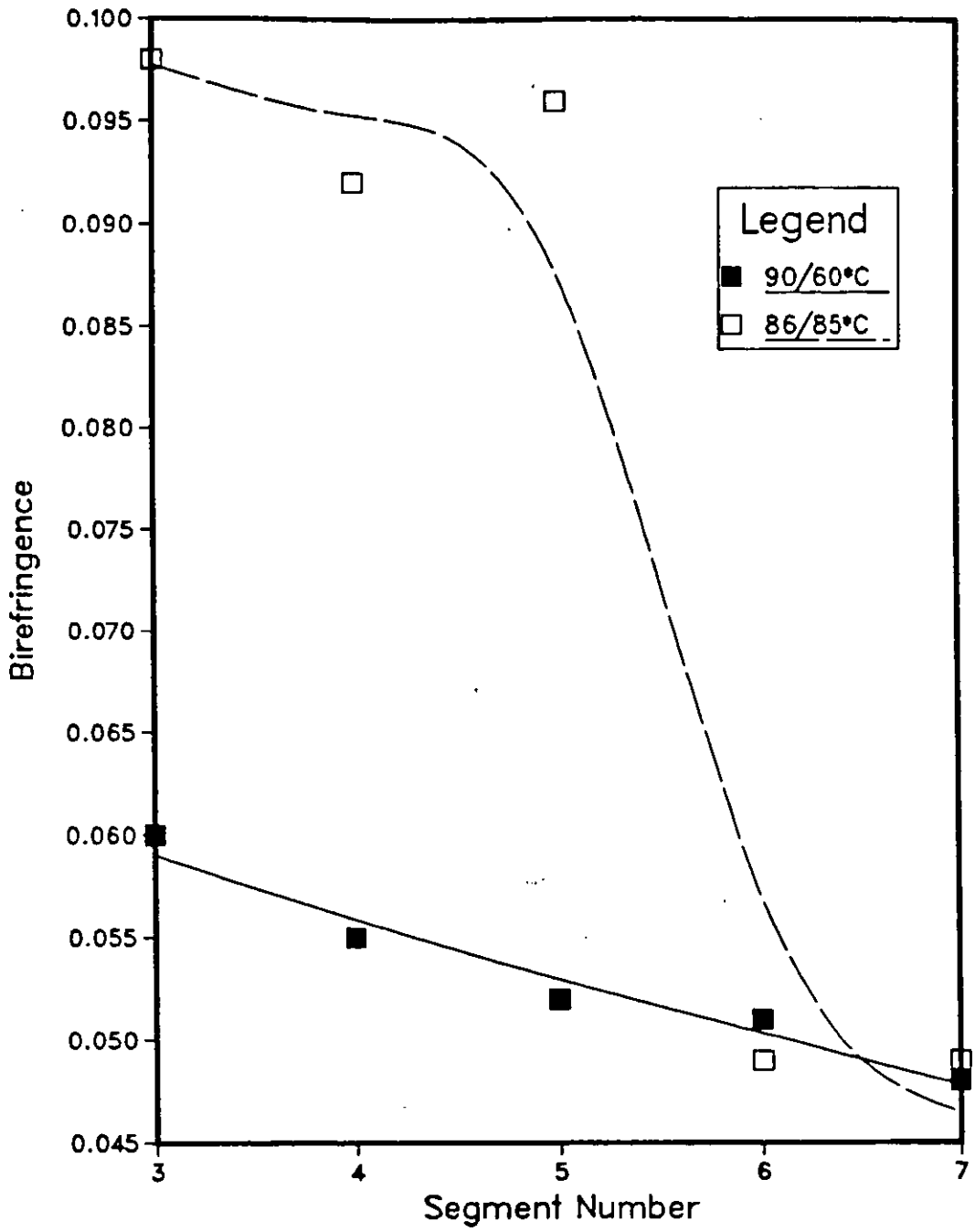

Figure 6.56 *Influence of processing conditions on sheet orientation in vacuum forming (deep draws)*
Legend:Sheet/ Mould temperatures

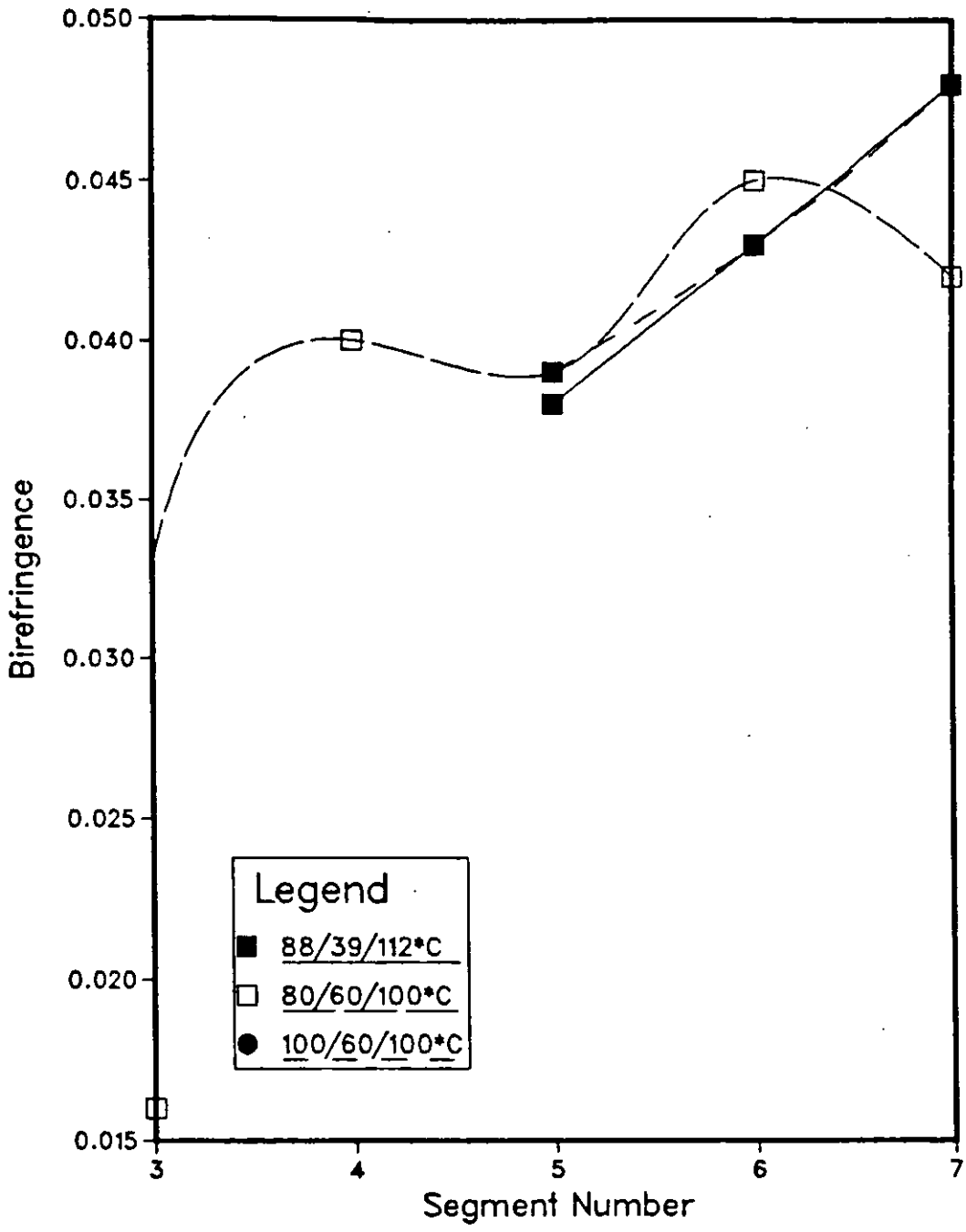

Figure 6.57 *Influence of processing conditions on sheet orientation in plug-assist (shallow draws)*
Legend: Sheet /Mould /Plug temperatures.

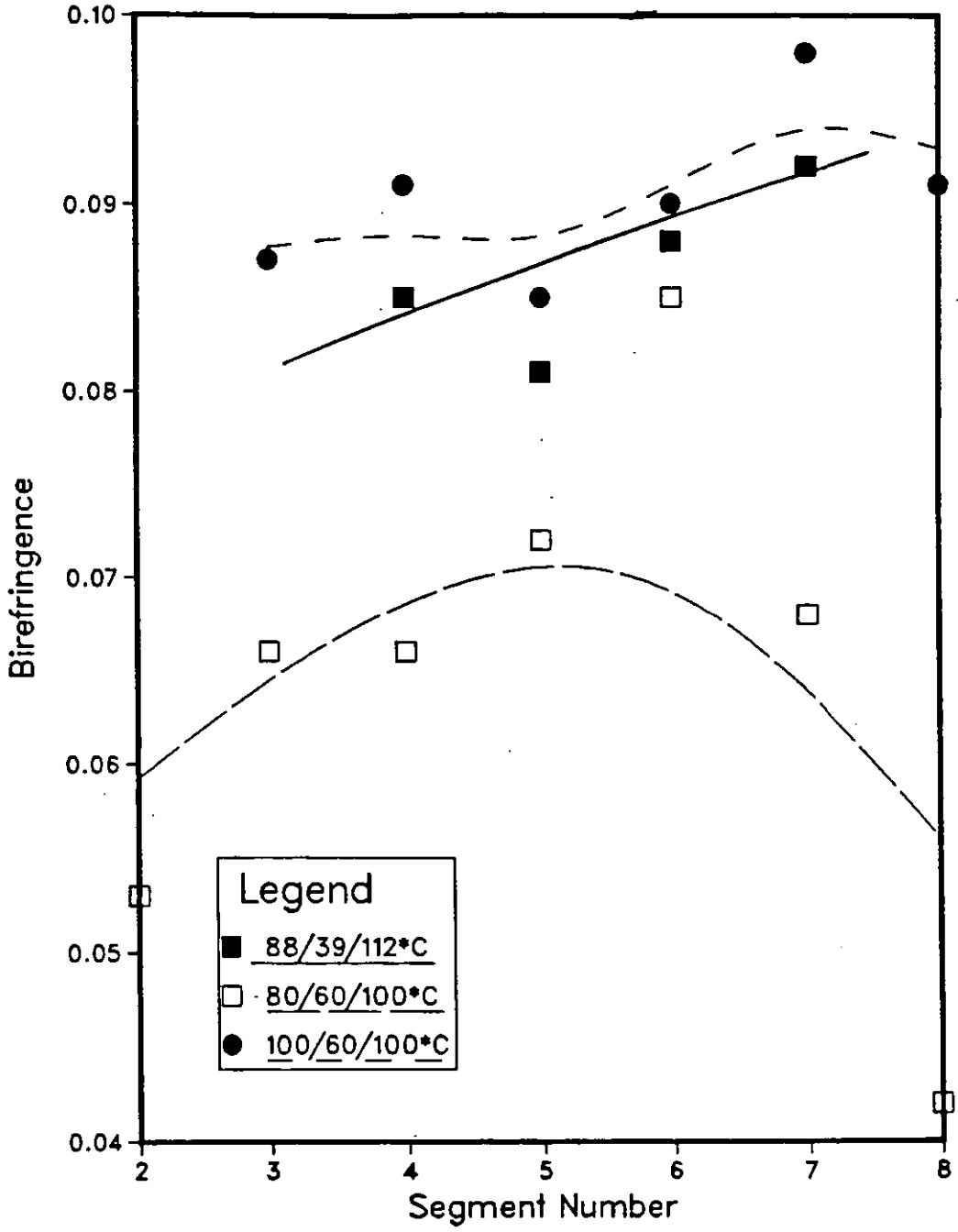

Figure 6.58 *Influence of processing conditions on sheet orientation in plug-assist (deep draws)*
Legend : Sheet / Mould / Plug temperatures.

6.9 Conclusions

The use of statistical experimental design for thermoforming has ensured in depth characterisation and understanding of PETP forming behaviour under a range of different processing conditions. Also, it has enabled the determination of the effect of each forming variable and the optimisation of forming conditions that will produce a product of desired properties.

A summary of the main points is as follows:

(i) There is a good agreement between the William's model and experimental data with respect to thickness distribution, especially for the vacuum formed containers. The slight deviation from the model prediction especially at the deep draws is due to the influence of strain hardening in PETP, since the model was designed for wholly amorphous plastics. The agreement with the model also shows that PETP is rubber-elastic within the thermoforming temperature range (80-110 °C) (especially in the shallow draws) up to the onset of crystallization.

(ii) Sheryshev's model was used to explain thermoforming processes of a crystasllizable polymer, PETP: Low cooling and stretch factors ensure near-isothermal conditions, which promote uniform deformation.

(iii) The change in volumetric capacity (shrinkage) of PETP containers showed that strain hardening behaviour in PETP not only improves thickness distribution, it also enhances thermal stability. Therefore, thermoformed amorphous PETP is more suitable for hot filling applications if strain-induced crystallisation can be induced.

(iv) The tensile properties of thermoformed PETP containers established that deformation in vacuum formed containers is predominantly bi-axial while plug-assist formed containers is more uniaxial. Biaxial deformation improves the toughness of the forming especially in the deep draws where strain-hardening is encouraged.

(v) The birefringence studies confirmed the effect of anisotropy in thermoforming PETP. In vacuum formed containers where the deformation is more biaxial, there was no preferential polarization of the molecular chains. Whereas, in the plug-assist forming, deformation is more uniaxial, thus there was preferential direction of polarization of the molecular chains.

(vi) The analysis of the factorial experiment in terms of the thickness distribution (taken as the most important dependent variable) enabled the determination of the optimum processing condition - summarised in table 6.34.

Forming Mode	**Draw ratio**	**Processing Conditions** sheet/mould or sheet/mould/plug °C
Vacuum forming	1:1	90 -100/80-85 °C
Vacuum forming	2:1	80-90/70-75 °C
Plug-assist forming	1:1	100 -112/75 -90/100 -112 °C
Plug-assist forming	2:1	80-90/50 -75/-100-112 °C

Table 6.34 Optimum thermoforming Processing conditions for amorphous PETP

Finally, draw ratio within the strain hardening regime of the stress-strain curve of PETP is essential to produce formings of more uniform thickness, and minimum shrinkage if reheated.

Chapter 7

General Conclusions and Recommendations

7.1 General Conclusions

The thermoforming behaviour of amorphous Poly(ethylene-terephthalate) PETP has been investigated; the sheet was wholly amorphous homopolymer PETP of O.71 I.V, having a T_g of 70°C, maximum crystallization temperature of 160 °C, and melting temperature of 250 °C. Thermoforming temperatures of amorphous PETP have been established within the range 70 - 130 °C.

Before determining the thermoforming behaviour of amorphous PETP, it was found that prevailing environmental humidity affects the response of the material. Moisture absorption was found to increase with increasing relative humidity which had a pronounced effect on mechanical properties. In order to maintain consistent mechanical properties, the sheet was kept in a constant relative humidity (50 %) room.

A summary of drawing behaviour, forming characteristics, optimum processing conditions and properties of formed containers is presented. The main conclusions for work done in these areas are as follows:

(i) Uniaxial tensile stress/strain behaviour of PETP:

The thermoforming characteristics of PETP sheet between 80 - 110 °C have been modelled by a uniaxial tensile testing. It has been established that PETP exhibits homogenous deformation within these temperature ranges. The stress/strain curve shows yielding (but no necking), a region of uniform stress and subsequent strain hardening. The strain hardening results from strain induced crystallization and can be described by the empirical relation:

$$\sigma = K (\varepsilon_t)^n$$

Where σ_t = true stress

ε_t= true strain

n = strain hardening index

K = constant

The strain hardening index 'n' is temperature dependent but was found to be relatively independent of strain rate; it decreases with increasing temperature. Strain hardening index can be directly related to thermoformability: It is proposed that high strain hardening indices promote uniform thickness in thermoformed parts.

The stress relaxation (at constant strain) behaviour of PETP is strain and temperature dependent, and shows that deformation of PETP obeys the kinetic theory of rubber elasticity below the strain hardening regime ($\varepsilon < 2$ within the range of temperature considered 80 - 110 °C)

(ii) Forming characteristics:

Thickness distribution improves with a decrease in sheet temperature. This agrees with (i), in that a high strain hardening index promotes thickness uniformity in formed parts. In addition, draw ratio must exceed the 'natural draw" (ε^N) regime of the stress-strain curve to promote formings of more uniform thickness.

A factorial experimental design (based on multivariate regression analysis) of the thermoforming process established the influence of each processing variable on some product characteristics of PETP:

(a) For simple (negative) vacuum forming, thickness distribution is mainly affected by sheet temperature. However, thermal shrinkage tests showed that both sheet and mould temperatures influence the production of formings of good thermal stability.

(b) In the plug-assist forming mode, there is a significant interaction between the sheet and plug temperatures, especially in the deep draws.

(c) It is concluded that, forming conditions which ensure near-isothermal deformation promote thickness uniformity and control shrinkage in formed articles, especially in the deep draws. This is because of combined influence of strain and thermally induced crystallinity. Therefore, the results contradict the general belief elsewhere in the literature that sheet temperature is the only important variable in thermoforming. For crystallizable polymers like PETP, each forming variable contributes to the appearance, structure and properties of formed articles.

(iii) Relation between Established Thermoforming Theories and PETP behaviour:

(a) Good agreement between Williams's predictive model and the practical thickness distributions especially for shallow draws was obtained. This confirmed that PETP can be modelled by rubber-elastic analysis below the strain hardening regime ($\varepsilon < 2$). The slight deviation at the deep draws is due to the influence of strain induced crystallization exhibited by PETP.

(b) The cooling and stretch factors defined in Sheryshev's models (cooling factor is a measure of heat exchange between the sheet and forming tools; stretch factor is a measure of sheet drawing from beyond that situated above the mould cavity in vacuum forming whilst in plug-assist forming it is a measure of

drawing from the plug surface) have been derived for a strain crystallizable PETP. A low cooling factor is indicative of near-isothermal conditions which promote slippage on the mould wall and uniform deformation in thermoformed parts. Also, a low stretch factor effects greater drawing either from the region beyond the mould cavity or from the plug surface which ensures evenness in thickness in formed parts. There is a good agreement between the working hypothesis of Sheryshev's model and the experimental results for PETP.

(iv) Properties of Formed Articles in PETP

The tensile and birefringence measurements of the formed containers indicate proof of gross anisotropy of mechanical and optical properties.

(a) In vacuum formed containers, the spherical bubble generated by vacuum action induces biaxial deformation, and parts exhibit ductile failure during tensile tests (in the hoop direction).

(b) In plug-assist formed containers, the deformation induced is more preferential (less biaxial) and the samples exhibit brittle failure since the tensile strain is applied in the hoop direction perpendicular to stretch (orientation) direction.

(c) Birefringence measurements provide proof of the postulations above. Vacuum formed containers were not birefringent (because of balanced orientation) while in the plug-assist formed containers, there was positive birefringence due to preferred orientation of the molecular chains.

(v) Optimization of Processing Conditions from the response surface (of the coefficient of thickness distribution and shrinkage) determined with respect to varying processing conditions to produce PETP formings of good characteristics, the following conditions are recommended: Vacuum forming sheet temperature (80 - 90 °C), mould temperature (70 - 85 °C) and plug-assist forming sheet temperature (80 - 90 °C), mould temperature (50 - 85 °C), plug temperature (100 - 112 °C).

7.2 Recommendations for further studies

(i) It is suggested that thermoforming behaviour of different grades (I.Vs) of PETP including co-polymers should be studied. It is hoped that it will show

a) the effect of varying molecular weight on PETP forming characteristics.

b) I.V changes on strain and thermal induced crystallinity at the thermoforming temperatures

and c) the influence of molecular weight on product properties.

(ii) The influence of plug geometry on formings should be investigated

(iii) For shallow draw forming, nucleated sheets should be considered in order to improve thickness distribution.

(iv) A more sophisticated thermoformer is required in order to reduce forming cycle time of PETP,.preferably a thermoformer with sliding forming stage, as opposed to sliding heating station, with constant heat bank at the forming station. In any case, pilot-scale proof trials are necessary, in order to assess the applicability of the project to commercial environment.

(v) Finally, the use of computer aided modelling for different geometries making use of existing theoretical thermoforming model including that suggested in this work may improve the understanding of polymer (amorphous or crystallizable) deformation during forming operations.

(vi) Other properties relevant to commercial products worth investigating include impact, puncture and burst strengths (especially for carbonated drinks packaging).

References

1 Carothers, W.H., Hill, J. W., J. Am.Chem. Soc. 54, 1579 (1952)

2 Whinfield, J. R., Dickson, J. T., U. S. Patent 2465, 319; Chem. Abstr. 43, 4896 (1949)

3 Goodman, I., Encyl. of Poly.Sci. Tech., Vol 11, p62

4 Hawtrone, J. M., Heffelfinger, C. J., Encyl. Poly. Sci Tech., Vol 1 p42

5 Brydson, J. A. "Plastics Materials" Chapter 25. p626, Butterworths scientific (1982)

6 Korshak, V.V., Vinogradova, S.V., "Polyesters" Pergamon Press (1965)

7 Goodman, I., Phys, J.A., "Polyesters" London Iliffe Book Ltd (1965)

8 Callander, D.D., Poly. Eng. Sci., 25, 453 (1985)

9 Anon.. Plastics and Rubber International 11, 28 (1986)

10 Siggel et al, to Glanzsstoff A. G., U.S Patent 3496, 143 Feb 17, (1970)

11 Przygocki, Wl, Wlochwicz, W., J. Appl. Polym Sci. 19, 2683 (1978)

12 Smoluk, G.R., Mordern Plastics Inter. 10, 28 (1984)

13 Hollander, E. R. Jr.,Plastics Technology, 22, 33 (Feb 1976)

14 Bocchi, L., "Experience and Developments in Thermoforming PET Containers for Carbonated Beverages" SPE 4th international conference on Biaxial Oriented Bottles and Containers in PET and other Engineering and Plastics resins (Oct 1983)

15 Griehl, W., Schnock, G., Textile Tech., 8, 408 (1957)

16 Wilfong, R.E, J. Polymer Sci 54, 385 (9161)

17 Challa, G., Makromol. Chem., 38; 105, 123, 138 (1960)

18 Challa, G., Rec. Tran. Chim. 79, 90 (1960)

19 Gregory, D.R., Watson, M.T., J. Polym. Sci, Part C; 30, 399 (1970)

20 Gregory, D.R., J. Appl. Polym. Sci. 16, 1479 (1972)

21 Cogswell, F.M., Poly. Eng Sci. 12, 64 (1972)

22 Cogswell, F.M, Trans. Soc. Rheol. 16:3, 383 (1972)

23 Denson, C.D., Poly. Eng. Sci. 13, 125 (1973)

24 Cogswell, F.M., Rheol. Acta. 8, 187 (1969)

25 Donald, D.J., Poehlein, G.W., Denson, C.D, Trans.Soc. Rheol 16:3, 42 (1972)

26 Throne, J.L., Plastics and Rubber Processing. 4, 129 (1979)

27 Denson, C.D., Gallo, R.J., Poly. Eng. Sci. 11, 174 (1971)

28 Malpass, V.E., White, C. H., "Laboratory Comparison of the Thermoforming Properties of Two ABS Materials" in "Basic Principles of Thermoforming" Bruins, P.F.(Ed). Gorden Breach Science Publishers (1973) 668.412

29 Lai, M.O., Holt, D.L., J. Appl. Polym. Sci. 19, 1209 (1975)

30 Rivlin, R.S., Saunders, D.W., Phil. Trans. 243, 251 (1951)

(31) Shmidt, L.R., Carley, J.P. Poly. Eng. Sci. 15, 51 (1975)
(32) deVries, A.J., Bonnebat, C., Poly. Eng.Sci. 16, 93 (1976)
33 Harris, R.L., Bruins, P.F. "A new Technique for Predicting Optimum Thermoforming Conditions" in "Basic Principles of Thermoforming" Bruins, P.F., (Ed) Gordon Breach Science Publishers (1973)
34 Tryon, M., Horowitz, E., "Infrared Spectroscopy" in"Analytical Chemistry of Polymers Part II", Kline, G. (Ed) chap VIII (1962), Interscience Publ. New York. London. p291
35 Billmeyer, F. W. Jr., "Text book of Polymer Science" 3rd Edition. Wiley-Interscience Publ. N.Y. (1971)
36 Vogel, A.I., "A text book of Practical Organic Chemistry" 4th edition. Longman Publ. London (1978)
37 Haslam, J., Willis, H.A., "Identification and Analysis of Plastics" Iliffe Publ. London (1965)
38 Bellamy, L.J. "The Infra-red Spectra of Complex Molecules" 2nd edition Chapman and Hall (1980)
39 Zbinden, R., "Infra-red Spectroscopy of High Polymers". Academic Press, New York (1964)
40 Cobbs, W.H. Jr., Burton, R.L., Polymer Sci .10, 275 (1953)
41 Weston. G.J., Chem and Ind. (London) 604 (1954)
42 Mann, J., Thomson, H.W., Proc. Roy. Soc (London). A211, 168 (1952)
43 Daniels, W.W., Kitson, R. E., J. Poly. Sci. 33, 161 (1958)
44 Miller, R. G. J., Willis, H. A., Trans. Faraday. 49, 433 (1953)
45 Weissberg, S.G., Rothman, S., Wales, M., "Molecular Weights and Sizes" in "Analytical Chemistry of Polymer Part II" Kline, G. (Ed) Chap I P1Interscience Publ. New York. London (1962)
46 Slade, P.E., "Polymer Molecular Weights" in "Polymer Molecular Weights Part I" Vol 4 Slade, P.E., (Ed), Marcel Dekker, Inc. New York (1975)
47 Carpenter, D.K., Westerman, L. "Viscometric Methods of studying Molecular Weight and Molecular Weight Distribution" in "Polymer Molecular Weights Part II" Vol 4 Slade, P.E. (Ed) Marcel Dekker, Inc New York (1975)
48 Cowie, J.M.G., "Polymers: Chemistry and Physics of Modern Materials" Inter text Books (1973)
49 Storenson, W.R., Ency. Poly.Sci. Tech. Vol 3. p182
50 Johnson, J.F., Ency. Poly. Sci. Tech. Vol 9. p182
51 Keavey, J. J., Eberlin, E.L.,J. Appl. Poly Sci. 3, 47 (1960)
52 Collins, E.A., Bares, J., Billmeyer, F.W. Jr., "Experiments in Polymer Science' Wiley (1973)

53 Gregory, D.R., Trans. Soc. Rheol. 17:1, 191 (1973)
54 Murphy, C.B., "Polymeric Materials" in "Differential Thermal Analysis" Vol 1 Mackenzie, R.C. (Ed) Academic Press London. New York (1970)
55 Ke, B., J. Poly. Sci. 42, 15 (1960)
56 Ke, B., J. Appl. Polym. Sci. 6, 624 (1962)
57 Richardson, M.J., Br. Polym. J.. 1, 132 (1969)
58 Allen, P.W. (Ed) "Techniques of Polymer Characterization" Butterworths Scientific Publications (1959) 547.84 All
59 Gooding, E.P., S.C.I. Monograph No 13, "Thermal Degradation of Polymers" (1961)
60 Marshall, I. Todd, A., Trans. Farad. Soc. 49, 67 (1953)
61 Kelleher, P.G., Wentz, R.P., Hellman, M.Y., Gilbert, E. H., Poly. Eng. Sci.23, 537 (1983)
62 Zimmerman, H., Kim, N.T., Poly. Eng. Sci. 20, 680, (1980)
63 Jabarin, S.A., Lofgren, E.A., Poly. Eng. Sci. 24, 1056 (1984)
64 Mc Mahon, W., Birds all, H.A., Johnson, G.R., and Camilli, C.T., J. Chem. Eng.Data 4, 57, (1959)
65 Ito, E., Kobayashi, Y., J. Appl. Poly. Sci. 25, 2145 (1980)
66 Gardner, R.J., Martin, J.R., SPE ANTEC Tech Papers 24 ,329 (1978)
67 Jabarin, S.A., Lofgren, E.A., Poly. Eng. Sci. 76, 620. (1986)
68 Van Amerongen, G.J. Rubber. Chem.Tech. 37, 1065 (1964)
69 Aminabhavi, T.M., Thomas, R.W., Cassidy, P.E., Poly.Eng.Sci .24, 1417 (1984)
70 Maron, G., Broutman, L.J. J.Appl . Poly. Sci. 26, 1493 (1981)
71 Shen, C.H., Springer, G.S., J. Comp. Mater., 10 ,2 (1976)
72 Gardner, R.J., Martin, J.R., SPE AMTEC Tech Papers 25 831 (1979)
73 Kishore, K., san Karahinghan Poly. Eng. Sci. 24, 1043 (1984)
74 Dulmage, W.J., Geddes. A.L., J. Poly. Sci. 321, 499 (1958)
75 Statton, W.O., Godard, G.M., J. Appl. Phys. 28 ,1111 (1957)
76 Heffelfinger, L.J., Schmidt, P.G., J. Appl. Poly. Sci. 9, 2661 (1965)
77 Dumbleton, J.H., Bowles, B.B., J. Polym. Sci. A - 2; 4, 951 (1966)
78 Dumbleton, J.H., J. Poly. Sci A-2; 7, 667 (1969)
79 Konig, J.L., Hannon, M.J., J. Macromol.Sci (Phys). B1, 119 (1967)
80 Prevorsek, D.L., Sibita, J.P., J. Macromol . Sci (Phys). B5, 617 (1971)
81 Yeh, G.S.Y.,Geil, P.H., J. Macromol. Sci (Phys). B1, 251 (1967)
82 Klement, J.J., Geil, P.H., J. Macromol. Sci (Phys). B5, 505 (1971)
83 Klement, J.J., Geil, P.H., J. Macromol. Sci (Phys). B5, 535 (1971)
84 Marshall, I., Thompson, A.B., J. Appl. Chem. 4,145 (1954)

85 Rietzh, F., Duckett, R.A., Ward, I.M., Polymer 20, 1133 (1979)
86 Engelaere, J.C., Cavrot, J.P., Rietsch, F., Polymer 23, 766 (1982)
87 Ward, I.M., (Ed) "Structure and Properties of Oriented Polymers". Applied Sci Publ. London (1975).
88 Padibjo, S.R., Ward, I.M., Polymer 24, 1103 (1983)
89 Pinnock, P.R., Ward, I.M., Trans.Fara. Soc. 62, 1308 (1966)
90 Pinnock, P.R., Ward, I.M., Br. J. Appl. Phys. 15, 1559 (1964)
91 Hughes, M.A., Sheldon, R.P., J. Appl Polym. Sci. 8, 1541 (1964)
92 Spruiell, J.E., McCord, D.E., Benerlein, R.A., Trans. Soc Rheol. 16, 353 (1972)
93 Misra, A., Stein, R.S., J. Poly. Sci Poly. Phys. Ed. 17, 235 (1979)
94 Hennessey, W.J., Spatorico, A.L., Poly. Eng. Sci. 19, 462 (1979)
95 Jabrin, S.A., Poly. Eng. Sci .24, 376 (1984)
96 Bonnebat, C., Ronllet, G., deVries, A.J., Poly. Eng. Sci 21 189 (1981)
97 deVries, A.J., Bonnebat,C., J. Poly. Sci: Poly.symp. 58, 109 (1977)
98 Nobbs, J.H., Bower, D.I., Ward, I., Patterson, D., Polymer 15 287 (1974)
99 Bhatt, G.M., Bell, J.P., J. Poly. Sci: Poly. Phys edn. 14, 575 (1976)
100 Smith, T.L., Trans. Soc. Rheol. 6, 61 (1962)
101 Meissner, J., Trans. Soc. Rheol. 16, 405 (1972)
102 Chang, H., Lodge, A.S., Rheol. Acta. 11, 127 (1972)
103 Lai, M.O., Holt, D.L., J. Appl Polym. Sci. 19, 1805 (1975)
104 J.J. Instrument Ltd "Infra-red non-contacting Extensometer Handbook"
105 Nielson, L.E., "Mechanical Properties of Polymers and composites" Vol 1. Mercel Debber Inc New York (1974)
106 Yang, H.H., Choinard, M.P., Ling, W .J., J. Poly. Sci: Poly Phys. Ed., 20 981 (1982)
107 Treloar, L.R.G. "The Physics of Rubber Elasticity" Clarendon Press, Oxford (1958)
108 Smith, F.S., Steward, R.D., Polymer 15, 283 (1974)
109 Smith, T.L., J. Poly. Sci. 32, 99 (1958)
110 Smith, T.L., Steadry, P.L., J. Appl. Phys. 31, 1892 (1960)
111 Bueche, F., J. Appl. Phys. 26, 1133 (1955)
112 Ward, I.M., "Mechanical Properties of Solid Polymers" 2nd edn. John Wiley and Son Ltd New York (1979)
113 Datsko, J. "Material Properties and Manufacturing Processes". John Wiley and Sons Ltd. New York (1966) 671. DAT
114 Budiansky, B., Wang, M.J., J. Mech. Phys, Solids. 14, 357 (1966)
115 Warshavsky, M. Tokita, M., SPE J. 26, 55 (1970)
116 Bahadur, S., Poly. Eng. Sci. 13, 266 (1973)
Principles of Vacuum Forming A. Thiel 668. 412.

117 Maruyama ,S., Imada, K., Takayanagi, M., Inter. J. Poly.Mater. 1, 211 (1972)
118 Forster, E.C., Heap, H., "The Rheology of Elastomers" Pergamon press, N.Y. (1957) P 190
119 Engelaere, J.C., Cavrot, J.P., Reietsch, F., Eur. Poly. J. 16, 721 (1980)
120 Broutman, L.J., Kalpajian, S., Chawla, J., Poly. Eng. Sci. 12, 150 (1972)
121 Farrow, G., Ward, I.M., Polymer 1, 330 (1960)
122 Chu, W.H., Yoon, D.Y., J. Polym. Sci: Polym Symp. 61, 17 (1977)
123 Rudd, J.F., Andrews, R.D., J. Appl. Physics 29, 1421 (1958)
124 Thomas, L.S., Cleerman, K.J. SPE. Journal 28, 61 (1972)
125 Cakmak, M., Spruiell, J.E., White, J.L., Poly. Eng. Sci. 24, 1390 (1984).
126 Bueche, F., "Physical Properties of Polymers". Interscience Publishers (1962)
127 Scott, K.W., Stein, R.S., J. Chem Phys. 21, 1272 (1953)
128 Andrews, R.D., Hoffman -Bang, N., Tobolsky, A.V.,J.Poly. Sci .3, 669 (1948)
129 Tobolsky, A.V., J. Appl. Phys.27, 673 (1956)
130 Meredith, R., Hsu, B., J. Poly. Sci. 61, 253 (1962)
132 Buchdahl, Rl, Nielsen, L.E., J. Appl. Phys. 22, 1344 (1951)
133 Bueche, F., J. Chem.Phys. 22, 603 (1954)
134 Rouse, E. Jr., J.Chem. Phys. 21, 1272 (1953)
135 Passaglia, E., Koppehele, H.P., J. Poly. Sci .33, 281 (1958)
136 McConnell, W., "The Oldest Infant" in 'Basic Principles of Thermoforming' Ed P.F. Bruins Gordon and Breach Science Publishers Ltd, London (1973)
137 Boyce, A.V., and Froehlich, J.E., Modern Plastics encyclopaedia, 54 10A, p384 (1977)
138 Childs, E.S., 'Thermoforming - Trends and Prospects' in 'Basic Principles of Thermoforming' P.E. Bruins Ed, Gordon and Breach science publishers ltd, London (1973)
139 Anony. Mordern Plastics 55: 1 p 41 (1978).
140 Butzko, R.L., 'Plastics Sheet Forming' Reinhold Pulb. Co. N.Y. (1958)
141 Platzer, N. 'Sheet Forming' in 'Processing of Thermoplastic Materials', E.C. Bernhadt Ed. Reinhold Publishing , N.Y. (1959)
142 Frados, J. Ed., 'Plastics Engineering Handbook' Van Nostrand Reinhold 10 (1960)
143 Stratton, B., Kunststoffe, 48, 68 (1958)
144 Progelhof, R.C., and Throne, J.L., Polym Eng. Sci 14, 810 (1974)
145 Quintiere,J.G., Throne, J.L, and Progelhof, R.C. Soc. Plast Eng. J. 29, (1) 35 (1973)
146 Davenport, R.C., Plastics Technology 2, 232 (1956)

147 Thiel, A., "Principles of Vacuum Forming" London Iliffe Books Lid (1965)
148 Throne, J.L., "Plastics Processing Engineering" Mercel Dekker Inc. New York. (1979) chapter 12
149 Harris, R., "Prototype Tooling for Thermoforming" Bruins, P.F. (Ed), Gordon and Breach, Science Publishers New York, (1973)
150 Ebell, P.C., Ph.D Thesis L.U.T (1981)
151 Kakouris, A.P., M.Phil Thesis L.U.T (1983)
152 Covas, J.A., Ph.D Thesis L.U.T (1986)
153 Wilkinson, D. Unpublished Results
154 Davis, O.L. (Ed), "The design and analysis of industrial Experiments" Longman Group Ltd London (1979)
155 Box, G.E.P., Hunter, W.G., Hunter, J.S., "Statistics for Experiments" John Wiley N. Y (1978)
156 Freakly, P.K., "Rubber Processing and Production organization" Plenum, (1985)
157 Cooper, B.E., "Statistics for Experiments" Pergamon Press Oxford (1969)
158 Box. G.E.P., Wilson, K.B., J Roy. Stat. Soc 13 1 (1951)
159 Box G.E.P., Biometrics 10 16 (1954)
160 Baker, R.J., Nelder, J.Al, "The GLIM System Release 3 Manual" Numerical Algorithms Group and Roy Stat Soc. London (1977)
161 Smith, H., Rose, A., Ind. Eng. Chem. 55, 25 (1963)
162 Hill, W.J., Hunter, W., Technometrics 87, 571 (1966)
163 Cochran, W.G. "Experimental Design" John Wiley N.Y. (1957)
164 Cox, D.R., "Planning of Experiments" John Wiley. N.Y. (1958)
165 Schmidt, L.R., Carley, J.F., Poly. Eng. Sci. 15, 51 (1975)
166 Williams,J. G., J. Strain Anal. 5, 49 (1970)
167 Ragab, A.R. Metals Technology 10, 340 (1983)
168 Ragab, A.R., Khorshied, S.A., Plastics and Rubber Processing and Applications 6, 21 (1986)
169 Rosenzweig, N, Nakis, M., Tadmor, S., Poly. Eng. Sci. 19, 946 (1979)
170 Crawford, R.J. "Plastics Engineering" Pergamon Press, Oxford (1981)
171 Sheryshev, M.A., Zhogolev, I.B. Salazkin., Soviet Plastics 11, 30 (1969)
172 Tsai, J.T. Poly. Eng Sci. 22, 265 (1982)
173 Sheryshev, M.A., Salazkin, K.A., Soviet Plastics 10, 28 (1970)
174 Haward, R.M., "The Physics of Glassy Polymers" Applied science Publishers Ltd (1973)

APPENDIX I

```
      DIMENSION C(6)
      CHARACTER *6 FNAM, FNAM1
      COMMON C
      REAL AZ(10,10),W(5000)
    6   Print *, 'Enter Filename'
      READ *, FNAM
      I = 1
   22     IF (I .GT. 1 .AND. FNAM(I:I) .EQ. ' ') THEN
      K = I - 1
      ELSE
      I = I + 1
      GOTO 22
      END IF
      FNAM1 = FNAM(1:K)
      OPEN (5, FILE = FNAM1, STATUS= 'OLD')
      READ (5,*) (C(I), I = 1,6)
      EXTERNAL RESP
      NW=5000
      NCONT=10
      ISM=1
      NIN=0
      NOUT=0
C     INITIALISE PLOTTING DEVICE
      WRITE (NOUT,*) 'DEVICE FOR OUTPUT ? '
      WRITE (NOUT,*) ' 0  FOR W1015       '
      WRITE (NOUT,*) ' 1  FOR W2019       '
      WRITE (NOUT,*) ' 2  FOR S5601       '
      WRITE (NOUT,*) ' 3  FOR S5664       '
      WRITE (NOUT,*) ' 4  FOR DTX5A       '
      WRITE (NOUT,*) ' 5  FOR SE281       '
      WRITE (NOUT,*) ' 6  FOR M6250       '
      WRITE (NOUT,*) ' 7  FOR C1051N      '
      PRINT *, 'ENTER 8 FOR CANON'
      READ (NIN,*) DTYPE
      IF (DTYPE .EQ. 0) THEN
      CALL T4010
      ELSE IF (DTYPE .EQ. 1) THEN
      CALL T4014
      ELSE IF (DTYPE .EQ. 2) THEN
      CALL S5601
      ELSE IF (DTYPE .EQ. 3) THEN
      CALL S5664
      ELSE IF (DTYPE .EQ. 4) THEN
      CALL DTX5A
      ELSE IF (DTYPE .EQ. 5) THEN
      CALL SE281
      ELSE IF (DTYPE .EQ. 6) THEN
      CALL M6250
      ELSE IF (DTYPE .EQ. 7) THEN
      CALL C1051N
      ELSE IF (DTYPE .EQ. 8) THEN
   24   CALL CNA2
      END IF
C
      CALL PICCLE
      CALL DEVPAP(250.0,150.0,1)
      CALL FUNCON(-1.414,1.414,-1.414,1.414,RESP,NCONT,ISM)
      CLOSE (5)
      PRINT *, 'DO YOU WANT A PLOT   1 FOR Y,  2   NO'
        READ *, NREP
        IF (NREP .EQ. 1) GOTO 24
      Print *, ' ANY MORE FILES   1  => Y  2  => N'
      READ *, NRP
      IF (NRP .EQ. 1) GOTO 6
      CALL DEVEND
      CALL GINEND
      END
C
      FUNCTION RESP(X,Y)
      DIMENSION C(6)
      COMMON C
      RESP = C(1) + C(2)*X + C(3)*Y + C(4)*X*X +
     &  C(5)*Y*Y + C(6)*X*Y
      RETURN
      END
```

APPENDIX II

```
C
C
        DIMENSION A(10),B(6)
      CHARACTER OLA *50,OLAV*12
       COMMON/BL/B
        EXTERNAL RESP
C     LIBRARY 'GINOGRAF'
C     LIBRARY 'GINOSURF'
C      LIBRARY 'GINO'
C      LIBRARY 'VAPPLB'
      CALL GINO
 15     PRINT *, ' FILE NAME :'
      READ (*,'(A)') OLA
      NRL = LENG(OLA)
      OLAV = OLA(1:NRL)
      OPEN (UNIT=8, FILE = OLAV,STATUS = 'OLD')
         READ (8,*)X1,X2,Y1,Y2
       DO 10 I = 1,10
 10     READ (8,*) A(I)
        CALL T4014
        CALL DEVPAP(210.0,297.0,0)
        CALL WINDO2 (12.0,297.0,0.0,210.0)
        CALL ERRMAX(30)
        WRITE (0,50)
 50     FORMAT ('IX=...IVX=...')
        READ(0,*) IX,IVX
      CALL PICCLE
        J = IX/3
        K = IX/2
        B(1) = A(1)+A(IX+1)*IVX+A(IX+4)*IVX*IVX
        B(2) = A(3-K)+A(8+J)*IVX
       B(3) = A(4-J)+A(9+K)*IVX
        B(4) = A(6-K)
        B(5) = A(7-J)
         B(6)=A(11-IX)
       DO 30 I = 1,6
 30     WRITE(0,40) B(I)
 40     FORMAT (6(F9.4/))
        CALL FUNCON(X1,X2,Y1,Y2,RESP,10,1)
      PRINT *,'DO YOU WANT PLOT ( 1 FOR Yes   2  No)'
      READ *, IPLOT
      CALL PICCLE
      CALL PICCLE
      IF (IPLOT .EQ.1)THEN
      CALL DEVEND
      CALL CNA2
      CALL FUNCON(X1,X2,Y1,Y2,RESP,10,1)
      END IF
      CALL GINEND
      PRINT *, ' CONTINUE  : TYPE  1 FOR YES     2 NO'
      READ *, ICONT
      CLOSE (8)
      IF (ICONT .EQ. 1 ) GOTO 15
        CALL EXIT
        END
C
        FUNCTION RESP(X,Y)
        DIMENSION B(6)
        COMMON/BL/B
        RESP= B(1)+B(2)*X+B(3)*Y+B(4)*X*X
     &+B(5)*Y*Y+B(6)*X*Y
        RETURN
        END
```